

EVOLUTION OF BARS IN GALAXIES:
EFFECTS ON STAR FORMATION AND STELLAR
DYNAMICS

Charlotte Donohoe-Keyes

A thesis submitted in partial fulfilment of the requirements of
Liverpool John Moores University
for the degree of
Doctor of Philosophy.

July 2021

Declaration

The work presented in this thesis was carried out at the Astrophysics Research Institute, Liverpool John Moores University. Unless otherwise stated, it is the original work of the author.

While registered as a candidate for the degree of Doctor of Philosophy, for which submission is now made, the author has not been registered as a candidate for any other award. This thesis has not been submitted in whole, or in part, for any other degree.

Charlotte Donohoe-Keyes
Astrophysics Research Institute
Liverpool John Moores University
IC2, Liverpool Science Park
146 Brownlow Hill
Liverpool
L3 5RF
UK

SEPTEMBER 17, 2021

Abstract

The majority of disc galaxies have a bar, and bars play a major role in the evolution of galaxies and their properties. Given the cumulative influence that bars can have over the properties of their host, determining the epoch of their formation becomes a fundamental step in understanding disc galaxy evolution. However, this is not a straightforward task. The stars that make up the bar are not necessarily formed there and bars can radially move both gas and stars within a galaxy which makes determining a bar's age from the properties of its stellar population unreliable. Additionally, while bars grow as they age, this is not a linear process and bar growth progresses differently for different galaxies. In this thesis I have explored how the effects of bars on the star formation and stellar dynamics of galaxies can be used to recover the ages of bars using a sample of cosmological zoom-in re-simulations of galaxies in isolated environments.

I first explored the effect of the bar on the star formation desert (SFD) in 6 of the isolated zoom-in cosmological re-simulations. The SFD is a region within the inner ring, lying either side of the bar in the area that the bar sweeps out. James and Percival (2016) found these regions had very little to no star formation and theorised that if star formation is suppressed by the bar the youngest stars in these regions should correspond to the age of the bar. I found that the removal of gas within the SFD occurs within 1-2 Gyr after the formation of the bar indicating there is little to no in-situ star formation after that time. We would, therefore, expect to see a sharp truncation in the star formation history. However, I found a gradual downturn in the star formation history of the SFD region in comparison to that of the bar, so all stars 1-2 Gyr younger than the bar must radially migrate into the SFD region. I propose that the onset of this

downturn could still be used to recover the age of the bar, although the interpretation is more difficult than anticipated. However, I also present the discovery that the SFD is a region where any young stars must be radial migrators. By combining this with a bar age it would allow us to probe the timescales and efficiency of radial migration and thus gain unparalleled insight into the chemo-dynamical evolution of the SFD region.

I also explored the effect of bars on galaxy stellar dynamics. As bars evolve they vertically thicken. Therefore, younger bars have a velocity dispersion similar to that of the disc while in older bars the difference is greater. I built on this by looking at features in the vertical velocity dispersion of the bar with a sample of 15 zoom-in cosmological re-simulations and 3 simulations of isolated galaxies.

I uncovered a special feature in the vertical velocity dispersion of the bar. The location of this feature is remarkably stable with time and on average is 1.5 kpc shorter than the initial length of the bar. By taking the difference between the σ_z of this feature and the bar ends I calculated a value I call $\Delta\sigma_z$. I was able to recover $\Delta\sigma_z$ in both cosmological and isolated simulations and found this value increases monotonically with the age of the bar at the same rate for all the bars in the sample.

The growth of $\Delta\sigma_z$ is influenced by two factors: the lengthening of the bar, and the vertical thickening of the bar. At early times after bar formation the lengthening of the bar is the main contributor to the increase seen in $\Delta\sigma_z$. However, after the bar buckles, the vertical thickening becomes the main contributor to the increase of $\Delta\sigma_z$. Therefore $\Delta\sigma_z$ is a powerful tracer of bar growth as it is entirely constrained by the evolution of the bar. Thus I present a new bar dating method which uses $\Delta\sigma_z$ to infer both the formation time of the bar and an estimate of the initial length of the bar. I have tested this new method on MUSE data of IC1438 and have found good agreement with literature data. This confirms that it is both possible to apply this method to current observational data and that the bar ages recovered are reasonable. This new method presents an exciting avenue for the reliable recovery of quantitative bar ages.

By applying these methods and findings to large statistical surveys we can begin to explore the time of disc settling and the onset of secular processes. I conclude that this

presents us with an exciting opportunity to explore how the formation of the bar can impact galaxy evolution.

Publications

In the course of completing the work presented in this thesis, the following papers have been submitted for publication in a refereed journal:

Donohoe-Keyes, C. E., Martig, M., James, P. A., Kraljic, K., “Redistribution of stars and gas in the star formation deserts of barred galaxies.”, 2019, MNRAS 489, 4992–5003.

This thesis is dedicated to my Grandma, who I know would have been proud of me.

Acknowledgements

First and foremost I would like to express my warmest thanks to my supervisors, Marie Martig and Phil James. They've swapped positions between first and second supervisor but I personally consider them both my first supervisor. They have been amazing in their support and encouragement of me and their willingness to put up with my stubborn pursuit of Chapter 4. This thesis has evolved significantly from what we originally set out to do and that is, in no small part, due to their willingness to trust in me and I in them. I couldn't have asked for two better people to support me in this endeavour. Not only did they support me academically but also emotionally. My Ph.D. has been hard fought and I come out of the other end with one pancreas down and sadly with the loss of my Grandmother. However, Phil and Marie have supported me through it all and I certainly wouldn't have made it without them.

I would also like to express my sincere gratitude to my viva examiners Karen Masters and Andreea Font for taking the time to carefully read through my thesis. I thoroughly enjoyed our discussion and their support for my work. Although I feel I must apologise for just saying "cool" in response to them telling me I had passed as I was rather overwhelmed.

I would also like to thank my A-level teachers Mike Pickard, Jill Smith and Tracylyn Stintson who encouraged me to pursue Astrophysics and with whom I have remained good friends. Their continued interest in my academic achievements has provided welcome support throughout both my undergraduate degree and Ph.D.

Thank you to everyone in the ARI office for being willing to try my food experimentation's and for some delightful discussions in the kitchen over coffee. I would like

to express my particular thanks to Robert Poole-McKenzie, Meghan Hughes, Thomas Sedgwick, Simon Pfeifer, and my Ph.D. brother Joaquín García de la Cruz, with whom I have had many stimulating discussions.

My warmest thanks are reserved for my friends and family. I wish to express my personal thanks to Emma and James who have kept me sane and humble at our weekly movie nights. This year has been difficult but I have always looked forward to Wednesday evening whether it be vampires, Lord of the Rings or Star Wars. I would also like to thank my partner Benjamin Mummery who has supported me continuously over the during of my Ph.D. and has always been ready to play his part as a rubber duck or proof reader as the need required. Finally I would like to express my deepest thanks to my Mum, my Grandad and my Grandma. They have supported and encouraged me through everything and I would not be where I am or who I am without them. Their support has shaped me into the determined person I am and that determination has been vital to making it through this Ph.D. I am especially thankful to my Grandma. Sadly she didn't get to see my complete my thesis but I know it would have made her proud as she was ever vocal about her pride in her little Astrophysicst.

“Clever girl”

- Robert Muldoon, Jurassic Park

“Dang it, Jim. I’m an astronomer, not a doctor! I mean, I am a doctor, but I’m not that kind of doctor. I have a doctorate, it’s not the same thing. You can’t help people with a doctorate. You just sit there and you’re useless!”

- Doctor Doppler, Treasure Planet

“I have passed through fire and deep water, since we parted. I have forgotten much that I thought I knew, and learned again much that I had forgotten.”

- J.R.R. Tolkien, The Lord of the Rings

Contents

Declaration	ii
Abstract	iii
Publications	vi
Acknowledgements	viii
Contents	xi
List of Tables	xv
List of Figures	xvi
1 Introduction	1
1.1 A general description of galaxy formation and evolution	4
1.1.1 Formation of primordial galaxies	4
1.1.2 Hierarchical growth	7
1.1.3 Physical processes in galaxy formation	9
1.1.4 The formation, growth and evolution of disc galaxies	14
1.2 Structure and dynamics of barred galaxies	24

1.2.1	Major properties of bars	24
1.2.2	The orbital structure of the bar	29
1.3	Effects of bars on galaxy evolution	34
1.3.1	Exchange of angular momentum	34
1.3.2	Formation of pseudo-bulges	35
1.3.3	Enhancing central star formation	36
1.3.4	Fueling AGN	37
1.3.5	Formation of rings	38
1.3.6	Suppression of star formation	40
1.4	Bar formation and destruction	42
1.4.1	Bar formation through disc instabilities	42
1.4.2	Bar slow down and growth	45
1.4.3	Are bars long-lived features?	46
1.5	Determining the time of bar formation	49
1.6	Layout for thesis	50
2	Methods	51
2.1	Simulation technique	51
2.2	Additional simulations	54
2.3	Bar detection	56
3	Redistribution of Stars and Gas in the Star Formation Deserts of Barred Galaxies	60
3.1	Introduction	60

3.2	Sample Selection	63
3.2.1	Defining the SFD	65
3.3	Results	65
3.3.1	Age Maps	65
3.3.2	Star Formation Histories	67
3.3.3	Gas Removal	71
3.3.4	Birth positions of SFD stars before & after bar formation . . .	71
3.3.5	Collective dynamics	76
3.4	Discussion	78
3.4.1	Limitations of the simulations	78
3.4.2	Potential bar dating method	79
3.5	Summary	82
4	Using bar kinematics to determine the age of the bar	84
4.1	Introduction	84
4.2	Sample selection	86
4.2.1	Simulations of isolated galaxies	86
4.3	A new method to determine the ages of bars	86
4.3.1	Velocity dispersion profiles in barred galaxies	87
4.3.2	Tracing σ_z through time	91
4.3.3	$\Delta\sigma_z$ as an age indicator	94
4.4	An explanation for the growth of $\Delta\sigma_z$ with time	97
4.5	Peak positions as an indicator for initial bar length	101

4.6	Application to observations	103
4.6.1	Effect of spatial resolution	103
4.6.2	Effect of inclination	105
4.6.3	Application to galaxy IC 1438	109
4.7	Summary	112
5	Summary and Future Work	115
5.1	Summary of main results	115
5.1.1	Dating bar formation using star formation histories	115
5.1.2	Dating bar formation using kinematics	116
5.2	Future work	118
5.2.1	Further investigations using simulations	118
5.2.2	Using Gaia and spectroscopic surveys to date the Galactic Bar	119
5.2.3	Using MaNGA for a statistical study of bar ages and radial migration	122
5.3	Concluding remarks	125
	Bibliography	126

List of Tables

3.1	Properties of the model galaxies taken from $z=0$. For each halo we provide the halo index number, the stellar mass (M_*) calculated by summing star particles to the R_{25} limit, the bar length (L_{bar}), and the bar strength (S_{bar}). The final column gives the bar formation epoch of the galaxy in lookback time.	63
-----	---	----

List of Figures

- 1.1 The Hubble Tuning Fork with the revised addition of lenticular (S0) galaxies. On the left-hand-side are the ellipticals or early-type galaxies, and on the right-hand-side are spirals or late-type galaxies which are further subdivided into barred and un-barred. Credit: SDSS, <http://skyserver.sdss.org/dr1/en/proj/advanced/galaxies/tuningfork.asp> 2
- 1.2 Comparison of the distribution of galaxies from galaxy redshift surveys (blue) and mock surveys from the Millennium simulation (Springel et al., 2006). There is a remarkably good agreement between predictions and observation of the Λ CDM model. 5
- 1.3 Timeline of the evolution of the Universe. After the Big Bang small perturbations are imprinted on the CMB at the time of recombination. These over-densities grow due to gravitational instabilities and collapse to form dark matter halos. Gas collapses along-side the dark matter and cools radiatively to form galaxies (image credit: NASA/WMAP science team). 7
- 1.4 A schematic showing the process of a galaxy merger (Baugh, 2006). Two halos which both contain a progenitor galaxy come close enough to become trapped in a gravitational well. The halos merge and the more massive galaxy is placed at the centre of this new halo. The smaller galaxy becomes a satellite of this halo and dynamical friction causes the satellite galaxy to spiral into the centre. If this processes is shorter than the halo lifetime then the galaxies merge. 8

1.5	The cumulative fraction of galaxy mergers predicted by the Eagle simulation (Font et al., 2017a). The merger mass ratio is given by $X = M_{sat}/M_{star,host}$. The solid lines represent a merger event defined by crossing the $r_{200}(z)$ radius, with dashed lines representing merger events defined at crossing a fixed radius of 20 kpc.	10
1.6	A schematic representation of the main mechanisms for gas accretion in galaxies (Putman, 2017). The red shows hot gas and the blue cool gas. a) Cold mode accretion bringing gas from inter-galactic filaments. b) Gas heated by feedback mechanism can cool and re-accrete back on the disc. c) Hot gas stripped from satellite galaxies or heated through merging events can cool and accrete onto the disc.	12
1.7	The various morphologies observed in the high redshift galaxies of the Hubble Ultra Deep Field (Elmegreen, 2007). Each row shows different examples of a single morphological class with redshift increasing from left to right. From top to bottom: chains (12% show this morphology), doubles (13%), tadpoles (11%), clump-clusters (19%), spirals (31%) and ellipticals (13%).	18
1.8	Comparisons of clumpy galaxies observed in i (rest-frame UV) and J (rest-frame optical) bands (Elmegreen, 2007). The clumpy morphology remains visible when observing in the J band which traces global mass distribution. This distinguishes these massive clumps as different objects from the star forming regions observed in local spiral galaxies.	19

1.9	Diagrammatic representation of the different processes involved in galaxy evolution (Kormendy, 2013). The top half represents fast processes happening on dynamical timescales, while the bottom half shows slow processes which happen over many galaxy rotations. The diagram is also divided horizontally with internal processes shown on the left and environmentally driven processes on the right. In the centre are processes which are present at all stages of galaxy evolution. As the Universe continues to expand secular processes are thought to become the dominate mode for further galaxy evolution.	21
1.10	Examples of boxy/peanut and barlens galaxies (Laurikainen et al., 2014a). The top row shows two galaxies with the characteristic X-shaped structure associated with the boxy/peanut bulges. The bottom row shows galaxies with a more boxy, or barlens-like shape. The galaxies on the left side are viewed nearly edge-on, while those on the right are closer to face-on views. The centre of each row is an unsharp mark of the left side galaxies clearly showing the X-shaped structure.	28
1.11	A schematic showing the 3 major resonances (dashed lines) seen in barred galaxies, the shape of their periodic orbits (solid lines) and an unclosed rosette orbit all in the rest-frame of the bar (Combes, 2001). At the inner Lindblad resonance (ILR) the orbit is elongated, oscillating twice in the radial direction, here the particle moves faster than the bar. At corotation (CR) there is only the epicyclic motion and the guiding centre of the orbit remains stationary in the bars rest-frame. At the outer Lindblad (OLR) resonance the orbit is again elongated with two radial oscillations, here a particle moves slower than the bar so appears to move backwards.	31

1.12	A schematic showing two of the most important families of periodic orbits in the bar (Contopoulos and Papayannopoulos, 1980). In this co-ordinate system the bar is parallel to the x-axis. The x1 family is extended parallel to the bar, while the x2 family is extended perpendicular to the bar.	33
2.1	Left: A plot showing $\phi_2(r)$ against galaxy radius for a single snapshot. The point where the phase deviates from being constant marks the length of the bar (black dashed line). Right: The face-on surface stellar density for the same galaxy and snapshot as left, showing the bar aligned along the y-axis.	57
2.2	Time evolution of bar length showing the raw data featuring the oscillation due to the interaction between the bar and the spiral arms (blue points) and the averaged bar length (black).	59
3.1	Top: R-band image of NGC 2543 showing the bar orientated parallel to the x-axis. Bottom: Continuum-subtracted $H\alpha$ image of the same galaxy showing the lack of $H\alpha$ emission in the SFD region (marked by the vertical black lines) (James and Percival, 2016).	61
3.2	Each plot represents a $40 \times 40 \times 40$ kpc box with the galaxy centred within the box. Left: Face-on surface stellar density maps with the total halo mass decreasing down the column. Middle: Average age maps displaying strong signals for the SFD desert feature. Right: Surface stellar density maps for the young stars, < 10 Myrs, also displaying the SFD feature with SF mainly located within the bar region and along the spiral arms of the galaxies.	64
3.3	The two ‘C’-shaped regions we define as the SFD.	66

3.4	For each of the simulated galaxies in the sample I present the age distribution of the $\text{SFR}_{\text{pc}^{-2}}$ taken from the SFD region, the bar, and the total galaxy at $z=0$. In each plot I display this age distribution normalised to the surface area of the corresponding regions, the age distribution normalised to an area of 1, and the residual (the bar minus the SFD age distribution). Marked on each plot by the vertical dashed line is the time of bar formation. This line coincides with the downturn in the age distribution of the SFD and, in most cases (see Section 3.3.2), the change of the residual from negative to positive.	68
3.5	Here I show the evacuation of gas from the SFD regions. Initially, the gas is diffuse before spiral arms begin to appear. When the bar forms, the central gas concentration elongates along the major axis of the bar, and the spiral arms strengthen. Once the bar is established the gas is removed from the SFD region progressively over 1-2 Gyr. Over time the size of the SFD changes corresponding to variations in the length of the bar.	70
3.6	The birth positions of SFD stars before and after the formation of the bar overlaid on the surface stellar density maps for galaxy 37. Upper: Birth positions of SFD stars before bar formation. Lower: Birth positions of SFD stars after the formation of the bar.	72
3.7	Top: the radial distribution of birth positions for stars born before the formation of the bar. The blue line shows the radial distribution for the SFD stars and orange the radial distribution for bar stars. Before the formation of the bar the stars are mainly born in the same region, within 6 kpc. Some stars are born in merging satellite galaxies, beyond 20 kpc. Bottom: the radial distribution of stars born after the formation of the bar, with blue representing the SFD and orange the bar. Bar stars are mainly born in the central regions while SFD stars are mainly born outside the radius of the bar.	73

3.8	Top: the fraction of stars born after the formation of the bar in the SFD, bar and disk selected to be SFD stars at $z=0$ for galaxy 37. Red represents the total SFD stars born at that time, green the number of SFD stars born in the disk, blue the number of SFD stars born in the bar, and orange the number of SFD stars born inside the SFD region. The majority of the stars ending up in the SFD after the bar is formed come from the disk. Very few stars come from the SFD region. Bottom: the fraction of stars selected to be bar stars at $z=0$ born in the SFD, bar and disk.	74
3.9	Tracking of SFD stars from their birth positions to $z=0$. Initially stars are born in the inner ring near the ends of the bar and along the spiral arms. They then move along the spiral arms and around the inner ring. Slowly stars begin to spiral from the inner ring into the SFD region. Finally the stars collect near the ends of the bar before circling back into the SFD selection region at $z=0$	77
4.1	The typical radial vertical velocity profiles for recently formed and evolved bars. Recently formed bars tend to have profiles similar to the disc, while in evolved bars the vertical velocity dispersion is much higher. (a) and (c) show the effect of a dynamically hot bulge, while (b) and (d) show the profile where the bulge and bar have similar kinematics (Gadotti and de Souza, 2005).	85
4.2	Here I show the diversity in kinematic profiles for the main sample. Each column shows the σ_z , the first derivative of σ_z and $ z $ for a different galaxy. The vertical black lines show the radial position for the bar ends.	87
4.3	Here I show the σ_z profiles for the rest of the sample, following on from Figure 4.2. Each subplot shows the σ_z profile along the bar for a different galaxy. The vertical black lines show the radial position for the bar ends.	88

4.4	Here I show a cartoon representation of the bin dimensions. The values for width, length and height are given as $W= 1$ kpc, $L= 0.25$ kpc and $H= 5$ kpc. These bins are repeated along the bar major axis extending out to the full simulation size of the box ± 20 kpc.	89
4.5	The σ_z evolution for bar major axis of one galaxy over time. Each plot shows both the σ_z and the first derivative of σ_z at a different time step. The peak position in the derivative (red) and bar length (black) is marked for each plot.	92
4.6	$\Delta\sigma_z$ against time for one galaxy. The points show $\Delta\sigma_z$ calculated using the unsmoothed bar lengths, with the line showing the $\Delta\sigma_z$ calculated using the smoothed bar lengths.	95
4.7	Top: $\Delta\sigma_z$ plotted against time since bar formation for all the galaxies in the main sample. The lines (light blue) show $\Delta\sigma_z$ for each individual galaxy. The filled region (blue) shows the inter-quartile range with the black line showing the median. Bottom: $\Delta\sigma_z$ of the isolated:N-body A (orange), isolated:N-body B (purple) and isolated:N-body+gas (red) plotted in comparison to the inter-quartile range of the main sample (blue filled region).	96
4.8	cartoon showing the two main factors affecting change in σ_z . The left hand side of each cartoon shows recently after bar formation, while the right hand side shows times much later than bar formation. Top: An idealised cartoon of the increase in $\Delta\sigma_z$ from the growth in length of the bar. Bottom: An idealised cartoon of the increase in $\Delta\sigma_z$ from the vertical thickening of the bar.	98
4.9	A cartoon showing what we would see if lengthening (left) or vertical thickening (right) is the dominant cause of $\Delta\sigma_z$	99

4.10	Example of galaxies where $\Delta\sigma_z$ is dominated by bar lengthening (top), kinematic thickening (middle) and a combination of both with bar lengthening dominated first (bottom).	100
4.11	The average peak position (orange) and bar length (blue) for one galaxy through time. The peak position remains remarkably stable and lies close to the initial bar length.	101
4.12	A histogram of the difference between the initial bar length and peak position for each snapshot of all the galaxies in the main sample. . . .	102
4.13	Top: σ_z profiles for one simulated galaxy at spatial resolutions of 250 pc (blue), 500 pc (orange), 750 pc (green) and 1000 pc (red). There is very little variation between the general shape of the profile, although at lower spatial resolutions the profile is smoother with less noise. Bottom: The first derivative of σ_z at spatial resolutions of 250 pc, 500 pc, 750 pc and 1000 pc. The peak position moves further out in radius with decreasing spatial resolution resulting in a lower $\Delta\sigma_z$ and an underestimation of the bar formation time.	106
4.14	Testing inclination with rotation about the y-axis (bar edge-on). The inter-quartile range for the main sample is plotted as the filled region with the median of the sample in black. The $\Delta\sigma_{los}$ values for one galaxy are plotted for inclinations of 0° (blue), 20° (orange), 45° (green) and 75° (blue) plotted for comparison.	107
4.15	Testing inclination with rotation about the x-axis (bar end-on). The inter-quartile range for the main sample is plotted as the filled region with the median of the sample in black. The $\Delta\sigma_{los}$ values for one galaxy are plotted for inclinations of 0° (blue), 20° (orange), 45° (green) and 75° (blue) plotted for comparison.	108

4.16	LHS: A colour map of galaxy IC1438 built using the TIMER MUSE data cube (Gadotti et al., 2018). RHS: A colour map of the stellar velocity dispersion of galaxy IC1438; where the bar is orientated in the same direction as in Figure 4.16. The colour bar shows indicates the plotted range in $km s^{-1}$	110
4.17	LHS: The extracted and binned velocity dispersion along the major axis of the bar. The bar length (black) and position of the peak radius (red) are marked with vertical lines. RHS: The first derivative of the velocity dispersion with the bar length and peak radius marked with vertical lines.	111
4.18	The $\Delta\sigma_z$ vs. time plot derived from the simulated galaxies with the $\Delta\sigma_z$ value for IC1438 marked (black dashed line).	112
5.1	Initial results with MaNGA data. Left: The $\Delta\sigma_z$ values for MaNGA galaxies 8331-12705 (orange) and 8935-610 (blue) plotted against the inter-quartile range of $\Delta\sigma_z$ for the simulations presented in Chapter 4 (blue filled region) and the median $\Delta\sigma_z$ of the simulation (black). Middle: SDSS g , r and i colour images of the MaNGA galaxies 8331-12705 (top) and 8935-610 (bottom). The magenta hexagon shows the size of MaNGAs IFU bundle. Right: The σ_z profiles for the MaNGA galaxies 8331-12705 (top) and 8935-610 (bottom). The peak positions of the first derivative (red) and the length of the bar (black) are marked with vertical lines.	124

Chapter 1

Introduction

A galaxy is a collection of stars, gas, and dark matter which is gravitationally bound together. Due to the significant timescales over which galaxies evolve, direct observation of their formation and evolution is not possible. However, by observing many galaxies at different evolutionary stages we can piece together the information important to understanding the details of their history.

One powerful tool in understanding galaxy evolution is the classification of their visual morphologies. The most recognisable scheme of galaxy morphology is credited to Edwin Hubble who created the ‘Hubble Tuning Fork’ (Hubble, 1926, see Figure 1.1). In this classification scheme Hubble divided galaxies into two main types: ellipticals which range in oblateness from E0 which are round to E7 which have a ellipticity of 0.7, and spirals classified from Sa to Sc based on the size of their bulges compared to their discs and how tightly wound their spiral arms are. Spirals were then further split based on the presence or absence of a bar into SBa-SBb-SBc and Sa-Sb-Sc respectively. Later added to the Hubble tuning fork were lenticular galaxies (Hubble, 1936), also referred to as S0 galaxies, which bridged the gap between ellipticals and spirals. There is an additional third classification which is not part of the original tuning fork comprising of irregular ‘I’ galaxies that show no dominant nuclei or rotational symmetry. This classification scheme has undergone multiple revisions since it was first introduced but perhaps the most notable was that done by de Vaucouleurs (1959) who

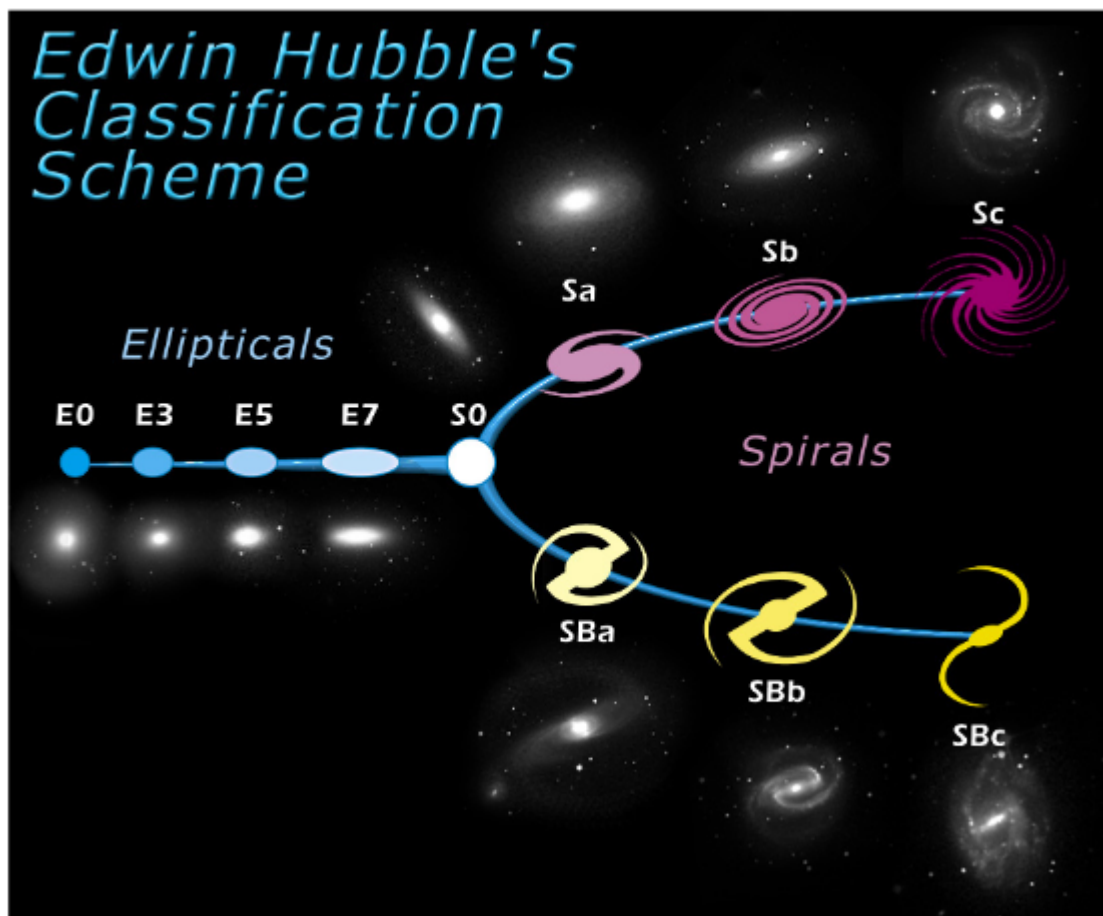


Figure 1.1: The Hubble Tuning Fork with the revised addition of lenticular (S0) galaxies. On the left-hand-side are the ellipticals or early-type galaxies, and on the right-hand-side are spirals or late-type galaxies which are further subdivided into barred and un-barred. Credit: SDSS, <http://skyserver.sdss.org/dr1/en/proj/advanced/galaxies/tuningfork.asp>

proposed two additional classes of spiral galaxy: ‘d’ for dwarf galaxies and ‘m’ for Magellanic spirals named after their prototype the Large Magellanic Cloud. de Vaucouleurs also added three sub-classes for each spiral type: SA for non-barred galaxies, SB for strongly barred galaxies and SAB for weakly barred galaxies.

In addition to their morphology, galaxies can also be classified by their colours. This colour classification led to the discovery of bimodality between the ‘blue cloud’ and ‘red sequence’, with the transition region between them commonly referred to as the ‘green valley’. The so-called ‘red sequence’ is predominantly populated by massive spheroidal systems, while the ‘blue cloud’ is mostly made up of spirals (Baldry et al., 2004; Bell et al., 2004; Driver et al., 2006; Faber et al., 2007; Blanton and Moustakas,

2009). However, both spirals and ellipticals can be found in both categories (Schawinski et al., 2009; Masters et al., 2010; Fraser-McKelvie et al., 2016). While these categories are linked to the colour of the galaxies it is actually the presence or absence of star formation which separates them (Noeske et al., 2007; Peng et al., 2010; Rodighiero et al., 2011).

Galaxies which lie in the red sequence have had their star formation quenched, while those in the blue cloud are actively star forming (Faber et al., 2007). The galaxies which reside in the green valley are few and are thought to be actively undergoing star formation quenching (Faber et al., 2007; Schawinski et al., 2007, 2014). There appears to be no clear causal link between galaxy morphological classification and presence within the green valley, although they tend to be of intermediate morphological types such as lenticulars or early-type barred galaxies (Schawinski et al., 2014; Cano-Díaz et al., 2016; Sánchez et al., 2019). These categories not only differ in star formation but stellar populations in galaxies residing in the blue cloud are younger than those in the green valley which are younger than those in the red cloud (Pan et al., 2013). These two factors support a evolutionary scenario in which galaxies transition from the blue cloud to the red sequence via the green valley as a result of some quenching mechanism (Bell et al., 2004; Faber et al., 2007), although it should be noted the reverse may be possible with red sequence galaxies being rejuvenated through the addition of fresh gas (Thomas et al., 2005, 2010).

However, the precise nature of the quenching mechanism is difficult to establish and there may be different mechanisms at play for different galaxies (Schawinski et al., 2014; Taylor and Kobayashi, 2015; Bremer et al., 2018; Eales et al., 2018). Both observations and simulations suggest at least two main evolutionary channels to quench galaxies: rapid quenching of early-type galaxies, and the gradual quenching of late-types through secular processes (Schawinski et al., 2014; Smethurst et al., 2015). There are many proposed quenching mechanisms which can be broadly divided into environmental and mass quenching. Environmental quenching pertains to processes which quench galaxies as a result of their interactions with their surrounding area such as strangulation (Balogh and Morris, 2000; Peng et al., 2015), ram pressure stripping

(Gunn and Gott, 1972; Moore et al., 1999; Barsanti et al., 2018), galaxy merging (Lotz et al., 2011), galaxy harassment (Moore et al., 1996), and tidal stripping (Merritt, 1983). Mass quenching pertains to those processes depending on the internal, or intrinsic, properties of galaxies such as AGN feedback (Di Matteo et al., 2005; Silk, 2013; Somerville and Davé, 2015; Penny et al., 2018), morphological quenching (Martig et al., 2009) and gas outflows from stellar feedback or supernovae explosions (Dekel and Silk, 1986; Dalla Vecchia and Schaye, 2008). In all cases these mechanisms act to deplete the reservoir of star-forming gas available to a galaxy, resulting in a suppression of the star formation rate.

Bars have been implicated as one mechanism through which a spiral galaxy may be gradually quenched (Gavazzi et al., 2015). In this thesis I focus on investigating the effects bars have on a galaxy's evolution through their influence on the star formation and stellar dynamics. In particular I explore how these effects might be able to indicate the time of bar formation and thus allow us to determine when discs begin to settle and secular processes begin to dominate a galaxy's evolution.

In this chapter I will first give a general overview of how galaxies are formed and the physical processes which influence their evolution. I shall then focus on describing the structure and properties of the bar, explaining the main effects of bars on galaxy evolution and their formation and destruction. Finally, I shall review the current methods used to determine the time of formation of the bar before outlining the layout of this thesis.

1.1 A general description of galaxy formation and evolution

1.1.1 Formation of primordial galaxies

The Lambda Cold Dark Matter (Λ CDM) model is the most favoured cosmological model successful at explaining the formation of large scale structure in the Universe

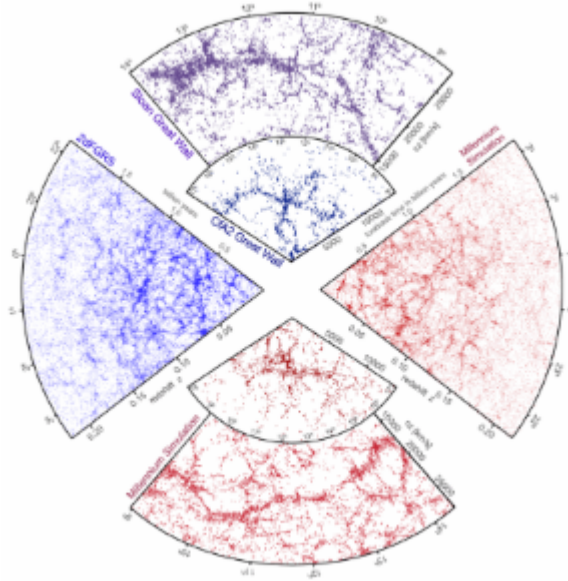


Figure 1.2: Comparison of the distribution of galaxies from galaxy redshift surveys (blue) and mock surveys from the Millennium simulation (Springel et al., 2006). There is a remarkably good agreement between predictions and observation of the Λ CDM model.

and which is in agreement with observations of the Cosmic Microwave Background (CMB) (see Figure 1.2) (Peebles, 1982; Blumenthal et al., 1984; Davis et al., 1985; Springel et al., 2006; Percival et al., 2007; Sánchez et al., 2009). Within this framework, observations point towards a Universe that is 13.7 billion years old comprised of 73.5% dark energy, 22% dark matter and 4.5% baryons (Cole et al., 2005; Percival et al., 2007; Kowalski et al., 2008; Dunkley et al., 2009; Vikhlinin et al., 2009; Rozo et al., 2010).

Fluctuations in the CMB

In this model the early universe is made up of a hot plasma of baryons, photons and dark matter. Small perturbations travel collisionally through this plasma as sound waves which creates over- and under-densities (Hu and White, 2004). In the cold dark matter (CDM) paradigm the dark matter component of this plasma only interacts gravitationally which acts to enhance some over-densities while negating others. When recombination begins (hydrogen begins to form) these density fluctuations become frozen and are preserved in the CMB.

Collapse of cold dark matter

The CDM contracts and then collapses into the over-dense regions, attracting more material from its surroundings causing the under-dense regions to become emptier. As the dark matter collapses it acquires angular momentum through tidal interactions or mergers with other collapsing halos and settles at virial equilibrium (White, 1984; Maller et al., 2002; Vitvitska et al., 2002). This process results in the filamentary cosmic web seen in the observations and cosmological simulations of today (Press and Schechter, 1974; Lacey and Cole, 1993; Frenk and White, 2012, see Figure 1.2).

Collapse of gas

Primordial gas collapses alongside the dark matter acquiring the same density profile and angular momentum (Rees and Ostriker, 1977; White and Frenk, 1991; Somerville and Davé, 2015). Unlike dark matter, gas can cool radiatively allowing it to collapse towards the centre of the dark matter halo. The collapsing gas settles into a rotationally supported disc whose orientation is determined by angular momentum (Abel et al., 2002; Bromm et al., 2009).

The first stars

Within these discs the gas cools forming H_2 molecules which collapse into dense clouds causing the formation of the first stars (Bromm et al., 2002; Bromm, 2013; Yoshida, 2008). While no examples of these ‘Population III’ stars have been observed, they are thought to be massive and, due to their size, short-lived. When they explode as supernovae they eject the heavy elements (metals) formed in their interiors, enriching the interstellar medium (Benson and Madau, 2003). The metals ejected by these dying stars allow for more efficient cooling of gas and the subsequent formation of Population II stars.

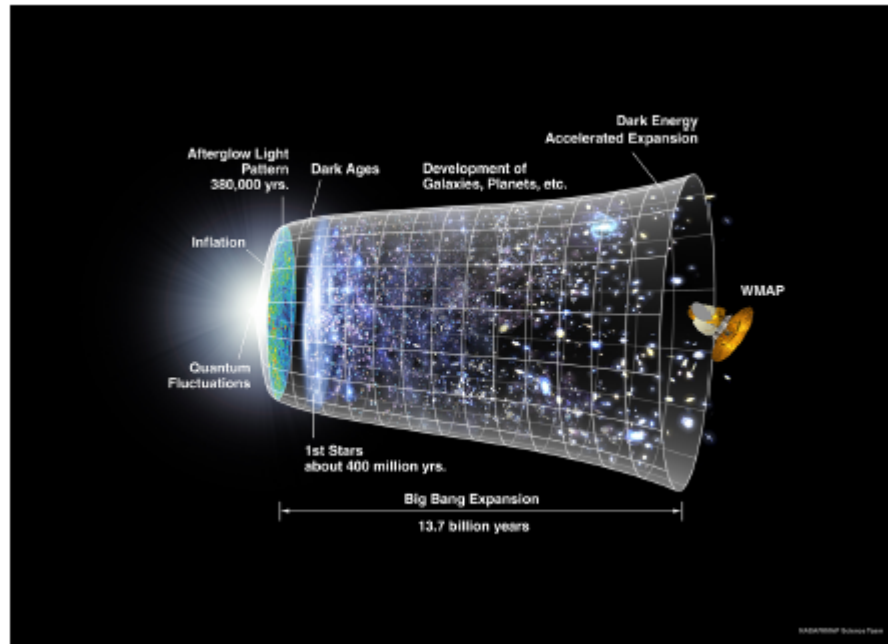


Figure 1.3: Timeline of the evolution of the Universe. After the Big Bang small perturbations are imprinted on the CMB at the time of recombination. These over-densities grow due to gravitational instabilities and collapse to form dark matter halos. Gas collapses along-side the dark matter and cools radiatively to form galaxies (image credit: NASA/WMAP science team).

1.1.2 Hierarchical growth

In Λ CDM small low mass structures are the first to form with objects of increasing size, mass and complexity forming later (Baugh et al., 1996; Baugh, 2006; Cole et al., 2000, see Figure 1.3). This formation scenario is commonly referred to as hierarchical growth (White and Rees, 1978; Baugh et al., 1999; Fakhouri and Ma, 2008).

Galaxies are more concentrated than the dark matter due to the dissipative cooling of gas so are able to survive the merging of their parent halos. This leads to a scenario where a dark matter halo contains one central massive galaxy with several satellite galaxies. As the satellite galaxies orbit the massive central galaxy they lose orbital energy as a result of dynamical friction (Chandrasekhar, 1943). When the satellite moves through the halo it attracts material to it causing a wake of higher density material to form behind it. This acts to break the forward motion of the satellite galaxy as it feels a stronger gravitational pull from the region it has just travelled through than the region it is about to enter. The loss of energy as a result of dynamical friction causes the satel-

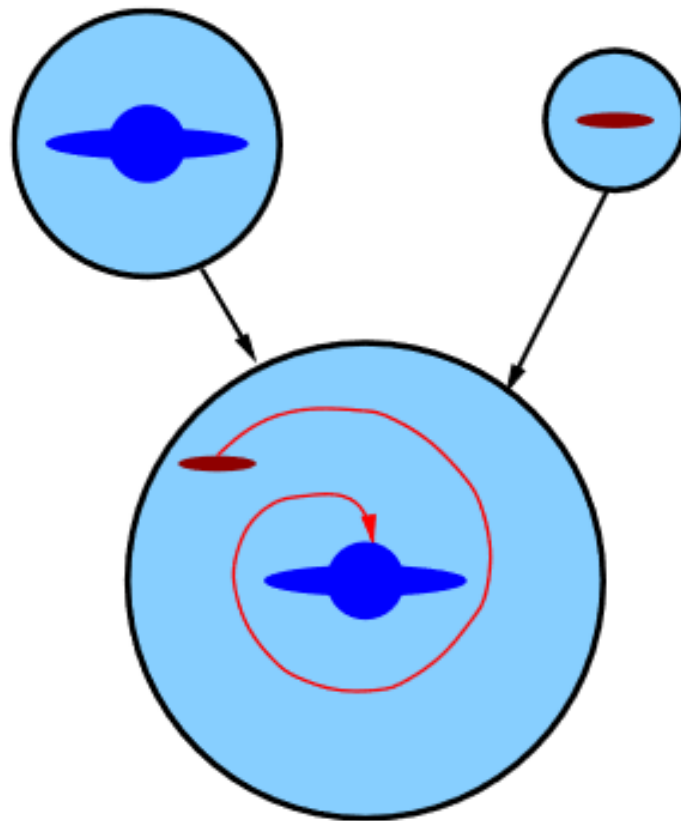


Figure 1.4: A schematic showing the process of a galaxy merger (Baugh, 2006). Two halos which both contain a progenitor galaxy come close enough to become trapped in a gravitational well. The halos merge and the more massive galaxy is placed at the centre of this new halo. The smaller galaxy becomes a satellite of this halo and dynamical friction causes the satellite galaxy to spiral into the centre. If this processes is shorter than the halo lifetime then the galaxies merge.

lite galaxy to spiral in towards the massive central galaxy (Binney, 1977, see Figure 1.4). If the timescale of this process is shorter than the time between halo mergers then the satellite galaxy will merge with the galaxy in the centre of the halo.

This process of galaxy merging is violent and can have dramatic effects on the morphologies and star formation histories of the resulting galaxies. In the next section I will review the physical processes involved in galaxy formation beginning with an overview of the consequences of galaxy mergers and then discussing another avenue for galaxy growth through gas accretion.

1.1.3 Physical processes in galaxy formation

Mergers

One of the key predictions of Λ CDM model, and a cornerstone idea for how galaxy formation occurs, is galaxy merging. Mergers have a significant impact on galaxy evolution through transforming galaxy morphology, changing galaxy kinematics, facilitating mass growth, and triggering star formation episodes.

Galaxy mergers can be broadly placed into two categories: major mergers which have mass ratios greater than 4:1, and minor mergers with mass ratios less than 1:4. These categories can both be further subdivided into dry and wet mergers. Dry mergers have a very low gas content so can be considered collisionless, while in wet mergers (which are gas rich) gas plays a much more significant role which can act to alter the morphological outcome of the merging event. As such the morphology of a galaxy at $z = 0$ is partially dependent on not only the mass ratio of the merging galaxies but also their gas content.

One would expect that in a hierarchical universe there should be a large number of mergers so constraining the merger rate over cosmic history is key for understanding galaxy evolution and for testing current evolutionary models. However, while there are many observational and theoretical studies on defining merger rates as a function of time, this is not a trivial process.

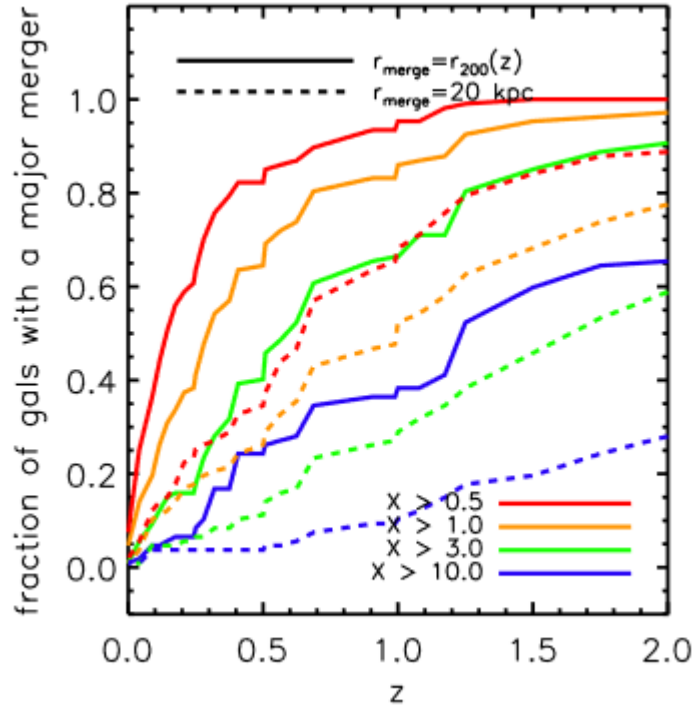


Figure 1.5: The cumulative fraction of galaxy mergers predicted by the Eagle simulation (Font et al., 2017a). The merger mass ratio is given by $X = M_{sat}/M_{star,host}$. The solid lines represent a merger event defined by crossing the $r_{200}(z)$ radius, with dashed lines representing merger events defined at crossing a fixed radius of 20 kpc.

Observational efforts in determining a merger rate rely on capturing a galaxy during the process. This can be through identifying galaxy pairs to find galaxies before the merge, or galaxies with distorted morphologies which can appear prior, during or post merger. However, the identification of galaxy pairs requires precise redshift measurements to eliminate background and foreground galaxies, and identifying the morphological distortions becomes increasingly difficult at higher redshifts (Patton et al., 1997, 2002; Le Fèvre et al., 2000; López-Sanjuan et al., 2011, 2012).

Another route for determining merger rates it to use statistical studies of large scale cosmological simulations (see Figure 1.5). This requires the use of halo finding algorithms and merging criteria. However, different algorithms can result in vastly different results and a merging halo does not guarantee galaxy mergers.

Despite the difficulties with measuring a merger rate it is generally agreed that merger fraction evolves as $(1+z)^m$, where m can take a value between 2 and 4. However,

most of these methods (the observational ones in particular) are biased towards major mergers as they cause stronger effects on the merging galaxies (Bluck et al., 2009, 2012; Bridge et al., 2010). Due to their smaller mass ratio the effects of minor mergers are weaker making it even more difficult to determine a merger rate.

Major mergers can quickly transform disc galaxies into ellipticals through violent relaxation. This is where strong fluctuations in the gravitational potential of chaotic systems allows particles to quickly exchange energy and settle back into equilibrium (Lynden-Bell, 1967). However, these events are expected to be rare. Minor mergers are both predicted (Maller et al., 2006; Stewart et al., 2008; Fakhouri and Ma, 2008; Kaviraj et al., 2009) and observed (Lin et al., 2004; Jogee et al., 2009; López-Sanjuan et al., 2010) to be at least 3-4 times more common than major mergers. While minor mergers result in less dramatic consequences such as the thickening of galactic discs, a high frequency of minor mergers may also result in morphological changes (Bournaud et al., 2007). However galaxy merging is not sufficient, on its own, to explain the evolution of galaxies.

Gas accretion

In addition to galaxy mergers, mass can also be assembled via gas accretion. In the Λ CDM model massive dark matter halos hosting galaxy clusters are predicted to reside in the nodes of a large filamentary structure called the “cosmic web”. Observational evidence for this cosmic web comes in the form of large surveys (Colless et al., 2001) which show that galaxies are also distributed along filaments which have large voids of space between them. Theory predicts that these filaments are made up of both dark matter and diffuse gas. While there is remarkably good agreement between simulations and the observed distribution of galaxies from both a statistical and qualitative standpoint, the diffuse gas component is rarely if ever observed (Hoyle et al., 2002; Springel et al., 2006; Umehata et al., 2019).

Gas accretion is an important process not only in the formation of galaxies but also in the sustainability of star formation in the universe: without continuous accretion galax-

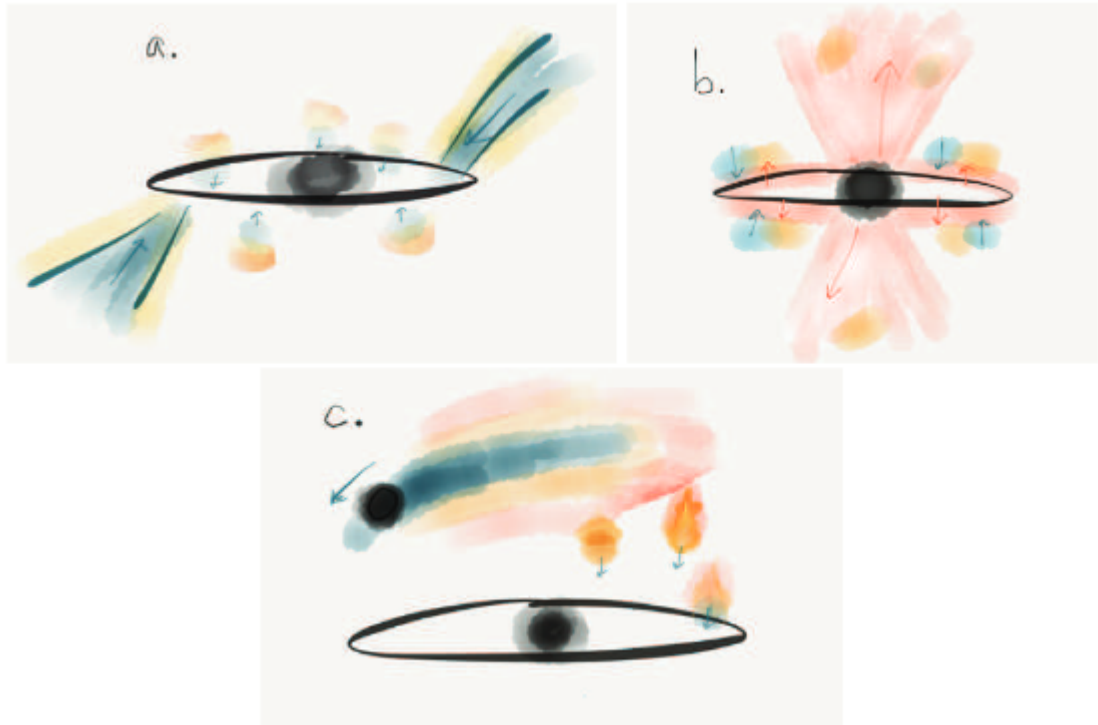


Figure 1.6: A schematic representation of the main mechanisms for gas accretion in galaxies (Putman, 2017). The red shows hot gas and the blue cool gas. a) Cold mode accretion bringing gas from inter-galactic filaments. b) Gas heated by feedback mechanism can cool and re-accrete back on the disc. c) Hot gas stripped from satellite galaxies or heated through merging events can cool and accrete onto the disc.

ies would exhaust their gas reserves within a few gigayears (Gyr) (Bigiel et al., 2008, 2011; Leroy et al., 2008, 2013; Rahman et al., 2012). High resolution cosmological simulations have found that gas accretion comes in two main flavours: hot and cold. These mechanisms are summarised in Figure 1.6. In hot mode accretion as the dark matter of a galaxy settles to virial equilibrium the infalling gas is shocked (Rees and Ostriker, 1977; Silk, 1977; Binney, 1977; White and Rees, 1978). If this gas is able to cool on a timescale shorter than the dynamical time then it is able to fall towards the centre and accrete onto the galaxy isotropically. If the cooling timescale is longer than the dynamical time then this gas is not able to cool and it forms a hot hydrostatic halo atmosphere which is stabilised against gravitational collapse by pressure (Birnboim and Dekel, 2003; Dekel and Birnboim, 2006). Specifically, hot mode accretion refers to gas accreted from the gas which has been shock heated to the virial temperature of the halo.

However, gas can also be heated as a result of various feedback mechanisms. These feedback mechanisms act to heat the gas, and in some cases expel it from the galaxy. The kinematic signatures of these feedback mechanisms heating gas into the halos of galaxies have been observed numerous times (Heckman et al., 1990; Shapley et al., 2003; Martin, 2005; Weiner et al., 2009; Rubin et al., 2014). While these processes can remove gas from a galaxy, the gas which is not removed from the galaxy through outflows can then cool and fall back onto the disc. While this process does not introduce new material in a global sense, it does act to prevent runaway star formation and to replenish the disc with gas. The most common candidates implicated in this process are supernovae possibly augmented by stellar winds (Heckman et al., 1990; Hopkins et al., 2012b) and active galactic nuclei (Silk and Rees, 1998; Bower et al., 2006; McNamara and Nulsen, 2007, AGN).

In cold mode accretion the gas is not heated allowing it to free-fall into the central regions of galaxies (Kereš et al., 2005, 2009). Cold accretion is thought to play a more dominant role at higher redshifts bringing gas directly from the cosmic web into the central regions of low mass halos and in low mass galaxies today via filaments and gas rich minor mergers. The high density of filamentary gas at early times facilitates rapid cooling rates and the lack of hot halos prevents the efficient shock heating of gas (Kereš et al., 2005; Benson and Bower, 2011). As halos begin to heat up towards later times shock heating becomes more efficient which prevents material reaching the galaxy at the centre, although cold gas may also be able to penetrate massive hot halos if the gas streams are sufficiently dense and cool efficiently (Dekel et al., 2009).

Cosmological simulations have predicted that most if not all galaxies experience a phase of growth facilitated by cold accretion (Kereš et al., 2005; van de Voort et al., 2011). As such, cold mode accretion is predicated to play a pivotal role in the formation and early growth of galaxies while hot mode accretion, which becomes more dominant at later times, is important in the continuous evolution of galaxies.

1.1.4 The formation, growth and evolution of disc galaxies

In this section I will describe how the processes involved in the formation, growth and evolution of galaxies affect the formation and preservation of disc galaxies.

Early violent processes

One of the long-standing issues in Λ CDM cosmology is recovering the local abundance of disc galaxies (Weinmann et al., 2006; Park et al., 2007). In the hierarchical galaxy formation scenario the vast majority of galaxies are expected to have undergone major merger events and in some cases multiple merging events (Toth and Ostriker, 1992; Stewart et al., 2008; Boylan-Kolchin et al., 2010). In a naive outlook one would expect very few disc galaxies would survive to today, however we commonly see disc galaxies in the local universe (Park et al., 2007; Kelvin et al., 2014).

Initial studies into the merging of disc galaxies were based on simulations involving little to no gas. In these cases the internal stellar structures of the discs were completely destroyed and the scattered stars form a spheroidal or ellipsoidal structure (Toomre and Toomre, 1972; Toomre, 1977; Hammer et al., 2009; Taranu et al., 2013; Deeley et al., 2017). This led to the (now discarded) conclusion that disc galaxies must evolve quiescently, with little to no merger events. While 1:1 mergers are generally considered to be rare for Milky Way-like systems it is expected that approximately 70% of them have undergone mergers with a mass ratio greater than 1:10 (Stewart et al., 2008; Font et al., 2017a). While not all of these are major mergers in the classical definition (mass ratio > 1:4) multiple minor mergers can result in the destruction of a disc. Even just looking at the major mergers, approximately 20-35% of all disc galaxies in the local universe are thought to have undergone major disc destroying mergers (López-Sanjuan et al., 2009). Therefore, to explain the local fraction of disc galaxies one must discard the paradigm which promotes a quiescent history for disc galaxy formation.

By including gas within galaxy mergers (making them no longer collisionless) it becomes easier to reconcile a hierarchically driven universe with the observed disc galaxy

population, although explaining bulgeless galaxies remains an outstanding issue. In fact, both isolated and cosmological simulations find that major mergers of discs can even result in a disc galaxy with the inclusion of gas (Athanasoula et al., 2016; Rodionov et al., 2017; Peschken et al., 2017; Sparre and Springel, 2017). In these scenarios the disc galaxies each contain a hot gaseous halo. The initial merger event results in the formation of a classical bulge through both the collisionless interaction between the stellar component and a rapid burst of merger driven star formation using up the cold gas of the discs. After some time the gas in the hot halo cools and is accreted onto the merger remnant alongside accretion from cold gas filaments. If this merging event happens at an intermediate or high redshift then the cumulative gas accretion, from cooling of hot gas and from cold filaments, results in a disc-dominated galaxy with a classical bulge as seen today.

Mergers between galaxies of unequal mass are both predicted (Maller et al., 2006; Stewart et al., 2008; Fakhouri and Ma, 2008; Kaviraj et al., 2009; Hopkins et al., 2009) and observed (Lin et al., 2004; Jogee et al., 2009; López-Sanjuan et al., 2010) to be 3-4 times more common than major mergers; this is especially the case at later times. While many minor mergers acting on one system can morphologically transform discs to ellipticals (this is actually the method proposed to produce realistic ellipticals) a minor merger will not usually destroy a galaxy disc. In fact, minor mergers have been implicated as an effective way to both vertically thicken and radially extend disc galaxies through dynamical friction (Hopkins et al., 2009). If there is a significant amount of gas within the galaxy disc, however, it can act to dampen this effect by absorbing some of the kinetic energy from the impact and through the re-formation of a thin stellar disc post-merger (Moster et al., 2010; Villalobos et al., 2010).

Minor mergers can also play a role in the formation of galaxy bulges. The accretion of a minor satellite causes instabilities in the disc. This results in a transfer of angular momentum causing stars to fall into the centre. The gas contained within the satellite also falls towards the galaxy centre as it cools and triggers central star formation resulting in the formation of a dispersion dominated bulge component. If these mergers are particularly gas rich they can result in the formation of massive clumps at large

radii which can cause clumpy irregular discs (Elmegreen, 1993; Taniguchi and Shioya, 2001; Robertson and Bullock, 2008; Bournaud et al., 2008; Overzier et al., 2008). Additionally, stars from the merging satellite may also spiral into the central regions of the galaxy helping to build up the bulge.

However, even when including gas rich mergers and minor mergers reconciling the currently accepted hierarchical galaxy formation scenario with the number of bulgeless galaxies observed in the universe is still a significant problem (Stinson et al., 2010). Many galaxies do not have bulges (Dutton, 2009), and even when considering massive galaxies many of them do not host classical bulges (Kormendy et al., 2010; Fisher and Drory, 2010). These galaxies may instead have a central component that looks similar to a bulge but with properties similar to the disc (referred to in the literature as a pseudo-bulge) (Kormendy and Kennicutt, 2004). This suggests that many disc galaxies have not undergone major merger events and instead have had a quieter history, acquiring their baryonic matter through other means.

Evidence suggests that the majority of a galaxy's baryonic matter is not obtained through mergers but through cold gas flows (Agertz et al., 2009; Ocvirk et al., 2008; Kereš et al., 2009; Brooks et al., 2009; Dekel et al., 2009). These cold gas flows are more dominant at higher redshifts for lower mass galaxies where the cold streams can easily penetrate through the hot halos (Ocvirk et al., 2008; Dekel et al., 2009). This can also result in turbulent, gas-rich discs which are prone to internal instabilities. The gas then fragments into massive star forming clumps (Bournaud et al., 2008; van Starckenburg et al., 2008) which (if the clumps are big enough) migrate into the galaxy centre providing another avenue for the formation of a galaxy bulge while preserving the disc (Elmegreen and Elmegreen, 2005; Genzel et al., 2008; Bournaud et al., 2008).

Discs at high redshift

Generally, bars are expected to form in discs once they are sufficiently massive and dynamically cold (Ostriker and Peebles, 1973; Sellwood and Wilkinson, 1993; Athanassoula and Misiriotis, 2002, see Section 1.4 for more details), and mark the onset of

secular processes (see Section 1.1.4). The formation of stellar bars in discs is expected to be a relatively quick process, occurring over a few Myr (Ostriker and Peebles, 1973; Athanassoula and Misiriotis, 2002; Athanassoula, 2003a). However, at high redshifts there are few galaxies which show morphologies like the disc galaxies we see in the local universe (Beckwith et al., 2006) with the presence of bars decreasing with increasing redshift. Instead as redshift increases we see an increase in galaxies with clumpier morphologies which are not just features in otherwise normal spirals and ellipticals (Elmegreen, 1993). Understanding why these discs do not form bars and for how long they remain stable against bar formation is key in determining the timescales of disc galaxy evolution. Deep surveys resolving these galaxies at $z \geq 1$ show these galaxies can generally be classified into chains and clump-clusters. In chain galaxies the clumps are aligned in a linear arrangement while clump clusters show a rounder arrangement of clumps (Elmegreen et al., 2004, see Figure 1.7).

These chain and clump-clusters tend to dominate star formation at high redshifts with the clumps themselves being massive star forming regions. Similarities in colours, apparent magnitudes and the distribution of the ratio of axes among clump cluster and chain galaxies show that clump-clusters are the face-on counterparts to chain galaxies (Elmegreen et al., 2004; Elmegreen and Elmegreen, 2005). While there is some debate on whether these clump systems could be interacting galaxies (Overzier et al., 2008), the general consensus is that they are the result of turbulent discs since their kinematics show ordered rotation which would not be the case if they were merging galaxies (Elmegreen et al., 2006; Bournaud et al., 2008).

When observing high redshift galaxies in the i -band it actually corresponds to their rest-frame UV . In local galaxies observations in the UV show a more clumpy fragmented structure. This means that the clumpy morphology we see in high redshift disc galaxies might only be a by-product of the band-shifting which results in us seeing them in their rest-frame UV (Kuchinski et al., 2001). However, Elmegreen et al. (2007) found that this clumpy morphology persists when observing in the J band (which corresponds to an optical rest-frame) which classifies these objects as different from local and high redshift spiral galaxies (see Figure 1.8).

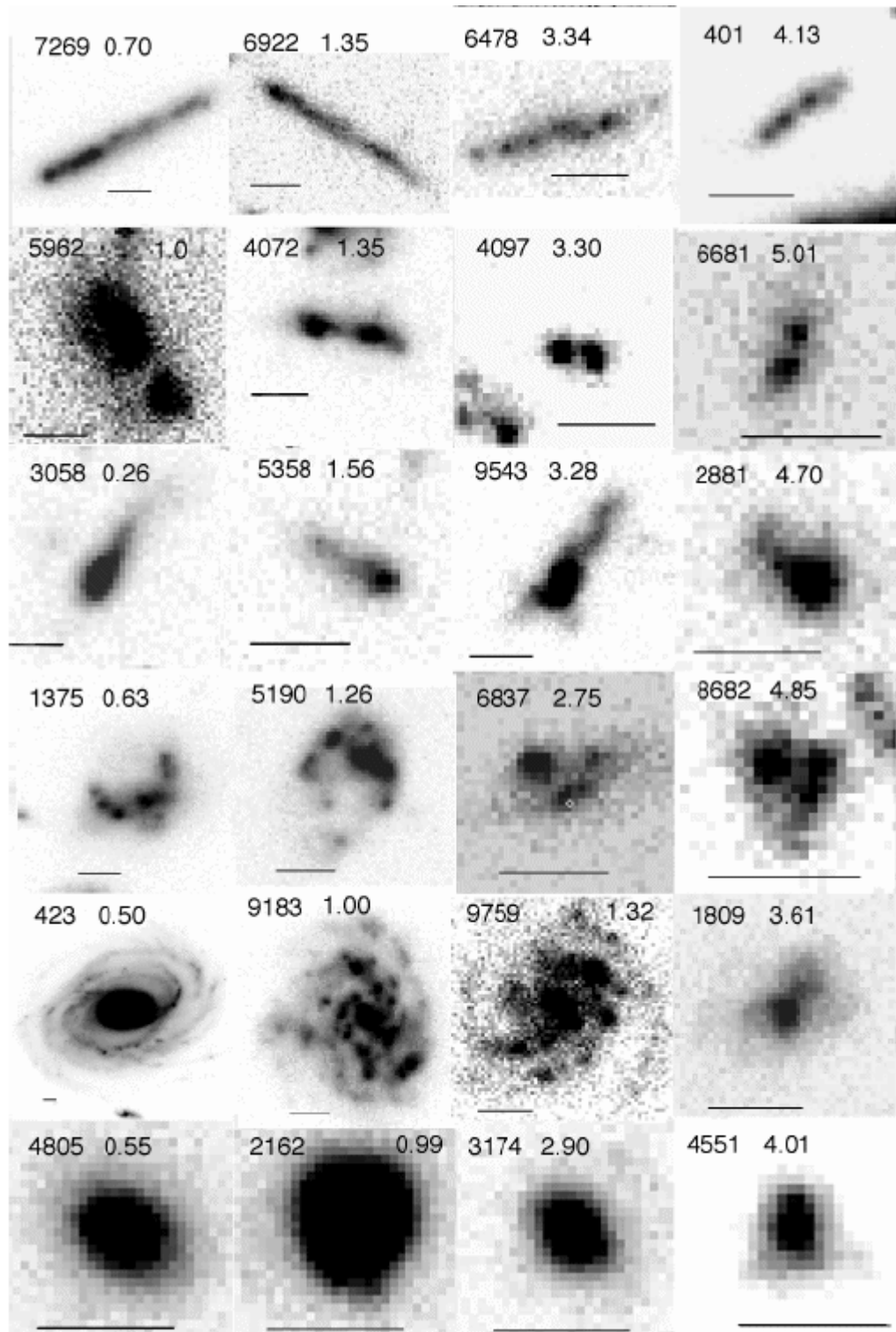


Figure 1.7: The various morphologies observed in the high redshift galaxies of the Hubble Ultra Deep Field (Elmegreen, 2007). Each row shows different examples of a single morphological class with redshift increasing from left to right. From top to bottom: chains (12% show this morphology), doubles (13%), tadpoles (11%), clump-clusters (19%), spirals (31%) and ellipticals (13%).

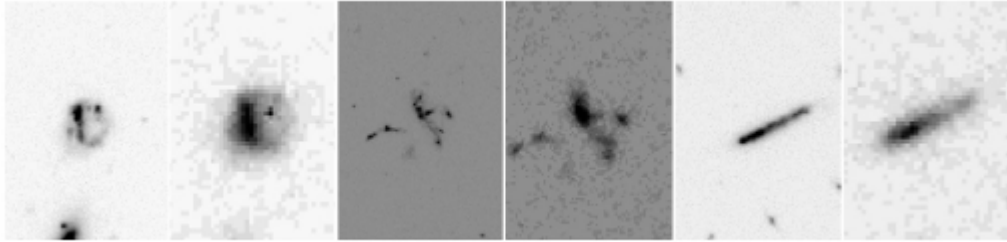


Figure 1.8: Comparisons of clumpy galaxies observed in i (rest-frame UV) and J (rest-frame optical) bands (Elmegreen, 2007). The clumpy morphology remains visible when observing in the J band which traces global mass distribution. This distinguishes these massive clumps as different objects from the star forming regions observed in local spiral galaxies.

There have been various debates over the origin of these clumps resulting in two possible formation scenarios. The clumps could be a result of external processes such as minor mergers or galaxy interactions (Hopkins et al., 2013; Mandelker et al., 2017). These clumps may be satellite galaxies in the process of merging or alternatively the merging event may induce instabilities within a disc. In these instabilities gas can accumulate to high enough densities that result in bursts of star formation. There has been some support for this from various observational studies (Puech et al., 2009; Puech, 2010; Wuyts et al., 2014; Straughn et al., 2015; Ribeiro et al., 2017; Zanella et al., 2019), however the preferred method is formation through violent instabilities within a turbulent disc. In this scenario the intense inflow of cold gas, which is predicted to be a dominant mode of mass growth in the early universe (Kereš et al., 2005; Dekel and Birnboim, 2006; Dekel et al., 2009), causes turbulence within the disc. Regions of dense gas cause gravitational instabilities driving turbulence in the disc which causes gas to collect in larger and larger clumps. When the densities of these clumps are high enough bursts of star formation are triggered forming the massive star forming regions observed in the chain and clump cluster galaxies (Bournaud et al., 2007, 2009; Dekel et al., 2009; Ceverino et al., 2010, 2012; Inoue et al., 2016). Observational support for this process, which is referred to as violent disc instability, comes from analysing the properties of these clumpy features (Elmegreen, 2007; Bournaud et al., 2008; Fisher et al., 2017). Although it has also been suggested that while violent disc instabilities are likely the origin of clumps in more massive galaxies the merger driven origin may better explain clump formation in low mass galaxies (Guo et al., 2015).

In addition to their origin the longevity and consequent evolution of these clumps is also a topic of some debate. In one scenario the clumps are short lived features being easily broken up by stellar feedback from their own starbursts which results in the thickening of the disc (Bassett et al., 2014; Inoue and Saitoh, 2014). Indeed there are several studies which support this narrative where clumps are quickly disrupted (Murray et al., 2010; Genel et al., 2012; Hopkins et al., 2012a; Buck et al., 2017). However, observed galacto-radial gradients in the colours of these clumps (Förster Schreiber et al., 2011; Shibuya et al., 2016) and ages calculated for the clumps themselves (Soto et al., 2017; Guo et al., 2018) suggests they are more long lived features. In simulations where clumps are long lived features they end up migrating towards the centre of the galaxy through dynamical friction and contribute to the build up of a bulge component which can then act to stabilise the disc against further instabilities (Bournaud et al., 2007; Elmegreen et al., 2008; Mandelker et al., 2014, 2017).

Secular evolution

[] While violent processes such as mergers and rapid internal evolution from violent disc instabilities play a pivotal role in shaping the early formation and evolution of disc galaxies, as the universe expands and mergers become less common (Toomre, 1977; Conselice et al., 2003) later evolution is thought to take place through internal secular processes. These secular processes act over timescales much larger than the dynamical time of the galaxy. Figure 1.9 represents this hypothesis visually. The top half of the figure denotes the fast processes, initial protogalactic collapse and galaxy-galaxy mergers. This is what we think of in the hierarchical collapse theory of the Universe's formation. These processes act quickly and can act to change the galaxy's structure and properties over fast timescales. While in the bottom half are secular processes. These processes can also act to transform the galaxy's properties and structure but much more slowly, much longer than a crossing time (the time taken for a star to complete one orbit). These fast and secular processes can be further split into those which occur internally (LHS of the figure), within the halo of the galaxy, and those which are caused by external perturbers (RHS of the figure). In the center of the figure

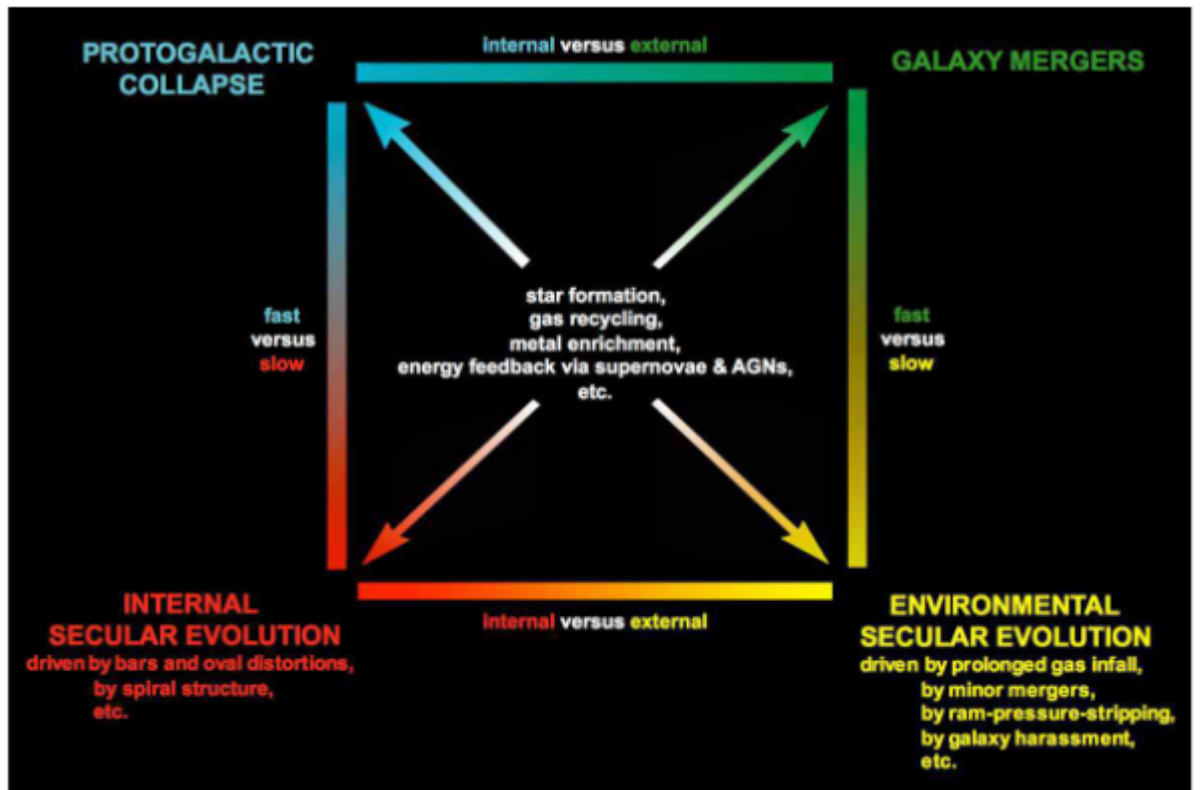


Figure 1.9: Diagrammatic representation of the different processes involved in galaxy evolution (Kormendy, 2013). The top half represents fast processes happening on dynamical timescales, while the bottom half shows slow processes which happen over many galaxy rotations. The diagram is also divided horizontally with internal processes shown on the left and environmentally driven processes on the right. In the centre are processes which are present at all stages of galaxy evolution. As the Universe continues to expand secular processes are thought to become the dominate mode for further galaxy evolution.

are processes which are present at all stages of galaxy evolution. As mergers become less common the secular processes will become the more dominant mode of galaxy evolution.

Thin discs, both stellar and gaseous, are prone to instabilities. At scales smaller than the Jeans length, L_J , a disc can be supported against instability by the random motion of its stars (velocity dispersion). At large scales, L_{rot} , the rotation of the disc supports it from collapse. Therefore, the disc is prone to instabilities at all radii satisfying $L_J < L < L_{rot}$. This has been extensively investigated by Toomre (1964) who developed the Toomre Q parameter for a stable stellar disc:

$$Q_s = \frac{\sigma_s \kappa}{3.36 G \Sigma_s} > 1 \quad (1.1)$$

where σ_s is the one-dimensional velocity dispersion of the stars in the radial direction, Σ_s is the stellar surface density of the disc and κ is the epicyclic frequency. Similarly, the stability of a gaseous disc is given by:

$$Q_g = \frac{\sigma_g \kappa}{\pi G \Sigma_g} > 1 \quad (1.2)$$

where σ_g is the one-dimensional velocity dispersion of the gas in the radial direction and Σ_g is the surface density of the gas disc.

However, it is rare that purely gaseous or stellar discs exist and predominantly the two appear in concert. This increases the likelihood of instability as where a gaseous disc might have been stable on its own, gravitational effects from the stellar disc can induce an instability in the gas disc and visa versa. This results in the combined Toomre parameter (Romeo and Wiegert, 2011) for a gas disc embedded in a stellar disc:

$$Q_{tot}^{-1} = \begin{cases} W Q_g^{-1} + Q_s^{-1} & \text{if } (Q_g > Q_s) \\ Q_g^{-1} + W Q_s^{-1} & \text{if } (Q_g < Q_s) \end{cases} \quad (1.3)$$

where

$$W = \frac{2\sigma_g\sigma_s}{\sigma_g^2 + \sigma_s^2}. \quad (1.4)$$

However, even if $Q > 1$ everywhere in the disc they can still be prone to instability.

The majority of disc galaxies contain bars (Eskridge et al., 2000; Erwin, 2005) making the bar instability (which I shall describe in more detail in Section 1.4.1) one of the most common non-axisymmetric instabilities. Other instabilities can result in other easily identifiable features of spiral galaxies such as the spiral arms themselves and oval distortions. These non-axisymmetric structures act to redistribute the angular momentum and material of the disc. In particular, they can act to move large amounts of gas into galaxy centres which can result in the formation of pseudo-bulges and cause discs to spread through movement of material to the outer regions.

While I shall go into more depth on how bars can drive the evolution of the disc galaxies which host them, I shall briefly introduce pseudo-bulges here. A pseudo-bulge, while having a superficial similarity to merger-built classical bulges, actually has properties more in line with that of the disc. Pseudo-bulges have flatter shapes than classical bulges, are more dominated by rotation than random motions, have nearly exponential surface brightness profiles, bluer colours, and may contain nuclear bars or even spiral structure within them (Kormendy, 1993; Kormendy et al., 2006; Andredakis and Sanders, 1994; Carollo et al., 1997; Gadotti and Dos Anjos, 2001; Erwin and Sparke, 2002; Fathi and Peletier, 2003; Fisher, 2006; Fisher and Drory, 2008a; Drory and Fisher, 2007).

As bars are thought to strongly drive gas towards the central regions resulting in the formation of a pseudo-bulge, the presence of a bar is a clear indicator that secular processes are occurring within a galaxy. Additionally, bars, and indeed discs, can be easily disrupted and destroyed by merging events (Pfenniger and Friedli, 1991; Athanassoula, 1996a, 1999; Berentzen et al., 2003; Sheth et al., 2012) so the presence of a bar is also indicative of a lack of major mergers. Thus, identifying when bars begin to form could allow us to determine when secular processes begin to have a more dominant role in the evolution of disc galaxies, which is key for understanding the cosmological history of the universe.

1.2 Structure and dynamics of barred galaxies

Bars are common and easily identified features of spiral galaxies. Optically, bars are found in over half of all local disc galaxies (Marinova and Jogee, 2007; Reese et al., 2007; Barazza et al., 2008). When also considering near-infrared imaging this fraction rises to approximately 70% (Knapen et al., 2000; Eskridge et al., 2000; Menéndez-Delmestre et al., 2007). There is substantial evidence that this fraction remains constant out to a redshift of $z \approx 1$ (Jogee et al., 2004; Elmegreen et al., 2004; Barazza et al., 2008). However, there is also significant evidence to the contrary with bar fraction rapidly declining with increasing redshift (Sheth et al., 2008; Melvin et al., 2014; Simmons et al., 2014).

There is also evidence that the bar fraction correlates with Hubble type, however the precise nature of this is widely debated. In some cases bar fraction is found to increase in early-type spirals which are massive, red, gas-poor, and bulge dominated (Sheth et al., 2008; Aguerri et al., 2009; Laurikainen et al., 2009; Cheung et al., 2013; Consolandi, 2016). There is also evidence that the opposite is true and bars are more likely to be found in late-type spirals which are less massive, blue, gas-rich, and disc dominated (Barazza et al., 2008, 2009; Aguerri et al., 2009; Buta et al., 2015; Erwin, 2018). Alternatively, it is also possible that both of these cases are true and indeed there is evidence of a bimodal peak of bar fraction in correlation with Hubble sequence with a peak in both early- and late-type spirals (Knapen, 1999; Nair and Abraham, 2010; Masters et al., 2011; Oh et al., 2012; Díaz-García et al., 2016).

1.2.1 Major properties of bars

Bars can be identified and categorised by their visual properties. They vary significantly in their length, how prominent the bar appears, and in the shape of the central region. In this section I will review the three main visual identifiers for bars: length, strength, and the presences of a boxy/peanut structure.

Bar length

One of the most easily identifiable characteristics of bars is their size or length. Although there are numerous methods with which bar lengths can be recovered, observed bars are, on-average, expected to have a typical radius of 2-5 kpc (Marinova and Jogee, 2007; Barazza et al., 2008; Durbala et al., 2008; Aguerri et al., 2009; Gadotti, 2011).

While in the Eagle simulation (Algorry et al., 2017) the range of bar lengths agrees well with the observational results of Gadotti (2011), bars in simulations are typically found to be longer (Berentzen et al., 1998; Athanassoula and Misiriotis, 2002; Valenzuela and Klypin, 2003; Holley-Bockelmann et al., 2005; Erwin, 2005). The deficit of short bars could be a result of having either too kinematically hot central regions or having large halos in comparison to the size of the disc (Valenzuela and Klypin, 2003). Additionally, bars in simulations can grow large quickly, within 1-2 Gyr of the bars formation (Martinez-Valpuesta et al., 2006), which may not actually be the case (I will touch on this further in Section 1.4.2). If the majority of bars lie within the 2-5 kpc range then at high redshifts observations may be biased towards only the largest bars, since resolving small bars at high redshifts becomes increasingly difficult. This may cause the observed bar fraction at higher redshift to be lower than the true bar fraction (Erwin, 2005).

It has been shown that bar lengths correlate with the galaxy type, with the bars in early-type spirals tending to be longer than their late-type counterparts (Erwin, 2005). However, this is not a smooth linear change and the smallest bars are usually found in galaxies of the morphological type Sbc (Martin, 1995; Laurikainen et al., 2007; Díaz-García et al., 2016; Font et al., 2017b). With morphology being linked with colour, there should also be a correlation between bar length and galaxy colour. Redder colours are a common feature of early-type discs so one would expect that redder galaxies should host longer bars, while late-type discs tend to be more blue as they are currently star forming so should host short bars. Indeed, Hoyle et al. (2011) find that longer bars are more commonly found in the redder galaxies in agreement with the previous studies which identified the link between bar lengths and morphology.

Bar length can also be linked with the prominence of the galaxy bulge. As the size of the bulge increases the bar length also increases (Hoyle et al., 2011). This is not an unexpected effect since bars are associated with the growth of pseudobulges through secular evolution. Indeed the link between increased bar length and increased bulge prominence is expected from simulations (Athanasoula and Martinet, 1980; Athanasoula, 2003a). This suggests that as the bar builds the bulge they increase with length through the exchange in angular momentum between the bars and the bulge they build. By making comparisons between observations and simulations Cheung et al. (2013) found a clear correlation between bars and pseudobulges in agreement with bar-driven secular evolution.

Bar strength

Generally bar strength is a parameter that measures the non-axisymmetric torques of the bar in galaxy discs (Laurikainen and Salo, 2002). Intuitively, the differences between a weak and strong bar are clear, with stronger bars appearing longer, encompassing a larger proportion of the galaxies mass and more visually distinct features, with their minor axis much smaller than their major. Weaker bars are shorter with the bar itself less easy to visually identify, and sometimes appearing more oval in shape. While there is no unique definition of bar strengths, there are various methods with which they can be measured.

Bar strengths can be recovered by measuring bar ellipticity (Martinet and Friedli, 1997; Whyte et al., 2002; Marinova and Jogee, 2007; Aguerri et al., 2009), comparisons of the surface brightness profiles of the major and minor bar axes (Kim et al., 2016), measuring bar torques (Combes and Sanders, 1981; Buta and Block, 2001; Laurikainen et al., 2007; Salo et al., 2010), and Fourier decomposition of the galaxy light (Aguerri et al., 2000; Athanasoula and Misiriotis, 2002; Laurikainen et al., 2005; Garcia-Gómez et al., 2017). Similarly to bar length, bar strength is also correlated with Hubble type, although the exact nature of the relationship between the strength of the bar and the galaxy morphology depends on the method for recovering bar strengths. If

bar strengths are calculated via bar torques then there is a clear increase of bar strength from early-type to late-type discs (Buta et al., 2004; Laurikainen et al., 2007). It is possible that there is a similar correlation when bar strength is measured through ellipticity, although if there is it is significantly weaker (Laurikainen et al., 2007). In fact Marinova and Jogee (2007) find that the ellipticity of the bar is independent of Hubble type.

The increase in bar strength with Hubble type seems in tension to the decrease in bar length with increasing Hubble type. Longer bars are more commonly found in early-type galaxies and indeed when using Fourier decomposition, which is closely associated with bar length, to measure strength the correlation between Hubble type is reversed (Laurikainen et al., 2007).

The disparity between the nature of the correlation of Hubble type and bar strength is due to the dilution of tangential forces caused by the bar in the more massive bulges of early-type discs (Buta et al., 2004). Therefore, while the bars in early-type discs are commonly longer, they have weaker torques resulting in weaker strengths when the bar torque method is implemented in calculating the strength of the bar.

Peanuts and boxy bulges

Nearly half of all edge-on disc galaxies display central components which are boxy-, peanut-, or X-shaped structures (these are commonly referred to as boxy/peanut or b/p bulges) (Lütticke et al., 2000; Yoshino and Yamauchi, 2015; Erwin and Debattista, 2017). While their nomenclature refers to them as bulges, and indeed they fall under a sub-classification of pseudobulges, numerical simulations have demonstrated that they are actually a feature of an edge-on bar (Combes et al., 1990; Martinez-Valpuesta et al., 2006).

While very few face-on barred galaxies show boxy, peanut or X-shaped structures, they do play host to barlenses. A barlens is a lens-like structure embedded in the bar which covers approximately half the length of the narrow bar (Laurikainen et al., 2011). Orientated along the major axis of the bar, their shapes can vary from oval to more

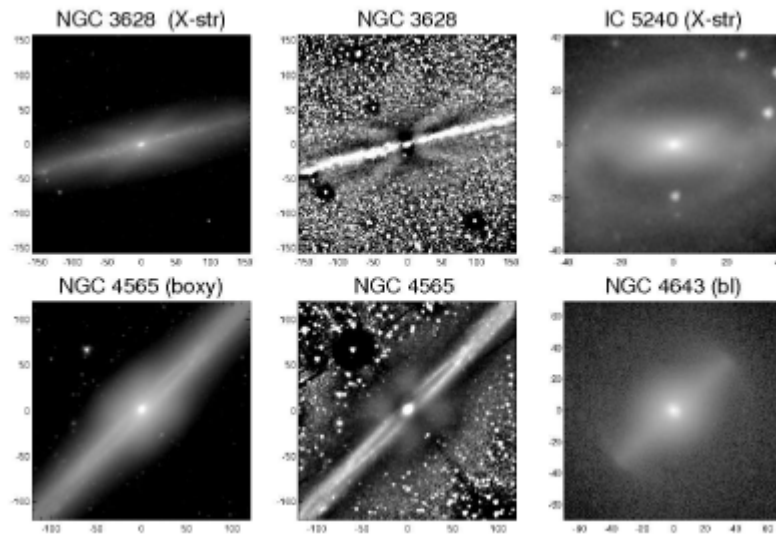


Figure 1.10: Examples of boxy/peanut and barlens galaxies (Laurikainen et al., 2014a). The top row shows two galaxies with the characteristic X-shaped structure associated with the boxy/peanut bulges. The bottom row shows galaxies with a more boxy, or barlens-like shape. The galaxies on the left side are viewed nearly edge-on, while those on the right are closer to face-on views. The centre of each row is an unsharp mark of the left side galaxies clearly showing the X-shaped structure.

circular (Laurikainen et al., 2013). Due to their roundness barlenses can be erroneously associated with classical bulges, however the similarity between the optical colours of barlenses and bars suggest they are actually a feature of the latter (see Figure 1.10) (Herrera-Endoqui et al., 2015).

If barlenses and boxy/peanuts are the same phenomena, as has been suggested (Laurikainen et al., 2007, 2014b; Athanassoula et al., 2015), then they should share observed properties. By looking at galaxy orientation in comparison to barlens morphology, Laurikainen et al. (2014b) (see also Laurikainen and Salo (2017); Salo and Laurikainen (2017)) found that the distribution of minor-to-major axis ratios (b/a) for galaxies with barlenses and boxy/peanut shapes is flat when both are considered together. This strongly implies that they are the same feature just seen at different inclinations. Additionally, boxy/peanuts show similar surface brightness profiles (Athanassoula et al., 2015), colours (Herrera-Endoqui et al., 2015) and kinematics (Debattista et al., 2005). Numerical simulations have found that the barlens is, indeed, a face-on view of the boxy/peanut (Athanassoula et al., 2015).

1.2.2 The orbital structure of the bar

The movement of stars is determined by the gravitational potential in which they are situated. Unlike systems with a central point mass like the solar system, in discs the mass is distributed radially. Gas is dissipational and can remove energy from a system, however angular momentum must remain conserved. Circular orbits have the minimum amount of energy for a given amount of angular momentum. Any stars born from this gas thus move on nearly circular orbits. In the inertial frame of the rotating disc stellar orbits can generally be defined as unclosed rosettes (Binney and Tremaine, 1987; Sellwood and Wilkinson, 1993).

Small radial deviations from the circular motion of the stars are called epicycles. The epicyclic motion for disc stars can effectively be broken down into two parts: the orbital motion of a guiding centre, and the rapid oscillations about the guiding centre. The frequency, κ , of these oscillations is given by the epicyclic approximation:

$$\kappa^2 = \frac{2v}{r} \left(\frac{v}{r} + \frac{dv}{dr} \right) \quad (1.5)$$

where v is circular rotation velocity as function of radius r , and the angular frequency of stars about the centre is $\Omega = v/r$ (Binney and Tremaine, 1987).

When non-asymmetric features are present in the galaxy they interact with the material in the disc distorting orbits. In particular, some orbits may experience resonances caused by coupling between the motion of the stellar material in the orbits and the motion of the non-axisymmetric structure.

Resonances

Bars interact with the galactic material resulting in distortion of the stellar orbits. Since bars also rotate within the disc they cause resonances to form. Resonances, in barred galaxies, form where the motion of the stars is coupled with the rotation of the bar (the particular rate of the bars rotation is referred to as its pattern speed Ω_p).

In the frame of the bar (where the bar is considered stationary) an orbit can be considered as resonant if it satisfies the condition:

$$l\kappa + m(\Omega - \Omega_p) = 0 \quad (1.6)$$

where $(l:m)$ are a pair of integers describing the resonance in the disc. Stars which are in resonant orbits will periodically return to the same position with respect to the bar, and they are closed orbits (Lichtenberg and Lieberman, 1983).

There are three important resonances in barred galaxies: corotation (0:1), the inner Lindblad resonance (-1:2), and the outer Lindblad resonance (1:2). A schematic representation of these resonances is shown in Figure 1.11. At the corotation radius gravitational and centrifugal forces cancel out in the rest frame of the bar so, as long as the pattern speed of the bar remains fixed, the positions of the stars do not change with respect to the bar. This means that if the pattern speed of the bar can be recovered then the corotation radius (R_{CR}) can be determined with:

$$R_{CR} = V_c / \Omega_p \quad (1.7)$$

where V_c is the circular velocity of the disc. Using this and the bar length (a_b) bars can be described by a distance independent parameter.

$$R = R_{CR} / a_b \quad (1.8)$$

Any self-consistent bar requires that $R > 1.0$, as such bars cannot extend beyond the corotation radius (Contopoulos, 1980; Athanassoula and Martinet, 1980). This parameter can also be used to categorise bars into fast ($1.0 < R < 1.4$) and slow ($R > 1.4$) rotators. The vast majority of bars lie in the fast regime (Elmegreen et al., 1996; Rautiainen et al., 2008; Portail et al., 2017) while only a few have been found to lie in the slow (Bureau et al., 1999; Rautiainen et al., 2008).

In addition to the corotation resonance, barred galaxies may also contain inner and outer Lindblad resonances. At these resonances the closed orbits have exactly two

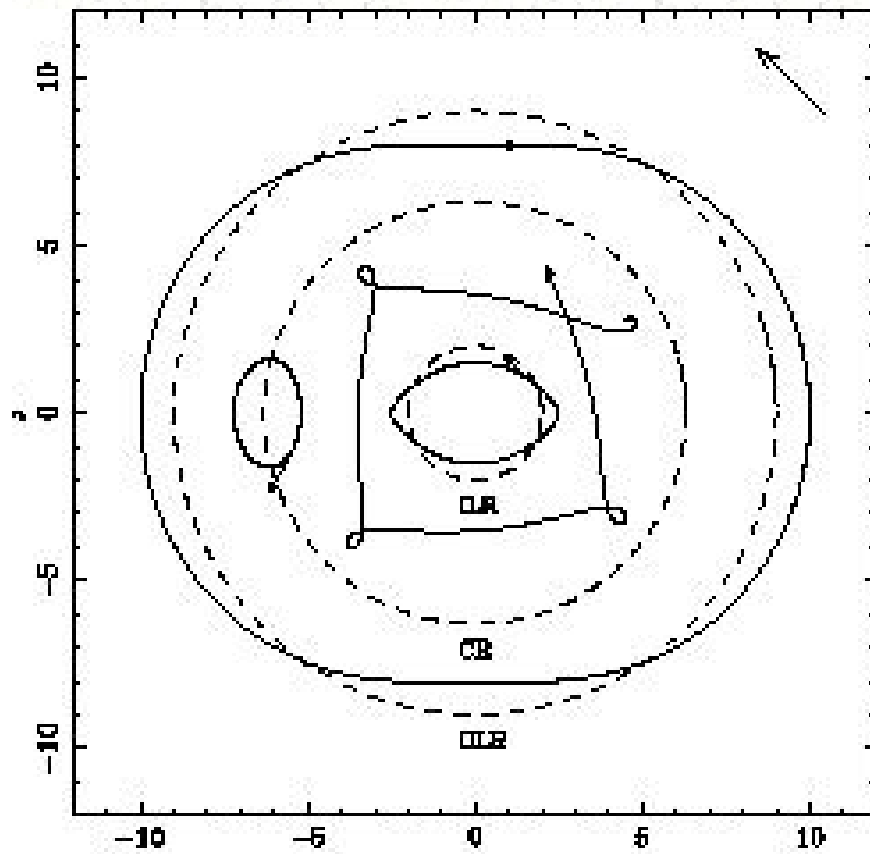


Figure 1.11: A schematic showing the 3 major resonances (dashed lines) seen in barred galaxies, the shape of their periodic orbits (solid lines) and an unclosed rosette orbit all in the rest-frame of the bar (Combes, 2001). At the inner Lindblad resonance (ILR) the orbit is elongated, oscillating twice in the radial direction, here the particle moves faster than the bar. At corotation (CR) there is only the epicyclic motion and the guiding centre of the orbit remains stationary in the bars rest-frame. At the outer Lindblad (OLR) resonance the orbit is again elongated with two radial oscillations, here a particle moves slower than the bar so appears to move backwards.

radial oscillations during one angular revolution resulting in a orbit with an ellipsoidal shape. At the inner Lindblad resonance, which lies inside the corotation radius, the star rotates faster than the bar. Therefore a particle will be at the top of its epicycle when the end of the bar swings by and will be at the top of its epicycle again when the opposite end of the bar swings by. Particles in the outer Lindblad resonance, which lies outside corotation, rotate slower than the bar. This means that a particle that will be at the top of its epicycle when the end of the bar swings by will be at the top of its epicycle again after two full rotations of the bar.

In some cases the inner and outer Lindblad resonances can be traced by rings. Interstellar gas collects at the resonances due to torque produced by the bar pattern. At these locations where the gas is dense it may result in star formation causing bluer star forming rings to form that trace the shape of the resonances (Athanasoula et al., 1982; Sellwood and Wilkinson, 1993; Rautiainen and Salo, 2000; Buta, 2017). As a result of this, many of these resonant rings are aligned with the bar (de Vaucouleurs, 1964; Schommer and Sullivan, 1976). In cases where there is not an alignment it is possible these resonances are the result of other physical mechanisms such as the pattern speed of the spiral arms which is decoupled from the bar (Comerón et al., 2014).

Important orbital families

As touched on in the previous sections, the presence of a bar disrupts the orbital structure of the disc. As such, there are several important orbital families associated with bars. These orbits are mostly periodic, meaning that they close after one or more revolutions of the bar and that the star will forever trace the same path (assuming there are no changes to the galaxy's structure).

The periodic orbits are the building blocks of a galaxy's structure, describing the shape of the stellar density distribution. Non-periodic orbits can become trapped, oscillating about one periodic with a similar shape forming an orbital family. Additionally, there are also chaotic orbits which can change in unpredictable ways; a small perturbation could result in a significant change in the orbit. There are numerous periodic orbits

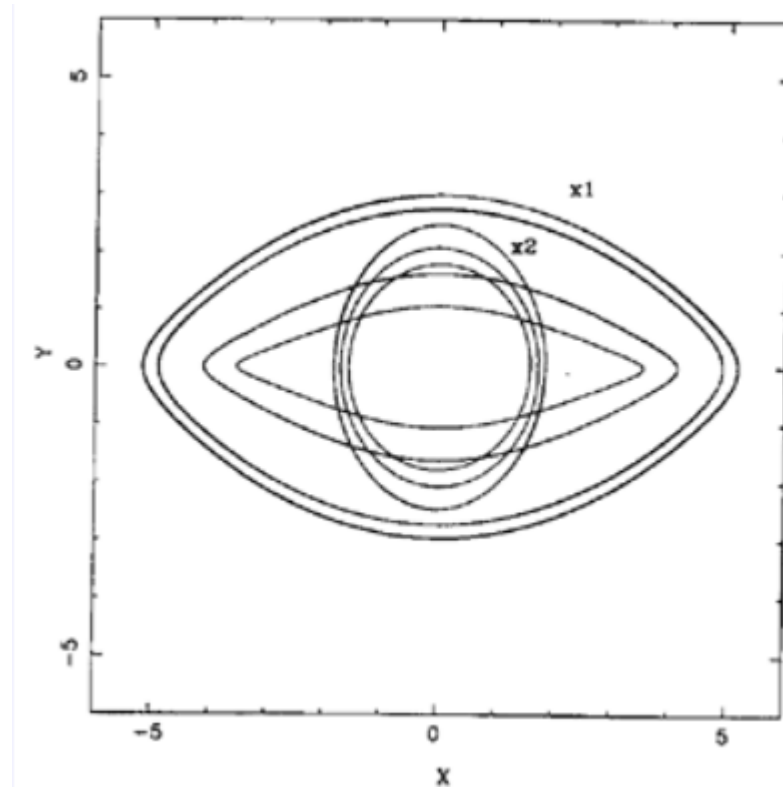


Figure 1.12: A schematic showing two of the most important families of periodic orbits in the bar (Contopoulos and Papayannopoulos, 1980). In this co-ordinate system the bar is parallel to the x-axis. The x1 family is extended parallel to the bar, while the x2 family is extended perpendicular to the bar.

contained within a galaxy but here I will only touch on those most important to the bar; the x1, x2, x3, and the retrograde x4 orbital families. The x1 and x2 orbital families are illustrated in Figure 1.12.

The x1-family are one of the most important orbits with regards to the bar and are generally considered to be the backbone of the bar. The x1 orbits are elongated along the major axis of the bar and can trap other orbits alongside them. These orbits are stable within corotation, becoming unstable outside it (Contopoulos and Papayannopoulos, 1980; Athanassoula et al., 1983; Contopoulos and Grosbol, 1989). As such, the bar does not exist beyond the corotation radius.

Other periodic orbits which are considered important for bar dynamics are the x2-family and x3-family. These orbits are perpendicular to the bar, acting to weaken it, and lie within the inner Lindblad resonance. The x3 orbits are more extended than the

x2 orbits but are always unstable.

The final important periodic orbit for the bar is the x4 orbit. This orbit is retrograde, meaning it appears to move backwards with respect to the bar's frame of reference. At small radii it is elongated perpendicular to the bar but becomes rounder with increasing radius (Athanasoula et al., 1983). These orbits have been associated with the formation of the boxy/peanut structure due to their prominence in the vertical direction (Athanasoula, 1990).

While the stars on these orbits are collisionless, the gas is not. Where these orbits intersect the gas can form shocks causing it to fall into the central regions to prevent further destabilisation. This prompts an exchange of angular momentum which causes the stellar orbits to elongate and the bar to grow. This process aids the formation of structures commonly associated with barred galaxies such as inner rings and pseudobulges (Kormendy and Kennicutt, 2004).

1.3 Effects of bars on galaxy evolution

Barred galaxies evolve through secular processes which transport angular momentum from the inner to the outer parts of a galaxy. The efficiency at which bars are able to redistribute angular momentum means that they are likely to play a key role in the evolution of disc galaxies via a number of processes. In this section I will touch on a few of the most important: (1) the formation of internal substructures such as pseudobulges and inner rings; (2) changing the rate of star formation; (3) the fueling of active galactic nuclei (AGN); and (4) redistribution of the stellar and gaseous components.

1.3.1 Exchange of angular momentum

Non-axisymmetric features in disc galaxies facilitate the transfer of angular momentum. Bars dynamically excite the galaxies in which they reside and are a key mechanism which allows for the transfer of angular momentum between the inner and outer

regions of the disc (Athanasoula, 2003b).

There are several different processes through which angular momentum can be transferred which are associated with the bar. Bars experience dynamical friction against the dark matter halo, transferring both energy and momentum, causing the bar to both slow and grow. As bars grow they can trap material in the disc onto elongated orbits, and the orbits of material in the bar may also become more elongated as a result (Athanasoula, 2003b). This requires angular momentum to be transferred to other parts of the galaxy to conserve the angular momentum of the disc.

As angular momentum is transferred, the bar slows and lengthens which causes an increase in the radii at which the corotation and Lindblad resonances lie (Chiba et al., 2021). This can be visualised like the rings of a growing tree with those orbits trapped at the core of the resonance being the first with newly trapped stars located at distances sequentially further from the resonance core (Chiba et al., 2021). Chiba and Schönrich (2021) used the sequential trapping of orbits in a tree ring structure to estimate that the corotation radius of the Milky Way has moved by more than 1.6 kpc since the formation of the Galactic bar.

1.3.2 Formation of pseudo-bulges

As I described in Section 1.2, the presence of the bar both signifies and drives secular evolution. The material that bars drive to the central regions acts to form a pseudo-bulge. Pseudo-bulges differ from classical bulges in several ways. Firstly, the surface brightness profile of pseudo-bulges is near exponential with the decline in light intensity (I) described by the Sérsic (1963) profile $I \propto r^{1/n}$ where $n < 2$ (Courteau et al., 1996; Carollo, 1999; Seigar et al., 2002; Fisher and Drory, 2008b); for classical bulges $n > 2$ (Fisher and Drory, 2008b). Additionally, pseudo-bulges show ongoing star formation and often have young populations of stars (Peletier et al., 2007), while classical bulges are considered to be red and dead generally having formed early in a galaxy's history. Indeed, specific star formation rates (sSFR) in the centres of barred galaxies are consistent with the formation of pseudo-bulges (Fisher et al., 2009),

making it plausible that these structures were formed through secular processes (Kormendy, 1979; Kormendy and Kennicutt, 2004), whereas classical bulges are thought to be built by mergers (Hopkins et al., 2012a; Martig et al., 2012). Finally, pseudo-bulges are more rotationally dominated (Kormendy, 1993; Falc3n-Barroso et al., 2006; Kormendy, 2008) with lower velocity dispersion than a classical bulge. This makes pseudo-bulges more similar to discs.

Pseudo-bulges often show internal structure when observed at high resolutions. Observations of the inner regions of pseudo-bulges show the existence of nuclear bars (Shaw et al., 1995; Erwin and Sparke, 2002; Erwin, 2004, 2011; Bittner et al., 2021), spiral arms (Courteau et al., 1996; Erwin and Sparke, 2002; Kim, 2018), nuclear rings (Erwin and Sparke, 2002; Li et al., 2015; Kim, 2018), and intense regions of star formation (Benedict et al., 2002; Knapen et al., 2006; Lin et al., 2017; Kim et al., 2020; Lin et al., 2020). Large-scale bars have been shown to contribute to the growth of pseudobulges in galaxies with gas (Cheung et al., 2013). It is also possible for both a pseudo-bulge and a classical bulge to exist in concert (M3endez-Abreu et al., 2014; Erwin et al., 2015), pointing towards a formation scenario for bulges that can be both secular and merger driven.

1.3.3 Enhancing central star formation

When a bar is present the gas inside the corotation radius tends to settle on the x_1 -family of periodic orbits which are aligned parallel to the major axis of the bar (Contopoulos and Papayannopoulos, 1980; Binney et al., 1991; Morris and Serabyn, 1996), while gas outside of corotation remains confined to the disc (Sanders and Huntley, 1976; Athanassoula, 1992; Berentzen et al., 1998; Kim and Seo, 2012; Cole et al., 2014). Because gas is collisional (unlike stars), the gas settled on the x_1 orbits shocks, losing angular momentum, falling into the central regions, and settling on x_2 orbits. The shocking process repeats until the gas settles near the inner Lindblad resonance (Simkin et al., 1980; Maciejewski, 2000). Here the gas may become trapped, unless other internal structures are present to funnel the gas further into the centre (Athanas-

soula, 1992; Quillen et al., 1995; Erwin and Sparke, 2002; Kim, 2018; Bittner et al., 2021). The build up of cold gas in the galaxy centre (Sakamoto et al., 1999; Sheth et al., 2005) can trigger intense episodes of star formation (Ellison et al., 2011; Catalán-Torrecilla et al., 2017). Indeed, many numerical simulations demonstrate this is an efficient way to supply gas to galaxy centres enhancing the efficiency of star formation there (Athanassoula, 1994; Sellwood and Wilkinson, 1993; Combes, 2001; Kim et al., 2011; Kim and Seo, 2012; Shin et al., 2017).

Observationally, barred galaxies are often found to have higher central gas concentrations and central star formation rates than their mass matched unbarred counterparts (Sakamoto et al., 1999; Knapen et al., 2002; Sheth et al., 2005; Ellison et al., 2011; Oh et al., 2012; Wang et al., 2012; Consolandi et al., 2017). Barred galaxies also tend to have younger and more metal-rich central regions than non-barred galaxies (Coelho and Gadotti, 2011; Ellison et al., 2011; Pérez and Sánchez-Blázquez, 2011). Observations of HI gas tends to show holes in the disc where the gas has been swept up by the bar and funneled into the central regions (Newnham et al., 2020). The effects described above tend to be stronger in galaxies with stronger bars (Ho et al., 1997; Gavazzi et al., 2015; Kim et al., 2017) which are more efficient at funneling gas into the galaxy centre (Athanassoula, 1994; Sheth et al., 2005; Kim and Seo, 2012).

1.3.4 Fueling AGN

An active galactic nucleus (AGN) is an energetic phenomenon powered by the accretion of gas onto a supermassive black hole (SMBH) located in the nucleus of a massive galaxy (Rees, 1984). Due to the efficiency at which bars funnel gas into the central regions of a galaxy, they are often associated with the fueling of AGN when they are present (Combes, 2003). While there is substantial evidence that this is the case (Hao et al., 2009; Oh et al., 2012; Alonso et al., 2013; Galloway et al., 2015), there is also a compelling amount of evidence in contradiction to this outlook (Lee et al., 2012; Cheung et al., 2015; Cisternas et al., 2015; Goulding et al., 2017).

These controversial results come down to a debate over how efficient bars are at trans-

porting material directly into the regions close to the SMBH (Knapen, 2005). One explanation is that smaller scale phenomena are needed to transport material from the central few pc down to the black hole. It has been proposed that the presence of small non-axisymmetric substructures, such as nuclear bars (Shlosman et al., 1989) or spirals (Martini et al., 2003), can bridge the gap between the gas transported by the bar and the accretion disc of the SMBH at the galaxy centre. Observational studies have found nuclear bars in galaxies with AGNs (Martini et al., 2001). However, they also revealed dust spirals which connect the bar to the nuclear region. While this is a promising mechanism for the transport of material down to the black hole, these dust spirals are present in both active and inactive galaxies (Martini et al., 2003). It may be the case that these different structures all act in concert and represent a hierarchy of mechanisms over different spatial scales which act to transport material down to the SMBH (Haan et al., 2009).

1.3.5 Formation of rings

The presence of a bar in a galaxy will often coincide with the presence of rings. There are three main types of rings (Buta et al., 2015) which are named based on their location in the galaxy: nuclear rings which are found in the central regions of a galaxy; inner rings which lie just outside the radius of the bar; and outer rings which lie further out in the disc.

Most rings in galaxies are thought to be formed from gas which collects near resonances in the disc. In numerical simulations, nuclear rings are linked to the presence of the inner Lindblad resonance, with inner rings commonly associated with the ultra-harmonic 4:1 resonance and outer rings associated with the outer Lindblad resonance (Athanasoula et al., 1982; Sellwood and Wilkinson, 1993; Rautiainen and Salo, 2000; Buta, 2017). However, collection of gas at resonances is not the only mechanism through which rings are thought to form.

The manifold theory is one alternative model that results in the formation of inner and outer rings (Romero-Gómez et al., 2006; Voglis et al., 2006; Romero-Gómez et al.,

2007; Tsoutsis et al., 2008; Athanassoula et al., 2009). In this theory the rings are formed as a result of gas and stars on chaotic orbits which are trapped in tubes that connect the Lagrangian points at the ends of the bar (Romero-Gómez et al., 2006, 2007; Athanassoula et al., 2009, 2010; Athanassoula, 2012), whereas nuclear rings may be formed due to the shocking of gas encountering the centrifugal barrier in the inner region of the galaxy (Kim and Seo, 2012).

If rings are the result of either manifolds or resonances then they should be aligned with the bar, and while some rings are so aligned, Comerón et al. (2014) found that nearly 50% of rings in late-type spirals have random orientations. This may be a result of measurement errors, since in later galaxy types rings are more difficult to define, or could be due to spiral modes rotating at a pattern speed different than that of the bar (Rautiainen and Salo, 2000).

The fraction of rings in galaxies increases with increasing stellar mass (Díaz-García et al., 2019), with inner rings being more common than outer rings (Buta and Combes, 1996; Comerón et al., 2014). They are found across all morphological types, however they are observed to be larger, relative to disc size, in early-type spirals with inner ring size increasing with increasing Hubble type (Díaz-García et al., 2019). While the outer ring size is not correlated with bar strength, the size of inner rings increases in radial extent and ellipticity with increasing bar strength (Díaz-García et al., 2019), however the link between strength and ellipticity is weaker than expected from numerical simulations (Sellwood and Wilkinson, 1993). This gives some support to the hypothesis that rings are formed as a result of resonances since as the bar grows in length and strength its pattern speed decreases which moves the resonances further out into the disc.

While rings are predominantly found in barred galaxies, about a third of galaxies which have rings have no bar (Díaz-García et al., 2019). A bar is generally considered important for the formation of rings (Schwarz, 1981; Sellwood and Wilkinson, 1993; Buta and Combes, 1996), although it may also be possible to form rings without the presence of a bar (Sil'chenko and Moiseev, 2006). It has been suggested that rings could outlive the bar, remaining after the bar has been dissolved (Athanassoula, 1996b). Al-

ternatively a bar might still exist but only be observable in the infra-red (Casasola et al., 2008).

1.3.6 **Suppression of star formation**

While there is evidence that bars can enhance the central star formation in galaxies at the nuclear scale, not all barred galaxies have high central gas concentrations or star formation rates (SFRs) when viewed at a larger scale encompassing the bar (Martinet and Friedli, 1997; Sheth et al., 2005; Cullen et al., 2007; Fisher et al., 2013; Abdurro'uf and Akiyama, 2017). This suppression of star formation in the central regions of barred galaxies was first noticed by Tubbs (1982). The very ability of bars to efficiently transport gas into the centre of a galaxy can result in the removal of gas from within the corotation radius of the bar: while gas inside corotation is funneled to the centre, gas outside corotation is driven outwards into the disc (Kalnajs, 1978; Bournaud and Combes, 2002; Combes, 2008; Spinoso et al., 2017) preventing the lost gas inside the corotation radius from being replaced. Alternatively, gas may be present but its star formation efficiency may be low. Strong bars which produce strong shocks combined with gas shearing could stabilise the gas against efficient star formation (Reynaud and Downes, 1998). Gas might also be stabilised as a result of the gas velocities induced by bars, even in regions of high density gas (Verley et al., 2007).

Observations of the bar region in narrow-band $H\alpha$ can reveal the complete suppression of star formation within the radial range swept out by the bar called the star formation desert (SFD) (James et al., 2009; James and Percival, 2015, 2018). Observations in HI reveal holes in the gas disc which the bar sweeps out confirming that it is likely that gas is removed from the region by the bar (Laine and Gottesman, 1998; Newnham et al., 2020). The appearance of a SFD often coincides with a slight increase in star formation in both the centre and the ends of the bar, and in the inner ring which surrounds the bar. Further supporting evidence of the suppression of star formation within the SFD comes from the deficit of core-collapse supernova observed in the radial range swept out by the bar (Hakobyan et al., 2016). Star formation deserts are also found in

simulations which confirm that strong bars are capable of depleting the gas in the bar region, effectively quenching star formation on approximately Gyr timescales (Fanali et al., 2015; Khoperskov et al., 2018; Spinoso et al., 2017) and leaving the region ‘red and dead’. However, whether bars can act to transform a galaxy from star forming in the ‘blue cloud’ to quenched on the ‘red sequence’, or if their suppression effects only effect the SFD, is still up for debate.

There is substantial evidence linking bars to galaxy quenching, however the exact nature of the process and its extent remains unclear. In comparisons with unbarred galaxies of the same mass, galaxies with bars have lower atomic gas fractions and star formation rates (Masters et al., 2012; Krishnarao et al., 2020). Bars are also more commonly found in optically redder galaxies than their unbarred counterparts (Masters et al., 2011; Vera et al., 2016; Kruk et al., 2018), with longer bars being more common in redder discs (Hoyle et al., 2011). The bar fraction is higher for galaxies of higher mass (Masters et al., 2012; Melvin et al., 2014; Gavazzi et al., 2015), with the bars in these galaxies also being stronger (Erwin, 2019). Bars are more numerous in galaxies with early-type morphology (Elmegreen and Elmegreen, 1985; Martin, 1995; Erwin, 2005; Menéndez-Delmestre et al., 2007; Lin et al., 2014; Díaz-García et al., 2016; Erwin, 2019) and galaxies in denser environments (Skibba et al., 2012). Evidence shows that the majority of the star formation in barred galaxies happens much earlier than their mass-matched unbarred counterparts (Fraser-McKelvie et al., 2020b) suggesting that barred galaxies are quenched earlier. The aforementioned evidence points towards a scenario in which bars quench the galaxy. However, simulations find that bars form more easily in gas-free discs (Athanasoula, 2013), such as those which have been quenched early. Disentangling these two scenarios, in which bars help quench a galaxy or form more easily because of quenching, is difficult because it requires knowledge of both the time of quenching and bar formation. There is currently a lack of methods with which we can observationally age date the bar and until more methods are made available the relationship between bars and quenching will remain unclear.

1.4 Bar formation and destruction

1.4.1 Bar formation through disc instabilities

Rotationally supported discs can become unstable when $Q < 1$ (this is the Toomre parameter as described in Section 1.3 Toomre (1964)). N-body simulations of isolated galaxies have shown that when a rotationally supported stellar disc becomes unstable a bar shaped structure is formed in response (Ostriker and Peebles, 1973; Toomre, 1977, 1981; Sellwood and Wilkinson, 1993; Binney and Tremaine, 1987). Toomre (1981) argued that the bar can be considered as a standing wave between corotation and the galaxy centre. The leading wave is reflected back at corotation, rotating it 180° into a trailing wave which amplifies the pattern through swing amplification, the superposition of a leading and trailing wave. This standing wave is a weak bar which then elongates and strengthens through the exchange of angular momentum between the inner and outer Lindblad resonances (Lynden-Bell and Kalnajs, 1972).

While the above is a good explanation for how bars might grow in isolated environments, bars are more frequently observed in dense environments such as clusters (Elmegreen et al., 1990). Interacting galaxies in dense environments can cause tidal distortions in the disc, these distortions cause non-axisymmetric instabilities that result in the formation of a bar (Noguchi, 1987). The resulting strengths of bars formed in this way are dependent on the mass ratios of the interacting galaxies and the mass ratios of the bulge and halo of the main disc (Noguchi, 1987). In comparison to bars formed in isolated environments, these bars tend to have slower pattern speeds and altered inner Lindblad resonance positions (Miwa and Noguchi, 1998).

Despite their generally destructive nature, even galaxy-galaxy mergers can result in the formation of a bar (Peirani et al., 2009; Lotz et al., 2010). When a minor merger occurs it is a relatively slow process in comparison to major mergers (Cavanagh and Bekki, 2020). As the minor galaxy spirals in, it causes tidal distortions in the disc which causes the bar to form (Peirani et al., 2009; Di Matteo et al., 2010). With each successive spiral, material is stripped from the minor galaxy until by the time it merges

with the disc it does not destructively warp or disturb it (Cavanagh and Bekki, 2020). The process is slightly different for major mergers which act on faster time scales. Most major mergers will destroy galaxy discs, however if the galaxies merge in very specific circumstances (related to their orientations) then a bar can survive (Cavanagh and Bekki, 2020).

The effect of gas on bar formation

The majority of the N-body simulations of bar formation discussed above do not include how the gaseous component of the disc responds to the bar. Gas is collisional so will form shocks where orbits intersect (Athanasoula, 1992). When included in simulations, the effects of gas on the formation of bars is varied. Athanasoula et al. (2013) found that bars in galaxies with a high gas fraction grow slowly, and Wozniak and Michel-Dansac (2009) reported that in some cases a high gas fraction may inhibit the formation of a bar completely. In contradiction, Robichaud et al. (2017) showed that bars can form earlier in discs with a high gas fractions if feedback from AGN is included. However, Berentzen et al. (2007) identified no link between bar formation time and galaxy gas fraction. In those simulations where a bar does form the inclusion of gas results in shorter and weaker bars (Berentzen et al., 1998; Athanasoula, 2003a; Berentzen et al., 2007; Athanasoula, 2013; Cheung et al., 2013).

The effect of the halo on bar formation

All galaxies are believed to reside inside large dark matter halos which make up the majority of their total mass. If the dark matter halo is massive, dynamically hot, and non-rotating it can act to stabilise the disc against perturbations and subsequent bar formation (Hohl, 1976; Efstathiou et al., 1982). A halo that rotates in the opposite direction to the disc can also act to suppress the formation of the bar (Saha and Naab, 2013). However, if the halo rotates in the same direction as the disc then it can act to encourage the formation of a bar (Saha and Naab, 2013).

The ability of a bar to grow is dependent on how efficiently angular momentum can be exchanged in a galaxy (Athanasoula, 2003a). In a static potential the dark matter halo is considered as rigid and so cannot contribute to the exchange of angular momentum with the bar. As a result the bar can only evolve by exchanging angular momentum with the outer Lindblad resonance in the disc removing angular momentum from the material in the bar and transporting it to the outer Lindblad resonance which allows the disc to spread. While the exchange of angular momentum in the disc is more efficient, the rate at which angular momentum is exchanged is also dependent on mass. As a result, bars develop slower in galaxies with rigid halos. However, if the galaxy is assumed to have a ‘live’ halo (made up of particles), then angular momentum can be absorbed at all resonances in the halo. While this is less efficient than absorption by the outer Lindblad resonance of the disc, the halo has significantly more mass allowing for bars to evolve quicker and, ultimately, stronger (Debattista and Sellwood, 1998; Athanasoula and Misiriotis, 2002; Saha et al., 2012).

Halo mass can also effect the rate of bar growth. If the mass of the halo dominates in the central regions it can delay the formation of the bar since it acts to dampen perturbations. However, if the disc mass dominates then the bar tends to form fast and earlier. In addition, the shape of the halos can also affect the formation time and evolution of the bar (Athanasoula, 2013). Triaxial halos cause bars to form faster but they grow more slowly and are weaker overall than bars which develop in galaxies with spherical halos.

Suppression of bar formation in ‘hot disks’

Simulations show that bar formation is delayed in dynamically hot discs (Athanasoula and Sellwood, 1986; Athanasoula, 2003a) due to the large amount of random motions preventing the bar instability from growing quickly. In some cases this may prevent bar formation from occurring at all (Sheth et al., 2012). These results are in agreement with the lack of bars observed in clump-cluster and chain galaxies seen at high redshifts as, while they do have rotation, they also have high amounts of dispersion in their discs.

Additionally, bars in simulations tend to form earlier in more massive discs compared to the more dispersion dominated low-mass discs.

1.4.2 Bar slow down and growth

The interaction between bars and the material of the disc through the exchange of angular momentum can result in the slow down of bar pattern speed. Because the length of the bar is limited by the radii of corotation, the decreases in pattern speed moves the radial position of corotation further into the disc. This allows for the trapping of more material onto elongated bar orbits, forging a longer and stronger bar (Lynden-Bell, 1979; Sellwood, 1981; Solway et al., 2012). In simulations where the bar slows due to dynamical friction with the halo bars can become almost as large as their discs (Athanasoula and Misiriotis, 2002; Martinez-Valpuesta et al., 2006; Villa-Vargas et al., 2009). However, as bars as large as discs are not seen in observations bar growth must be mediated by more than just dynamical friction with the halo (Erwin, 2005). A substantial gas component can delay or even halt the formation of the bar, and in cases where the bar does form result in weaker bars overall. Alternatively, bar growth can be interrupted by a process called buckling.

Instability and buckling

The orbits in bars, and indeed galaxies, are not constrained to just two-dimensional motion but also extend up into the vertical plane. The vertical motion of stars in the bar can result in the distortion of material up out of the disc plane.

While the precise nature of this distortion is still debated, there are currently three popular mechanisms proposed. Firstly, as the bar grows it can become dynamically unstable which causes the bar to buckle vertically out of the plane of the disc, effectively thickening the central regions (Binney, 1981; Pfenniger and Friedli, 1991; Skokos et al., 2002; Portail et al., 2015; Collier, 2020). This instability is commonly referred to as the fire-hose instability. Secondly, the vertical motions of stars in the bar

may gradually increase through interactions with vertical resonances (Quillen et al., 2014). Finally, stars on $x1$ orbits may become trapped within a vertical resonance of the bar, gradually building up its vertical height (Quillen, 2002; Sellwood and Gerhard, 2020).

Numerical simulations find that the bar buckles out of the plane shortly after its formation (Pfenniger and Friedli, 1991; Sotnikova and Rodionov, 2003; Martinez-Valpuesta and Shlosman, 2004), with the buckling phase itself only lasting for a few hundred Myr (Athanasoula et al., 2016). After buckling, the resulting bar is weaker but much thicker in vertical height (Martinez-Valpuesta et al., 2006). Due to the rapidity of the buckling phase, very few observations show bars in the process of buckling (Erwin and Debattista, 2016; Li et al., 2017). However, simulations show that the buckled bar settles into a boxy/peanut shape commonly associated with edge-on bars. In some cases it may be possible for the bar to undergo several buckling episodes. These secondary buckling events act over longer time periods, taking between 2-3 Gyr (Martinez-Valpuesta et al., 2006; Łokas, 2019), but are expected to occur less frequently than the initial buckling episodes (Smirnov and Sotnikova, 2019).

Gas can also have significant effects on the onset and outcome of buckling bars. Bars are efficient transporters of gas to the central regions. The build up of central mass through bars in gas rich discs can act to either completely suppress the buckling instability (Berentzen et al., 1998; Debattista et al., 2006; Berentzen et al., 2007; Villa-Vargas et al., 2010; Athanasoula, 2013) or result in the destruction of the bar (Bournaud and Combes, 2002; Bournaud et al., 2005). The lack of buckled bars with boxy/peanuts or barlens structures in late-type galaxies (Erwin and Debattista, 2017; Li et al., 2017) points towards the former being the case.

1.4.3 Are bars long-lived features?

Bars have been found present in galaxies up to $z \approx 2$ and they clearly have an influence on galaxy evolution. As bars are implicated in the formation of pseudo-bulges through secular processes, a pivotal issue is the long-term stability of bars: can a bar

be destroyed, and if so can it then be reformed?

Bar destruction

As bars are efficient in funneling material into the central regions, determining their stability in the presence of a central mass concentration such as a super-massive black hole is important. Some models find that bars rapidly dissolve in the presence of central mass concentrations (Bournaud and Combes, 2002; Bournaud et al., 2005; Hozumi and Hernquist, 2005; Hozumi, 2012). In contrast, others have shown that unrealistically massive black hole masses 4% of the total stellar mass are required for the destruction of large-scale bars (Shen and Sellwood, 2004; Athanassoula, 2005; Debattista et al., 2006). However, Du et al. (2017) found that a black hole mass $\approx 0.1\%$ of the total stellar mass would effectively destroy short bars (where short is considered as $< 1.5\text{kpc}$) irrespective of whether they co-exists with a larger outer bar. In cases where the bar is not destroyed it can be weakened as the central mass concentration can alter the orbital structure of the central regions (Bournaud et al., 2005).

The first self-consistent numerical simulations containing gas showed that bars can be destroyed (Friedli and Benz, 1993). While initially this was thought to be the result of the build up of a central mass component, the gas itself can also act to destroy the bar: gas is driven into the central regions of galaxies by bar torques, but the gas also exerts an opposite torque which can weaken and destroy the bar (Combes, 2008). While simulations show that an unrealistically massive central mass concentration is required for bar destruction (Shen and Sellwood, 2004), the gas infall need only be 1-2% of the disc mass to destroy a bar (Friedli et al., 1994; Berentzen et al., 1998; Bournaud et al., 2005; Combes, 2008). The bars in these gas-rich galaxies are short-lived and predicted to be destroyed within 1-2 Gyr of formation (Bournaud et al., 2005).

Galaxy-galaxy interactions and mergers could also result in the destruction of a bar since they can alter the dynamics of the galaxy. However, major mergers can destroy the disc as well resulting in the formation of a spheroid. Although minor mergers or an interaction between the galaxy and a satellite could disrupt and destroy the bar, since

bars can be tidally induced by such events they may reform after the disc has once again settled.

Bar reformation

If a bar is destroyed then the disc will be dynamically hot and must cool before a bar can be formed again. As mentioned previously in this section, a bar that is destroyed through a minor merger or galaxy-galaxy interaction may reform after a disc has settled. Bars which have been destroyed by gas inflow may also reform once new gas has been accreted, replenishing the disc and making it again unstable to bar formation (Combes, 2008). Those bars which have been destroyed by a central mass concentration will be prevented from reformation as a result of the altered dynamical structure of the galaxy (Sellwood and Moore, 1999).

Observational evidence of bar destruction and reformation is difficult to come by since we only ever see a snapshot of a galaxy's evolution. In simulations Bournaud and Combes (2002) and Combes (2008) found that galaxies can have multiple episodes of bar formation if the galaxy has a high gas accretion rate. However, each cycle of bar destruction and reformation requires additional accretion of mass, and since bars can easily transport material into the centre of the galaxy, the disc becomes more centrally concentrated acting to stabilise the disc against further bar formation (Sellwood and Moore, 1999).

However, some statistical surveys show that the bar fraction remains constant out to a redshift of $z \approx 1$ and in massive galaxies strong bars have been found up to redshifts of $z \approx 2$ (Simmons et al., 2014) which implies that either bars are long-lived features or that barred galaxies are destroyed and reformed in equal measure. Although I have described several methods through which bars can be destroyed it appears difficult to destroy them once they become sufficiently strong (Athanasoula, 2005). Indeed, there are several theoretical predictions from simulations that find bars are actually robust and long-lived structures (Debattista et al., 2006; Curir et al., 2008; Kraljic et al., 2012a).

1.5 Determining the time of bar formation

Many observational methods have been proposed for the recovery of bar ages which could not only shed light on the lifetime of bars but also constrain the evolution of bar properties and the time of disc settling with cosmological epoch. As previously mentioned, studies of bar fraction with redshift indicate that bars are in place early and seem to have lifetimes which exceed 2 Gyr (Jogee et al., 2004).

More specific investigations into bar ages used optical spectroscopy to investigate the properties of the stellar populations in bars, recovering a wide range of ages (Pérez et al., 2009; Pérez and Sánchez-Blázquez, 2011; Gadotti and de Souza, 2006). However, these results must be taken with a element of caution since ages are recovered for the stellar populations in the bar which may not related to the age of the bar itself (Wozniak, 2007). An alternative method proposes that the age of the stellar population in the nuclear ring could be related to the age of the bar since nuclear rings are thought to form only after the formation of the bar itself (Gadotti et al., 2015).

Looking at the influence of a bar on the galaxy, (James and Percival, 2016) proposed that the region which the bar sweeps out, the star formation desert (SFD), could be closely linked with the time of bar formation since bars are expected to remove gas from the region inside corotation on fast timescales. By recovering the star formation history of this region a truncation time might be recovered which identified a lower limit on the time of bar formation. Alternatively, looking at the star formation history of the central regions on the barred galaxy could show a peak in star formation around the time of bar formation (Carles et al., 2016) due to the same process, the efficient movement of gas inside the corotation radius into the centre of the galaxy.

Aside from using the properties of the stellar populations, other methods proposed for recovering bar ages use properties of the bar itself. Gadotti and de Souza (2005) measured the vertical velocity dispersion of bars in simulations and found that older bars have a higher velocity dispersion than younger bars. Kim et al. (2014) found that the light profiles of bars changes from exponential and disc-like to flat as the bar becomes older. While both of these methods could be used to determine whether a bar

is recently formed or old they do not recover specific bar ages.

1.6 Layout for thesis

In this thesis I analyse the effects bars have on the star formation and stellar dynamics of their host galaxies using numerical simulations. In Chapter 2 I give an overview of the technique used for the high resolution simulations in which I do the majority of my analysis, as well as the numerical method used to recover the bar properties.

Chapter 3 is devoted to analysis of the effect of the bar on the star formation in the star formation desert region and its implications for determining the time of bar formation. I also explore how the star formation desert might be an important asset for understanding the influence of the bar on radial migration.

In Chapter 4 I explore the effects of the bar on the stellar dynamics, describing how the bars kinematical properties can provide insight into bar formation times and even bar evolution.

In Chapter 5 I provide my final conclusions and present potential avenues for future work.

Chapter 2

Methods

As described in the previous chapter, bars are an extremely complex phenomenon that can have a significant impact on the structure and evolution of a galaxy. One way in which we can study the impact of bars is through numerical simulations. In this thesis I have used zoom-in cosmological re-simulations to study the effects of bars on the dynamics and star formation of galaxies. In this chapter I describe the simulation technique and also the algorithm used to recover bar length and strength properties.

2.1 Simulation technique

In this thesis I analyse barred galaxies from a sample of zoom-in cosmological re-simulations presented in Martig et al. (2012). These are simulations performed in a cosmological context which achieve a high resolution at a galactic scale. The technique requires two parts. First, the full history of a galaxy is extracted from a low-resolution cosmological simulation. Second, this is used in a high resolution re-simulation of only the target galaxy including mergers and gas accretion as prescribed by the cosmological simulation. I describe each part of the simulation process in more detail in the following subsections.

Cosmological simulation

The entire history of a galaxy is extracted from a low resolution dark matter-only cosmological simulation run with the adaptive mesh refinement code RAMSES (Teyssier, 2002). The simulation box has a comoving length of $20 h^{-1}$ Mpc and contains 512^3 particles each with a mass of $6.9 \times 10^6 M_{\odot}$. Halos are detected with the HOP algorithm (Eisenstein and Hut, 1998) and those of interest are selected such that at $z=0$ they are considered isolated with no massive halos found within a 2 Mpc radius.

Once a halo of interest is identified the most massive progenitor is identified in each snapshot tracing back to the main progenitor at a redshift of $z=5$. A spherical boundary defined by the virial radius of the main halo at $z=0$ is then considered. At high redshift the diffuse particles and halos within this boundary are considered as part of the initial conditions. All halos and diffuse particles crossing this boundary in each snapshot are then recorded to build-up the merger and accretion history of the galaxy from $z=5$ to $z=0$.

High resolution re-simulation

The target halos are then re-simulated at higher resolution. The re-simulations begin at $z=5$ with a seed galaxy containing stars, gas and dark matter. The total galaxy mass is divided into 17% baryons and 83% dark matter (with the dark matter mass as the mass from the initial cosmological simulation). Gas content is prescribed according to redshift and galaxy mass. For large discs at high redshift the gas fraction is 30% reducing to 15% at lower redshifts in accordance to high and low redshift observations. For small galaxies ($M \leq 10^{11} M_{\odot}$) gas fraction is always 30% of the baryonic mass. This galaxy's evolution is followed down to $z=0$ with mergers, as well as dark matter and gas accretion, prescribed by the cosmological simulation. Tests have shown that the initial properties of the seed galaxies have little impact on the evolution of the galaxy from $z=5$ to $z=0$ due to the small mass of the seed and the rapid evolution at high redshifts (Martig et al., 2009). I refer the reader to Martig et al. (2012) for details on the properties of the incoming galaxies.

The zoom-in re-simulations have a spatial resolution of 150 pc, mass resolution of $1.5 \times 10^4 M_\odot$ for gas particles, of $7.5 \times 10^4 M_\odot$ for star particles (or $1.5 \times 10^4 M_\odot$ for star particles formed during the simulation from the gas) and $3 \times 10^5 M_\odot$ for dark matter particles in a box of 800 kpc. Gravity for gas, stars and dark matter is modelled using the particle mesh-code described in Bournaud and Combes (2002) and Bournaud et al. (2003), with gas dynamics modelled using a sticky particle algorithm. The sticky particle algorithm impedes the accuracy of the simulation at high mass due to the poor treatment of the hot gas phase, thus limiting us to low mass galaxies where the cold mode gas accretion is dominant.

Star formation is modeled using a Kennicutt-Schmidt relation (Kennicutt, 1998) with a 1.5 exponent and a star formation threshold of $0.03 M_\odot \text{pc}^{-3}$. This means that the star formation rate surface density scales by power of 1.5 of the gas surface density. Kinetic feedback from supernovae is included such that 20 percent of supernova energy is redistributed to the gas particles, and stellar mass loss is also taken into account (Martig et al., 2012).

Simulations performed in this way have the advantage of a lower computation time allowing for the potential of statistical studies. Additionally, galaxies with all types of merger histories can be explored, including mergers at $z \approx 0$. This is in contrast to standard zoom simulations which need to include and follow all of the components of a galaxy at high resolution from the initial stages down to $z=0$, which could result in the high-resolution sub-volume being very large.

However, there are also disadvantages with one of the most significant being the large number of free parameters in the structure and baryonic content of galaxies interacting with the main galaxy. This is especially true of the galaxies at $z=5$ where there is little observational data available for comparison.

The resulting galaxies at $z = 0$ have inner and thick disc scale heights that vary between 0.1 to 1 kpc and 0.5 to 3 kpc respectively (García de la Cruz et al., 2021). The bulge fractions range between a B/T of 0.02 and 0.80 with bulges varying in radial size between 0.6 and 12.5 kpc (Martig et al., 2012). However, even with this large variation

the simulations are unable to account for the large number of observed bulgeless galaxies. In addition the simulated galaxies tend to be in more isolated environments than their mass-matched observed counterparts. There also does not appear to be any correlation between bulge content and stellar mass in the simulations. This differs from the expected trend in observations which finds higher bulge fractions associated with higher stellar masses (Weinzirl et al., 2009). However, this could be a result of the limited sample size or differences between the methods used to measure stellar mass in simulations and observations.

The majority of the simulated galaxies have a low Sérsic index, with many falling below 2 which indicates that the majority of the bulges are likely pseudobulges in agreement with observations of local discs (Laurikainen et al., 2007). Additionally, 70% of the simulated disc galaxies contain bars which matches the observed bar fraction of 60-70% when galaxies are viewed in the infra-red (Eskridge et al., 2000; Marinova and Jogee, 2007).

2.2 Additional simulations

In addition to the simulations described above I also use three simulations of galaxies in isolated environments. Two of the simulations are collisionless N-body simulations (*isolated:N-body A* and *isolated:N-body B*) which are presented in Fragkoudi et al. (2017) while, the third is a hydrodynamical simulation run with RAMSES (*isolated:N-body+gas*) to be presented in Fragkoudi & Bieri, in prep. In all cases the simulations start with a fully formed disc at the time of bar formation. Here I summarise the most important details with the full details of these simulations given in Chapter .

The *isolated:N-body* simulations were run employing the Tree-SPH code of Semelin and Combes (2002) without the SPH component of the code as neither *isolated:N-body A* or *B* contain gas. The *isolated:N-body* simulations contain both a thin and thick disc with respective scaleheights of 0.3 and 0.9 kpc. The number of total disc particles is $n_{disc} = 1 \times 10^6$ each with a mass of $m_{disc} = 9.2 \times 10^4 M_{\odot}$ making a

combined baryonic disc mass (thin+thick disc) of $M_* = 1 \times 10^{11} M_\odot$ with the mass of the thick disc comprising 30% of the combined disc mass. The dark matter halo contains $n_{halo} = 5 \times 10^5$ particles, each with a mass of $3.2 \times 10^5 M_\odot$ making for a total halo mass of $M_H = 1.6 \times 10^{11} M_\odot$. A Plummer sphere (fixed potential halo) is used to model the dark matter halo which has a characteristic radius of $r_H = 10 \text{ kpc}$. Both isolated:N-body A and B are simulated with time steps of $\Delta t = 0.25 \text{ Myr}$ which begin at the time of bar formation. Isolated:N-body A has a peanut that forms shortly after the time of bar formation, while in isolated:N-body B the formation of the peanut is delayed by several Gyr. I refer the reader to Fragkoudi et al. (2017) for more details on the simulation method for both isolated:N-body A and B.

The third simulation I use (isolated:N-body+gas) is a simulation of an isolated Milky Way-mass galaxy with both a collisionless and collisional component, i.e. a stellar disc+dark matter component, together with a gaseous disc. This model is part of a suite of models that will be presented elsewhere (Fragkoudi & Bieri, in prep.). Here I describe the main properties of this simulation. The simulation is run with the adaptive mesh refinement (AMR) code RAMSES code (Teyssier, 2002). The AMR grid is refined using a quasi-Lagrangian strategy, where the maximum resolution reached in the simulation is 48 pc.

The initial conditions are created with the MCMC code DICE (Perret et al., 2014; Perret, 2016). The total mass of the halo and galaxy is $M_{tot} = 2 \times 10^{12} M_\odot$. The mass fraction in the dark matter, stellar and gaseous components corresponds to 98.5%, 1.425% and 0.075% of the total mass, respectively. The dark matter and stellar component is modelled using 2×10^6 and 1×10^6 particles respectively. The dark matter halo is modelled as a Navarro-Frenk-White (Navarro et al., 1997) profile with a scale-radius of 3 kpc. The stars and gas are modelled as exponential discs, with a scale lengths of 3 kpc and 4 kpc respectively.

Gas in the simulation cools via atomic and metal-dependant cooling processes. Primordial gas cooling is implemented according to Katz et al. (1996), including collisional excitation, collisional ionisation, recombination and free-free emission, with an additional contribution based on abundances from Sutherland and Dopita (1993). For gas

below 10^4 K, we use the standard prescription implemented in RAMSES which uses the rates from Rosen and Bregman (1995). Once gas becomes dense enough star formation is allowed to take place. The star formation is modelled as a Schmidt law; star formation is triggered when the gaseous density ρ_{gas} is larger than 1 cm^{-3} with an efficiency of $\epsilon_{\star} = 1\%$,

$$\dot{\rho}_{\star} = \epsilon_{\star} \rho_{\text{gas}} / t_{\text{ff}} \quad (2.1)$$

where $\dot{\rho}_{\star}$ is the local star formation rate and $t_{\text{ff}} = \sqrt{3\pi/(32G\rho_{\text{gas}})}$ is the free-fall time computed at the gas density ρ_{gas} . AMR cells with temperature greater than 2×10^5 K are not allowed to form stars.

Supernova feedback is implemented by assuming that a fraction of the stellar population will explode as supernovae (here, $\eta_{SN} = 0.2$). The thermal energy of the supernovae is injected into the 27 parent cells surrounding the stellar particle. Each supernova is assumed to produce 10^{51} ergs of energy. AGN feedback is not included. More details on the feedback implementation can be found in Dubois and Teyssier (2008).

2.3 Bar detection

The focus of this thesis resides in identifying the effects of bars on the star formation and dynamics of an evolving galaxy, and as such the identification of the bars and their properties is pivotal to this thesis. While bars can be identified visually, I identified bars through the automatic detection method presented in Kraljic et al. (2012a). This method allows for the simultaneous identification of the presence of the bar in addition to its length and strength via the azimuthal spectral analysis of surface density profiles of face-on galaxies. This is done by considering the stellar surface density of each galaxy in polar coordinates which is decomposed into its Fourier components:

$$\Sigma(r, \theta) = \Sigma_0(r) + \sum_m A_m(r) \cos(m\theta - \phi_m(r)) \quad (2.2)$$

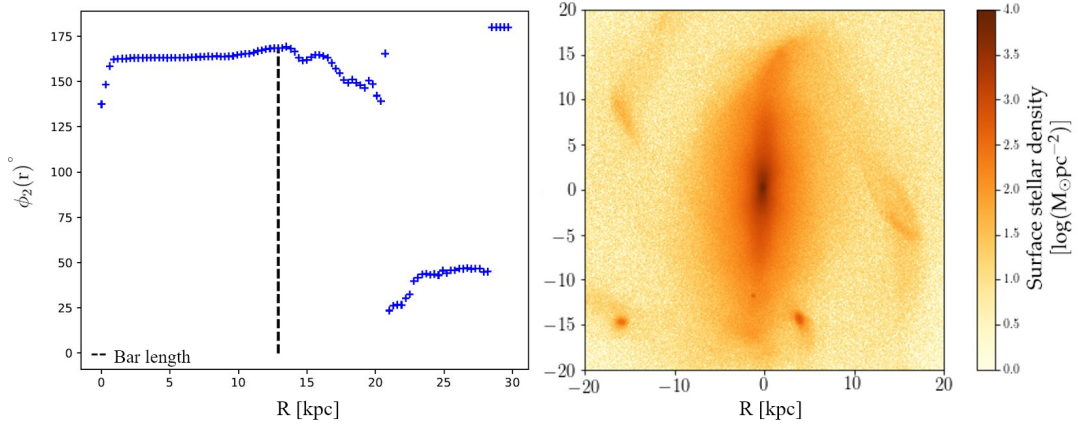


Figure 2.1: Left: A plot showing $\phi_2(r)$ against galaxy radius for a single snapshot. The point where the phase deviates from being constant marks the length of the bar (black dashed line). Right: The face-on surface stellar density for the same galaxy and snapshot as left, showing the bar aligned along the y-axis.

where the stellar surface density is $\Sigma(r, \theta)$, θ is the azimuthal angle in the frame where the bar is fixed and r is the radial distance. The Fourier amplitude is given by A_m , with the phase given by ϕ_m . The azimuthally-average profile of the stellar surface density is given by $\Sigma_0(r)$. To center the galaxy for the analysis the center of stellar mass within the central 10 kpc is determined.

The presence of a bar is typically associated with even-mode phase signatures, with the $m=2$ mode being the most prominent in the bar detection region. Even-modes are associated with those features which are symmetric such as bars and spiral arms, while odd-modes tend to highlight any asymmetric features. The bar and spiral arms, when an even number of arms are present, are both symmetrical features and thus both show up when looking at the $m=2$ mode, however the bar has a phase $\phi_2(r)$ which is constant with radius while with spiral arms the phase varies. So by looking for a region of constant phase in the center of the galaxy, a bar can be identified and its length measured (see Figure 2.1).

The minimum criterion for identifying the presence of a bar is defined as a constant phase $\phi_2(r) \pm 5^\circ$ within a bar region starting between 900 and 1500 pc. The phase must be constant for a minimum of 1500 pc. The exclusion of the very central regions ≤ 900 pc accounts for small variation in Φ_2 which are produced by off-centering (a result of

the resolution limit) and central asymmetries which can cause the mis-identification of bars. No bars are visually identified as starting their constant ϕ_2 phase at a radii ≥ 1500 pc so by limiting between 900 and 1500 pc all systems which can visually be identified as bars are always identified. The requirement of the minimum constant phase extent of 1500 pc excludes nuclear bars or very weak bars since typically most bars have a length ≥ 2 kpc (Barazza et al., 2008).

After a bar has been found its length (determined by the extent of the constant phase Φ_2) and strength are measured. To calculate strength the definition proposed by Aguerri et al. (1998) is used:

$$S \equiv r_{\text{bar}}^{-1} \int_0^{r_{\text{bar}}} \frac{A_2}{A_0} dr \quad (2.3)$$

where the radial limit of the bar is defined by r_{bar} and A_2 and A_0 represent the Fourier amplitudes for the 0th and 2nd modes.

At high redshifts bars may still be mis-identified, especially if they are weak. Bars tend to grow in both strength and length with time, they are also considered as a transition point for the onset of secular evolution which indicates when discs begin to settle. Galaxies forming at high redshift exist in chaotic environments and usually undergo merging events which can result in spheroid-dominated galaxies. These galaxies have flattened central isophotes which can be mistakenly identified as bars with the aforementioned method, however this actually corresponds to a triaxial part of the spheroid. To reduce this effect true bars are identified by requiring that the strengths of the $m=2$ mode must be greater than, or equivalent to, 0.3 in two orthogonal edge-on projections.

The advantage of this method comes from the ability to simultaneously detect bars, and measure their lengths and strengths making it ideal for statistical analysis. In this thesis I record the lengths and strengths for each snapshot of the simulated galaxies.

However, Hilmi et al. (2020) found that bar lengths and strengths measured in this way can be over estimated up to $\approx 100\%$ and $\approx 15\%$ respectively. This discrepancy is caused by bar-spiral arm coupling and interference from overlapping bar and spiral

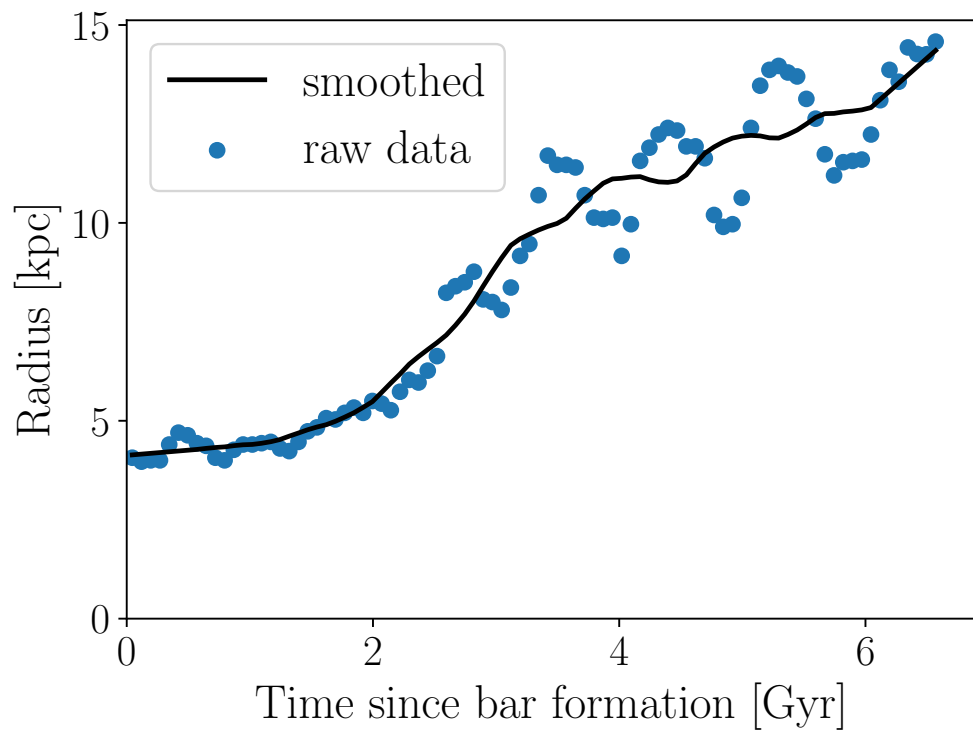


Figure 2.2: Time evolution of bar length showing the raw data featuring the oscillation due to the interaction between the bar and the spiral arms (blue points) and the averaged bar length (black).

modes. The length increases caused by these interactions oscillate over a time period of 60-200 Myr. In Figure 2.2 I show bar length over time. The oscillations in bar length are clear in the raw data after 3 Gyr. To combat this effect I choose to smooth the bar length measurements using a rolling mean over a window of 9 snapshots giving a rolling window of 333 Myr allowing for the full coverage of any oscillation events.

Chapter 3

Redistribution of Stars and Gas in the Star Formation Deserts of Barred Galaxies

3.1 Introduction

The formation of a bar has been linked with the time of disc settling and the onset of secular processes (Gadotti and Dos Anjos, 2001). This makes the recovery of bar ages an important step towards a complete understanding of galaxy evolution. However, the majority of bar dating methods, as described in Section 1.5, rely on dating the underlying stellar population. This must be done with some caution since the age of the stellar population within the bar may not necessarily be related with the bar formation epoch. An alternative way to approach the recover of a bar formation time could come from investigating the influence of the bar on its surroundings.

James and Percival (2016, 2018) used a feature first noticed by James et al. (2009), which they named the ‘star formation desert’ (SFD), to determine the ages of the bars. They define the SFD as a region lying within the inner ring, either side of the bar in the area the bar sweeps out that shows little to no $H\alpha$ emission (see Figure 3.1).

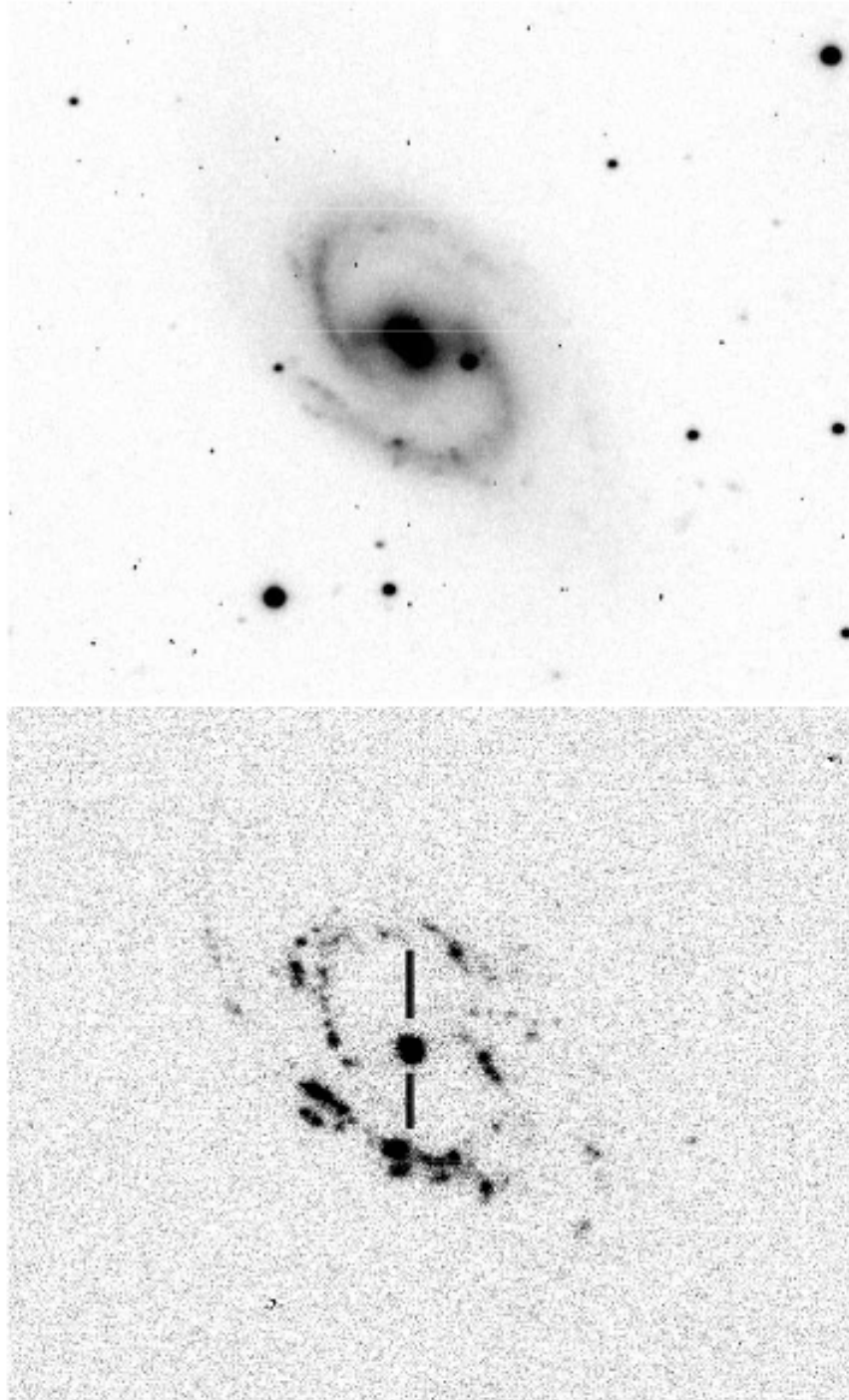


Figure 3.1: Top: R-band image of NGC 2543 showing the bar orientated parallel to the x-axis. Bottom: Continuum-subtracted $H\alpha$ image of the same galaxy showing the lack of $H\alpha$ emission in the SFD region (marked by the vertical black lines) (James and Percival, 2016).

These regions also display a deficit in surface stellar density (Gadotti and de Souza, 2003; Gadotti, 2008; Kim et al., 2016) and suppressed star formation (Hakobyan et al., 2015). To model the star formation histories in those regions James and Percival (2016, 2018) assumed a truncated star formation model and found that SFD regions can be very old. If the truncation of star formation is caused by the bar, this feature can be used to determine the epoch of bar formation. This leads to some interesting questions:

- Is the SFD region observable in simulations? Can the mechanism behind this cessation of star formation be determined?
- Is it a result of gas being dynamically heated against star formation, or is the gas being removed by the formation of the bar? If the gas is removed then where does it go?
- Can the properties of the SFD be used as a method for determining the formation epoch of the bar?
- Are the SFD stars only born before the formation of the bar and, if they are not, where do the later-forming stars come from?
- Is the cessation of star formation in the SFDs related to a global downturn in star formation?

In this chapter I attempt to answer these questions by presenting a numerical analysis of a sample of simulated galaxies selected from Martig et al. (2012). The structure of this chapter is as follows: Section 2.1 contains a description of the simulation techniques used to produce our sample, a description of the sample itself and the method used to obtain the properties of the bars. Section 3.3 contains my results and analysis of stars within the SFD region in comparison with the bar and global galaxy properties. Section 3.4 contains my discussion of the main results in terms of determining the epoch of bar formation and the analysis of the stars within the SFD region. My main conclusions are presented in Section 3.5.

The work presented in this chapter has been published in Donohoe-Keyes et al. (2019).

Halo	M_* [$10^{10}M_\odot$]	L_{bar} [kpc]	S_{bar}	T_{bar} [Gyr]
37	12.0	6.0	0.70	8.5
45	10.2	6.6	0.76	6.8
82	3.81	4.4	0.38	2.0
92	4.38	5.6	0.71	6.8
106	4.29	3.1	0.45	6.6
128	2.69	3.3	0.74	4.7

Table 3.1: Properties of the model galaxies taken from $z=0$. For each halo we provide the halo index number, the stellar mass (M_*) calculated by summing star particles to the R_{25} limit, the bar length (L_{bar}), and the bar strength (S_{bar}). The final column gives the bar formation epoch of the galaxy in lookback time.

3.2 Sample Selection

From the sample of 33 simulated galaxies described in Martig et al. (2012) I select 6 that display a wide range of star formation histories, masses, and bar lengths, strengths, and formation epochs. By selecting this limited sample I can do a more detailed analysis while still being able to explore the diversity of the larger sample.

Column 1 of Figure 3.2 shows the surface stellar density maps of the galaxies face-on at $z=0$, ranked in order of largest halo mass (top) to lowest (bottom). The main properties are highlighted in Table 3.1.

All of the galaxies begin with a merger-intense phase which contributes to the build up of a hot stellar component for ages greater than 9 Gyr. After this the disk builds with features such as spiral arms, and, more pivotal to the focus of this chapter, the bars and star formation desert regions. Halo 106 differs from this scenario by having three epochs of bar formation with the first two being destroyed by mergers. For this case I list properties relevant to the final bar, for which the bar formation epoch is given in the final column of Table 3.1.

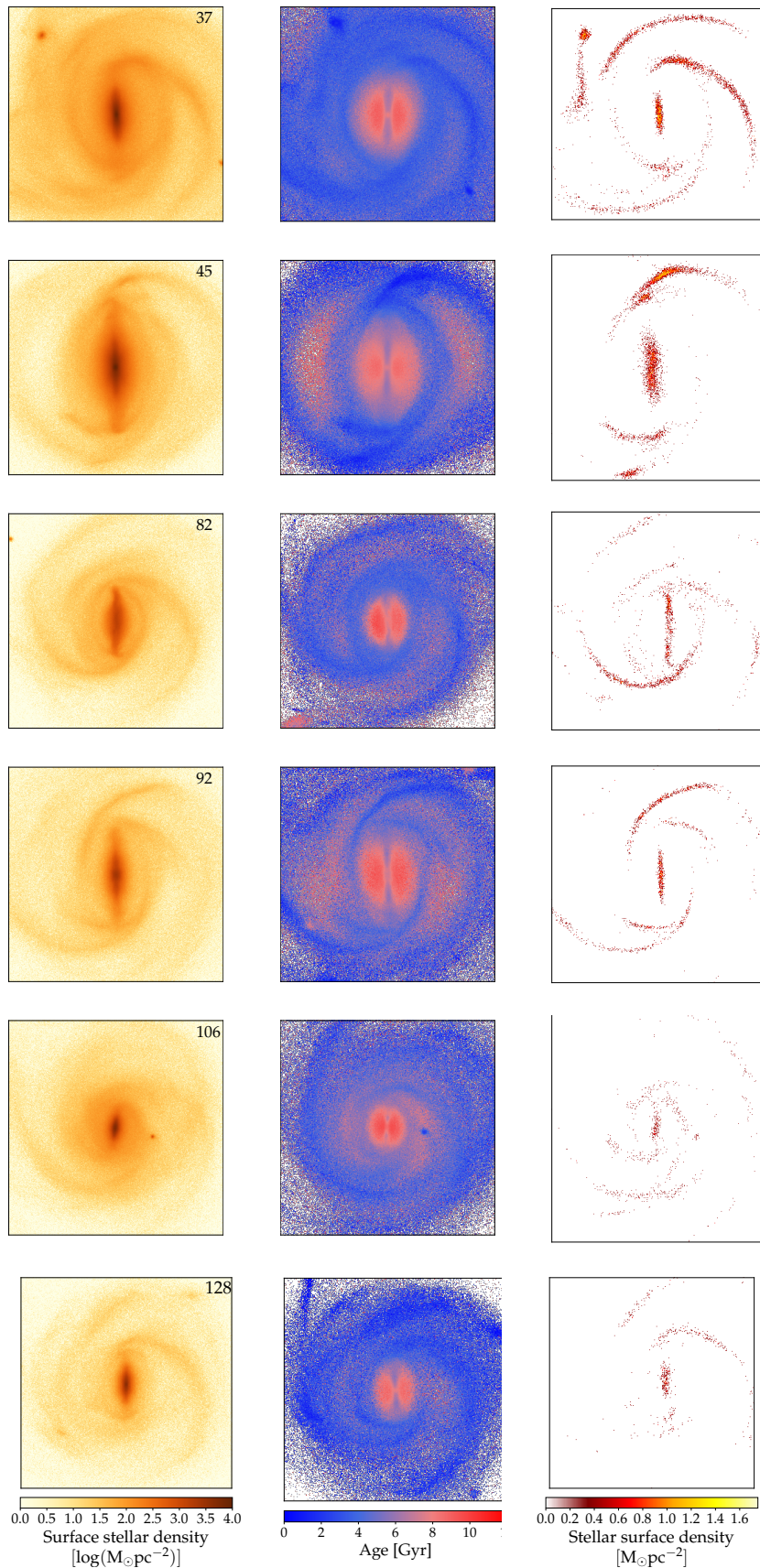


Figure 3.2: Each plot represents a $40 \times 40 \times 40$ kpc box with the galaxy centred within the box. Left: Face-on surface stellar density maps with the total halo mass decreasing down the column. Middle: Average age maps displaying strong signals for the SFD desert feature. Right: Surface stellar density maps for the young stars, <10 Myrs, also displaying the SFD feature with SF mainly located within the bar region and along the spiral arms of the galaxies.

3.2.1 Defining the SFD

Figure 3.2, column 2 shows the mean age maps for the sample of simulated galaxies. The blue colour highlights younger stellar populations while the red shows older populations. In all of the galaxies in the sample there is a region either side of the bar, within the region the bar sweeps out, displaying consistently older populations. This coincides with the SFD region seen observationally in James and Percival (2015). The size of the SFD is closely associated with bar length and it never extends further than the radius of the bar. The SFD region is bordered by the inner ring which contains a younger population. In all the cases the bar appears to be a younger feature than the SFD but, in these simulated galaxies, older than the ring and disk.

I define the SFD as the region encompassed in a ring excluding the bar and the bulge. I fit the shape of the ring as an ellipse using the bar length as the major axis and take the width of the bar as 1 kpc. Additionally, I remove stars which are associated with the bulge from the SFD by removing an inner ellipse shaped region and then removing the bar itself. This results in two ‘C’-shaped regions shown in Figure 3.3.

Finally I remove ‘interloper’ stars. These are stars which are only passing through the SFD region at the point of selection. To remove them from the SFD sample I define a z-axis (perpendicular to the plane of the galaxy) limit of 2 kpc either side of the central plane on a snapshot 0.075 Gyr from the selection snapshot and compare the stellar IDs to those in the selection snapshot, only keeping the stars which appear in both snapshots.

3.3 Results

3.3.1 Age Maps

To determine whether the SFD region in the simulated galaxy sample is a result of a lack of star formation I refer to the young star maps shown in Figure 3.2, column

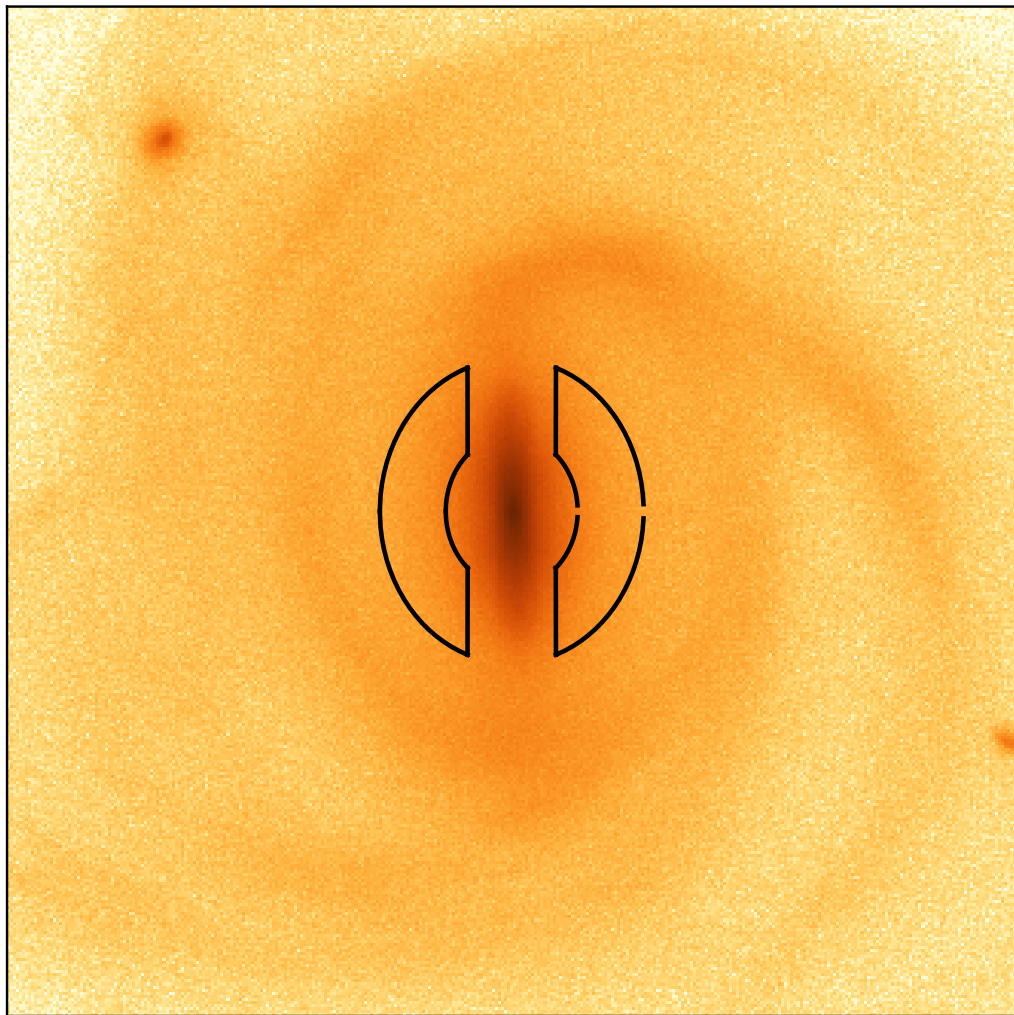


Figure 3.3: The two 'C'-shaped regions we define as the SFD.

3. Here I present the surface stellar density of stars less than 10 Myr old, at $z=0$. High concentrations of young stars are seen within the bar, the spiral arms, and along the inner ring. Some of the rings are populated fully with young stars, while others exhibit broken profiles. For those that do show broken inner rings, the stars are more concentrated at the regions connecting to the ends of the bar. Very few, if any, young stars are seen in the SFD regions. When making side-by-side comparisons between the age and young star maps it is clear that they both highlight the SFD region, the age maps through the older mean age populations and the young star maps through a lack of young stars.

However, the figures presented in this section only show the mean age population and do not tell us about the distribution in ages within the SFD region in comparison to the bar and global populations. To understand how the age distributions differ between regions we need to investigate how the age distributions change with respect to lookback time.

3.3.2 Star Formation Histories

From the mean stellar age maps in Figure 3.2 centre column there is a clear difference between the mean ages of stellar populations within the SFDs, bars, and inner rings of the galaxies.

In Figure 3.4 I plot the age distribution of the SFR pc^{-2} for stars found in the bar and SFD regions, together with the age distribution of the SFR pc^{-2} for all stars found within a $20 \times 20 \text{ kpc}^2$ box with a height of 4 kpc. The top section of each plot shows the bar, SFD, and global age distributions normalised by area. The onset of the bar is marked with a black dashed line. The bar always shows a ~ 10 times higher surface density in the age distribution when compared to the SFD and global galaxy, reflecting the higher mass surface density in the bar. The shape of the age distributions for the bar and global galaxy are actually very similar, and the formation of the bar does not seem to have any impact on star formation globally in the galaxy. By contrast, the age distribution of the SFD shows a relative lack of young stars after the formation of the

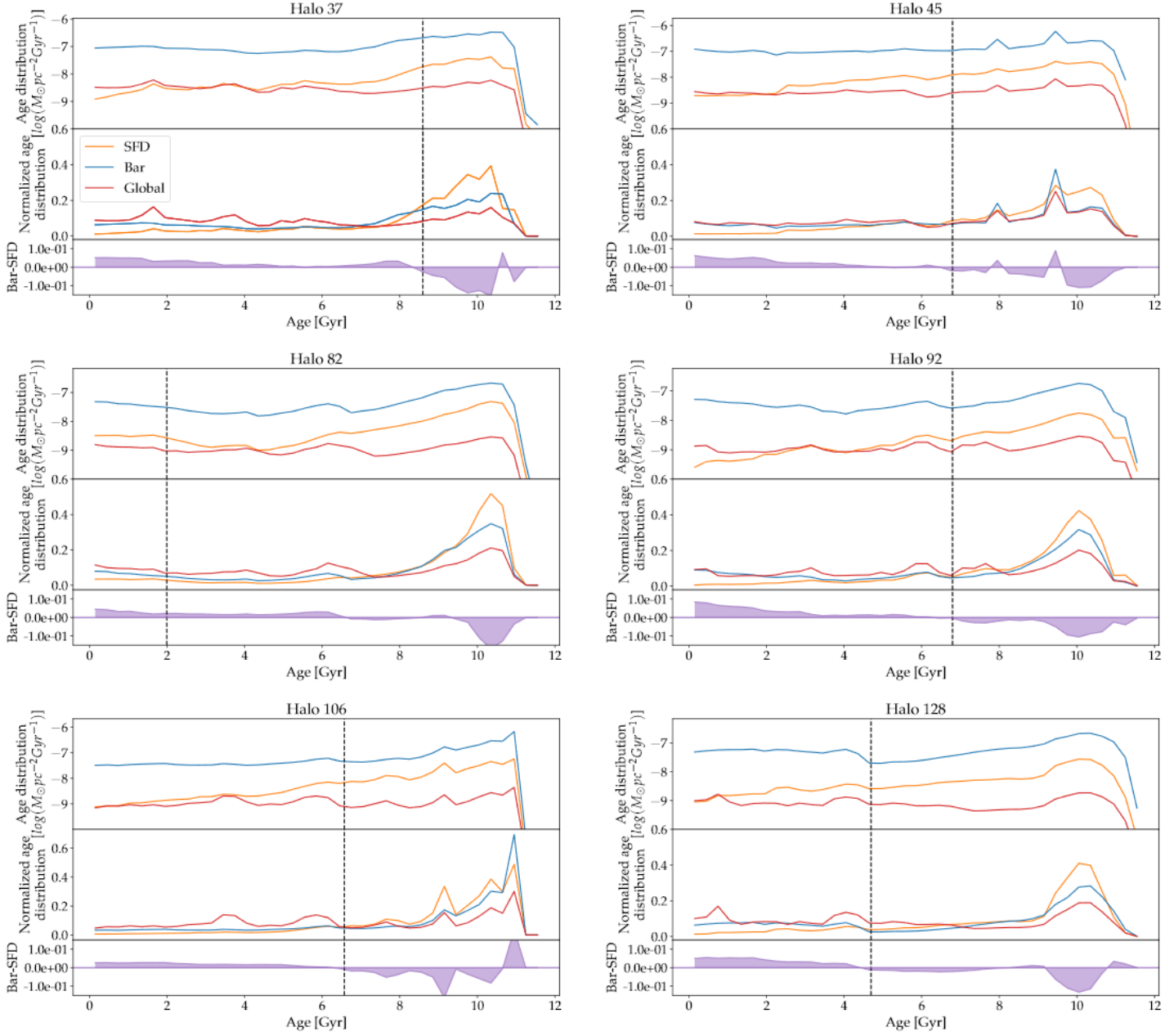


Figure 3.4: For each of the simulated galaxies in the sample I present the age distribution of the SFRpc^{-2} taken from the SFD region, the bar, and the total galaxy at $z=0$. In each plot I display this age distribution normalised to the surface area of the corresponding regions, the age distribution normalised to an area of 1, and the residual (the bar minus the SFD age distribution). Marked on each plot by the vertical dashed line is the time of bar formation. This line coincides with the downturn in the age distribution of the SFD and, in most cases (see Section 3.3.2), the change of the residual from negative to positive.

bar.

For galaxies 37, 45, 92, 106, and 128 the drop in the age distribution of the SFD coincides with the onset of the bar. However, in galaxy 82, the drop happens long before the formation of the bar (see Section 3.4.2 for more details).

To better compare the shapes of the different age distributions, I normalize them to 1 and plot them in the middle panels of each plot. In all cases the global and bar age distributions follow similar shapes, while the SFD gradually drops relative to that of the bar after bar formation. I highlight this effect by showing the difference between the age distributions of the bar and SFD in the bottom panels. For the majority of cases this difference moves from negative to positive after bar formation (corresponding to a change to a lower value for the SFD after bar formation). As the galaxy continues to evolve the residual difference between the bar and SFD tends to increase which we associate with a suppression in the star formation of the SFD region.

Again, galaxy 82 remains an outlier. The transfer of the residual from negative to positive occurs ~ 5 Gyr before the onset of the bar. While this is not associated with the formation of the bar, there is a ring-like feature which does form during this period.

In all galaxies the age distribution of the stars in the SFD does not show a sudden drop at the time of bar formation, contrary to what could have been expected from the mean age maps which show a striking contrast between the mean ages of the SFD and the bar regions. For almost all of the galaxies there is a more gradual decrease in the age distribution of the SFD. If this is a true representation of the star formation histories in observed galaxies, this will make using the SFDs to time the formation of the bar harder than expected. However, there is information in the shape of the difference between the SFD and bar age distributions. Once the bar has formed, for almost all the galaxies, there is a change from negative to positive in the difference between the SFD and the bar. This difference is subtle, but it does imply that there is a suppression of star formation within the SFD after the formation of the bar.

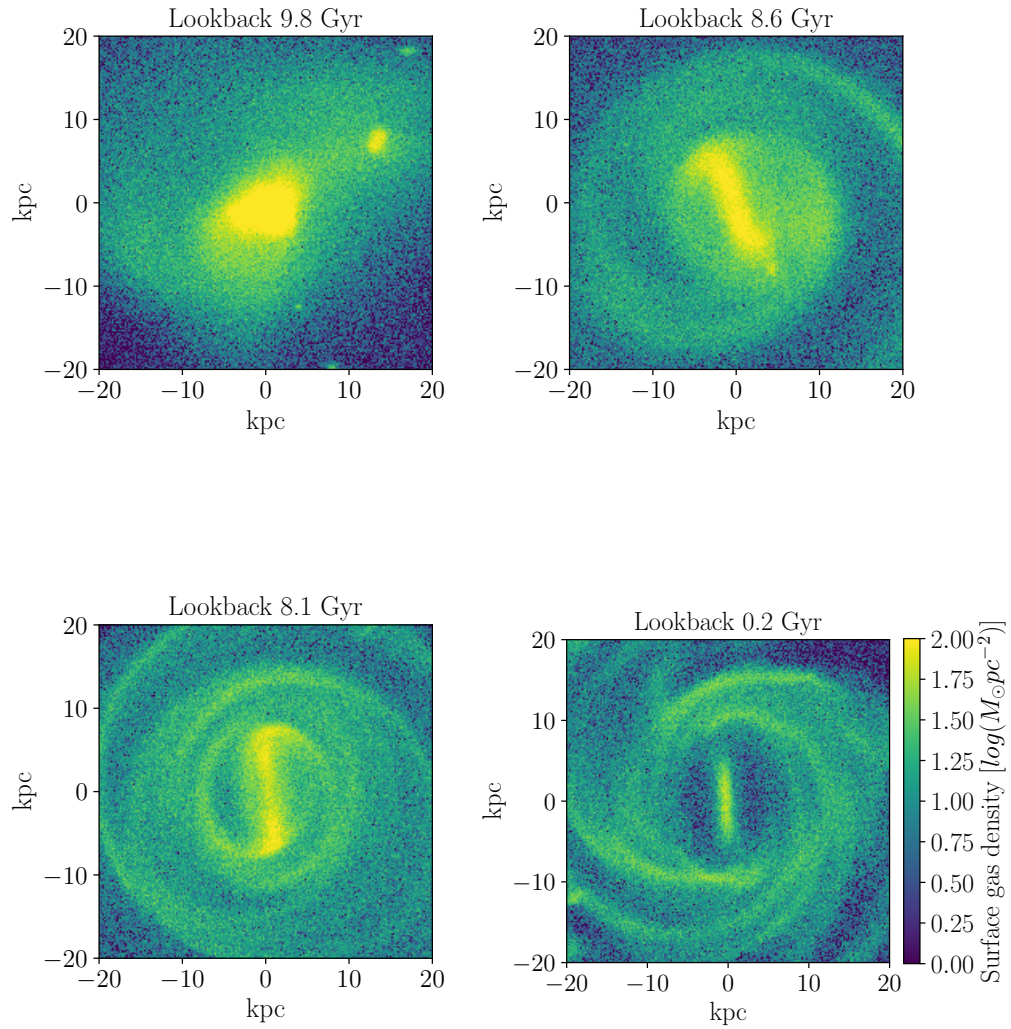


Figure 3.5: Here I show the evacuation of gas from the SFD regions. Initially, the gas is diffuse before spiral arms begin to appear. When the bar forms, the central gas concentration elongates along the major axis of the bar, and the spiral arms strengthen. Once the bar is established the gas is removed from the SFD region progressively over 1-2 Gyr. Over time the size of the SFD changes corresponding to variations in the length of the bar.

3.3.3 Gas Removal

To understand the drop in star formation in the SFD after the bar forms, I now explore how the gas disk responds to bar formation. As an example, in Figure 3.5 I present the time evolution of the gas in galaxy 37.

Before the bar forms (top left panel, lookback time of 9.8 Gyr), the gas density peaks in the center and does not show any other overdensities. The slight lopsidedness is due to tidal effects following a fly-by. As the gas disk grows and cools, it first develops spiral arms. A bar then starts to form at a lookback time of 8.6 Gyr (top right panel). At first, the gas density contrast between the bar and its surroundings is small, but after ~ 1 Gyr the gas within the bar region starts to be collected by the bar. After 500 Myr (bottom left panel) the bar has strengthened and it becomes clear that there is a deficit of gas within the SFD region, with the bar surrounded by a ring connected to clear spiral arms. By $z=0$, there is very little gas remaining inside the SFD region (bottom right panel).

In all six galaxies, the gas in the central regions follows a similar evolution, although the bars form at different times. The removal of gas from the SFD region is a relatively fast process, taking between 1-2 Gyr. This also means that star formation within the SFD is quickly suppressed after the bar forms. However, the star formation histories in Figure 3.4 (discussed in Section 3.3.2) do not show a sharp decline around the time of bar formation and instead imply a more gradual decline in the age distribution of the SFD region. With no gas to continue forming young stars in the SFD after the bar formed, the younger population found in that region must be coming from elsewhere in the galaxy.

3.3.4 Birth positions of SFD stars before & after bar formation

From Figure 3.4 it is clear that there is no truncation in the age distribution associated with the onset of the bar: instead it is a gradual process with the number of young stars in the SFD decreasing after the formation of the bar. However, when looking at the

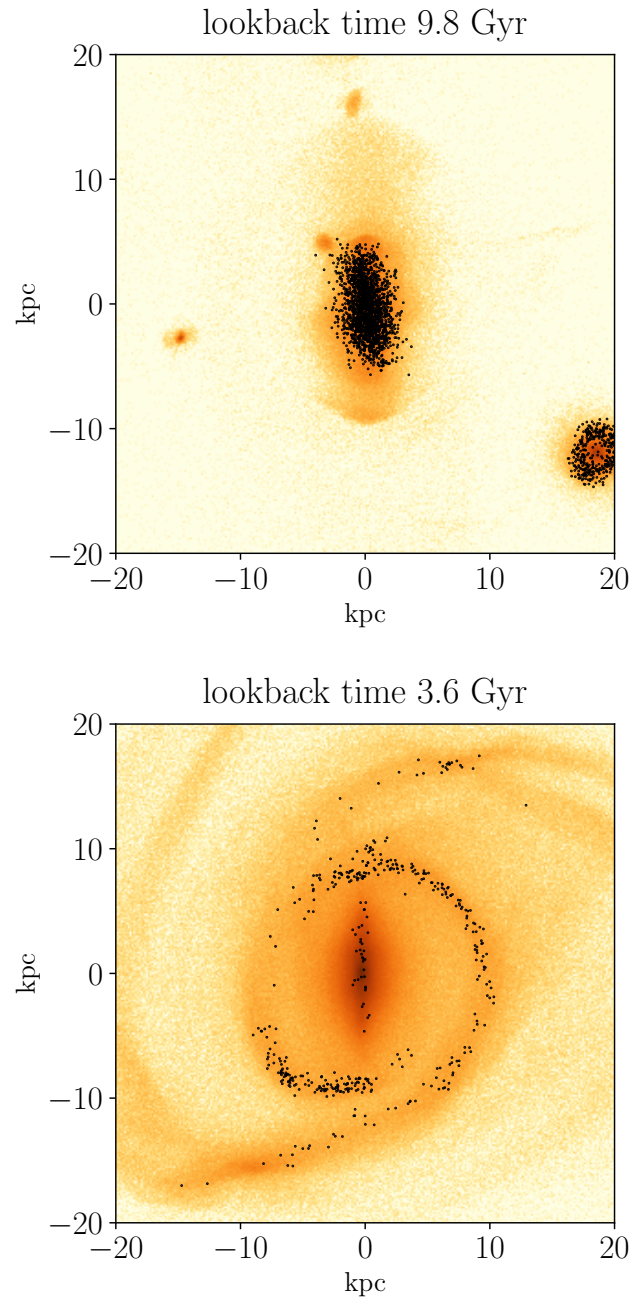


Figure 3.6: The birth positions of SFD stars before and after the formation of the bar overlaid on the surface stellar density maps for galaxy 37. Upper: Birth positions of SFD stars before bar formation. Lower: Birth positions of SFD stars after the formation of the bar.

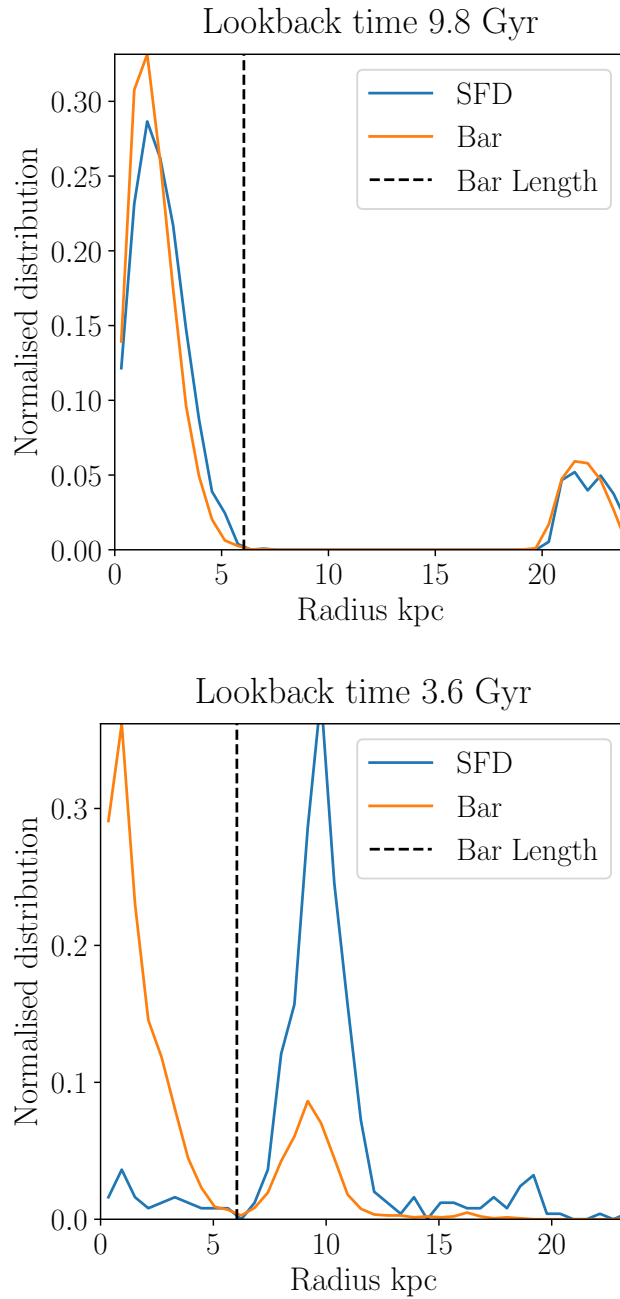


Figure 3.7: Top: the radial distribution of birth positions for stars born before the formation of the bar. The blue line shows the radial distribution for the SFD stars and orange the radial distribution for bar stars. Before the formation of the bar the stars are mainly born in the same region, within 6 kpc. Some stars are born in merging satellite galaxies, beyond 20 kpc. Bottom: the radial distribution of stars born after the formation of the bar, with blue representing the SFD and orange the bar. Bar stars are mainly born in the central regions while SFD stars are mainly born outside the radius of the bar.

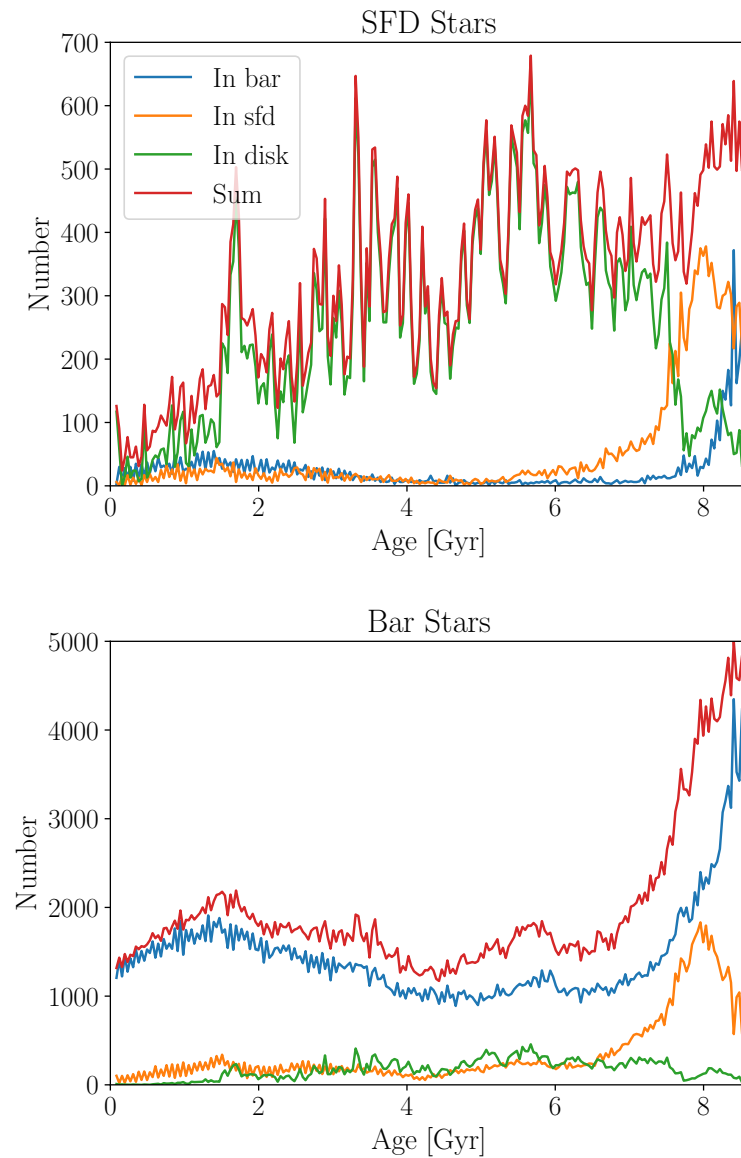


Figure 3.8: Top: the fraction of stars born after the formation of the bar in the SFD, bar and disk selected to be SFD stars at $z=0$ for galaxy 37. Red represents the total SFD stars born at that time, green the number of SFD stars born in the disk, blue the number of SFD stars born in the bar, and orange the number of SFD stars born inside the SFD region. The majority of the stars ending up in the SFD after the bar is formed come from the disk. Very few stars come from the SFD region. Bottom: the fraction of stars selected to be bar stars at $z=0$ born in the SFD, bar and disk.

evolution of the gas density within the SFD after bar formation there is a distinct lack of gas in the SFD within about 1 Gyr. This is a relatively fast process and does not match up with what I inferred from the age distribution plots, which show a gradual downturn in the age distribution. This implies that the SFD region, after the formation of the bar, is being supplemented with young stars from elsewhere in the galaxy.

Figure 3.6 shows the birth positions of stars found in the SFD at $z=0$ and born before and after the formation of the bar, for galaxy 37. Before the formation of the bar, the stars are born throughout the galaxy. After the formation of the bar there is a distinct difference: the SFD stars are born mainly in the inner ring surrounding the bar with some along the spiral arms.

No stars are born within the defined SFD regions. This explains the disparity between Figures 3.4 and 3.5. There are no stars forming within the SFD region but younger stars are coming into the SFD from the inner ring and spiral arms, which explains the gradual drop of the SFD age distribution.

Figure 3.7 shows the distribution of birth radii of SFD and bar stars born before (upper) and after (lower) the formation of the bar for galaxy 37 at the same ages as Figure 3.6. This further supports the conclusion that the SFD is being supplemented with young stars from outside the inner ring and that in the SFD star formation is suppressed. This is a trend that can be seen in all of the galaxies in the sample. For all cases, before bar formation the SFD and bar stars are coming from the same regions. However, stars ending up in the bar and SFD that form after the onset of the bar come from two different regions. SFD stars come mainly from outside the bar radius (mainly from the inner ring and the spiral arms), while bar stars are mainly born inside the bar radius with a portion coming from the spiral arms.

Figure 3.8 shows the number of stars being born in the disk, SFD and bar for galaxy 37. The top plot in Figure 3.8 shows that almost all (75.2%) of the SFD stars born after the formation of the bar are coming from the region we define as the disk, with only a small fraction (8.1%) coming from the SFD. The bar also contributes a minor fraction (16.6%) of SFD stars which may represent some of the bar stars we were not

able to remove from the SFD sample selection. At ~ 1.5 Gyr there is a drop in the age distribution which coincides with a drop in the contribution of SFD stars from the disk. This could be accounted for by the time it takes stars from the disk to migrate to the SFD region. In that case, when I take the SFD sample from the final snapshot ($z=0$) I am missing out on disk stars which would become SFD stars after this time.

The lower half of Figure 3.8 shows the number of bar stars being born in the same region defined for the top plot of the same figure. The majority (73.8%) of bar stars are born within the bar, with a small contribution (17.7%) from the disk and a negligible amount (8.6%) coming from the SFD. At late times, less than 1 Gyr, there is no contribution from the disk.

By looking at the three plots discussed in this section in conjunction with Figure 3.4 I find that before the formation of the bar the population in the SFD and bar regions come from the same regions, which is supported by the similarities of the SFD and bar age distributions. However, after the formation of the bar there is a disparity in the regions in which bar and SFD stars are born. The star formation in the SFD region is truncated quickly as gas is removed from the SFD, but young stars are being born in the disk which migrate into the SFD. To determine how the stars from the disk and ring migrate into the SFD I need to track their progression from their birth positions to the SFD region.

3.3.5 Collective dynamics

After the formation of the bar the SFD region is supplemented with young stars which are born along the inner ring and spiral arms. To determine how these stars end up in the SFD we track the progression of stars born at a lookback time of 3 Gyr to $z=0$ in Figure 3.9. The plot at 3 Gyr shows the birth positions of the SFD stars. Correlating with the results from Section 3.3.4, the stars are born mainly along the inner ring and spiral arms with very few being born in the bar and SFD. Within 300 Myr the stars begin to move along the spiral arms and inner ring. By 1.2 Gyr almost all of the stars are moving along the inner ring and are beginning to fall towards the SFD

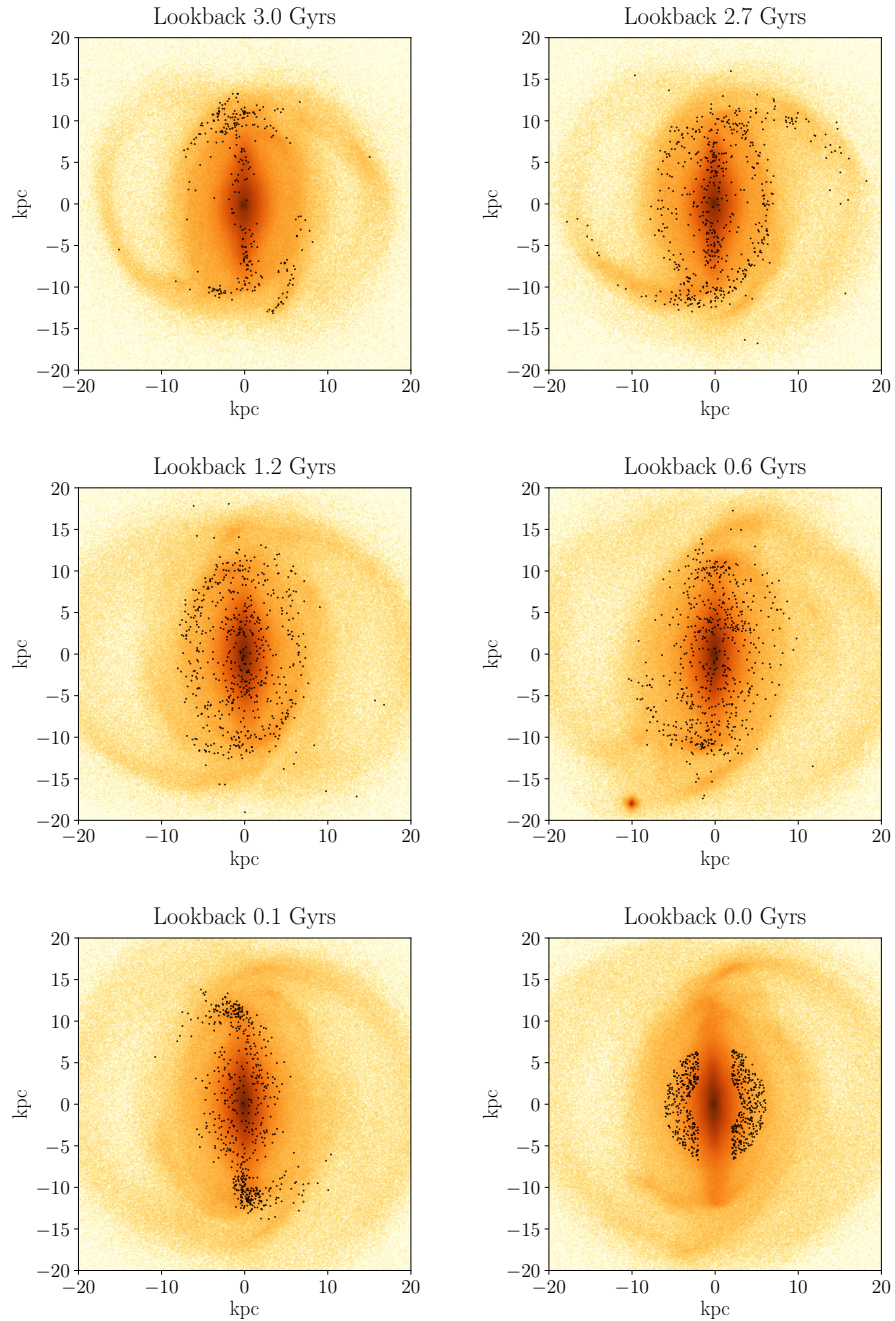


Figure 3.9: Tracking of SFD stars from their birth positions to $z=0$. Initially stars are born in the inner ring near the ends of the bar and along the spiral arms. They then move along the spiral arms and around the inner ring. Slowly stars begin to spiral from the inner ring into the SFD region. Finally the stars collect near the ends of the bar before circling back into the SFD selection region at $z=0$.

region by 600 Myr. At 100 Myr the stars are collected near the ends of the bar before they reach their selection point in the SFD regions at 0 Gyr. This implies that it takes approximately 2.4 Gyr before ring stars begin to reach the SFD region, which supports my conclusion that the reduction in SFD stars being born in the disk for the final 1.5 Gyr seen in Figure 3.8 could be a result of the time taken for disk stars to migrate to the SFD.

3.4 Discussion

3.4.1 Limitations of the simulations

A number of previous papers have explored the properties of simulated disks in the Martig et al. (2012) sample, and have found those disks to be realistic overall, when compared to a range of observational data. Most importantly for this work, Kraljic et al. (2012b) showed that the fraction of barred galaxies in the simulated sample ($\sim 70\%$) is consistent with observations in the local universe, and that the time evolution of the fraction of barred galaxies matches observations by Sheth et al. (2008) and Simmons et al. (2014). Additionally, in the simulations, bars, on average, form later in low mass galaxies, which agrees with Sheth et al. (2008). Martig et al. (2014a,b) have further shown that the vertical structure of the disks is well resolved, and that some galaxies are a good match to observations of the Milky Way.

Overall, this is a strong indication that global stellar dynamics is adequately modelled in the simulations, in spite of a spatial resolution of only 150 pc. The global distribution of gas in the central regions also appears to be consistent with observations. In particular the absence of gas within SFDs is clear in the observations of molecular gas shown by George et al. (2019). I note that a recent paper by Rosas-Guevara et al. (2019) using the IllustrisTNG100 simulation also finds rapid consumption of gas within the central regions of barred galaxies.

However, a resolution of 150 pc does not allow us to properly track the movement

of gas particles within the central regions, or to follow the formation of features like nuclear disks. The motion of gas particles along the bar is also not properly modelled, and for instance I do not see dense gas lanes along the leading edges of the bars.

Additionally, the Kennicutt-Schmidt relation used to model star formation is based solely on the local gas density, and does not account for dynamical heating from shocks halting the collapse of dense gas regions. Indeed, observations suggest that the star formation efficiency might be reduced in bars (Momose et al., 2010).

An imperfect modelling of star formation might be the reason why a majority of the simulated bars are star forming, which is not the case of bars generally in the Local Universe. Star forming bars do exist (Martin and Friedli, 1997; Verley et al., 2007), but a detailed comparison of the fraction of star-forming bars in simulations and observations (controlling for environment and mass) is beyond the scope of this work.

With all of this in consideration, the simulations might overestimate star formation in bars, but probably model SFDs adequately in terms of the global dynamics of gas and stars.

3.4.2 Potential bar dating method

For all of the galaxies in the sample, the number of young stars (born after the bar formed) drops with time for the SFD compared to the bar. In five out of the six galaxies, the time of bar formation closely coincides with a change in the sign of the “bar-SFD” residual age distribution (galaxy 82 is the exception, and with this case the residual changes sign long before the bar forms). This suggests the possibility to use the sign of the residual as an indicator of the epoch of bar formation. However, this signal appears to be very subtle, and consists in a gradual downturn in the age distribution instead of the sharp truncation assumed by James and Percival (2016, 2018) to model star formation histories in their sample of observed SFDs. This is because young stars coming from the disk are migrating to the SFD, and are “polluting” it with a young population that should not be present if only in-situ star formation happened. In the

following two subsections, I first explore the possible reasons for the strange behaviour of galaxy 82 and then discuss the usefulness of the method to date bar formation with observational data.

The unusual behaviour of galaxy 82

Galaxy 82 is the only galaxy in which the change of sign of the Bar-SFD residual does not coincide with the epoch of bar formation. Within the full sample of 33 galaxies, galaxy 82 is unique in forming a bar as recently as 2 Gyr ago - all others formed their bars no later than 4 Gyr ago. To understand whether galaxy 82's strangeness could come from having a very young bar, the simulation was run for a further 3 Gyr. I can confirm that even after 3 more Gyr, the age distributions still look different from the ones for the other simulated galaxies. Those differences are probably due to galaxy 82's very unique formation history that in turn could explain why it formed its bar so late.

At early times (10 Gyr) it consists of a central low density disk that persists throughout its evolution up until the time of bar formation. Additionally, at this time (from 10 to 9 Gyr) it undergoes the accretion of a satellite which leaves a gaseous ring surrounding the central disk.

The ring quickly undergoes fragmentation which is then followed by the formation of spiral arms. After the spiral arms have strengthened, the central regions become bar unstable leading to the formation of the bar. This varies drastically from the other evolutionary histories for the galaxies in the sample. Furthermore, there is a spatial segregation of the bar and SFD stars' birth positions well before the epoch of bar formation (with SFD stars being born at the edge of the low density disk, in the ring, and along the spiral arms while the bar stars are primarily born in the central disk), which is a feature I see only after the formation of the bar in the rest of our sample. This spatial segregation is most likely the cause of the early bar-SFD residual sign change, although what precisely leads to the segregation of the birth positions is not entirely clear.

Application to observational data

The method I propose to date bar formation in a galaxy relies on a very weak signal, which makes applying the SFD bar dating method more complex than previously suggested in James and Percival (2016, 2018). Indeed, this method relies on the accurate recovery of SFH shapes for the bar and SFD. Spectra at old ages look very similar to one another and the effect of age and metallicity can be degenerate, which will make finding a bar formation signal for early bars more challenging. Bar and SFD average ages differ by approximately 2 Gyr, which makes comparisons between the SFHs of the components for early bars difficult given the constraints stated above. Additionally, if I have overestimated the star formation efficiency of the bar in the simulations then the signal could be even weaker than anticipated.

Should a signal be found in observational data, then there is the additional problem that the bar formation time cannot be reliably determined for all simulated galaxies in the sample. Even considering that galaxy 82 may be an unusual case it can not be assumed that any signal found is directly related to bar formation. However, the SFD bar dating method could be used in conjunction with several other methods. By measuring the vertical velocity dispersion (Gadotti and de Souza, 2005) or shape of the light profiles (Kim et al., 2014) we can determine if the bars are old or young and so better constrain the region of the SFH where we would expect to see a signal. In cases where these age indicators disagree the studied galaxy could be flagged as having an unusual history.

A lower limit on the epoch of bar formation could also be defined by looking at the ages of nuclear disks (Gadotti et al., 2015), which form after the formation of the bar. Additionally, we might also be able to date bar formation by comparing the metallicities of bar and SFD stars as a function of age, due to the spatial segregation in birth positions of bar and SFD stars younger than the bar.

3.5 Summary

James and Percival (2015) first described the properties of star formation deserts, regions swept up by bars with very low levels of line emission and little recent star formation. James and Percival (2016, 2018) then proposed that the cessation of star formation in those regions was due to the formation of the bar. This would mean that finding a sharp truncation in star formation histories in SFDs could be a way to determine the epoch of bar formation.

In this chapter, I investigated the validity of these conclusions by studying the properties of SFDs using zoom-in cosmological re-simulations. From the sample of Martig et al. (2012), I chose 6 simulated disk galaxies with bar formation times ranging from 2 to 8 Gyr ago. I found that the formation of the bar does not appear to have an effect on the global star formation rate of the galaxies but affects the distribution of gas and star formation within the central regions. At $z = 0$, I found both sides of the bar regions are dominated by old stars, and that resemble the observed SFDs. However, the SFDs in the simulated galaxies actually contain stars of all ages:

- SFD stars older than the bar are born in similar regions to similarly old stars that end up in the bar.
- When the bar forms, it efficiently removes gas from the SFD on 1 Gyr timescales, which quickly truncates the local star formation.
- SFD stars younger than the bar are not formed in-situ but are born in the disk and migrate to the SFD (unlike bar stars of similar ages, which are mostly born in-situ).

If there were no radial migration of young stars from the disk to the SFD, then the age distribution of SFD stars would show a truncation within ~ 1 Gyr after the time of bar formation. However, this is not the case, and the SFD age distributions show a gradual downturn instead of a truncation, which makes recovering the epoch of bar formation more complicated than James and Percival (2016, 2018) anticipated. The

different shapes of age distributions for SFD and bar stars can provide an indication of when the bar formed, but the signal is weak and potentially hard to detect. This might still be used to date bars, especially in conjunction with other methods.

SFDs could also be used to investigate radial migration. Indeed, they are unique regions with no in-situ star formation: stars younger than the bar all come from the disk (outside of the bar radius). This can provide an uncontaminated sample of stars only affected by radial migration.

While I focused on only 6 galaxies here I found the distinct signatures of the SFD present in all the barred galaxies from the simulations presented in Martig et al. (2012). Given the analysis I have presented here and the care take to represent the range of galaxies within the original sample of 6, I would also expect that these galaxies would show similar trends.

Chapter 4

Using bar kinematics to determine the age of the bar

4.1 Introduction

In Chapter 1 Section 1.3 I described how bars can heavily influence a galaxy's evolutionary path. One way in which they do this is through their impact on stellar dynamics. While a recently formed bar has a vertical extent similar to that of the disc, as they evolve they grow thicker in the vertical direction resulting in the boxy/peanut shape associated with barred galaxies. This process can be fast (~ 1 Gyr) in the case of violent buckling, or can correspond to a gradual continual growth (Gadotti and de Souza, 2005). As such, it follows that by studying the vertical growth of the bar in comparison with the disc it may be possible to determine the formation time of the bar.

Gadotti and de Souza (2005) used precisely this concept to distinguish between recently formed and evolved bars using the face-on vertical velocity dispersion of 14 observed galaxies. They found that in recently formed bars the vertical velocity dispersion is similar to that of the galaxy disc, whereas evolved bars have a vertical velocity dispersion significantly higher than the disc (see Figure 4.1). However, in cases where the bulge is dynamically hotter than the bar the distinction between recently formed

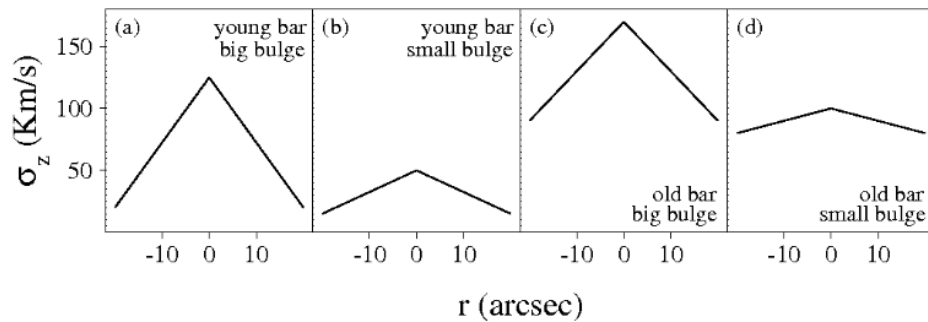


Figure 4.1: The typical radial vertical velocity profiles for recently formed and evolved bars. Recently formed bars tend to have profiles similar to the disc, while in evolved bars the vertical velocity dispersion is much higher. (a) and (c) show the effect of a dynamically hot bulge, while (b) and (d) show the profile where the bulge and bar have similar kinematics (Gadotti and de Souza, 2005).

and evolved bars is less clear. While this does not result in a quantitative measurement of bar age, it does confirm that the vertical velocity dispersion of a bar increases with its age.

It is clear that bars can have significant effects on the kinematics of the central regions of galaxies. While Gadotti and de Souza (2005) showed that kinematics could be used to distinguish between recently formed and evolved bars the question remains of whether this can be taken further to refine bar age estimates. In this chapter I build on the work in Gadotti and de Souza (2005) by first exploring how the profile of the vertical velocity dispersion of the bar changes over time using zoom-in cosmological resimulations. I then present a new method I have developed for recovering the formation time of the bar and investigating the mechanisms behind it. I explore the feasibility of this method on observational data before finally summarising this chapter.

The work presented in this chapter is from a paper in preparation (Donohoe-Keyes et al. in-prep).

4.2 Sample selection

From the sample of 33 zoom-in cosmological re-simulations presented in Martig et al. (2012), I selected 15 galaxies which showed clear bars, this includes the 6 galaxies selected for the analysis presented in Chapter 3. This barred galaxy sample has a wide range of masses, star formation histories, and bar lengths, strengths and formation times. This allows for the exploration of the kinematics of a diverse range of bars. A brief description of the simulation technique is given in Chapter 2.

4.2.1 Simulations of isolated galaxies

To test the robustness of my results, I also use three simulations of isolated galaxies. Two of them are collisionless simulations, first presented in Fragkoudi et al. (2017), which I will refer to in the text as *isolated:N-body A* and *isolated:N-body B*, the third simulation is a hydrodynamical simulation run with RAMSES which I will refer to as *isolated:N-body+gas*. The relevant details of these simulations are highlighted in Section 2.2.

4.3 A new method to determine the ages of bars

Gadotti and de Souza (2005) proposed that the difference between the σ_{los} of the bar and disk could be used to distinguish between recently formed and evolved bars. They demonstrated that bars with σ_{los} profiles similar to their disks are recently formed while those that have a σ_{los} much removed from the disk are likely more evolved bars. However, bars with significant central bulge masses also displayed large differences between their σ_{los} values in the bar and disk even when recently formed. In this section I use numerical simulations to explore how the shape of the velocity dispersion of the bar evolves over time and how a key feature within the bar's velocity dispersion can provide a quantitative age for the bar.

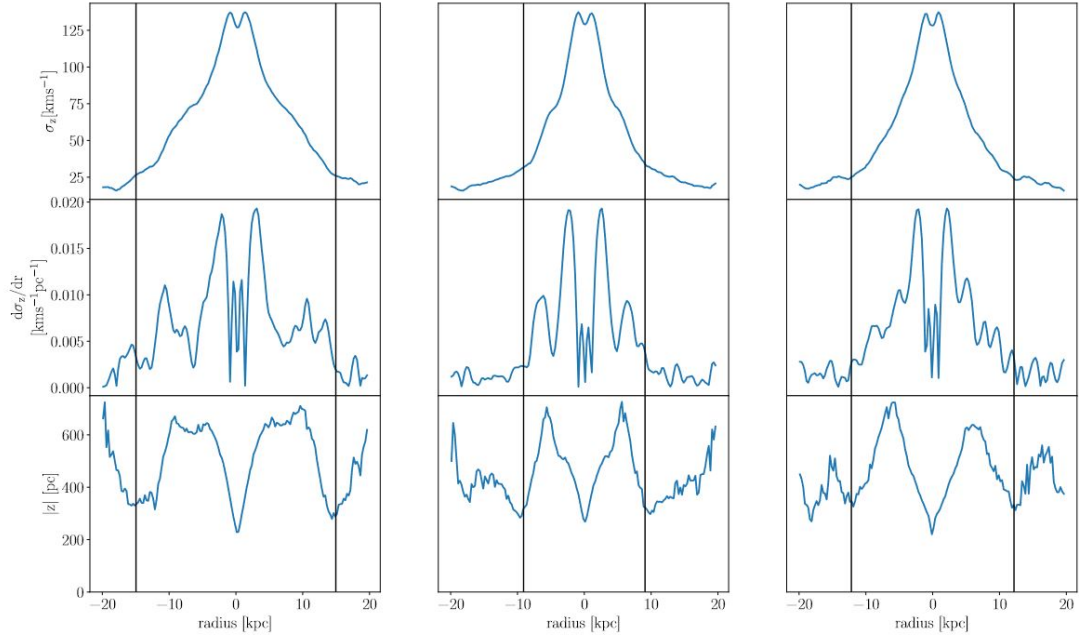


Figure 4.2: Here I show the diversity in kinematic profiles for the main sample. Each column shows the σ_z , the first derivative of σ_z and $|z|$ for a different galaxy. The vertical black lines show the radial position for the bar ends.

4.3.1 Velocity dispersion profiles in barred galaxies

To understand how the velocity dispersion changes over time I will first describe how I extract the vertical velocity dispersion along the bar for multiple snapshots. I then explain what features can be seen in the velocity dispersion and how they compare with other properties of the bar using three different simulated galaxies as examples.

In observations we can recover all of the kinematical information on a object by fitting a model to its line-of-sight velocity distribution (LOSVD). The now universally accepted model developed by van der Marel and Franx (1993) describes the LOSVD as a summation of orthogonal functions - the Gauss-Hermite series - where each moment describes a different parameter. The 0th, 1st, 2nd, 3rd and 4th moments correspond to the surface brightness (μ), mean velocity (V), velocity dispersion (σ), skewness (h_3) and kurtosis (h_4) respectively. To replicate this method in simulations we must first bin the particles so that we can construct a LOSVD. I group particles into bins (see Figure 4.4) of $1 \times 0.25 \times 5$ kpc ($w \times l \times h$) along the bar major axis creating a single local velocity distribution associated with each bin. By then using the Gauss-Hermite series

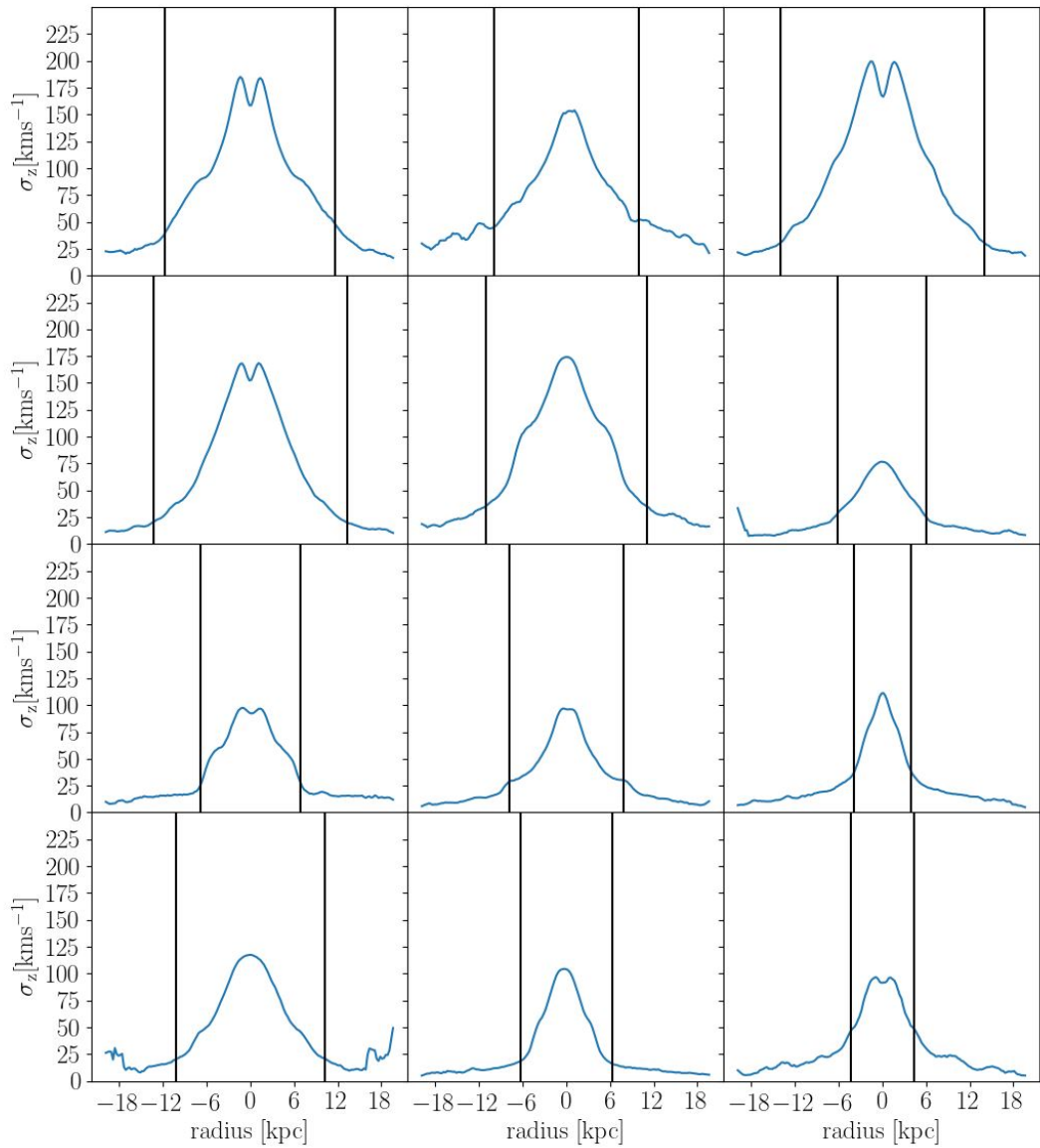


Figure 4.3: Here I show the σ_z profiles for the rest of the sample, following on from Figure 4.2. Each subplot shows the σ_z profile along the bar for a different galaxy. The vertical black lines show the radial position for the bar ends.

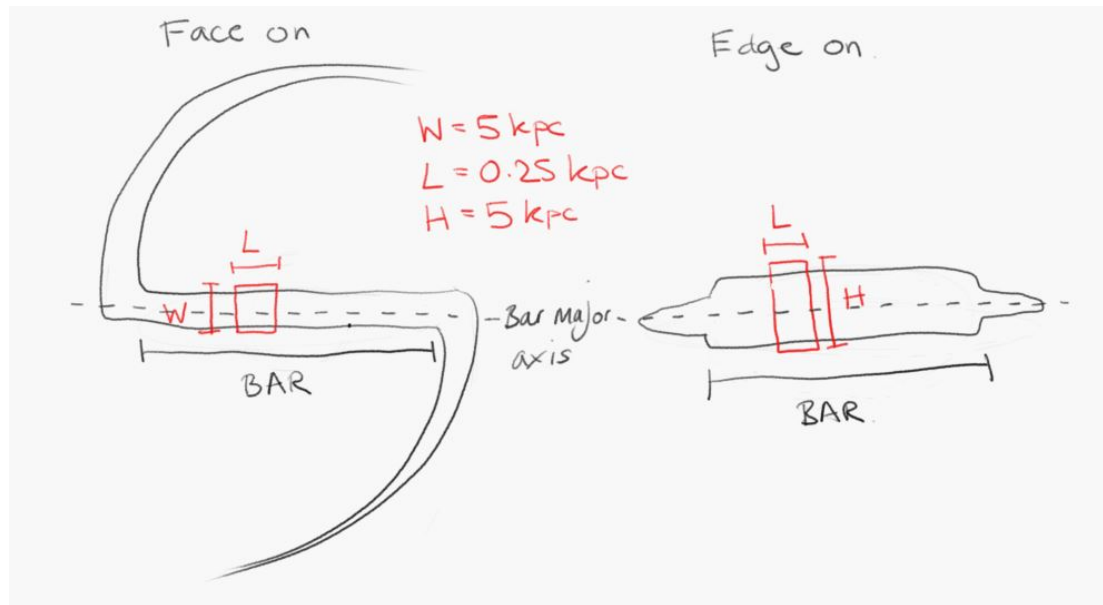


Figure 4.4: Here I show a cartoon representation of the bin dimensions. The values for width, length and height are given as $W = 1$ kpc, $L = 0.25$ kpc and $H = 5$ kpc. These bins are repeated along the bar major axis extending out to the full simulation size of the box ± 20 kpc.

I can recover each of the parameters described above. In this case while I do recover all of the moments described I focus on only the 2nd moment, σ , which describes the velocity dispersion of each bin. I note that for the simulated galaxies I refer to σ_z not σ_{los} , this is because in simulations we can orientate the galaxy precisely face-on and so can be confident in our extraction of σ in the z -plane. However, in observations determining the orientation of a galaxy is not straight forward and in many cases a galaxy is inclined to some degree. Attempts can be made to correct for this inclination using de-projection but this requires assumptions about the galaxies shape and can induce large errors. Thus when observing galaxies σ_{los} is used to account for the fact that we are, more often than not, observing a galaxy at some degree of inclination.

In Figure 4.2 I present σ_z (top row), the first derivative of σ_z with respect to radius (middle row) and $|z|$ which gives the median height of particles in the z plane (bottom row) for a single time step. Each column represents a different galaxy selected from the sample defined in Section 4.2 with the bar length marked by the black lines. Galaxies were chosen to show the variety of σ_z profiles seen in the sample. In Figure 4.3 I show only the σ_z profiles for the rest of the sample.

Looking at the σ_z (top row) for each of the galaxies there is a range of profile shapes. In the left-hand case the profile shows a central peak with a steep gradient that then plateaus into a distinct shoulder-like feature as the bar's radius increases before once again decreasing with a slightly shallower gradient out to the bar ends. The central case shows a similar behaviour, however the shoulder-like feature is less distinct than in the left-hand case. Overall this profile is also much broader than the previous case. In the right-hand case the profile is more peaked with no noticeable shoulder-like feature present. This varied range in profiles is also apparent in other simulations (Debattista et al., 2005; Iannuzzi and Athanassoula, 2015) as well as observational studies of face-on bar kinematics (Seidel et al., 2015). In all of the vertical velocity dispersion profiles shown, there is a central σ -drop indicating that the central regions of these galaxies contain a dynamically cool component such as a nuclear disc (Wozniak and Champavert, 2006; Emsellem et al., 2001; Márquez et al., 2003; Emsellem, 2006; Peletier et al., 2007). Additionally, in all of the profiles there is a transition to a shallower gradient associated with transition between the bar and the dynamically cooler disc.

By taking the first derivative of σ_z with respect to radius (middle row) I explore further the different gradient transitions seen in the σ_z profiles. In all cases I find a central minimum bordered by two clear peaks. These peaks are symmetrical with respect to the bar radius and, in the cases where the shoulder-like feature is visible in the σ_z profile, lie close to where the shoulder-like feature begins. In the left-hand and central plots where the shoulder-like feature is clearly visible there is an additional peak that lies just outside the shoulder-like feature's radius. In the right-hand plot there is a small plateau between the symmetrical peaks and the bar ends, which may correspond to the edge of a gradient change similar to the shoulder-like feature seen in the other two cases, but if there is a shoulder-like feature present in the σ_z profile it is very weak and not easily visible.

In previous work, Debattista et al. (2005) found no clear link between features in the σ_z profile and the peanut suggesting that if there is some signature in the σ_z profile it is buried within the noise. To determine if the peaks I find in the first derivative are associated with the peanut (the buckled region of the bar), I present $|z|$ in the bottom

panel of Figure 4.2 for each of these examples. The peanut structure becomes clearly visible as an M-shaped structure in the $|z|$ profiles. In all cases the σ_z derivative peaks lie well within the radial bounds of the peanut structure described in $|z|$. While this does indicate that the peaks could be the result of the more dynamically hot component which makes up the peanut structure, they do not seem to correspond directly to the features seen in the $|z|$ profiles. However, for the two galaxies which show prominent shoulder-like features there is a correlation with the position of the second peak and the extent of the peanut structure as seen in the $|z|$ profiles but a more detailed analysis of this correlation is beyond the scope of this paper.

Overall, while I do find a variety of σ_z profiles I find a common symmetrical peak feature in the first derivative of σ_z . The radius of this peak feature lies within the buckled region of the bar which contains an older dynamically hotter stellar component. In the next section I explore the evolution of this peak feature over time to determine if it can be used to trace the evolution of the bar.

4.3.2 Tracing σ_z through time

In the previous section I showed the variety of different profiles seen in σ_z and found that they all displayed a common symmetrical peak feature in the first derivative. In this section I will explore how the σ_z profile and the symmetrical peak features change with time.

In Figure 4.5 I present the evolution of σ_z and the first derivative over 3 snapshots. Each snapshot represents a different time in the evolution of this galaxy with the early times soon after bar formation shown in the top two panels and the final snapshot representing the current epoch in the bottom two panels. I mark out the radius of the bar with black vertical lines and the position of the derivative peaks with the red vertical lines. The growth in height of σ_z can be seen progressing from early to late times with the σ_z in central regions of the bar growing from 100 - 140 kms^{-1} from formation to the current epoch. Also clearly evident is the effect of bar growth. At early times the bar ends lie along the slope of the central σ_z peak; as the bar lengthens

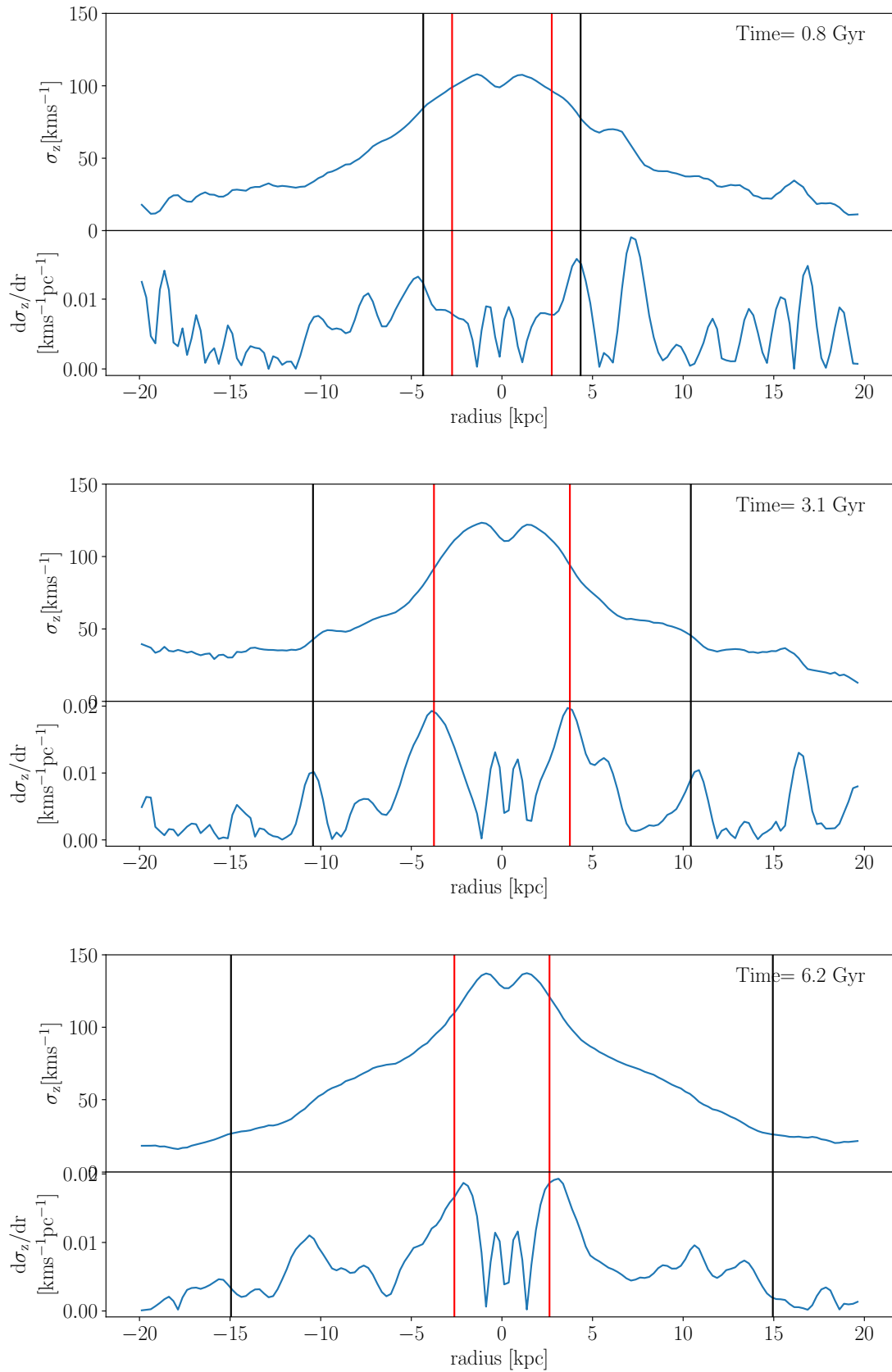


Figure 4.5: The σ_z evolution for bar major axis of one galaxy over time. Each plot shows both the σ_z and the first derivative of σ_z at a different time step. The peak position in the derivative (red) and bar length (black) is marked for each plot.

the ends of the bar become dynamically colder similar to what is seen in the disc. This gives us an overall change in bar end σ_z from $80 - 30 \text{ km s}^{-1}$ over the bar's evolution.

There is not only a change in the values of σ_z within the bar but also a change in the shape of the σ_z profile. I noted in the previous section that there are a variety of profiles and one of the distinct profile shapes showed a shoulder-like feature. This feature was also evident in the first derivative through symmetrical peaks and in the cases where the shoulder-like features were strong there are multiple peaks.

In Figure 4.5 I show the evolution of a simulated galaxy with strong shoulder-like features. At early times, where the bar has just formed, there is no shoulder-like feature visible in σ_z and this is reflected in the first derivative with no clear peak features being present within the bar's radius. Although I do note that when looking at the full extent of the σ_z profile into the disc there is a broader peak feature that extends beyond the bar's radius. As the bar continues to evolve and the difference between central and bar end σ_z values diverge and the shoulder-like feature begins to develop. In the central panels there is a weak shoulder-like feature in the σ_z profile and clear symmetrical peaks in the first derivative. In the bottom plots I show the σ_z profile along with the first derivative for the final epoch. In the σ_z profile there is a strong shoulder-like feature and this is reflected in the first derivative by strong central symmetrical peaks and a secondary set of peaks that lie closer to the bar ends. Overall I find that as the bar evolves these shoulder-like features develop and strengthen, and that this is reflected in the derivative where the characteristic peak features appear and become more prominent as the bar evolves.

To determine the relationship between the age of the bar and this shoulder-like feature, I calculate a variable I shall refer to as $\Delta\sigma_z$. To calculate $\Delta\sigma_z$ I determine the value of σ_z at the location of the central symmetrical peaks I find in the derivative. I then take the averaged value of σ_z from both of these peaks. I then subtract from this the value of σ_z averaged over a 1 kpc range at the bar ends. By averaging the σ_z at the bar ends over the additional 1 kpc I account for the variability in bar length found due to the connection and dis-connection of the spiral arms between snapshots. I calculated this $\Delta\sigma_z$ value in all snapshots from the time of bar formation to the present epoch.

In Figure 4.6 I show the time evolution of $\Delta\sigma_z$ from bar formation to present epoch for one galaxy. The time of bar formation starts at $t=0$ Gyr. There is a clear monotonic increase in the $\Delta\sigma_z$ value with age. At early times when the strength of the shoulder-like feature is small I recover small values for $\Delta\sigma_z$ and as the age of the bar increases so does the $\Delta\sigma_z$ value. However, there are small variations in the slope of this monotonic increase which closely follows the shape of the unsmoothed evolution of bar length with time shown in Figure 2.2. This indicates that this $\Delta\sigma_z$ might be closely linked with bar growth as well as bar age (see Section 4.4). It is clear that the deviations that seen in the bar growth can strongly affect the $\Delta\sigma_z$ value recovered and while taking a σ_z for the bar ends averaged over 1 kpc lessens the effect of the oscillating bar length it still impacts the $\Delta\sigma_z$ value. I choose to calculate $\Delta\sigma_z$ using the smoothed bar length to mitigate this oscillation effect in further plots. However, the relation between age and $\Delta\sigma_z$ presents us with a promising avenue for the recovery of bar ages. In the next section I will explore the time evolution of $\Delta\sigma_z$ for all of the galaxies in the sample.

4.3.3 $\Delta\sigma_z$ as an age indicator

In the previous section I explored how the σ_z profile of one simulated galaxy evolves over time. Using features recovered in the first derivative of this profile I calculated a parameter I call $\Delta\sigma_z$ that shows a monotonic increase with bar age. In this section I will calculate the $\Delta\sigma_z$ values over the evolution of all the galaxies in the sample to determine if the monotonic increase found between $\Delta\sigma_z$ and bar age is robust.

In Figure 4.7 I present the $\Delta\sigma_z$ values for the full sample defined in Section 4.2. The blue band represents the inter-quartile range and the dark blue line shows the median for this sample. In all cases $t=0$ represents the time of bar formation and I follow the evolution of the bar up to the current epoch. The relationship between $\Delta\sigma_z$ and age described in the previous section roughly holds for all of the galaxies in this sample. I find a clear monotonic increase in $\Delta\sigma_z$ with bar age. Although it should be noted that the confidence interval is broad, there is clearly a robust difference between young and old bars. However, there are also fewer bars at older ages and as such there is a

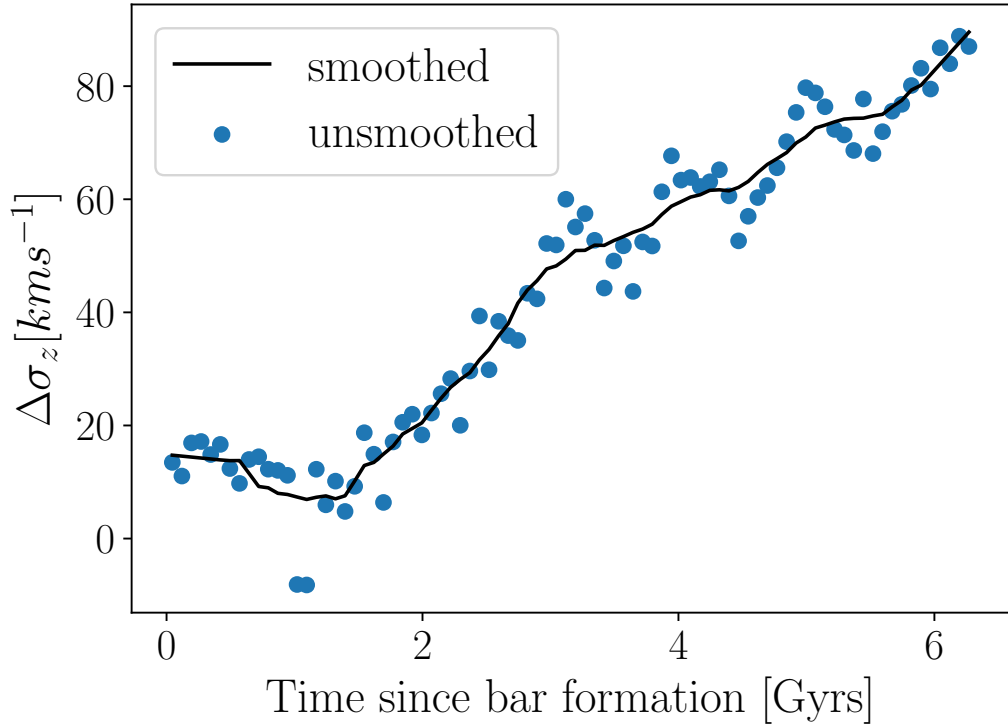


Figure 4.6: $\Delta\sigma_z$ against time for one galaxy. The points show $\Delta\sigma_z$ calculated using the unsmoothed bar lengths, with the line showing the $\Delta\sigma_z$ calculated using the smoothed bar lengths.

saturation in the case of the older bars. Despite this, it appears clear that the $\Delta\sigma_z$ value recovered from the σ_z profile can be used as an indicator for bar age.

As a secondary comparison, I perform the former analysis on the three isolated galaxies described in Section 4.2.1. I show the $\Delta\sigma_z$ values over the evolution of the bar from the time of bar formation in Figure 4.7 as three coloured lines. The red line shows the isolated:N-body+gas simulation while the yellow and purple show the isolated:N-body A and isolated:N-body B simulations respectively. In all cases I find the same monotonic increase in $\Delta\sigma_z$ with bar age. This further proves the robustness of using $\Delta\sigma_z$ as a bar age indicator. Additionally, with the trend being apparent even in collisionless systems it indicates that the relation between $\Delta\sigma_z$ and age is likely to be governed by the stellar dynamics of the bar and not a result of gas dynamics or star formation.

While global trends in all the galaxies in the samples show the monotonic increase in

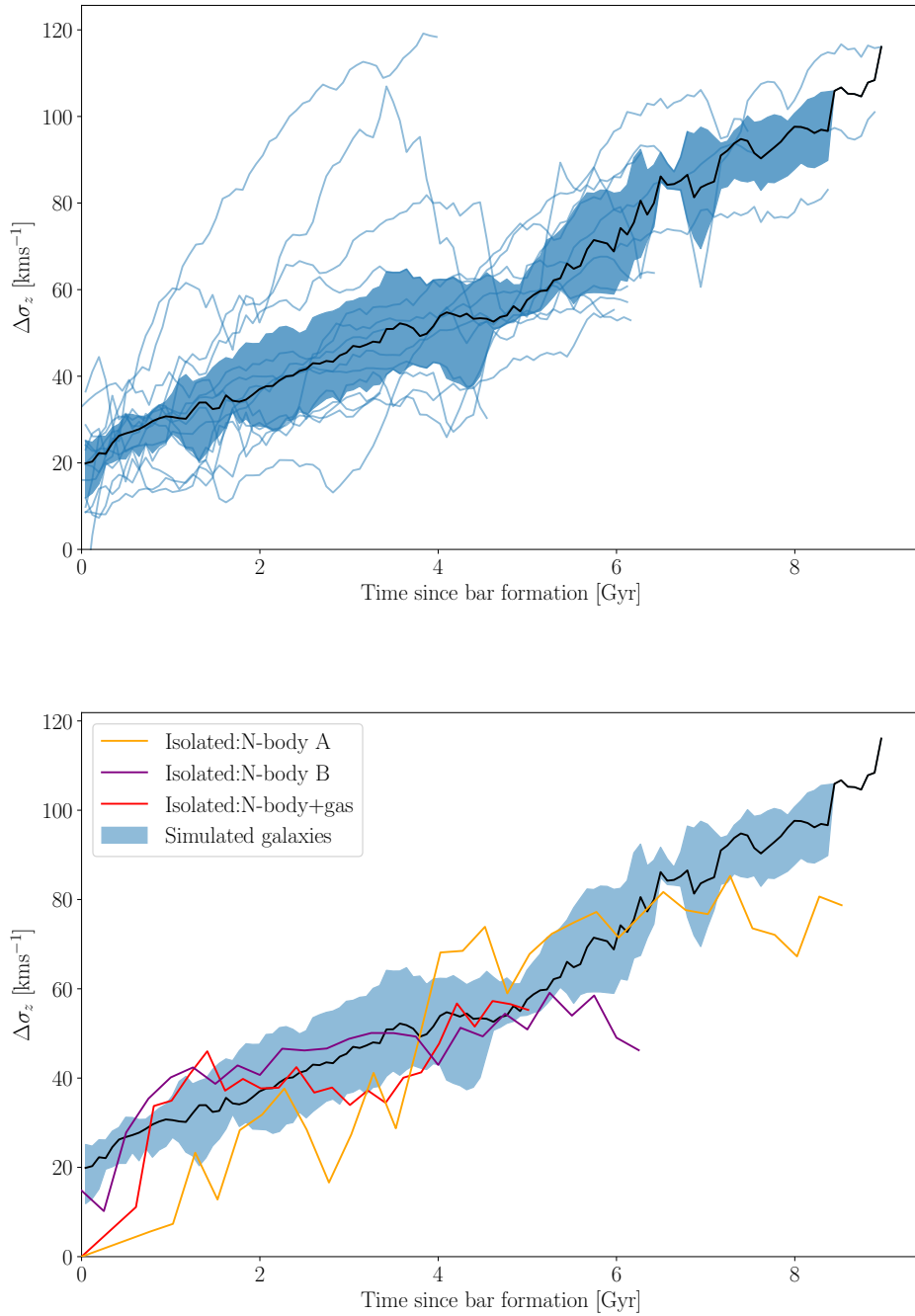


Figure 4.7: Top: $\Delta\sigma_z$ plotted against time since bar formation for all the galaxies in the main sample. The lines (light blue) show $\Delta\sigma_z$ for each individual galaxy. The filled region (blue) shows the inter-quartile range with the black line showing the median. Bottom: $\Delta\sigma_z$ of the isolated:N-body A (orange), isolated:N-body B (purple) and isolated:N-body+gas (red) plotted in comparison to the inter-quartile range of the main sample (blue filled region).

$\Delta\sigma_z$ with age, I do find deviations from the trend shown in Figure 4.7. I found three galaxies in the original sample that showed higher than expected $\Delta\sigma_z$ values when compared to the global trend. These galaxies all had higher central masses than the general sample although they did not show indications of classical-like bulges. However, all had experienced mergers close to the time of bar formation making up 2-10% of the host galaxy's mass. These mergers serve to elevate the $\Delta\sigma_z$ values recovered, however they still show a monotonic increase with age if elevated above the norm for the sample.

Overall I confirm that the trend seen in the previous section applies to all of the galaxies in the sample. I also confirm this trend in three other simulations, two of which are collisionless which indicates that the underlying cause contributing to the monotonic trend found is governed by stellar dynamics. This is even more evident when considering how large mergers cause an elevation in this trend as they can substantially alter the underlying dynamics of a galaxy. In the next section I will explore the underlying mechanisms that are causing the $\Delta\sigma_z$ increase with age.

4.4 An explanation for the growth of $\Delta\sigma_z$ with time

In the previous section I demonstrated a relation between $\Delta\sigma_z$ and bar age. In this section I will explore the two possible mechanisms that underlie this relation. One mechanism is kinematic thickening caused by internal instabilities or vertical heating. The other mechanism is bar lengthening which comes from defining $\Delta\sigma_z$ as the difference in velocity dispersion at the characteristic radius and the ends of the bar. When the bar lengthens the ends of the bar move further into the disk where σ_z is lower. I will describe how each of these mechanisms influence $\Delta\sigma_z$ and the test I have developed to determine which mechanism is dominant for the galaxies in this sample.

To differentiate between the two mechanisms I must first describe how they influence $\Delta\sigma_z$. Kinematic thickening can occur in two ways: the bar can buckle through internal instabilities causing a significant and sudden distortion out of the plane, or the process

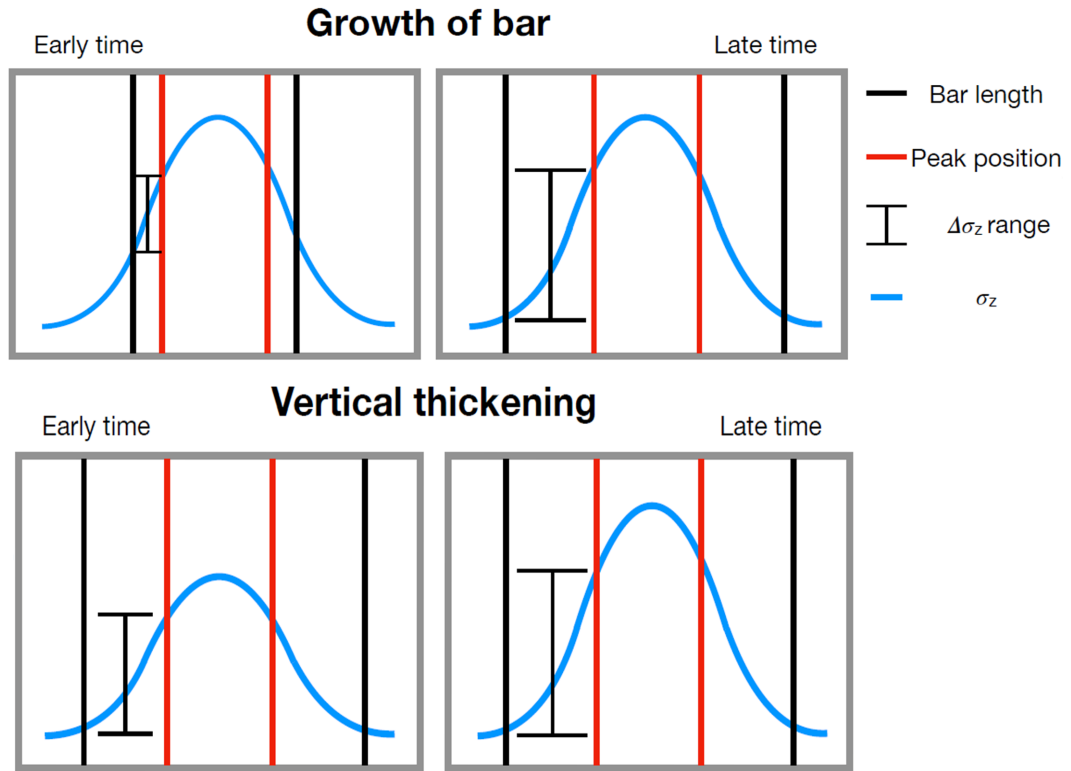


Figure 4.8: cartoon showing the two main factors affecting change in σ_z . The left hand side of each cartoon shows recently after bar formation, while the right hand side shows times much later than bar formation. Top: An idealised cartoon of the increase in $\Delta\sigma_z$ from the growth in length of the bar. Bottom: An idealised cartoon of the increase in $\Delta\sigma_z$ from the vertical thickening of the bar.

can be gradual, vertically heating the bar over time. In the bottom panels of Figure 4.8 I present an idealised scenario affected only by kinematic thickening. The thickening causes a change in height of the σ_z profile, this change causes an increase in $\Delta\sigma_z$.

However, $\Delta\sigma_z$ can also be increased via bar lengthening. In the top panels of Figure 4.8 I show the idealised scenario for this case. With no intrinsic change in the σ_z profile bar lengthening pushes apart the reference points for calculating $\Delta\sigma_z$.

In any galaxy either or indeed both mechanisms can be happening. To determine which mechanism influences the $\Delta\sigma_z$ relation I developed the following test: I fix the bar length and peak position at their final distances in kpc from the galaxy center and re-calculate $\Delta\sigma_z$ through time. By choosing to fix these reference points I eliminate any influence of bar lengthening on $\Delta\sigma_z$. In Figure 4.9 I show what we would see for each idealised case. If the dominant mechanism is kinematic thickening the test

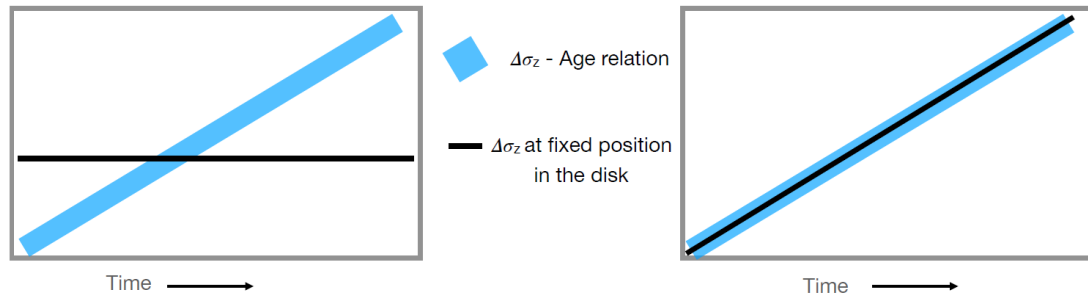


Figure 4.9: A cartoon showing what we would see if lengthening (left) or vertical thickening (right) is the dominant cause of $\Delta\sigma_z$.

should reproduce the $\Delta\sigma_z$ -age relation, increasing with time. If, instead, the dominant mechanism is bar lengthening the test should show no increase with time. No real galaxy will conform to these idealised cases but by applying this test I can determine how the two mechanisms influence $\Delta\sigma_z$.

The results of this test fell into three categories represented in Figure 4.10. In the first category bar lengthening dominates. In this category I found 2 galaxies. In the second category kinematic thickening is the dominant influence. I found 4 of the 15 galaxies in the sample fell into this category. In the final category both mechanisms occur but they dominate at different times. In this category I found 7 galaxies. In all 7 of these galaxies, bar lengthening initially dominates but then kinematic thickening takes over. The transition between which mechanism is influencing $\Delta\sigma_z$ always occurs close to the buckling time. Buckling marks a dramatic change in the structure of the bar by causing a significant vertical distortion of its stellar distribution and an increase in the vertical velocity dispersion. The correlation between the test and $\Delta\sigma_z$ seen in the kinematic thickening regime post bar buckling implies that the peak position lies within the buckled region which continues to thicken throughout the bar's subsequent evolution.

The two mechanisms that dominate the evolution of $\Delta\sigma_z$ are intrinsically linked to both the structural and dynamical evolution of the bar. The first mechanism, bar lengthening, dominates initially with bar buckling marking the time of transition into the second mechanism where kinematic thickening dominates. This makes $\Delta\sigma_z$ a powerful tracer of bar growth, being both a property solely of the bar and constrained entirely by the

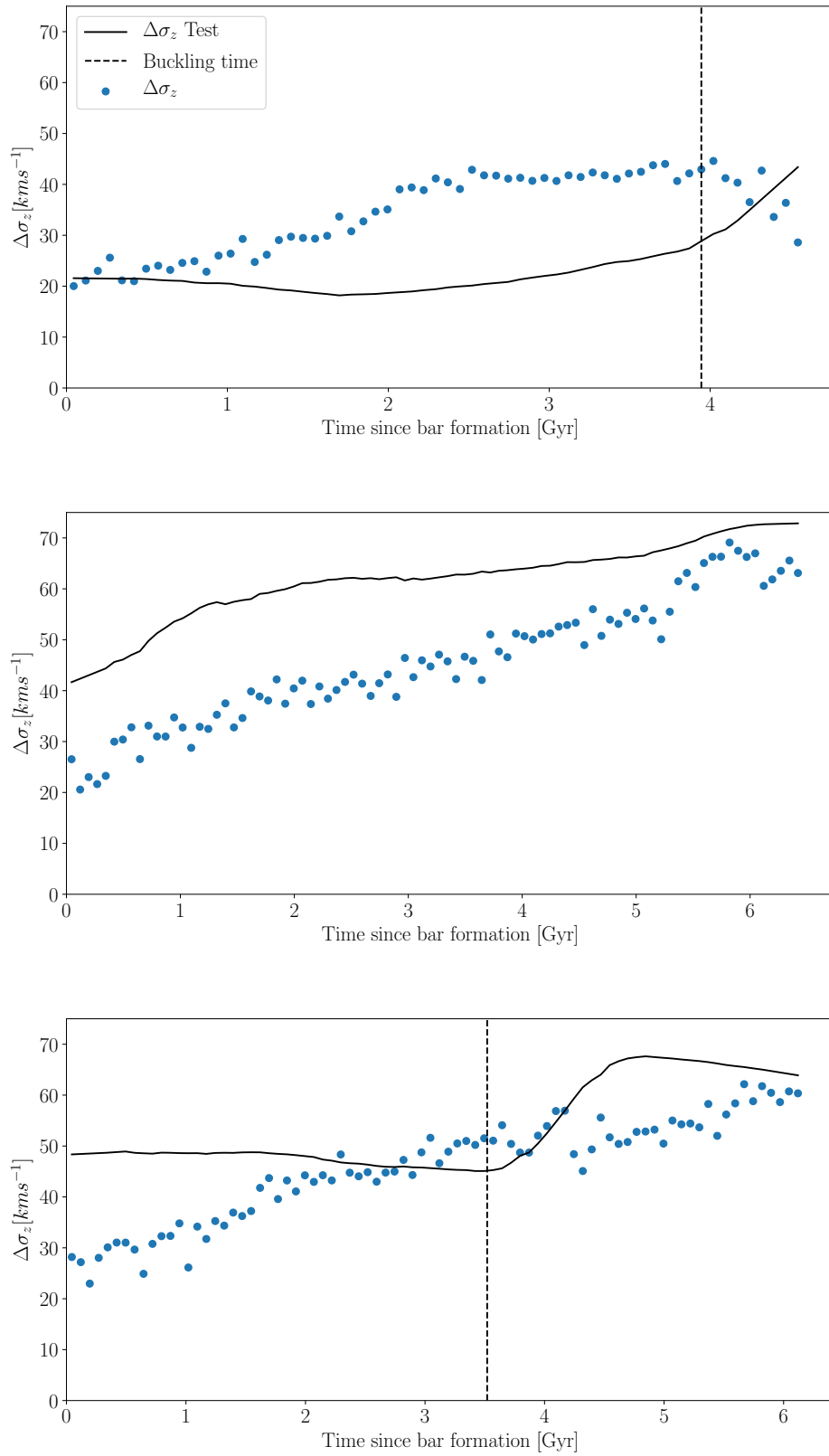


Figure 4.10: Example of galaxies where $\Delta\sigma_z$ is dominated by bar lengthening (top), kinematic thickening (middle) and a combination of both with bar lengthening dominated first (bottom).

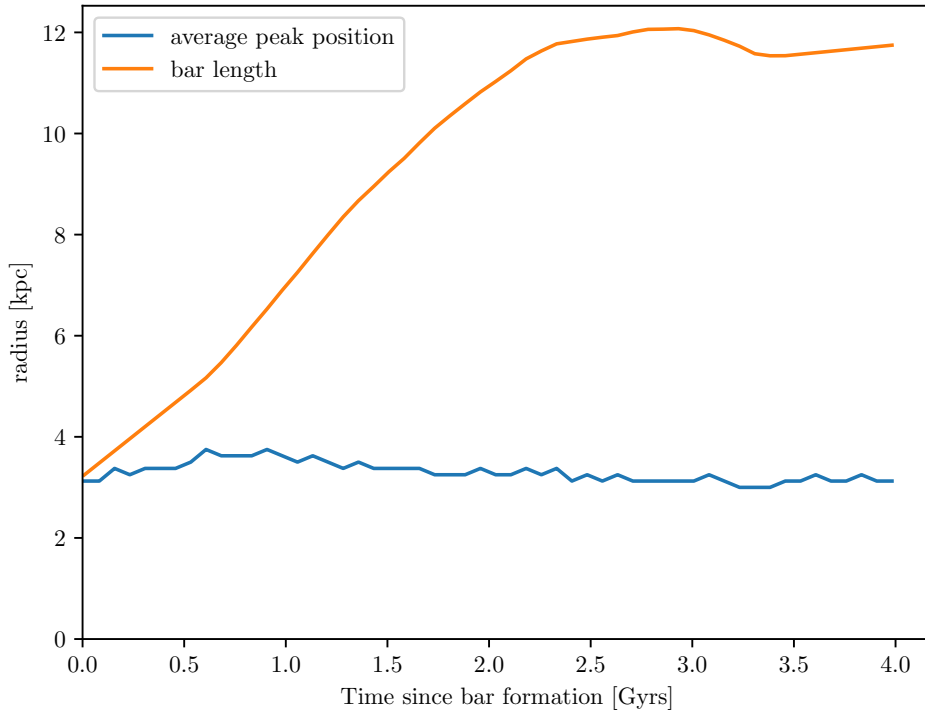


Figure 4.11: The average peak position (orange) and bar length (blue) for one galaxy through time. The peak position remains remarkably stable and lies close to the initial bar length.

bar's evolution.

4.5 Peak positions as an indicator for initial bar length

In the previous section I established the two mechanisms underlying the growth of $\Delta\sigma_z$ with time as kinematic thickening and bar lengthening. I now look in more detail at the characteristic position, which I introduced in Section 4.3 as the peak in the radial slope of the velocity dispersion, used to define $\Delta\sigma_z$. I will see how this radius, which I refer to as the peak radius, changes as a function of time and relates to properties of the bar.

To start this discussion I will look at the evolution of the peak radius with time for one galaxy. In Figure 4.11 I show the time evolution of bar length (orange) and peak radius (blue). While the bar length increases over the full 4 Gyr lifetime of this bar, the peak

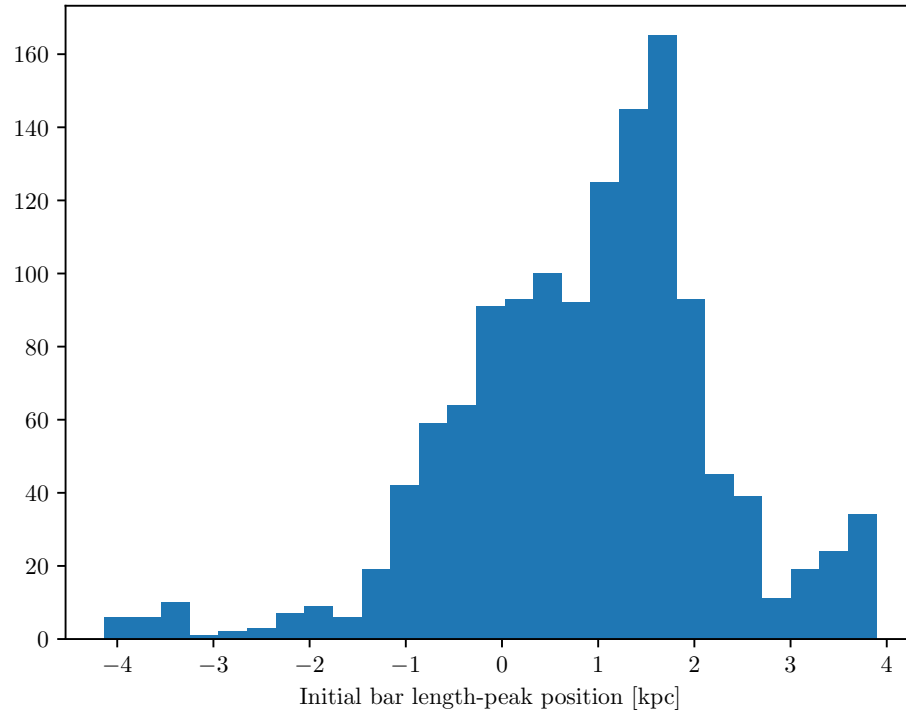


Figure 4.12: A histogram of the difference between the initial bar length and peak position for each snapshot of all the galaxies in the main sample.

radius remains remarkably stable. Of particular note is the similarity of the peak radius with the initial length of the bar. When I applied this analysis across the full sample I found a similar scenario: while the bar length increases the peak radius remains stable. In some of the galaxies there are deviations in the peak radius which occur at similar times to bar buckling. Additionally, while I find that the peak positions across the full sample are similar to the initial bar length there are some deviations from this trend.

In Figure 4.12 I present a histogram of the difference between the initial bar length and the peak radius for each snapshot across the full sample. On average the peak radius is 1.5 kpc shorter than the initial bar length however, I do see differences as great as ± 4 kpc for a handful of snapshots. Despite this, the majority of the sample lie within the 0-2 kpc difference range. This suggest that the peak radius could be used as an estimate for the initial length of the bar which, combined with a bar age, can allow for estimates on bar growth. The position of the peak radius and its association with the initial bar

length indicates that the peak in the radial slope of the velocity dispersion could be related to a change in orbital structure between initial and evolved bar. Although this presents a promising avenue for determining the rate of bar growth, exploring it further is beyond the scope of this thesis.

4.6 Application to observations

Thus far I have discussed this work in a theoretical context with the application to observations in mind. In this section I will explore the effects of changing bin widths and inclination on the $\Delta\sigma_z$ -age relation. I will then apply the method to an observational example, recovering a bar age.

4.6.1 Effect of spatial resolution

In observations one of the key limitations impacting data is the spatial resolution which we can recover using an instrument. Current large IFU (integral field unit) surveys such as MaNGA (Bundy et al., 2015), CALIFA (Sánchez et al., 2012) and SAMI (Bryant et al., 2015) can reach spatial resolutions down to 1 kpc which is much larger than the 250pc resolution I have been using in our theoretical study of $\Delta\sigma_z$. In this section I aim to understand how the $\Delta\sigma_z$ -age relation could be affected by lower resolutions more inline with current IFU surveys.

In the top panel of Figure 4.13 I show the σ_z profile of one simulated galaxy from the sample for 4 different bin widths 250, 500, 750 and 1000 pc. In all cases I do not see much deviation between the σ_z profiles over the range of bin widths. All show a central peak with a σ -drop and the shoulder-like features as described in Section 4.3.1. Unsurprisingly, there is a smoothing effect when moving to a larger bin width with the 250pc profile showing more noise than the 1000pc profile which is the smoothest.

In the bottom panel I present the first derivative of these σ_z profiles. In the first derivative I see a clearer deviation between the different bin widths. While the general trend

of two central symmetrical peaks remains similar, there is a distinct difference between the first derivative from the finest binning (250pc) to the broadest (1000 pc). At the finest binning there is significant noise. Additionally, at this resolution I also find two very clear and thin central peaks associated with the σ -drop feature like those seen in Figure 4.2. At lower resolutions these thin central peaks are completely smoothed away. This smoothing at lower resolutions is also apparent in the peak profiles themselves, as they become smoother and less prominent at larger bin widths. This also results in the position of the derivative peaks being offset at larger bins. As the bin width increases the position of the peak also increases, moving to larger radii.

The relation between $\Delta\sigma_z$ and age, and the recovery of the initial bar lengths rely on the accurate recovery of the peak positions. In Figure 4.13 I show that the peak position changes over the range of bin widths. As bin width increases the peak position (and hence initial bar length estimate) also increases. This increase averages to a +1 kpc difference between the smallest and largest bin width across the sample. Since $\Delta\sigma_z$ also relies on the peak position this translates to a -25 km s^{-1} average difference in $\Delta\sigma_z$ between the smallest and largest bin widths. When comparing with the $\Delta\sigma_z$ -age relation I recovered for the 250 pc bin width this would result in an underestimate of the bars age with an over estimate for the bars initial length. However, at all resolutions the peak feature can still be recovered as it relies more on the general shape of the σ_z profile and the shoulder-like features which remain present even with increasing bin width.

It is clear that changing the spatial resolution will affect the recovery of both bar ages and initial bar lengths using this method, with lower resolutions (larger bin widths) resulting in an underestimate in bar ages and an over estimate in initial bar lengths. However, I do find that the ages and initial bar lengths change consistently across bin widths. $\Delta\sigma_z$ decreases by an average 25 km s^{-1} when comparing between 250pc and 1000pc bin widths, as such while changing the spatial resolution would affect the recovered age for the bar it can be accounted for by adding 25 km s^{-1} to the recovered $\Delta\sigma_z$ when determining bar ages using lower resolution data. Additionally, the relation could be re-calibrated for different bin widths which would allow for a more accurate

recovery of bar ages specific to the resolution of the observational data the method is being applied to.

4.6.2 Effect of inclination

In the previous section I found that while the spatial resolution affects the recovery of $\Delta\sigma_z$ this change is small and consistent allowing us to use a correction value of $+25 \text{ kms}^{-1}$ when applying the method to resolutions of 1000pc. Another key limitation in observational data is the inclination of the observed galaxy. In my analysis so far I have only looked at recovering $\Delta\sigma_z$ with the galaxy orientated face on. In reality, however, galaxies are observed in many different inclinations hence only allowing us to recover a σ_{los} . In this section I will explore how changing the inclination of the galaxy effects the recovery of a $\Delta\sigma$ value.

In Figure 4.14 I overlay the $\Delta\sigma_{los}$ values for one galaxy at multiple inclinations with the galaxy rotated about the y-axis such that at 90° the bar is viewed edge-on. I find that there is little difference in the $\Delta\sigma_{los}$ values recovered for inclinations up to 20° . At 45° the $\Delta\sigma_{los}$ I recover is lower than expected but still within the range of expected values. At the highest inclinations (75° - 90°) there is a more significant change in the recovered $\Delta\sigma_{los}$ with values falling at the lower limits of the $\Delta\sigma_z$ -age relation found from the simulations.

In Figure 4.15 I repeat the same process as described for Figure 4.14 but rotate about the x-axis such that the bar is face-on at 0° and would be end-on at 90° . Much like with the rotation about the y-axis at inclinations up to 20° I find that there is little difference in the recovered $\Delta\sigma_{los}$. However at higher inclinations the difference in the recovered $\Delta\sigma_{los}$ values is more significant. As I increase the degree of inclination the recovered $\Delta\sigma_{los}$ values become smaller which would result in an underestimate of the age of the bar. Additionally, at higher inclinations the recovered $\Delta\sigma_{los}$ values plateau at the early ages soon after bar formation. The duration of this plateau increases as the inclination angle increases.

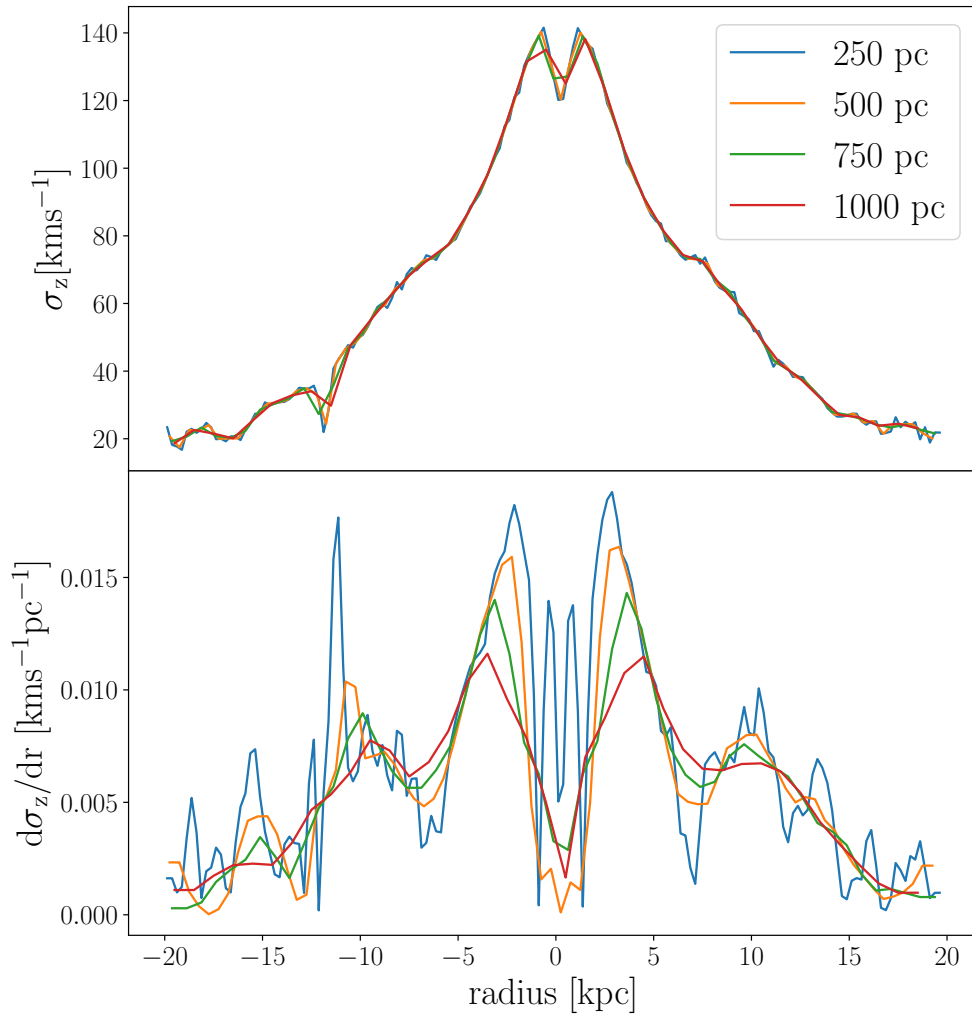


Figure 4.13: Top: σ_z profiles for one simulated galaxy at spatial resolutions of 250 pc (blue), 500 pc (orange), 750 pc (green) and 1000 pc (red). There is very little variation between the general shape of the profile, although at lower spatial resolutions the profile is smoother with less noise. Bottom: The first derivative of σ_z at spatial resolutions of 250 pc, 500 pc, 750 pc and 1000 pc. The peak position moves further out in radius with decreasing spatial resolution resulting in a lower $\Delta\sigma_z$ and an underestimation of the bar formation time.

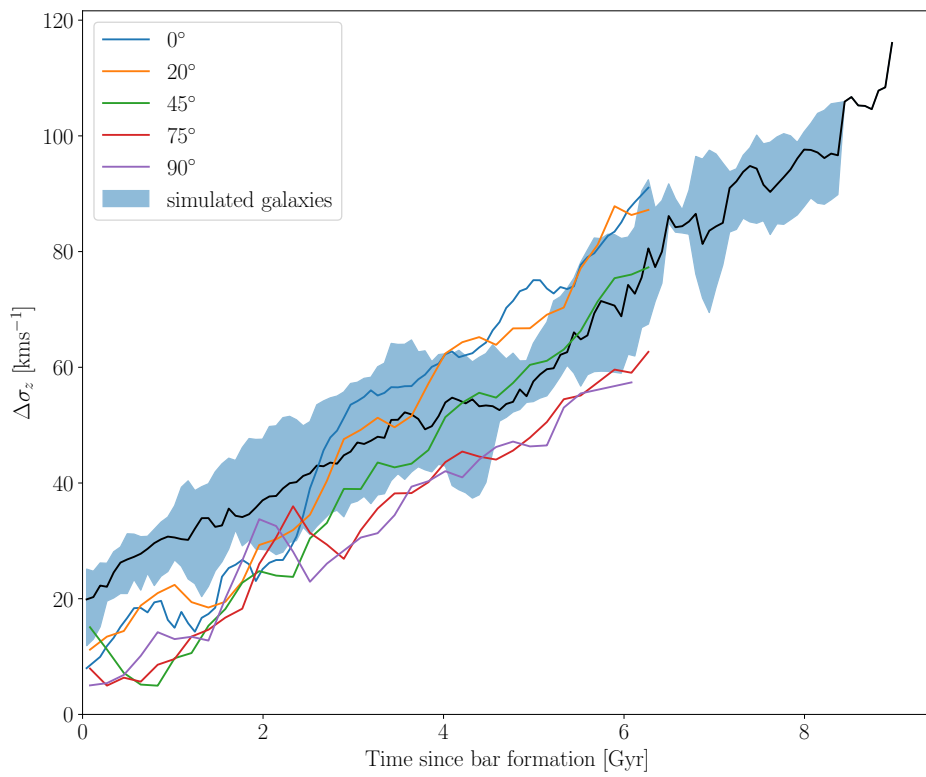


Figure 4.14: Testing inclination with rotation about the y-axis (bar edge-on). The inter-quartile range for the main sample is plotted as the filled region with the median of the sample in black. The $\Delta\sigma_{los}$ values for one galaxy are plotted for inclinations of 0° (blue), 20° (orange), 45° (green) and 75° (blue) plotted for comparison.

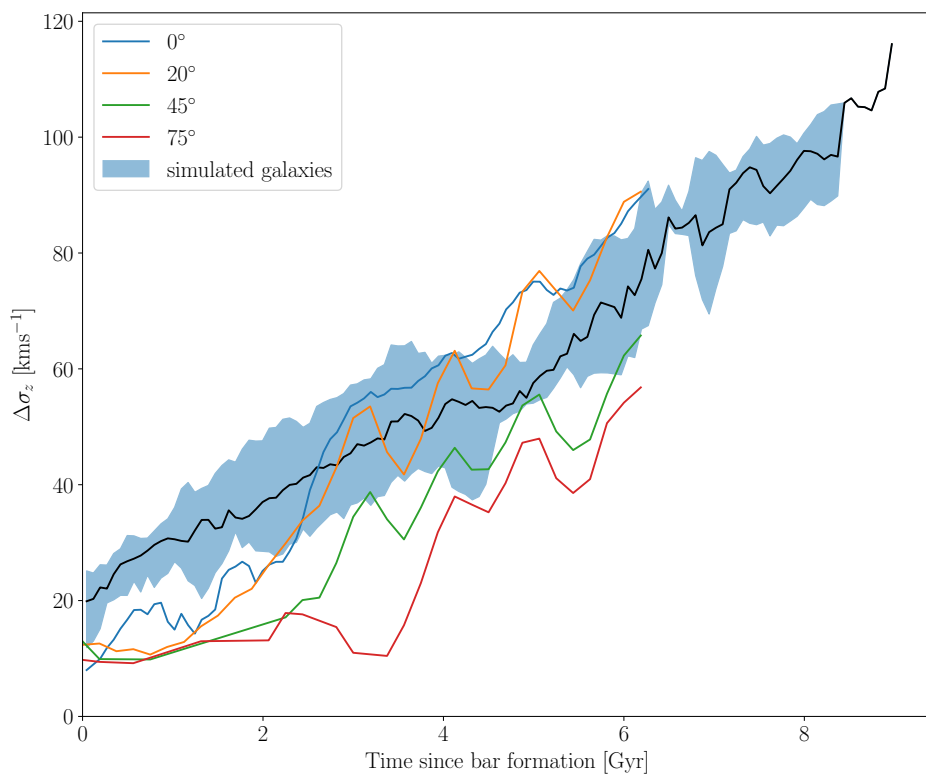


Figure 4.15: Testing inclination with rotation about the x-axis (bar end-on). The inter-quartile range for the main sample is plotted as the filled region with the median of the sample in black. The $\Delta\sigma_{los}$ values for one galaxy are plotted for inclinations of 0° (blue), 20° (orange), 45° (green) and 75° (blue) plotted for comparison.

Overall I find that increasing inclination causes a decrease in the value of $\Delta\sigma_{los}$ recovered. It is clear the rotations about the x-axis cause much more significant change in the ability to recover $\Delta\sigma_{los}$ values for the bar while for rotations about the y-axis we are still able to recover a $\Delta\sigma_{los}$ within the inter-quartile range even up to edge-on inclinations. The ability to recover $\Delta\sigma_{los}$ values even at edge-on inclinations for rotations about the y-axis supports my hypothesis that it is likely that the peaks seen in the first derivative of σ_z are the result of orbital structures within the bar.

4.6.3 Application to galaxy IC 1438

To further test if my method can be applied to data, I apply it to one galaxy from the sample of 24 strongly barred galaxies in the Time Inference with MUSE in Extragalactic Rings (TIMER) survey (Gadotti et al., 2019). The galaxies in the TIMER sample are all selected from the Spitzer Survey of Stellar Structure in Galaxies (S⁴G Sheth et al. (2010)) and were observed using the Multi-Unit spectroscopic Explorer (MUSE Bacon et al. (2010) which is an integral field spectrograph mounted on the Very Large Telescope (VLT) located at the Paranal Observatory in Chile. This spectrograph has a spectral range from 4750 Å to 9300 Å with a spectral sampling of 1.25 Å. The instrument offers a 1' x 1' field of view with a spatial resolution of 0.2'' per pixel when operated in the wide field mode, and the galaxies were observed with a typical seeing of 0.8'' to 0.9'' (Gadotti et al., 2018). IC 1438 was observed with a spatial resolution of 164 pc/arcsecond (Bittner et al., 2020). This allows for the recovery of detailed maps in both spatial and velocity resolution which is key for the application of bar dating method I have developed.

The data are reduced using version 1.6 of the MUSE data reduction pipeline (Weilbacher et al., 2012, 2020). In particular, the TIMER data is flux and wavelength calibrated with bias, flat-fielding and illumination corrections applied. Telluric features and the sky background are removed by exploiting a principal component analysis. The observations are then accurately registered astrometrically. Full details of the observations and data reduction pipeline are presented in Gadotti et al. (2019).

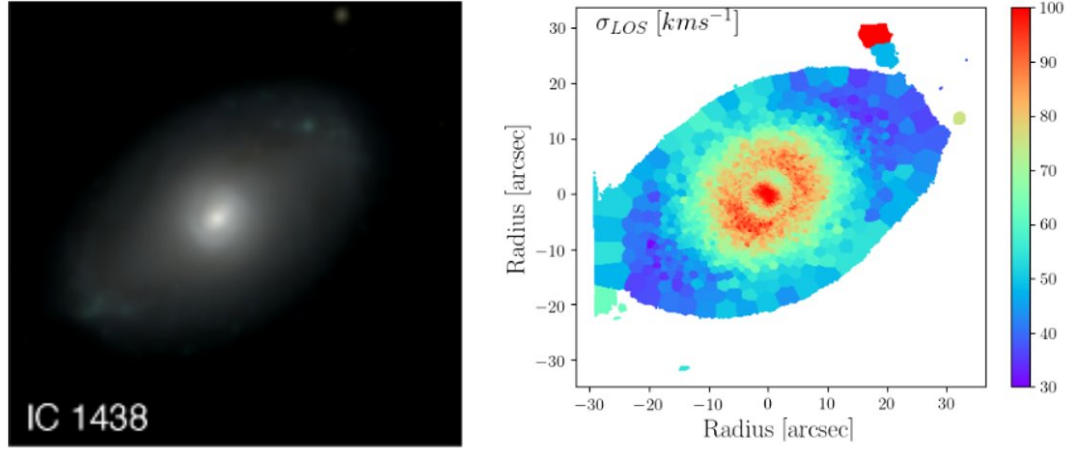


Figure 4.16: LHS: A colour map of galaxy IC1438 built using the TIMER MUSE data cube (Gadotti et al., 2018). RHS: A colour map of the stellar velocity dispersion of galaxy IC1438; where the bar is orientated in the same direction as in Figure 4.16. The colour bar shows indicates the plotted range in $km.s^{-1}$.

Recovery of stellar kinematics is performed using the Galaxy IFU Spectroscopy Tool (GIST) pipeline (Bittner et al., 2019, 2020). GIST uses the adaptive Voronoi tessellation routine of Cappellari and Copin (2003) to spatially bin the data with a minimum signal-to-noise ratio of 40. The stellar kinematics (V, σ, h_3, h_4) were extracted using the PPXF-module which utilises the penalised pixel-fitting (pPXF) method (Cappellari and Emsellem, 2004; Cappellari, 2017) using the full wavelength range.

From the available TIMER galaxies I select galaxy IC1438 because the TIMER data covers the full bar, and because of its low inclination angle of 24° , since in Section 4.6.2 I have shown that high inclination angles can result in a lower $\Delta\sigma_{los}$ value and thus age than expected. This galaxy has a bar of length of $23''$ at a position angle of 121° (see Figure 4.16), full properties are given in Gadotti et al. (2019). In Figure 4.16 I also present a colour map of the velocity dispersion. I apply a mask along the bar with a width of 1kpc to extract the σ_{los} along the bar's major axis. At the same time σ_{los} data is binned such that each bin corresponds to a width of 250pc smoothing the data slightly and adjusting the spatial resolution so that it is the same as used for the analysis performed on the simulations.

In Figure 4.17 I present both the extracted σ_{los} profile for the major axis of the bar and the first derivative of the σ_{los} profile with the position of the bar ends and derivative

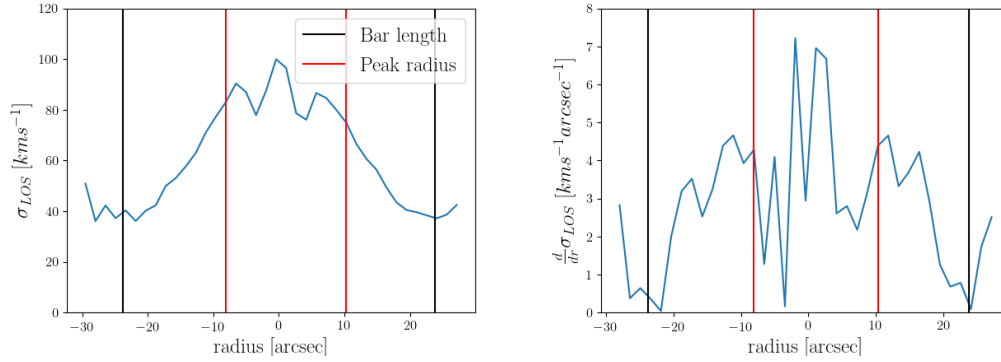


Figure 4.17: LHS: The extracted and binned velocity dispersion along the major axis of the bar. The bar length (black) and position of the peak radius (red) are marked with vertical lines. RHS: The first derivative of the velocity dispersion with the bar length and peak radius marked with vertical lines.

peaks marked. It has general similarities with the σ_z profiles of the simulations, such as the central peak with the σ_z decreasing towards the bar ends. However, unlike the simulations the profile presents a clear central peak bordered by two secondary peaks. These secondary peaks appear to lie just outside of the radius of the inner ring and correspond to the high velocity dispersion ring seen in Figure 4.17. While the derivative peaks are not as clear as in the simulations it is still possible to identify them. I calculate a $\Delta\sigma_z$ in the same way as described in Section 4.1.2 recovering a $\Delta\sigma_z$ of 40 kms^{-1} . In Figure 4.18 I present the $\Delta\sigma_z$ vs. age plot for the full simulation sample with the $\Delta\sigma_{los}$ value for IC1438 plotted in the dashed line. This gives a bar age estimate of 1.4 Gyr to 4.4 Gyr.

There are no direct bar age estimates for IC1438 in the literature, however Gadotti et al. (2015) postulated that the age of the stellar population in the inner ring could be used as a lower limit for the bar age. Bittner et al. (2020) found that spaxels in the nuclear disc and ring of IC1438 have an average age between 2.5 and 5 Gyr. This is in good agreement with the estimate we find using our new method. This demonstrates that not only does the $\Delta\sigma_z$ method produce reasonable age estimates, but most importantly that this method can be used with current observational data.

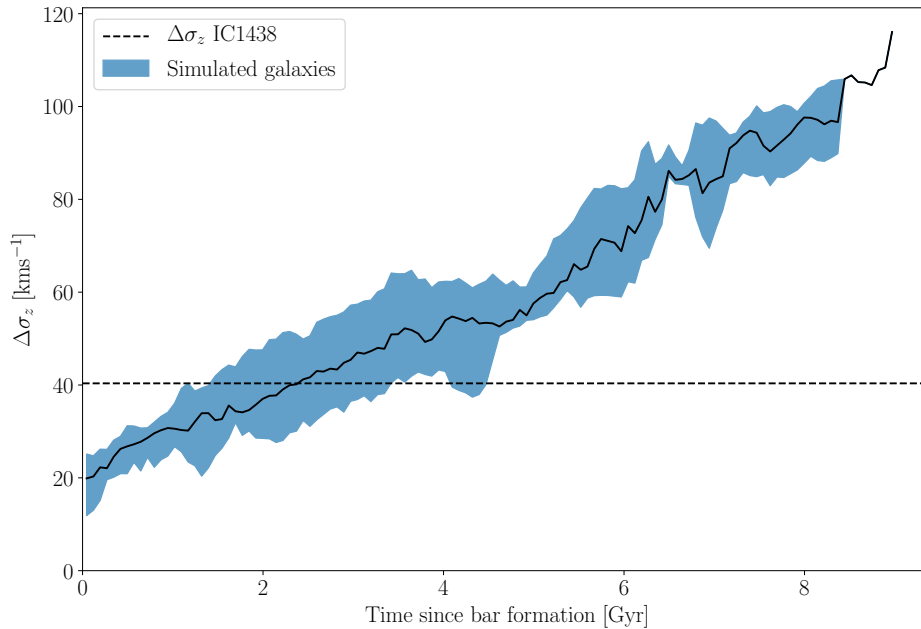


Figure 4.18: The $\Delta\sigma_z$ vs. time plot derived from the simulated galaxies with the $\Delta\sigma_z$ value for IC1438 marked (black dashed line).

4.7 Summary

Gadotti and de Souza (2005) first explored the link between the vertical velocity dispersion of the bar and its formation time. They proposed that it was possible to distinguish between recently formed and evolved bars by how different the vertical velocity dispersion of the bar is from the disc. While this method does not provide a quantitative estimate of bar age they did find that recently formed bars have a velocity dispersion similar to the disc with the difference being much greater in more evolved bars.

In this chapter I built on this work by studying how the shape of the bar's vertical velocity dispersion changes over time using 15 isolated zoom-in cosmological re-simulations (Martig et al., 2012). I found that not only does the vertical velocity dispersion increase with time but the shape of the radial profile of σ_z changes. As the bar evolves symmetrical shoulder-like features develop in the majority of the sample.

I derive a value, $\Delta\sigma_z$, which is the difference between the vertical velocity dispersion of the shoulder-like feature and the bar ends. The $\Delta\sigma_z$ value increases monotonically

with time; it is small for recently formed bars and higher for more evolved bars. This relationship is found both in cosmological and in isolated simulations, proving that it is robust. Therefore, by determining $\Delta\sigma_z$ for the bar one can recover the time of bar formation.

The position of the shoulder-like feature is remarkably stable as a function of time for any one galaxy. On average, the position of this feature is 1.5 kpc shorter than the initial bar length. This indicates that shoulder-like feature could be related to a change in orbital structure between the initial and evolved bar. If this is the case then by determining the location of this feature in observational data, the initial length of the bar could be recovered in addition to the age of the bar. This presents a promising avenue for constraining the rate of bar lengthening in galaxies.

The increase of $\Delta\sigma_z$ over time is influenced by two different factors. The first is bar lengthening; as the bar increases in length the reference point for the $\Delta\sigma_z$ value moves further out into the disc. Since σ_z on average decreases as a function of radius for the galaxy this results in an increase in $\Delta\sigma_z$. The second is kinematic thickening which increases the vertical velocity dispersion of the bar through internal instabilities or vertical heating. The increase of $\Delta\sigma_z$ is initially dominated by bar lengthening with kinematic thickening becoming dominant after the bar buckles, making $\Delta\sigma_z$ a powerful tracer of bar growth.

Finally, I tested how spatial resolution and galaxy inclination affect the measurements of $\Delta\sigma_z$. Lower resolutions smooth the vertical velocity profile causing the shoulder-like feature to be identified at a larger radius. This results in a younger bar age than would be expected. However this change appears to be systematic with $\Delta\sigma_z$ values decreasing by 25 kms^{-1} between resolutions of 250 pc and 1000 pc, so we might be able to correct for this effect. Increasing the inclination also results in an underestimate of the bar age with the most significant underestimates seen when the bar is inclined end-on. I therefore propose that this method is best applied to data of a similar resolution to the simulations presented here with a face-on inclination.

Having established the potential of this method I have applied it to MUSE data of

IC1438 and found good agreement with age estimates of the nuclear ring and disc. I have confirmed that not only is it possible to use this method with observational data but also that the bar age recovered is reasonable. This new method presents an exciting opportunity for the recovery of bar ages which are key in understanding the timescales of galaxy evolution.

Chapter 5

Summary and Future Work

5.1 Summary of main results

In this thesis I have explored the effects of bars on the star formation and stellar dynamics of galaxies. By analysing the concurrent evolution of bars and galaxies using a sample of isolated and cosmological zoom-in re-simulations I developed two methods for recovering the formation time of the bar. In addition, I identified the star formation desert region of the bar as an uncontaminated region of radially migrated stars. I summarise the findings of my thesis below.

5.1.1 Dating bar formation using star formation histories

The SFD is a region within the inner ring, lying either side of the bar in the areas that the bar sweeps out. James and Percival (2016) found these regions had very little to no star formation and theorised that if star formation is suppressed by the bar the youngest stars in these regions should correspond to the age of the bar. In Chapter 3 I explored this hypothesis further with a sample of 6 zoom-in cosmological re-simulations (Donohoe-Keyes et al., 2019).

Looking at the average age maps revealed old regions located either side of the bar with

a deficit of star younger than 10 Myr, confirming the presence of the SFD phenomenon. The removal of gas within the SFD occurs within 1-2 Gyr after the formation of the bar indicating there is little to no in-situ star formation after that time. We would, therefore, expect to see a sharp truncation in the star formation rate. However, I found a gradual downturn in the star formation rate of the SFD region in comparison to that of the bar. While the SFD regions do appear on average older than the bar, they actually contain stars of all ages. While looking at the star formation rate of the SFD could still provide information of the formation time of bars, the interpretation is more difficult than anticipated.

Since gas is removed quickly after bar formation, all stars 1-2 Gyr younger than the bar must radially migrate into the SFD region. The discovery of this radially migrated sample provides us with unparalleled insight into a region where any young stars must be radial migrators. Combining this with bar age would allow us to probe the timescales and efficiency of radial migration. By separating out the stellar populations formed before and after the bar we can gain unparalleled insight into the chemo-dynamical evolution of the SFD region.

5.1.2 Dating bar formation using kinematics

As bars evolve they vertically thicken. Younger bars have a velocity dispersion similar to that of the disc while in older bars the difference is greater (Gadotti and de Souza, 2005). However, bars with significant central bulge masses also show large differences between the bar and disc even when recently formed. In Chapter 4 I used the relationship between the bars age and the increase in the bars velocity dispersion by looking at features in the vertical velocity dispersion of the bar with a sample of 15 zoom-in cosmological re-simulations and 3 simulations of isolated galaxies.

I uncovered a special feature located within the bar radius. This feature appears in the first derivation of the velocity dispersion as two symmetrical peaks within the bars radius and I refer to it as the peak position. By taking the difference between the σ_z of the peak position and the bar ends I produced a value I call $\Delta\sigma_z$. The $\Delta\sigma_z$ increases

monotonically with time allowing the age of the bar to be found. I was able to recover $\Delta\sigma_z$ in both in cosmological and isolated simulations, demonstrating that this feature is robust. By using $\Delta\sigma_z$ we can infer a time of bar formation free from the uncertainties introduced by other methods. The location of the peak position is remarkably stable and on average it is 1.5 kpc shorter than the initial length of the bar. This provides a promising avenue for recovering initial bar length and, combined with a bar age, could be used to constrain the growth rate of bars.

The $\Delta\sigma_z$ value is influenced by two factors: the lengthening of the bar, and the vertical thickening of the bar. At early stages the lengthening of the bar is the main contributor, however, after the time of buckling the vertical thickening dominates. Therefore $\Delta\sigma_z$ is a powerful tracer of bar growth being constrained entirely by the bar's evolution.

To determine how the method was affected by inclination I recovered $\Delta\sigma_{los}$ values for one galaxy orientated at multiple inclinations with the bar edge-on and end-on. I found that at edge-on inclinations $\Delta\sigma_{los}$ remained in good agreement with the $\Delta\sigma_z$ trend found from the face on orientation of the simulations with only a small decrease in the $\Delta\sigma_{los}$ recovered with increasing inclination angle. However, in end on orientations the recovered $\Delta\sigma_{los}$ decreases significantly with increasing inclination.

Having established the potential of this method within simulations I have tested it on MUSE data of IC1438. I find good agreement with literature data, confirming that it is possible to apply this method to current observational data and that the bar ages recovered are reasonable. This new method presents an exciting avenue for the reliable recovery of quantitative bar ages furnishing us with new insights in our understanding of the timescales of disc galaxy evolution.

5.2 Future work

5.2.1 Further investigations using simulations

The work presented in this thesis provides two methods through which a bar formation time can be recovered. However, both of these methods have been developed using the same suite of simulations. By repeating the analysis presented in this work across a larger cosmological sample we could investigate how the properties of the galaxies influence the results.

In Chapter 3 I confirmed the presence of the SFD region in simulations. Observationally, not all bars are observed with an SFD region so it would be of interested to see how the presence of the SFD correlates with galaxy properties. Additionally, one of the key results from that work is that the SFD is the result of gas being removed from the bar region on timescales of 1-2 Gyrs. By repeating my analysis on a large cosmological suit it would be possible to determine how this gas removal timescale is correlated with the properties of the galaxy and the galaxy bar. Furthermore, in this work I found that, after the time of bar formation, stars which are younger than the bar in the SFD have all radially migrated there. Further work could be done to determine on what timescale these stars migrate into the SFD and if this process changes over the evolution of the galaxy.

In Chapter 4 I presented a new method for the recovery of bar ages using $\Delta\sigma_z$. To further develop this method I propose re-calibrating it with a larger cosmological sample. By testing this method against a statistically large sample with galaxy properties more representative of the large range of properties seen observationally, we would be able to test how galaxy properties influence $\Delta\sigma_z$ against the norm. This will also test the method against a large variety of galaxies thus allowing us to determine its limitations for application to observations.

5.2.2 Using Gaia and spectroscopic surveys to date the Galactic Bar

The Milky Way provides us with a wealth of data that makes it an ideal laboratory for exploring the 3-dimensional properties of the bar not available in any other system. Even so, with the plethora of data available dating the age of the bar remains a persistent problem. The most common methods for to determine a Galactic bar age rely on the age of the underlying stellar populations (Ng et al., 1996; Sevenster, 1999; Cole and Weinberg, 2002; Bovy et al., 2019; Baba and Kawata, 2020), but as discussed many times in this thesis, this does not necessarily correspond to the age of the bar. An alternative method uses the response of the disc to the formation of the bar to provide an age estimate but can give vastly different ages dependent on if the bar is evolving or not (Minchev and Famaey, 2010). As a consequence of these methods the true age of the Galactic bar remains an open issue with estimates varying widely from 2 to 8 Gyrs. Using the data available from the recent and upcoming Milky Way surveys I would like to propose three potential projects aimed at developing and adapting my techniques for application to the Milky Way.

Dating the Milky Way bar using kinematics

During my PhD one of the novel methods I developed for determining bar ages relies solely on the kinematical response of stars within the bar. By applying my method I removed the need for assumptions on the nature and origin of the underlying stellar population and their association with the bar. Additionally, I negated the uncertainty introduced into the bar age from having to assume a stable or evolving bar.

The first stage of this analysis will involve using simulations to modify the criteria I found to estimate the epoch of bar formation for the Milky Way. This would involve translating these criteria into Gaia observables (parallaxes, proper motions and line-of-sight velocities) to recover the $\Delta\sigma_z$ signature as an observer positioned within the Galactic plane. This would require the proper motions of stars to extract the vertical

velocity dispersion for the bar. This analysis would also allow us to determine what constraints should be considered when applying this method to observational data. Specific focus should be given to limitations such as the maximum height above the plane at which the signal can be found as well as the extent of the bar required in order to recover the signal.

This can then be used to directly compare the results from the simulated data with the data available from Milky Way surveys by making use of the existing Gaia data 2 release as well the Gaia early data release 3 which can be bolstered by the full release of DR3 expected in early 2022. Although, this may be difficult on account of dust obscuring observations towards the galactic center. However, by combining both Gaia and APOGEE (Majewski et al., 2017), which observed in the near-IR and can see through the galactic dust, we would have access to a rich resource that will allow us to recover the signal with which we will be able to date the age of the Milky Way bar. Given that the method I developed is based solely on the kinematical properties of the bar and does not require assumptions of the bars evolutionary phase, or on the stellar ages of bar stars I would expect to recover a more reliable age estimate than previous techniques have produced.

Investigating in-plane tracers of bar age

The optimal way to confirm an estimate of the Galactic bar age is to have another independent age estimate with which to compare. Due to the nature of previous age estimates and the uncertainties introduced by their assumptions, comparisons between bar ages must be approached with caution. In the most ideal scenario we would have two or more age dating methods independent of the underlying stellar population properties.

By comparing extracted in-plane velocity dispersions across multiple simulated galaxies with different bar ages (Martig et al., 2012) we can determine if tracers of the bar formation can be recovered in an edge-on plane. The in-plane motions and line-of-sight velocities can be explored using the GDR3 and WEAVE which is expected to

be in its final science stage in the same time-frame as Gaia DR3, to which it is complementary. As the first and only high-resolution optical multi-object spectrograph in the northern hemisphere it will provide the necessary resolution to recover radial velocities too faint for Gaia and allow for detailed analysis of chemical abundances. If the signatures of bar formation can be recovered then we would be able to develop a method which can be applied to the observational data and then compare results with previous work to produce a robust age for the Galactic bar.

Investigating radial migration within the Milky Way

In my previous research I explored a region within barred galaxies termed the SFD, which contained an uncontaminated sample of radially migrated stars and presenting an exciting opportunity for galactic archaeology by offering a route to explore radial migration within a galaxy in more detail. The recent and upcoming surveys of the Milky Way will provide a unique laboratory to investigate not only the effect of radial migration on the galactic center but also the rate of this process over the Milky Way's evolution.

By expanding on my previous work exploring the properties of the SFD in simulations to a more detailed study of Milky Way-like simulated galaxies (Martig et al., 2012) we would be able to make predictions on characteristic radial migration timescales. With WEAVE and Gaia we have access to the kinematical information necessary to resolve the star formation desert population within the Milky Way allowing for direct comparisons with the predictions from the simulations. By filtering the extracted SFD population for those stars with ages younger than the Galactic bar we could explore the rate of radial migration during the evolution of the bar and from the abundances we would be able to explore the origins of these stars.

These projects will provide a route for the detailed exploration of the formation history of the Milky Way and its bar. By pinpointing the time for the formation of the Milky Way bar we will have an estimate of when the Milky Way disc settled and secular evolution began to take place. In addition we will be able to explore how the Milky

Way bar influenced the subsequent chemical evolution of the Milky Way by exploring the rate of radial migration from within the star formation desert region.

5.2.3 Using MaNGA for a statistical study of bar ages and radial migration

Determining bar ages

A major question remaining in the study of barred galaxy evolution is whether the formation of the bar is correlated to galaxy disc quenching. Evidence suggests that bars in high-mass galaxies are already in place at high redshift and contain more evolved stellar populations with less current star formation than their unbarred counterparts (Fraser-McKelvie et al., 2020a). However, without an estimate of bar age we are unable to confirm if the bar helps to cause this cessation in star formation. By applying the method I have developed for dating bars using kinematics in conjunction with star formation histories we could explore how the formation time of the bar relates to the rate of star formation at different times. By doing this for a statistically large and diverse sample of barred galaxies, such as that sampled by MaNGA, we would begin to understand whether bars correlated to disc quenching.

While bars are commonly associated with quenching, we also find star forming bars, mostly in low-mass galaxies. There are currently two proposed scenarios to explain these low-mass star forming bars. We could be seeing recently formed bars or alternatively a different type of bar than those seen in high-mass galaxies that can form stars due to lower gas shear within the bar (Fraser-McKelvie et al., 2020b). Previous studies of barred galaxies in MaNGA revealed 5 different categories when looking at $H\alpha$ (Fraser-McKelvie et al., 2020a): star formation along the bar, star formation predominantly in the center of the galaxy, star formation in a ring around the bar region, star formation at the ends of the bar and those with no star formation. By using the kinematic method I have developed we could recover the ages of the bar for galaxies in each of these categories to determine if they represent different stages of bar evolution

or if they are associated with different types of bars. Bar growth is not entirely understood either. Studies from simulations suggest that bars continually grow throughout their evolution but their rate of growth is poorly constrained. One advantage of the method I have developed is the recovery of an initial bar length. By recovering initial bar lengths and ages we could explore the rate of bar growth within different barred galaxies. By making comparisons with simulations we could further our understanding of how bars evolve within galaxies of all types and masses and the consequences of their evolution on other galactic components.

In the Figure 5.1 I present my initial results with MaNGA. Galaxy 8331-12705 is a high-mass galaxy with a long bar of 14.3 kpc showing no current star formation along the bar, while galaxy 8935-6104 is a low mass galaxy with a star forming bar of length 2.3 kpc. I can confirm that for these galaxies the higher mass, longer bar formed first, while the bar in the lower mass galaxy formed much more recently. This new method presents an exciting avenue for the reliable recovery of bar ages furnishing us with new insights in our understanding of the timescales of disc galaxy evolution.

Radial migration

Bars exert strong torques in their host galaxy redistributing both stars and gas through radial migration impacting not only star formation but the stellar properties of other galactic components. During my PhD I discovered that star formation within the SFD region is suppressed after bar formation. Any stars younger than the age of the bar can only have got there through radial migration with stars taking approximately 1-2 Gyrs to migrate to the SFD from the inner ring or disk. By recovering the age of the bar we are able to extract the uncontaminated radially migrated stars from the SFD region. It would be interesting to investigate this further by determining the rate of the radial migration within this region by making comparisons between simulations and observations over a range of different barred galaxies. With this we would be able to further our understanding of the influence of bars. This can then be applied in the analysis of the stellar populations of other galactic components by comparing with

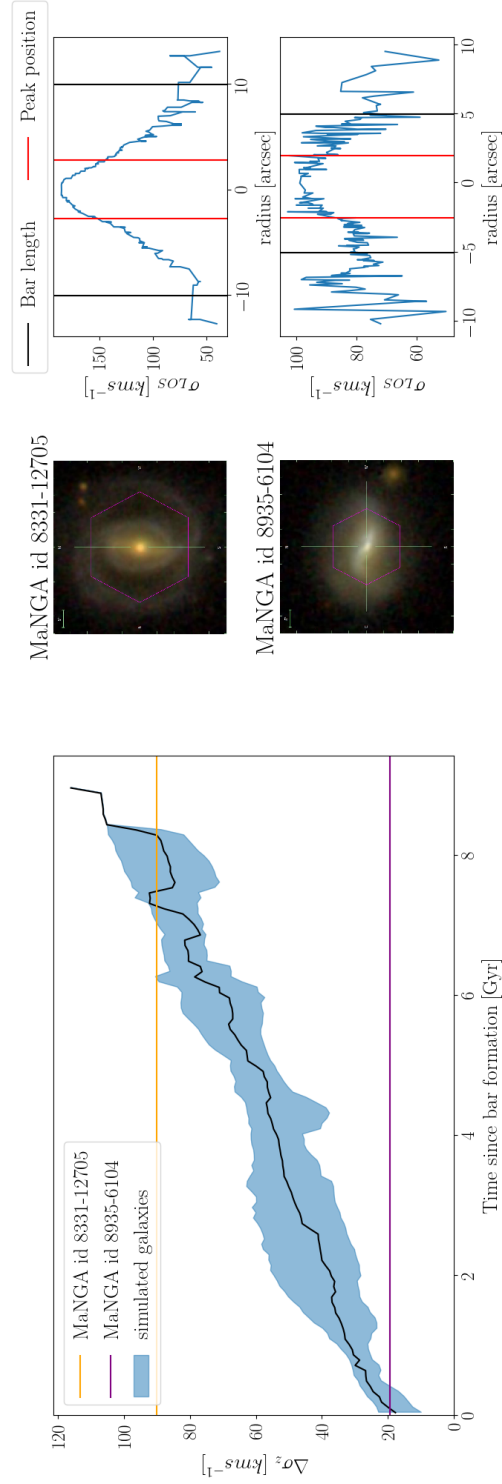


Figure 5.1: Initial results with MaNGA data. Left: The $\Delta\sigma_z$ values for MaNGA galaxies 8331-12705 (orange) and 8935-610 (blue) plotted against the inter-quartile range of $\Delta\sigma_z$ for the simulations presented in Chapter 4 (blue filled region) and the median $\Delta\sigma_z$ of the simulation (black). Middle: SDSS g , r and i colour images of the MaNGA galaxies 8331-12705 (top) and 8935-610 (bottom). The magenta hexagon shows the size of MaNGAs IFU bundle. Right: The σ_z profiles for the MaNGA galaxies 8331-12705 (top) and 8935-610 (bottom). The peak positions of the first derivative (red) and the length of the bar (black) are marked with vertical lines.

unbarred galactic counterparts to uncover how bars influence the properties of other spatially distinct components through radial migration.

5.3 Concluding remarks

The formation of a bar is a keystone event in galaxy evolution. It marks a time of transition from fast evolutionary processes, such as mergers, to secular evolutionary processes, of which bars are heavy drivers. In this thesis I have presented two methods through which bar formation times can be recovered. Further than this I have investigated the processes which underlie these methods. By recovering bar ages we will be able to define the time of onset for secular evolution. By taking this work further we may also be able to quantify what influences bars have on the evolution of a galaxy and over what timescales they act. This would allow us to predict the evolutionary paths of barred galaxies, including our own galaxy, the Milky Way.

Bibliography

- Abdurro'uf and Akiyama, M. (2017). Understanding the scatter in the spatially resolved star formation main sequence of local massive spiral galaxies. *MNRAS*, 469(3):2806–2820.
- Abel, T., Croft, R. C., and Hernquist, L. (2002). On the 'initial' Angular Momentum of Galaxies. In Natarajan, P., editor, *The Shapes of Galaxies and their Dark Halos*, pages 119–122.
- Agertz, O., Teyssier, R., and Moore, B. (2009). Disc formation and the origin of clumpy galaxies at high redshift. *MNRAS*, 397(1):L64–L68.
- Aguerri, J. A. L., Beckman, J. E., and Prieto, M. (1998). Bar Strengths, Bar Lengths, and Corotation Radii, Derived Photometrically for 10 Barred Galaxies. *AJ*, 116:2136–2153.
- Aguerri, J. A. L., Méndez-Abreu, J., and Corsini, E. M. (2009). The population of barred galaxies in the local universe. I. Detection and characterisation of bars. *A&A*, 495(2):491–504.
- Aguerri, J. A. L., Muñoz-Tuñón, C., Varela, A. M., and Prieto, M. (2000). Characterizing bar structures: application to NGC 1300, NGC 7479 and NGC 7723. *A&A*, 361:841–849.
- Algorry, D. G., Navarro, J. F., Abadi, M. G., Sales, L. V., Bower, R. G., Crain, R. A., Dalla Vecchia, C., Frenk, C. S., Schaller, M., Schaye, J., and Theuns, T. (2017). Barred galaxies in the EAGLE cosmological hydrodynamical simulation. *MNRAS*, 469(1):1054–1064.

- Alonso, M. S., Coldwell, G., and Lambas, D. G. (2013). Effect of bars in AGN host galaxies and black hole activity. *A&A*, 549:A141.
- Andredakis, Y. C. and Sanders, R. H. (1994). Exponential bulges in late-type spirals : an improved description of the light distribution. *MNRAS*, 267:283–296.
- Athanassoula, E. (1990). Bar shapes and orbital stochasticity. *Annals of the New York Academy of Sciences*, 596:181–186.
- Athanassoula, E. (1992). The existence and shapes of dust lanes in galactic bars. *MNRAS*, 259:345–364.
- Athanassoula, E. (1994). Gas Dynamics and Star Formation in and Around Bars (Invited paper). In Shlosman, I., editor, *Mass-Transfer Induced Activity in Galaxies*, page 143.
- Athanassoula, E. (1996a). Evolution of Bars in Isolated and in Interacting Disk Galaxies. In Buta, R., Crocker, D. A., and Elmegreen, B. G., editors, *IAU Colloq. 157: Barred Galaxies*, volume 91 of *Astronomical Society of the Pacific Conference Series*, page 309.
- Athanassoula, E. (1996b). Evolution of Bars in Isolated and in Interacting Disk Galaxies. In Buta, R., Crocker, D. A., and Elmegreen, B. G., editors, *IAU Colloq. 157: Barred Galaxies*, volume 91 of *Astronomical Society of the Pacific Conference Series*, page 309.
- Athanassoula, E. (1999). N-body Simulations of Interacting Disc Galaxies. In Sellwood, J. A. and Goodman, J., editors, *Astrophysical Discs - an EC Summer School*, volume 160 of *Astronomical Society of the Pacific Conference Series*, page 351.
- Athanassoula, E. (2003a). What determines the strength and the slowdown rate of bars? *MNRAS*, 341(4):1179–1198.
- Athanassoula, E. (2005). Dynamical Evolution of Barred Galaxies. *Celestial Mechanics and Dynamical Astronomy*, 91(1-2):9–31.

- Athanassoula, E. (2012). Manifold-driven spirals in N-body barred galaxy simulations. *MNRAS*, 426(1):L46–L50.
- Athanassoula, E. (2013). *Bars and secular evolution in disk galaxies: Theoretical input*, page 305.
- Athanassoula, E., Bienayme, O., Martinet, L., and Pfenniger, D. (1983). Orbits as building blocks of a barred galaxy model. *A&A*, 127(2):349–360.
- Athanassoula, E., Bosma, A., Creze, M., and Schwarz, M. P. (1982). On the sizes of rings and lenses in disk galaxies. *A&A*, 107:101–106.
- Athanassoula, E., Laurikainen, E., Salo, H., and Bosma, A. (2015). On the nature of the barlens component in barred galaxies: what do boxy/peanut bulges look like when viewed face-on? *MNRAS*, 454(4):3843–3863.
- Athanassoula, E., Machado, R. E. G., and Rodionov, S. A. (2013). Bar formation and evolution in disc galaxies with gas and a triaxial halo: morphology, bar strength and halo properties. *MNRAS*, 429(3):1949–1969.
- Athanassoula, E. and Martinet, L. (1980). A correlation between the lengths of bars and the sizes of bulges. *A&A*, 87(3):L10.
- Athanassoula, E. and Misiriotis, A. (2002). Morphology, photometry and kinematics of N -body bars - I. Three models with different halo central concentrations. *MNRAS*, 330(1):35–52.
- Athanassoula, E., Rodionov, S. A., Peschken, N., and Lambert, J. C. (2016). Forming Disk Galaxies in Wet Major Mergers. I. Three Fiducial Examples. *ApJ*, 821(2):90.
- Athanassoula, E., Romero-Gómez, M., Bosma, A., and Masdemont, J. J. (2010). Rings and spirals in barred galaxies - III. Further comparisons and links to observations. *MNRAS*, 407(3):1433–1448.
- Athanassoula, E., Romero-Gómez, M., and Masdemont, J. J. (2009). Rings and spirals in barred galaxies - I. Building blocks. *MNRAS*, 394(1):67–81.

- Athanassoula, E. and Sellwood, J. A. (1986). Bi-symmetric instabilities of the Kuz'min/Toomre disc. *MNRAS*, 221:213–232.
- Athanassoula, L. (2003b). *Angular Momentum Redistribution and the Evolution and Morphology of Bars*, volume 626, pages 313–326.
- Baba, J. and Kawata, D. (2020). Age dating the Galactic bar with the nuclear stellar disc. *MNRAS*, 492(3):4500–4511.
- Bacon, R., Accardo, M., Adjali, L., Anwand, H., Bauer, S., Biswas, I., Blaizot, J., Boudon, D., Brau-Nogue, S., Brinchmann, J., Caillier, P., Caponni, L., Carollo, C. M., Contini, T., Couderc, P., Daguisé, E., Deiries, S., Delabre, B., Dreizler, S., Dubois, J., Dupieux, M., Dupuy, C., Emsellem, E., Fechner, T., Fleischmann, A., François, M., Gallou, G., Gharsa, T., Glindemann, A., Gojak, D., Guiderdoni, B., Hansali, G., Hahn, T., Jarno, A., Kelz, A., Koehler, C., Kosmowski, J., Laurent, F., Le Floch, M., Lilly, S. J., Lizon, J. L., Loupiau, M., Manescau, A., Monstein, C., Nicklas, H., Olaya, J. C., Pares, L., Pasquini, L., Pécontal-Rousset, A., Pelló, R., Petit, C., Popow, E., Reiss, R., Remillieux, A., Renault, E., Roth, M., Rupprecht, G., Serre, D., Schaye, J., Soucail, G., Steinmetz, M., Streicher, O., Stuijk, R., Valentin, H., Vernet, J., Weilbacher, P., Wisotzki, L., and Yerle, N. (2010). The MUSE second-generation VLT instrument. In McLean, I. S., Ramsay, S. K., and Takami, H., editors, *Ground-based and Airborne Instrumentation for Astronomy III*, volume 7735 of *Society of Photo-Optical Instrumentation Engineers (SPIE) Conference Series*, page 773508.
- Baldry, I. K., Glazebrook, K., Brinkmann, J., Ivezić, Ž., Lupton, R. H., Nichol, R. C., and Szalay, A. S. (2004). Quantifying the Bimodal Color-Magnitude Distribution of Galaxies. *ApJ*, 600(2):681–694.
- Balogh, M. L. and Morris, S. L. (2000). $H\alpha$ photometry of Abell 2390. *MNRAS*, 318(3):703–714.
- Barazza, F. D., Jablonka, P., Desai, V., Jogee, S., Aragón-Salamanca, A., De Lucia, G., Saglia, R. P., Halliday, C., Poggianti, B. M., Dalcanton, J. J., Rudnick, G., Milvang-

- Jensen, B., Noll, S., Simard, L., Clowe, D. I., Pelló, R., White, S. D. M., and Zaritsky, D. (2009). Frequency and properties of bars in cluster and field galaxies at intermediate redshifts. *A&A*, 497(3):713–728.
- Barazza, F. D., Jogee, S., and Marinova, I. (2008). Bars in Local Galaxies: Evidence for a Higher Optical Bar Fraction in Disk-Dominated Galaxies. In Funes, J. G. and Corsini, E. M., editors, *Formation and Evolution of Galaxy Disks*, volume 396 of *Astronomical Society of the Pacific Conference Series*, page 351.
- Barsanti, S., Owers, M. S., Brough, S., Davies, L. J. M., Driver, S. P., Gunawardhana, M. L. P., Holwerda, B. W., Liske, J., Loveday, J., Pimblet, K. A., Robotham, A. S. G., and Taylor, E. N. (2018). Galaxy and Mass Assembly (GAMA): Impact of the Group Environment on Galaxy Star Formation. *ApJ*, 857(1):71.
- Bassett, R., Glazebrook, K., Fisher, D. B., Green, A. W., Wisnioski, E., Obreschkow, D., Cooper, E. M., Abraham, R. G., Damjanov, I., and McGregor, P. J. (2014). DYNAMO - II. Coupled stellar and ionized-gas kinematics in two low-redshift clumpy discs. *MNRAS*, 442(4):3206–3221.
- Baugh, C. M. (2006). A primer on hierarchical galaxy formation: the semi-analytical approach. *Reports on Progress in Physics*, 69(12):3101–3156.
- Baugh, C. M., Cole, S., and Frenk, C. S. (1996). Evolution of the Hubble sequence in hierarchical models for galaxy formation. *MNRAS*, 283(4):1361–1378.
- Baugh, C. M., Cole, S., Frenk, C. S., Benson, A. J., and Lacey, C. G. (1999). Early-Type Galaxies in the Hierarchical Universe. In Carral, P. and Cepa, J., editors, *Star Formation in Early Type Galaxies*, volume 163 of *Astronomical Society of the Pacific Conference Series*, page 227.
- Beckwith, S. V. W., Stiavelli, M., Koekemoer, A. M., Caldwell, J. A. R., Ferguson, H. C., Hook, R., Lucas, R. A., Bergeron, L. E., Corbin, M., Jogee, S., Panagia, N., Robberto, M., Royle, P., Somerville, R. S., and Sosey, M. (2006). The Hubble Ultra Deep Field. *AJ*, 132(5):1729–1755.

- Bell, E. F., Wolf, C., Meisenheimer, K., Rix, H.-W., Borch, A., Dye, S., Kleinheinrich, M., Wisotzki, L., and McIntosh, D. H. (2004). Nearly 5000 Distant Early-Type Galaxies in COMBO-17: A Red Sequence and Its Evolution since $z=1$. *ApJ*, 608(2):752–767.
- Benedict, G. F., Howell, D. A., Jørgensen, I., Kenney, J. D. P., and Smith, B. J. (2002). NGC 4314. IV. Photometry of Star Clusters with the Hubble Space Telescope: History of Star Formation in the Vicinity of a Nuclear Ring. *AJ*, 123(3):1411–1432.
- Benson, A. J. and Bower, R. (2011). Accretion shocks and cold filaments in galaxy formation. *MNRAS*, 410(4):2653–2661.
- Benson, A. J. and Madau, P. (2003). Early preheating and galaxy formation. *MNRAS*, 344(3):835–846.
- Berentzen, I., Athanassoula, E., Heller, C. H., and Fricke, K. J. (2003). Numerical simulations of interacting gas-rich barred galaxies: vertical impact of small companions. *MNRAS*, 341(1):343–360.
- Berentzen, I., Heller, C. H., Shlosman, I., and Fricke, K. J. (1998). Gas-driven evolution of stellar orbits in barred galaxies. *MNRAS*, 300(1):49–63.
- Berentzen, I., Shlosman, I., Martinez-Valpuesta, I., and Heller, C. H. (2007). Gas Feedback on Stellar Bar Evolution. *ApJ*, 666(1):189–200.
- Bigiel, F., Leroy, A., Walter, F., Brinks, E., de Blok, W. J. G., Madore, B., and Thornley, M. D. (2008). The Star Formation Law in Nearby Galaxies on Sub-Kpc Scales. *AJ*, 136(6):2846–2871.
- Bigiel, F., Leroy, A. K., Walter, F., Brinks, E., de Blok, W. J. G., Kramer, C., Rix, H. W., Schruba, A., Schuster, K. F., Usero, A., and Wiesemeyer, H. W. (2011). A Constant Molecular Gas Depletion Time in Nearby Disk Galaxies. *ApJL*, 730(2):L13.
- Binney, J. (1977). The physics of dissipational galaxy formation. *ApJ*, 215:483–491.

- Binney, J. (1981). Resonant excitation of motion perpendicular to galactic planes. *MNRAS*, 196:455–467.
- Binney, J., Gerhard, O. E., Stark, A. A., Bally, J., and Uchida, K. I. (1991). Understanding the kinematics of Galactic Centre gas. *MNRAS*, 252:210.
- Binney, J. and Tremaine, S. (1987). *Galactic dynamics*.
- Birnboim, Y. and Dekel, A. (2003). Virial shocks in galactic haloes? *MNRAS*, 345(1):349–364.
- Bittner, A., de Lorenzo-Cáceres, A., Gadotti, D. A., Sánchez-Blázquez, P., Neumann, J., Coelho, P., Falcón-Barroso, J., Fragkoudi, F., Kim, T., Martín-Navarro, I., Méndez-Abreu, J., Pérez, I., Querejeta, M., and van de Ven, G. (2021). Galaxies within galaxies in the TIMER survey: stellar populations of inner bars are scaled replicas of main bars. *A&A*, 646:A42.
- Bittner, A., Falcón-Barroso, J., Nedelchev, B., Dorta, A., Gadotti, D. A., Sarzi, M., Molaeinezhad, A., Iodice, E., Rosado-Belza, D., de Lorenzo-Cáceres, A., Fragkoudi, F., Galán-de Anta, P. M., Husemann, B., Méndez-Abreu, J., Neumann, J., Pinna, F., Querejeta, M., Sánchez-Blázquez, P., and Seidel, M. K. (2019). The GIST pipeline: A multi-purpose tool for the analysis and visualisation of (integral-field) spectroscopic data. *A&A*, 628:A117.
- Bittner, A., Sánchez-Blázquez, P., Gadotti, D. A., Neumann, J., Fragkoudi, F., Coelho, P., de Lorenzo-Cáceres, A., Falcón-Barroso, J., Kim, T., Leaman, R., Martín-Navarro, I., Méndez-Abreu, J., Pérez, I., Querejeta, M., Seidel, M. K., and van de Ven, G. (2020). Inside-out formation of nuclear discs and the absence of old central spheroids in barred galaxies of the TIMER survey. *A&A*, 643:A65.
- Blanton, M. R. and Moustakas, J. (2009). Physical Properties and Environments of Nearby Galaxies. *ARA&A*, 47(1):159–210.
- Bluck, A. F. L., Conselice, C. J., Bouwens, R. J., Daddi, E., Dickinson, M., Papovich, C., and Yan, H. (2009). A surprisingly high pair fraction for extremely massive galaxies at $z \sim 3$ in the GOODS NICMOS survey. *MNRAS*, 394(1):L51–L55.

- Bluck, A. F. L., Conselice, C. J., Buitrago, F., Grützbauch, R., Hoyos, C., Mortlock, A., and Bauer, A. E. (2012). The Structures and Total (Minor + Major) Merger Histories of Massive Galaxies up to $z \sim 3$ in the HST GOODS NICMOS Survey: A Possible Solution to the Size Evolution Problem. *ApJ*, 747(1):34.
- Blumenthal, G. R., Faber, S. M., Primack, J. R., and Rees, M. J. (1984). Formation of galaxies and large-scale structure with cold dark matter. *Nature*, 311:517–525.
- Bournaud, F. and Combes, F. (2002). Gas accretion on spiral galaxies: Bar formation and renewal. *A&A*, 392:83–102.
- Bournaud, F., Combes, F., and Semelin, B. (2005). The lifetime of galactic bars: central mass concentrations and gravity torques. *MNRAS*, 364(1):L18–L22.
- Bournaud, F., Daddi, E., Elmegreen, B. G., Elmegreen, D. M., Nesvadba, N., Vanzella, E., Di Matteo, P., Le Tiran, L., Lehnert, M., and Elbaz, D. (2008). Observations and modeling of a clumpy galaxy at $z = 1.6$. Spectroscopic clues to the origin and evolution of chain galaxies. *A&A*, 486(3):741–753.
- Bournaud, F., Duc, P. A., and Masset, F. (2003). The large extent of dark matter haloes probed by the formation of tidal dwarf galaxies. *A&A*, 411:L469–L472.
- Bournaud, F., Elmegreen, B. G., and Martig, M. (2009). The Thick Disks of Spiral Galaxies as Relics from Gas-rich, Turbulent, Clumpy Disks at High Redshift. *ApJL*, 707(1):L1–L5.
- Bournaud, F., Jog, C. J., and Combes, F. (2007). Multiple minor mergers: formation of elliptical galaxies and constraints for the growth of spiral disks. *A&A*, 476(3):1179–1190.
- Bovy, J., Leung, H. W., Hunt, J. A. S., Mackereth, J. T., García-Hernández, D. A., and Roman-Lopes, A. (2019). Life in the fast lane: a direct view of the dynamics, formation, and evolution of the Milky Way’s bar. *MNRAS*, 490(4):4740–4747.

- Bower, R. G., Benson, A. J., Malbon, R., Helly, J. C., Frenk, C. S., Baugh, C. M., Cole, S., and Lacey, C. G. (2006). Breaking the hierarchy of galaxy formation. *MNRAS*, 370(2):645–655.
- Boylan-Kolchin, M., Springel, V., White, S. D. M., and Jenkins, A. (2010). There’s no place like home? Statistics of Milky Way-mass dark matter haloes. *MNRAS*, 406(2):896–912.
- Bremer, M. N., Phillipps, S., Kelvin, L. S., De Propriis, R., Kennedy, R., Moffett, A. J., Bamford, S., Davies, L. J. M., Driver, S. P., Häußler, B., Holwerda, B., Hopkins, A., James, P. A., Liske, J., Percival, S., and Taylor, E. N. (2018). Galaxy and Mass Assembly (GAMA): Morphological transformation of galaxies across the green valley. *MNRAS*, 476(1):12–26.
- Bridge, C. R., Carlberg, R. G., and Sullivan, M. (2010). The CFHTLS-Deep Catalog of Interacting Galaxies. I. Merger Rate Evolution to $z = 1.2$. *ApJ*, 709(2):1067–1082.
- Bromm, V. (2013). Formation of the first stars. *Reports on Progress in Physics*, 76(11):112901.
- Bromm, V., Coppi, P. S., and Larson, R. B. (2002). The Formation of the First Stars. I. The Primordial Star-forming Cloud. *ApJ*, 564(1):23–51.
- Bromm, V., Yoshida, N., Hernquist, L., and McKee, C. F. (2009). The formation of the first stars and galaxies. *Nature*, 459(7243):49–54.
- Brooks, A. M., Governato, F., Quinn, T., Brook, C. B., and Wadsley, J. (2009). The Role of Cold Flows in the Assembly of Galaxy Disks. *ApJ*, 694(1):396–410.
- Bryant, J. J., Owers, M. S., Robotham, A. S. G., Croom, S. M., Driver, S. P., Drinkwater, M. J., Lorente, N. P. F., Cortese, L., Scott, N., Colless, M., Schaefer, A., Taylor, E. N., Konstantopoulos, I. S., Allen, J. T., Baldry, I., Barnes, L., Bauer, A. E., Bland-Hawthorn, J., Bloom, J. V., Brooks, A. M., Brough, S., Cecil, G., Couch, W., Croton, D., Davies, R., Ellis, S., Fogarty, L. M. R., Foster, C., Glazebrook, K., Goodwin, M., Green, A., Gunawardhana, M. L., Hampton, E., Ho, I. T., Hopkins, A. M., Kewley,

- L., Lawrence, J. S., Leon-Saval, S. G., Leslie, S., McElroy, R., Lewis, G., Liske, J., López-Sánchez, Á. R., Mahajan, S., Medling, A. M., Metcalfe, N., Meyer, M., Mould, J., Obreschkow, D., O’Toole, S., Pracy, M., Richards, S. N., Shanks, T., Sharp, R., Sweet, S. M., Thomas, A. D., Tonini, C., and Walcher, C. J. (2015). The SAMI Galaxy Survey: instrument specification and target selection. *MNRAS*, 447(3):2857–2879.
- Buck, T., Macciò, A. V., Obreja, A., Dutton, A. A., Domínguez-Tenreiro, R., and Granato, G. L. (2017). NIHAO XIII: Clumpy discs or clumpy light in high-redshift galaxies? *MNRAS*, 468(3):3628–3649.
- Bundy, K., Bershady, M. A., Law, D. R., Yan, R., Drory, N., MacDonald, N., Wake, D. A., Cherinka, B., Sánchez-Gallego, J. R., Weijmans, A.-M., Thomas, D., Tremonti, C., Masters, K., Coccatto, L., Diamond-Stanic, A. M., Aragón-Salamanca, A., Avila-Reese, V., Badenes, C., Falcón-Barroso, J., Belfiore, F., Bizyaev, D., Blanc, G. A., Bland-Hawthorn, J., Blanton, M. R., Brownstein, J. R., Byler, N., Cappellari, M., Conroy, C., Dutton, A. A., Emsellem, E., Etherington, J., Frinchaboy, P. M., Fu, H., Gunn, J. E., Harding, P., Johnston, E. J., Kauffmann, G., Kinemuchi, K., Klaene, M. A., Knapen, J. H., Leauthaud, A., Li, C., Lin, L., Maiolino, R., Malanushenko, V., Malanushenko, E., Mao, S., Maraston, C., McDermid, R. M., Merrifield, M. R., Nichol, R. C., Oravetz, D., Pan, K., Parejko, J. K., Sanchez, S. F., Schlegel, D., Simmons, A., Steele, O., Steinmetz, M., Thanjavur, K., Thompson, B. A., Tinker, J. L., van den Bosch, R. C. E., Westfall, K. B., Wilkinson, D., Wright, S., Xiao, T., and Zhang, K. (2015). Overview of the SDSS-IV MaNGA Survey: Mapping nearby Galaxies at Apache Point Observatory. *ApJ*, 798(1):7.
- Bureau, M., Freeman, K. C., Pfitzner, D. W., and Meurer, G. R. (1999). The Shape and Figure Rotation of the Dark Halo of NGC 2915. *AJ*, 118(5):2158–2171.
- Buta, R. and Block, D. L. (2001). A Dust-penetrated Classification Scheme for Bars as Inferred from Their Gravitational Force Fields. *ApJ*, 550(1):243–252.
- Buta, R. and Combes, F. (1996). Galactic Rings. *Fund. Cosmic Phys.*, 17:95–281.

- Buta, R., Laurikainen, E., and Salo, H. (2004). The Distribution of Maximum Relative Gravitational Torques in Disk Galaxies. *AJ*, 127(1):279–294.
- Buta, R. J. (2017). Galactic rings revisited. II. Dark gaps and the locations of resonances in early-to-intermediate-type disc galaxies. *MNRAS*, 470(4):3819–3849.
- Buta, R. J., Sheth, K., Athanassoula, E., Bosma, A., Knapen, J. H., Laurikainen, E., Salo, H., Elmegreen, D., Ho, L. C., Zaritsky, D., Courtois, H., Hinz, J. L., Muñoz-Mateos, J.-C., Kim, T., Regan, M. W., Gadotti, D. A., Gil de Paz, A., Laine, J., Menéndez-Delmestre, K., Comerón, S., Erroz Ferrer, S., Seibert, M., Mizusawa, T., Holwerda, B., and Madore, B. F. (2015). A Classical Morphological Analysis of Galaxies in the Spitzer Survey of Stellar Structure in Galaxies (S4G). *ApJS*, 217(2):32.
- Cano-Díaz, M., Sánchez, S. F., Zibetti, S., Ascasibar, Y., Bland-Hawthorn, J., Ziegler, B., González Delgado, R. M., Walcher, C. J., García-Benito, R., Mast, D., Mendoza-Pérez, M. A., Falcón-Barroso, J., Galbany, L., Husemann, B., Kehrig, C., Marino, R. A., Sánchez-Blázquez, P., López-Cobá, C., López-Sánchez, Á. R., and Vilchez, J. M. (2016). Spatially Resolved Star Formation Main Sequence of Galaxies in the CALIFA Survey. *ApJL*, 821(2):L26.
- Cappellari, M. (2017). Improving the full spectrum fitting method: accurate convolution with Gauss-Hermite functions. *MNRAS*, 466(1):798–811.
- Cappellari, M. and Copin, Y. (2003). Adaptive spatial binning of integral-field spectroscopic data using Voronoi tessellations. *MNRAS*, 342(2):345–354.
- Cappellari, M. and Emsellem, E. (2004). Parametric Recovery of Line-of-Sight Velocity Distributions from Absorption-Line Spectra of Galaxies via Penalized Likelihood. *PASP*, 116(816):138–147.
- Carles, C., Martel, H., Ellison, S. L., and Kawata, D. (2016). The mass dependence of star formation histories in barred spiral galaxies. *MNRAS*, 463(1):1074–1087.
- Carollo, C. M. (1999). The Centers of Early- to Intermediate-Type Spiral Galaxies: A Structural Analysis. *ApJ*, 523(2):566–574.

- Carollo, C. M., Stiavelli, M., de Zeeuw, P. T., and Mack, J. (1997). Spiral Galaxies with WFPC2. I. Nuclear Morphology, Bulges, Star Clusters, and Surface Brightness Profiles. *AJ*, 114:2366.
- Casasola, V., Combes, F., García-Burillo, S., Hunt, L. K., León, S., and Baker, A. J. (2008). Molecular gas in Nuclei of GALaxies (NUGA). X. The Seyfert 2 galaxy NGC 3147. *A&A*, 490(1):61–76.
- Catalán-Torrecilla, C., Gil de Paz, A., Castillo-Morales, A., Méndez-Abreu, J., Falcón-Barroso, J., Bekeraite, S., Costantin, L., de Lorenzo-Cáceres, A., Florido, E., García-Benito, R., Husemann, B., Iglesias-Páramo, J., Kennicutt, R. C., Mast, D., Pascual, S., Ruiz-Lara, T., Sánchez-Menguiano, L., Sánchez, S. F., Walcher, C. J., Bland-Hawthorn, J., Duarte Puertas, S., Marino, R. A., Masegosa, J., Sánchez-Blázquez, P., and CALIFA Collaboration (2017). Star Formation in the Local Universe from the CALIFA Sample. II. Activation and Quenching Mechanisms in Bulges, Bars, and Disks. *ApJ*, 848(2):87.
- Cavanagh, M. K. and Bekki, K. (2020). Bars formed in galaxy merging and their classification with deep learning. *A&A*, 641:A77.
- Ceverino, D., Dekel, A., and Bournaud, F. (2010). High-redshift clumpy discs and bulges in cosmological simulations. *MNRAS*, 404(4):2151–2169.
- Ceverino, D., Dekel, A., Mandelker, N., Bournaud, F., Burkert, A., Genzel, R., and Primack, J. (2012). Rotational support of giant clumps in high-*z* disc galaxies. *MNRAS*, 420(4):3490–3520.
- Chandrasekhar, S. (1943). Dynamical Friction. I. General Considerations: the Coefficient of Dynamical Friction. *ApJ*, 97:255.
- Cheung, E., Athanassoula, E., Masters, K. L., Nichol, R. C., Bosma, A., Bell, E. F., Faber, S. M., Koo, D. C., Lintott, C., Melvin, T., Schawinski, K., Skibba, R. A., and Willett, K. W. (2013). Galaxy Zoo: Observing Secular Evolution through Bars. *ApJ*, 779(2):162.

- Cheung, E., Trump, J. R., Athanassoula, E., Bamford, S. P., Bell, E. F., Bosma, A., Cardamone, C. N., Casteels, K. R. V., Faber, S. M., Fang, J. J., Fortson, L. F., Kocevski, D. D., Koo, D. C., Laine, S., Lintott, C., Masters, K. L., Melvin, T., Nichol, R. C., Schawinski, K., Simmons, B., Smethurst, R., and Willett, K. W. (2015). Galaxy Zoo: Are bars responsible for the feeding of active galactic nuclei at $0.2 < z < 1.0$? *MNRAS*, 447(1):506–516.
- Chiba, R., Friske, J. K. S., and Schönrich, R. (2021). Resonance sweeping by a decelerating Galactic bar. *MNRAS*, 500(4):4710–4729.
- Chiba, R. and Schönrich, R. (2021). Tree-ring structure of Galactic bar resonance. *MNRAS*.
- Cisternas, M., Sheth, K., Salvato, M., Knapen, J. H., Civano, F., and Santini, P. (2015). The Role of Bars in AGN Fueling in Disk Galaxies Over the Last Seven Billion Years. *ApJ*, 802(2):137.
- Coelho, P. and Gadotti, D. A. (2011). Bars Rejuvenating Bulges? Evidence from Stellar Population Analysis. *ApJL*, 743(1):L13.
- Cole, A. A. and Weinberg, M. D. (2002). An Upper Limit to the Age of the Galactic Bar. *ApJL*, 574(1):L43–L46.
- Cole, D. R., Debattista, V. P., Erwin, P., Earp, S. W. F., and Roškar, R. (2014). The formation of stellar nuclear discs in bar-induced gas inflows. *MNRAS*, 445(4):3352–3369.
- Cole, S., Lacey, C. G., Baugh, C. M., and Frenk, C. S. (2000). Hierarchical galaxy formation. *MNRAS*, 319(1):168–204.
- Cole, S., Percival, W. J., Peacock, J. A., Norberg, P., Baugh, C. M., Frenk, C. S., Baldry, I., Bland-Hawthorn, J., Bridges, T., Cannon, R., Colless, M., Collins, C., Couch, W., Cross, N. J. G., Dalton, G., Eke, V. R., De Propriis, R., Driver, S. P., Efstathiou, G., Ellis, R. S., Glazebrook, K., Jackson, C., Jenkins, A., Lahav, O., Lewis, I., Lumsden, S., Maddox, S., Madgwick, D., Peterson, B. A., Sutherland, W.,

- and Taylor, K. (2005). The 2dF Galaxy Redshift Survey: power-spectrum analysis of the final data set and cosmological implications. *MNRAS*, 362(2):505–534.
- Colless, M., Dalton, G., Maddox, S., Sutherland, W., Norberg, P., Cole, S., Bland-Hawthorn, J., Bridges, T., Cannon, R., Collins, C., Couch, W., Cross, N., Deeley, K., De Propris, R., Driver, S. P., Efstathiou, G., Ellis, R. S., Frenk, C. S., Glazebrook, K., Jackson, C., Lahav, O., Lewis, I., Lumsden, S., Madgwick, D., Peacock, J. A., Peterson, B. A., Price, I., Seaborne, M., and Taylor, K. (2001). The 2dF Galaxy Redshift Survey: spectra and redshifts. *MNRAS*, 328(4):1039–1063.
- Collier, A. (2020). Violent buckling benefits galactic bars. *MNRAS*, 492(2):2241–2249.
- Combes, F. (2001). Fueling the AGN. In Aretxaga, I., Kunth, D., and Mújica, R., editors, *Advanced Lectures on the Starburst-AGN*, page 223.
- Combes, F. (2003). AGN Fueling: The observational point of view. In Collin, S., Combes, F., and Shlosman, I., editors, *Active Galactic Nuclei: From Central Engine to Host Galaxy*, volume 290 of *Astronomical Society of the Pacific Conference Series*, page 411.
- Combes, F. (2008). Gaseous flows in galaxies. In Bureau, M., Athanassoula, E., and Barbuy, B., editors, *Formation and Evolution of Galaxy Bulges*, volume 245, pages 151–160.
- Combes, F., Debbasch, F., Friedli, D., and Pfenniger, D. (1990). Box and peanut shapes generated by stellar bars. *A&A*, 233:82.
- Combes, F. and Sanders, R. H. (1981). Formation and properties of persisting stellar bars. *A&A*, 96:164–173.
- Comerón, S., Salo, H., Laurikainen, E., Knapen, J. H., Buta, R. J., Herrera-Endoqui, M., Laine, J., Holwerda, B. W., Sheth, K., Regan, M. W., Hinz, J. L., Muñoz-Mateos, J. C., Gil de Paz, A., Menéndez-Delmestre, K., Seibert, M., Mizusawa, T., Kim, T., Erroz-Ferrer, S., Gadotti, D. A., Athanassoula, E., Bosma, A., and Ho, L. C. (2014). ARRAKIS: atlas of resonance rings as known in the S⁴G. *A&A*, 562:A121.

- Conselice, C. J., Bershad, M. A., Dickinson, M., and Papovich, C. (2003). A Direct Measurement of Major Galaxy Mergers at $z \sim 3$. *AJ*, 126(3):1183–1207.
- Consolandi, G. (2016). Automated bar detection in local disk galaxies from the SDSS. The colors of bars. *A&A*, 595:A67.
- Consolandi, G., Dotti, M., Boselli, A., Gavazzi, G., and Gargiulo, F. (2017). Bars as seen by Herschel and Sloan. *A&A*, 598:A114.
- Contopoulos, G. (1980). How far do bars extend. *A&A*, 81(1-2):198–209.
- Contopoulos, G. and Grosbol, P. (1989). Orbits in barred galaxies. *A&A Rev.*, 1(3-4):261–289.
- Contopoulos, G. and Papayannopoulos, T. (1980). Orbits in weak and strong bars. *A&A*, 92(1-2):33–46.
- Courteau, S., de Jong, R. S., and Broeils, A. H. (1996). Evidence for Secular Evolution in Late-Type Spirals. *ApJL*, 457:L73.
- Cullen, H., Alexander, P., Green, D. A., Clemens, M., and Sheth, K. (2007). The unusual distribution of molecular gas and star formation in Arp 140. *MNRAS*, 374(4):1185–1197.
- Curir, A., Mazzei, P., and Murante, G. (2008). Star formation and bar instability in cosmological halos. *A&A*, 481(3):651–659.
- Dalla Vecchia, C. and Schaye, J. (2008). Simulating galactic outflows with kinetic supernova feedback. *MNRAS*, 387(4):1431–1444.
- Davis, M., Efstathiou, G., Frenk, C. S., and White, S. D. M. (1985). The evolution of large-scale structure in a universe dominated by cold dark matter. *ApJ*, 292:371–394.
- de Vaucouleurs, G. (1959). General Physical Properties of External Galaxies. *Handbuch der Physik*, 53:311.

- de Vaucouleurs, G. (1964). Interpretation of velocity distribution of the inner regions of the Galaxy. In Kerr, F. J., editor, *The Galaxy and the Magellanic Clouds*, volume 20, page 195.
- Debattista, V. P., Carollo, C. M., Mayer, L., and Moore, B. (2005). The Kinematic Signature of Face-On Peanut-shaped Bulges. *ApJ*, 628(2):678–694.
- Debattista, V. P., Mayer, L., Carollo, C. M., Moore, B., Wadsley, J., and Quinn, T. (2006). The Secular Evolution of Disk Structural Parameters. *ApJ*, 645(1):209–227.
- Debattista, V. P. and Sellwood, J. A. (1998). Dynamical Friction and the Distribution of Dark Matter in Barred Galaxies. *ApJL*, 493(1):L5–L8.
- Deeley, S., Drinkwater, M. J., Cunnamea, D., Bland-Hawthorn, J., Brough, S., Cluver, M., Colless, M., Davies, L. J. M., Driver, S. P., Foster, C., Grootes, M. W., Hopkins, A. M., Kafle, P. R., Lara-Lopez, M. A., Liske, J., Mahajan, S., Phillipps, S., Power, C., and Robotham, A. (2017). Galaxy and Mass Assembly (GAMA): formation and growth of elliptical galaxies in the group environment. *MNRAS*, 467(4):3934–3943.
- Dekel, A. and Birnboim, Y. (2006). Galaxy bimodality due to cold flows and shock heating. *MNRAS*, 368(1):2–20.
- Dekel, A., Birnboim, Y., Engel, G., Freundlich, J., Goerdt, T., Mumcuoglu, M., Neistein, E., Pichon, C., Teyssier, R., and Zinger, E. (2009). Cold streams in early massive hot haloes as the main mode of galaxy formation. *Nature*, 457(7228):451–454.
- Dekel, A. and Silk, J. (1986). The Origin of Dwarf Galaxies, Cold Dark Matter, and Biased Galaxy Formation. *ApJ*, 303:39.
- Di Matteo, P., Qu, Y., Lehnert, M. D., van Driel, W., and Jog, C. J. (2010). Minor mergers and their impact on the kinematics of galaxy discs. In *EAS Publications Series*, volume 45 of *EAS Publications Series*, pages 389–392.

- Di Matteo, T., Springel, V., and Hernquist, L. (2005). Energy input from quasars regulates the growth and activity of black holes and their host galaxies. *Nature*, 433(7026):604–607.
- Díaz-García, S., Díaz-Suárez, S., Knapen, J. H., and Salo, H. (2019). Inner and outer rings are not strongly coupled with stellar bars. *A&A*, 625:A146.
- Díaz-García, S., Salo, H., Laurikainen, E., and Herrera-Endoqui, M. (2016). Characterization of galactic bars from 3.6 μm S⁴G imaging. *A&A*, 587:A160.
- Donohoe-Keyes, C. E., Martig, M., James, P. A., and Kraljic, K. (2019). Redistribution of stars and gas in the star formation deserts of barred galaxies. *MNRAS*, 489(4):4992–5003.
- Driver, S. P., Allen, P. D., Graham, A. W., Cameron, E., Liske, J., Ellis, S. C., Cross, N. J. G., De Propris, R., Phillipps, S., and Couch, W. J. (2006). The Millennium Galaxy Catalogue: morphological classification and bimodality in the colour-concentration plane. *MNRAS*, 368(1):414–434.
- Drory, N. and Fisher, D. B. (2007). A Connection between Bulge Properties and the Bimodality of Galaxies. *ApJ*, 664(2):640–649.
- Du, M., Debattista, V. P., Shen, J., Ho, L. C., and Erwin, P. (2017). Black Hole Growth in Disk Galaxies Mediated by the Secular Evolution of Short Bars. *ApJL*, 844(2):L15.
- Dubois, Y. and Teyssier, R. (2008). On the onset of galactic winds in quiescent star forming galaxies. *A&A*, 477(1):79–94.
- Dunkley, J., Spergel, D. N., Komatsu, E., Hinshaw, G., Larson, D., Nolta, M. R., Odegard, N., Page, L., Bennett, C. L., Gold, B., Hill, R. S., Jarosik, N., Weiland, J. L., Halpern, M., Kogut, A., Limon, M., Meyer, S. S., Tucker, G. S., Wollack, E., and Wright, E. L. (2009). Five-Year Wilkinson Microwave Anisotropy Probe (WMAP) Observations: Bayesian Estimation of Cosmic Microwave Background Polarization Maps. *ApJ*, 701(2):1804–1813.

- Durbala, A., Sulentic, J. W., Buta, R., and Verdes-Montenegro, L. (2008). Photometric characterization of a well-defined sample of isolated galaxies in the context of the AMIGA project. *MNRAS*, 390(3):881–905.
- Dutton, A. A. (2009). On the origin of exponential galaxy discs. *MNRAS*, 396(1):121–140.
- Eales, S. A., Baes, M., Bourne, N., Bremer, M., Brown, M. J. I., Clark, C., Clements, D., de Vis, P., Driver, S., Dunne, L., Dye, S., Furlanetto, C., Holwerda, B., Ivison, R. J., Kelvin, L. S., Lara-Lopez, M., Leeuw, L., Loveday, J., Maddox, S., Michałowski, M. J., Phillipps, S., Robotham, A., Smith, D., Smith, M., Valiante, E., van der Werf, P., and Wright, A. (2018). The causes of the red sequence, the blue cloud, the green valley, and the green mountain. *MNRAS*, 481(1):1183–1194.
- Efstathiou, G., Lake, G., and Negroponte, J. (1982). The stability and masses of disc galaxies. *MNRAS*, 199:1069–1088.
- Eisenstein, D. J. and Hut, P. (1998). HOP: A New Group-Finding Algorithm for N-Body Simulations. *ApJ*, 498(1):137–142.
- Ellison, S. L., Patton, D. R., Nair, P., Simard, L., Mendel, J. T., McConnachie, A. W., and Scudder, J. M. (2011). Gas Flows in Galaxies: the Relative Importance of Mergers and Bars. In Carignan, C., Combes, F., and Freeman, K. C., editors, *Tracing the Ancestry of Galaxies*, volume 277, pages 178–181.
- Elmegreen, B. G. (1993). Star Formation at Compressed Interfaces in Turbulent Self-gravitating Clouds. *ApJl*, 419:L29.
- Elmegreen, B. G., Bournaud, F., and Elmegreen, D. M. (2008). Bulge Formation by the Coalescence of Giant Clumps in Primordial Disk Galaxies. *ApJ*, 688(1):67–77.
- Elmegreen, B. G. and Elmegreen, D. M. (1985). Properties of barred spiral galaxies. *ApJ*, 288:438–455.
- Elmegreen, B. G. and Elmegreen, D. M. (2005). Stellar Populations in 10 Clump-Cluster Galaxies of the Hubble Ultra Deep Field. *ApJ*, 627(2):632–646.

- Elmegreen, B. G., Elmegreen, D. M., Chromey, F. R., Hasselbacher, D. A., and Bissell, B. A. (1996). Light Profiles and Pattern Speeds for Bars in Early- and Late-Type Galaxies. *AJ*, 111:2233.
- Elmegreen, B. G., Elmegreen, D. M., Vollbach, D. R., Foster, E. R., and Ferguson, T. E. (2006). On the Origin of Exponential Disks at High Redshift. In *American Astronomical Society Meeting Abstracts #207*, volume 207 of *American Astronomical Society Meeting Abstracts*, page 138.12.
- Elmegreen, D. M. (2007). Clumpy Galaxies in the Early Universe. In Combes, F. and Palouš, J., editors, *Galaxy Evolution across the Hubble Time*, volume 235, pages 376–380.
- Elmegreen, D. M., Elmegreen, B. G., and Bellin, A. D. (1990). Statistical Evidence That Galaxy Companions Trigger Bars and Change the Spiral Hubble Type. *ApJ*, 364:415.
- Elmegreen, D. M., Elmegreen, B. G., and Hirst, A. C. (2004). Discovery of Face-on Counterparts of Chain Galaxies in the Tadpole Advanced Camera for Surveys Field. *ApJL*, 604(1):L21–L23.
- Emsellem, E. (2006). The origin of sigma-drops: mapping stellar kinematics and populations in spirals. *arXiv e-prints*, pages astro-ph/0610834.
- Emsellem, E., Greusard, D., Combes, F., Friedli, D., Leon, S., Pécontal, E., and Wozniak, H. (2001). Dynamics of embedded bars and the connection with AGN. I. ISAAC/VLT stellar kinematics. *A&A*, 368:52–63.
- Erwin, P. (2004). Double-barred galaxies. I. A catalog of barred galaxies with stellar secondary bars and inner disks. *A&A*, 415:941–957.
- Erwin, P. (2005). How large are the bars in barred galaxies? *MNRAS*, 364(1):283–302.
- Erwin, P. (2011). Double-barred galaxies. *Memorie della Societa Astronomica Italiana Supplementi*, 18:145.

- Erwin, P. (2018). The dependence of bar frequency on galaxy mass, colour, and gas content - and angular resolution - in the local universe. *MNRAS*, 474(4):5372–5392.
- Erwin, P. (2019). What determines the sizes of bars in spiral galaxies? *MNRAS*, 489(3):3553–3564.
- Erwin, P. and Debattista, V. P. (2016). Caught in the Act: Direct Detection of Galactic Bars in the Buckling Phase. *ApJL*, 825(2):L30.
- Erwin, P. and Debattista, V. P. (2017). The frequency and stellar-mass dependence of boxy/peanut-shaped bulges in barred galaxies. *MNRAS*, 468(2):2058–2080.
- Erwin, P., Saglia, R. P., Fabricius, M., Thomas, J., Nowak, N., Rusli, S., Bender, R., Vega Beltrán, J. C., and Beckman, J. E. (2015). Composite bulges: the coexistence of classical bulges and discy pseudo-bulges in S0 and spiral galaxies. *MNRAS*, 446(4):4039–4077.
- Erwin, P. and Sparke, L. S. (2002). Double Bars, Inner Disks, and Nuclear Rings in Early-Type Disk Galaxies. *AJ*, 124(1):65–77.
- Eskridge, P. B., Frogel, J. A., Pogge, R. W., Quillen, A. C., Davies, R. L., DePoy, D. L., Houdashelt, M. L., Kuchinski, L. E., Ramírez, S. V., Sellgren, K., Terndrup, D. M., and Tiede, G. P. (2000). The Frequency of Barred Spiral Galaxies in the Near-Infrared. *AJ*, 119(2):536–544.
- Faber, S. M., Willmer, C. N. A., Wolf, C., Koo, D. C., Weiner, B. J., Newman, J. A., Im, M., Coil, A. L., Conroy, C., Cooper, M. C., Davis, M., Finkbeiner, D. P., Gerke, B. F., Gebhardt, K., Groth, E. J., Guhathakurta, P., Harker, J., Kaiser, N., Kassin, S., Kleinheinrich, M., Konidaris, N. P., Kron, R. G., Lin, L., Luppino, G., Madgwick, D. S., Meisenheimer, K., Noeske, K. G., Phillips, A. C., Sarajedini, V. L., Schiavon, R. P., Simard, L., Szalay, A. S., Vogt, N. P., and Yan, R. (2007). Galaxy Luminosity Functions to $z \sim 1$ from DEEP2 and COMBO-17: Implications for Red Galaxy Formation. *ApJ*, 665(1):265–294.
- Fakhouri, O. and Ma, C.-P. (2008). The nearly universal merger rate of dark matter haloes in Λ CDM cosmology. *MNRAS*, 386(2):577–592.

- Falcón-Barroso, J., Bacon, R., Bureau, M., Cappellari, M., Davies, R. L., de Zeeuw, P. T., Emsellem, E., Fathi, K., Krajnović, D., Kuntschner, H., McDermid, R. M., Peletier, R. F., and Sarzi, M. (2006). The SAURON project - VII. Integral-field absorption and emission-line kinematics of 24 spiral galaxy bulges. *MNRAS*, 369(2):529–566.
- Fanali, R., Dotti, M., Fiacconi, D., and Haardt, F. (2015). Bar formation as driver of gas inflows in isolated disc galaxies. *MNRAS*, 454(4):3641–3652.
- Fathi, K. and Peletier, R. F. (2003). Do bulges of early- and late-type spirals have different morphology? *A&A*, 407:61–74.
- Fisher, D. B. (2006). Central Star Formation and PAH Profiles in Pseudobulges and Classical Bulges. *ApJ*, 642(1):L17–L20.
- Fisher, D. B., Bolatto, A., Drory, N., Combes, F., Blitz, L., and Wong, T. (2013). The Molecular Gas Density in Galaxy Centers and how it Connects to Bulges. *ApJ*, 764(2):174.
- Fisher, D. B. and Drory, N. (2008a). Distinguishing Pseudobulges and Classical Bulges. In Funes, J. G. and Corsini, E. M., editors, *Formation and Evolution of Galaxy Disks*, volume 396 of *Astronomical Society of the Pacific Conference Series*, page 309.
- Fisher, D. B. and Drory, N. (2008b). The Structure of Classical Bulges and Pseudobulges: the Link Between Pseudobulges and Sérsic Index. *AJ*, 136(2):773–839.
- Fisher, D. B. and Drory, N. (2010). Bulges of Nearby Galaxies with Spitzer: Scaling Relations in Pseudobulges and Classical Bulges. *ApJ*, 716(2):942–969.
- Fisher, D. B., Drory, N., and Fabricius, M. H. (2009). Bulges of Nearby Galaxies with Spitzer: The Growth of Pseudobulges in Disk Galaxies and its Connection to Outer Disks. *ApJ*, 697(1):630–650.
- Fisher, D. B., Glazebrook, K., Abraham, R. G., Damjanov, I., White, H. A., Obreschkow, D., Basset, R., Bekiaris, G., Wisnioski, E., Green, A., and Bolatto,

- A. D. (2017). Connecting Clump Sizes in Turbulent Disk Galaxies to Instability Theory. *ApJl*, 839(1):L5.
- Font, A. S., McCarthy, I. G., Le Brun, A. M. C., Crain, R. A., and Kelvin, L. S. (2017a). The Diversity of Assembly Histories Leading to Disc Galaxy Formation in a Λ CDM Model. *PASA*, 34:e050.
- Font, J., Beckman, J. E., Martínez-Valpuesta, I., Borlaff, A. S., James, P. A., Díaz-García, S., García-Lorenzo, B., Camps-Fariña, A., Gutiérrez, L., and Amram, P. (2017b). Kinematic Clues to Bar Evolution for Galaxies in the Local Universe: Why the Fastest Rotating Bars are Rotating Most Slowly. *ApJ*, 835(2):279.
- Förster Schreiber, N. M., Shapley, A. E., Genzel, R., Bouché, N., Cresci, G., Davies, R., Erb, D. K., Genel, S., Lutz, D., Newman, S., Shapiro, K. L., Steidel, C. C., Sternberg, A., and Tacconi, L. J. (2011). Constraints on the Assembly and Dynamics of Galaxies. II. Properties of Kiloparsec-scale Clumps in Rest-frame Optical Emission of $z \sim 2$ Star-forming Galaxies. *ApJ*, 739(1):45.
- Fragkoudi, F., Di Matteo, P., Haywood, M., Gómez, A., Combes, F., Katz, D., and Semelin, B. (2017). Bars and boxy/peanut bulges in thin and thick discs. I. Morphology and line-of-sight velocities of a fiducial model. *A&A*, 606:A47.
- Fraser-McKelvie, A., Aragón-Salamanca, A., Merrifield, M., Masters, K., Nair, P., Emsellem, E., Kraljic, K., Krishnarao, D., Andrews, B. H., Drory, N., and Neumann, J. (2020a). SDSS-IV MaNGA: spatially resolved star formation in barred galaxies. *MNRAS*, 495(4):4158–4169.
- Fraser-McKelvie, A., Brown, M. J. I., Pimblet, K. A., Dolley, T., Crossett, J. P., and Bonne, N. J. (2016). A photometrically and spectroscopically confirmed population of passive spiral galaxies. *MNRAS*, 462(1):L11–L15.
- Fraser-McKelvie, A., Merrifield, M., Aragón-Salamanca, A., Peterken, T., Kraljic, K., Masters, K., Stark, D., Fragkoudi, F., Smethurst, R., Boardman, N. F., Drory, N., and Lane, R. R. (2020b). SDSS-IV MaNGA: The link between bars and the early cessation of star formation in spiral galaxies. *MNRAS*, 499(1):1116–1125.

- Frenk, C. S. and White, S. D. M. (2012). Dark matter and cosmic structure. *Annalen der Physik*, 524(9-10):507–534.
- Friedli, D. and Benz, W. (1993). Secular evolution of isolated barred galaxies. I. Gravitational coupling between stellar bars and interstellar medium. *A&A*, 268:65–85.
- Friedli, D., Benz, W., and Kennicutt, R. (1994). On the Influence of Bars and Star Formation on Galactic Abundance Gradients. *ApJl*, 430:L105.
- Gadotti, D. A. (2008). Image decomposition of barred galaxies and AGN hosts. *MNRAS*, 384:420–439.
- Gadotti, D. A. (2011). Secular evolution and structural properties of stellar bars in galaxies. *MNRAS*, 415(4):3308–3318.
- Gadotti, D. A. and de Souza, R. E. (2003). NGC 4608 and NGC 5701: Barred Galaxies without Disks? *ApJl*, 583:L75–L78.
- Gadotti, D. A. and de Souza, R. E. (2005). The Vertical Stellar Kinematics in Face-On Barred Galaxies: Estimating the Ages of Bars. *ApJ*, 629(2):797–815.
- Gadotti, D. A. and de Souza, R. E. (2006). On the Lengths, Colors, and Ages of 18 Face-on Bars. *ApJS*, 163(2):270–281.
- Gadotti, D. A. and Dos Anjos, S. (2001). Stellar Populations, Bars and Secular Evolution in Late-Type Galaxies. In Funes, J. G. and Corsini, E. M., editors, *Galaxy Disks and Disk Galaxies*, volume 230 of *Astronomical Society of the Pacific Conference Series*, pages 237–238.
- Gadotti, D. A., Sánchez-Blázquez, P., Falcón-Barroso, J., Husemann, B., Seidel, M., Leaman, R., Leung, G., van de Ven, G., Querejeta, M., Fragkoudi, F., de Lorenzo-Cáceres, A. d., Méndez-Abreu, J., Pérez, I., Kim, T., Martínez-Valpuesta, I., Coelho, P., Donohoe-Keyes, C., Martig, M., and Neumann, J. (2018). Investigating the Formation and Evolution of Massive Disc Galaxies with the MUSE TIMER Project. *The Messenger*, 173:28–32.

- Gadotti, D. A., Sánchez-Blázquez, P., Falcón-Barroso, J., Husemann, B., Seidel, M. K., Pérez, I., de Lorenzo-Cáceres, A., Martínez-Valpuesta, I., Fragkoudi, F., Leung, G., van de Ven, G., Leaman, R., Coelho, P., Martig, M., Kim, T., Neumann, J., and Querejeta, M. (2019). Time Inference with MUSE in Extragalactic Rings (TIMER): properties of the survey and high-level data products. *MNRAS*, 482(1):506–529.
- Gadotti, D. A., Seidel, M. K., Sánchez-Blázquez, P., Falcón-Barroso, J., Husemann, B., Coelho, P., and Pérez, I. (2015). MUSE tells the story of NGC 4371: The dawning of secular evolution. *A&A*, 584:A90.
- Galloway, M. A., Willett, K. W., Fortson, L. F., Cardamone, C. N., Schawinski, K., Cheung, E., Lintott, C. J., Masters, K. L., Melvin, T., and Simmons, B. D. (2015). Galaxy Zoo: the effect of bar-driven fuelling on the presence of an active galactic nucleus in disc galaxies. *MNRAS*, 448(4):3442–3454.
- García de la Cruz, J., Martig, M., Minchev, I., and James, P. (2021). On the flaring of thick discs of galaxies: insights from simulations. *MNRAS*, 501(4):5105–5120.
- García-Gómez, C., Athanassoula, E., Barberà, C., and Bosma, A. (2017). Measuring bar strength using Fourier analysis of galaxy images. *A&A*, 601:A132.
- Gavazzi, G., Consolandi, G., Dotti, M., Fanali, R., Fossati, M., Fumagalli, M., Viscardi, E., Savorgnan, G., Boselli, A., Gutiérrez, L., Hernández Toledo, H., Giovanelli, R., and Haynes, M. P. (2015). H α 3: an H α imaging survey of HI selected galaxies from ALFALFA. VI. The role of bars in quenching star formation from $z = 3$ to the present epoch. *A&A*, 580:A116.
- Genel, S., Naab, T., Genzel, R., Förster Schreiber, N. M., Sternberg, A., Oser, L., Johansson, P. H., Davé, R., Oppenheimer, B. D., and Burkert, A. (2012). Short-lived Star-forming Giant Clumps in Cosmological Simulations of $z \approx 2$ Disks. *ApJ*, 745(1):11.
- Genzel, R., Burkert, A., Bouché, N., Cresci, G., Förster Schreiber, N. M., Shapley, A., Shapiro, K., Tacconi, L. J., Buschkamp, P., Cimatti, A., Daddi, E., Davies, R., Eisenhauer, F., Erb, D. K., Genel, S., Gerhard, O., Hicks, E., Lutz, D., Naab, T.,

- Ott, T., Rabien, S., Renzini, A., Steidel, C. C., Sternberg, A., and Lilly, S. J. (2008). From Rings to Bulges: Evidence for Rapid Secular Galaxy Evolution at $z \sim 2$ from Integral Field Spectroscopy in the SINS Survey. *ApJ*, 687(1):59–77.
- George, K., Joseph, P., Mondal, C., Subramanian, S., Subramaniam, A., and Paul, K. T. (2019). Insights on bar quenching from a multiwavelength analysis: The case of Messier 95. *A&A*, 621:L4.
- Goulding, A. D., Mattheae, E., Greene, J. E., Hickox, R. C., Alexander, D. M., Forman, W. R., Jones, C., Lehmer, B. D., Griffis, S., Kanek, S., and Oulmakki, M. (2017). Galaxy-scale Bars in Late-type Sloan Digital Sky Survey Galaxies Do Not Influence the Average Accretion Rates of Supermassive Black Holes. *ApJ*, 843(2):135.
- Gunn, J. E. and Gott, J. Richard, I. (1972). On the Infall of Matter Into Clusters of Galaxies and Some Effects on Their Evolution. *ApJ*, 176:1.
- Guo, Y., Closson Ferguson, H., Bell, E. F., Conselice, C., Koo, D. C., Ravindranath, S., Giavalisco, M., Dekel, A., Faber, S. M., Primack, J. R., Mandelker, N., and Candels (2015). The formation and evolution of clumpy galaxies from $z=3$ to $z=0.5$. In *American Astronomical Society Meeting Abstracts #225*, volume 225 of *American Astronomical Society Meeting Abstracts*, page 426.06.
- Guo, Y., Rafelski, M., Bell, E. F., Conselice, C. J., Dekel, A., Faber, S. M., Giavalisco, M., Koekemoer, A. M., Koo, D. C., Lu, Y., Mandelker, N., Primack, J. R., Ceverino, D., de Mello, D. F., Ferguson, H. C., Hathi, N., Kocevski, D., Lucas, R. A., Pérez-González, P. G., Ravindranath, S., Soto, E., Straughn, A., and Wang, W. (2018). Clumpy Galaxies in CANDELS. II. Physical Properties of UV-bright Clumps at $0.5 \leq z < 3$. *ApJ*, 853(2):108.
- Haan, S., Schinnerer, E., Emsellem, E., García-Burillo, S., Combes, F., Mundell, C. G., and Rix, H.-W. (2009). Dynamical Evolution of AGN Host Galaxies—Gas In/Out-Flow Rates in Seven NUGA Galaxies. *ApJ*, 692(2):1623–1661.
- Hakobyan, A. A., Karapetyan, A. G., Barkhudaryan, L. V., Mamon, G. A., Kunth, D., Petrosian, A. R., Adibekyan, V., Aramyan, L. S., and Turatto, M. (2015). Su-

- pernovae and their host galaxies – III. The impact of bars and bulges on the radial distribution of supernovae in disc galaxies. *Monthly Notices of the Royal Astronomical Society*, 456(3):2848–2860.
- Hakobyan, A. A., Karapetyan, A. G., Barkhudaryan, L. V., Mamon, G. A., Kunth, D., Petrosian, A. R., Adibekyan, V., Aramyan, L. S., and Turatto, M. (2016). Supernovae and their host galaxies - III. The impact of bars and bulges on the radial distribution of supernovae in disc galaxies. *MNRAS*, 456(3):2848–2860.
- Hammer, F., Flores, H., Puech, M., Yang, Y. B., Athanassoula, E., Rodrigues, M., and Delgado, R. (2009). The Hubble sequence: just a vestige of merger events? *A&A*, 507(3):1313–1326.
- Hao, L., Jogee, S., Barazza, F. D., Marinova, I., and Shen, J. (2009). Bars in Starbursts and AGNs - A Quantitative Reexamination. In Jogee, S., Marinova, I., Hao, L., and Blanc, G. A., editors, *Galaxy Evolution: Emerging Insights and Future Challenges*, volume 419 of *Astronomical Society of the Pacific Conference Series*, page 402.
- Heckman, T. M., Armus, L., and Miley, G. K. (1990). On the Nature and Implications of Starburst-driven Galactic Superwinds. *ApJS*, 74:833.
- Herrera-Endoqui, M., Díaz-García, S., Laurikainen, E., and Salo, H. (2015). Catalogue of the morphological features in the Spitzer Survey of Stellar Structure in Galaxies (S⁴G). *A&A*, 582:A86.
- Hilmi, T., Minchev, I., Buck, T., Martig, M., Quillen, A. C., Monari, G., Famaey, B., de Jong, R. S., Laporte, C. F. P., Read, J., Sanders, J. L., Steinmetz, M., and Wegg, C. (2020). Fluctuations in galactic bar parameters due to bar-spiral interaction. *MNRAS*, 497(1):933–955.
- Ho, L. C., Filippenko, A. V., and Sargent, W. L. W. (1997). The Influence of Bars on Nuclear Activity. *ApJ*, 487(2):591–602.
- Hohl, F. (1976). Suppression of bar instability by a massive halo. *AJ*, 81:30–36.

- Holley-Bockelmann, K., Weinberg, M., and Katz, N. (2005). Bar-induced evolution of dark matter cusps. *MNRAS*, 363(3):991–1007.
- Hopkins, P. F., Kereš, D., and Murray, N. (2013). Accretion does not drive the turbulence in galactic discs. *MNRAS*, 432(4):2639–2646.
- Hopkins, P. F., Kereš, D., Murray, N., Quataert, E., and Hernquist, L. (2012a). Stellar feedback and bulge formation in clumpy discs. *MNRAS*, 427(2):968–978.
- Hopkins, P. F., Quataert, E., and Murray, N. (2012b). Stellar feedback in galaxies and the origin of galaxy-scale winds. *MNRAS*, 421(4):3522–3537.
- Hopkins, P. F., Somerville, R. S., Cox, T. J., Hernquist, L., Jogee, S., Kereš, D., Ma, C.-P., Robertson, B., and Stewart, K. (2009). The effects of gas on morphological transformation in mergers: implications for bulge and disc demographics. *MNRAS*, 397(2):802–814.
- Hoyle, B., Masters, K. L., Nichol, R. C., Edmondson, E. M., Smith, A. M., Lintott, C., Scranton, R., Bamford, S., Schawinski, K., and Thomas, D. (2011). Galaxy Zoo: bar lengths in local disc galaxies. *MNRAS*, 415(4):3627–3640.
- Hoyle, F., Outram, P. J., Shanks, T., Croom, S. M., Boyle, B. J., Loaring, N. S., Miller, L., and Smith, R. J. (2002). The 2dF QSO Redshift Survey - IV. The QSO power spectrum from the 10k catalogue. *MNRAS*, 329(2):336–348.
- Hozumi, S. (2012). Destructible Bars in Disk Galaxies under the Dynamical Influence of a Massive Central Black Hole. *PASJ*, 64:5.
- Hozumi, S. and Hernquist, L. (2005). Secular Evolution of Barred Galaxies with Massive Central Black Holes. *PASJ*, 57:719–731.
- Hu, W. and White, M. (2004). The Cosmic Symphony. *Scientific American*, 290(2):44–53.
- Hubble, E. P. (1926). Extragalactic nebulae. *ApJ*, 64:321–369.
- Hubble, E. P. (1936). *Realm of the Nebulae*.

- Iannuzzi, F. and Athanassoula, E. (2015). 2D kinematic signatures of boxy/peanut bulges. *MNRAS*, 450(3):2514–2538.
- Inoue, S., Dekel, A., Mandelker, N., Ceverino, D., Bournaud, F., and Primack, J. (2016). Non-linear violent disc instability with high Toomre’s Q in high-redshift clumpy disc galaxies. *MNRAS*, 456(2):2052–2069.
- Inoue, S. and Saitoh, T. R. (2014). Properties of thick discs formed in clumpy galaxies. *MNRAS*, 441(1):243–255.
- James, P. A., Bretherton, C. F., and Knapen, J. H. (2009). The $H\alpha$ galaxy survey. VII. The spatial distribution of star formation within disks and bulges. *A&A*, 501(1):207–220.
- James, P. A. and Percival, S. M. (2015). Discovery of kpc-scale line emission in barred galaxies, not linked to AGN or star formation. *MNRAS*, 450(4):3503–3513.
- James, P. A. and Percival, S. M. (2016). Stellar population constraints on the ages of galactic bars. *MNRAS*, 457(1):917–925.
- James, P. A. and Percival, S. M. (2018). Star formation suppression and bar ages in nearby barred galaxies. *MNRAS*, 474(3):3101–3109.
- Jogee, S., Barazza, F. D., Rix, H.-W., Shlosman, I., Barden, M., Wolf, C., Davies, J., Heyer, I., Beckwith, S. V. W., Bell, E. F., Borch, A., Caldwell, J. A. R., Conselice, C. J., Dahlen, T., Häußler, B., Heymans, C., Jahnke, K., Knapen, J. H., Laine, S., Lubell, G. M., Mobasher, B., McIntosh, D. H., Meisenheimer, K., Peng, C. Y., Ravindranath, S., Sanchez, S. F., Somerville, R. S., and Wisotzki, L. (2004). Bar Evolution over the Last 8 Billion Years: A Constant Fraction of Strong Bars in the GEMS Survey. *ApJL*, 615(2):L105–L108.
- Jogee, S., Miller, S. H., Penner, K., Skelton, R. E., Conselice, C. J., Somerville, R. S., Bell, E. F., Zheng, X. Z., Rix, H.-W., Robaina, A. R., Barazza, F. D., Barden, M., Borch, A., Beckwith, S. V. W., Caldwell, J. A. R., Peng, C. Y., Heymans, C., McIntosh, D. H., Häußler, B., Jahnke, K., Meisenheimer, K., Sanchez, S. F., Wisotzki, L.,

- Wolf, C., and Papovich, C. (2009). History of Galaxy Interactions and Their Impact on Star Formation Over the Last 7 Gyr from GEMS. *ApJ*, 697(2):1971–1992.
- Kalnajs, A. J. (1978). A Confrontation of Density Wave Theories with Observations. In Berkhuijsen, E. M. and Wielebinski, R., editors, *Structure and Properties of Nearby Galaxies*, volume 77, page 113.
- Katz, N., Weinberg, D. H., and Hernquist, L. (1996). Cosmological Simulations with TreeSPH. *ApJS*, 105:19.
- Kaviraj, S., Devriendt, J. E. G., Ferreras, I., Yi, S. K., and Silk, J. (2009). Identifying the progenitor set of present-day early-type galaxies: a view from the standard model. *A&A*, 503(2):445–458.
- Kelvin, L. S., Driver, S. P., Robotham, A. S. G., Taylor, E. N., Graham, A. W., Alpaslan, M., Baldry, I., Bamford, S. P., Bauer, A. E., Bland-Hawthorn, J., Brown, M. J. I., Colless, M., Conselice, C. J., Holwerda, B. W., Hopkins, A. M., Lara-López, M. A., Liske, J., López-Sánchez, Á. R., Loveday, J., Norberg, P., Phillipps, S., Popescu, C. C., Prescott, M., Sansom, A. E., and Tuffs, R. J. (2014). Galaxy And Mass Assembly (GAMA): stellar mass functions by Hubble type. *MNRAS*, 444(2):1647–1659.
- Kennicutt, Robert C., J. (1998). The Global Schmidt Law in Star-forming Galaxies. *ApJ*, 498(2):541–552.
- Kereš, D., Katz, N., Fardal, M., Davé, R., and Weinberg, D. H. (2009). Galaxies in a simulated Λ CDM Universe - I. Cold mode and hot cores. *MNRAS*, 395(1):160–179.
- Kereš, D., Katz, N., Weinberg, D. H., and Davé, R. (2005). How do galaxies get their gas? *MNRAS*, 363(1):2–28.
- Khoperskov, S., Haywood, M., Di Matteo, P., Lehnert, M. D., and Combes, F. (2018). Bar quenching in gas-rich galaxies. *A&A*, 609:A60.
- Kim, E., Hwang, H. S., Chung, H., Lee, G.-H., Park, C., Cervantes Sodi, B., and Kim, S. S. (2017). Star Formation Activity of Barred Spiral Galaxies. *ApJ*, 845(2):93.

- Kim, M., Choi, Y.-Y., and Kim, S. S. (2020). Effect of bars on evolution of SDSS spiral galaxies. *MNRAS*, 494(4):5839–5850.
- Kim, S. S., Saitoh, T. R., Jeon, M., Figer, D. F., Merritt, D., and Wada, K. (2011). Nuclear Star-forming Ring of the Milky Way: Simulations. *ApJ*, 735(1):L11.
- Kim, T., Gadotti, D. A., Athanassoula, E., Bosma, A., Sheth, K., and Lee, M. G. (2016). Evidence of bar-induced secular evolution in the inner regions of stellar discs in galaxies: what shapes disc galaxies? *MNRAS*, 462(4):3430–3440.
- Kim, T., Gadotti, D. A., Sheth, K., Athanassoula, E., Bosma, A., Lee, M. G., Madore, B. F., Elmegreen, B., Knapen, J. H., Zaritsky, D., Ho, L. C., Comerón, S., Holwerda, B., Hinz, J. L., Muñoz-Mateos, J.-C., Cisternas, M., Erroz-Ferrer, S., Buta, R., Laurikainen, E., Salo, H., Laine, J., Menéndez-Delmestre, K., Regan, M. W., de Swardt, B., Gil de Paz, A., Seibert, M., and Mizusawa, T. (2014). Unveiling the Structure of Barred Galaxies at 3.6 μm with the Spitzer Survey of Stellar Structure in Galaxies (S⁴G). I. Disk Breaks. *ApJ*, 782(2):64.
- Kim, W.-T. (2018). Nuclear Rings, Nuclear Spirals, and Mass Accretion to Black Holes in Disk Galaxies. In *Journal of Physics Conference Series*, volume 1031 of *Journal of Physics Conference Series*, page 012005.
- Kim, W. T. and Seo, W. Y. (2012). Gas Dynamics in Central Regions of Barred Galaxies: Hydrodynamic Models. In Pogorelov, N. V., Font, J. A., Audit, E., and Zank, G. P., editors, *Numerical Modeling of Space Plasma Slows (ASTRONUM 2011)*, volume 459 of *Astronomical Society of the Pacific Conference Series*, page 79.
- Knapen, J. H. (1999). Observations of Barred Galaxies. In Beckman, J. E. and Mahoney, T. J., editors, *The Evolution of Galaxies on Cosmological Timescales*, volume 187 of *Astronomical Society of the Pacific Conference Series*, pages 72–87.
- Knapen, J. H. (2005). Structure and star formation in disk galaxies. III. Nuclear and circumnuclear H α emission. *A&A*, 429:141–151.
- Knapen, J. H., Allard, E. L., Mazzuca, L. M., Sarzi, M., and Peletier, R. F. (2006). Star formation in the central regions of galaxies. *arXiv e-prints*, pages astro-ph/0611061.

- Knapen, J. H., Pérez-Ramírez, D., and Laine, S. (2002). Circumnuclear regions in barred spiral galaxies - II. Relations to host galaxies. *MNRAS*, 337(3):808–828.
- Knapen, J. H., Shlosman, I., and Peletier, R. F. (2000). A Subarcsecond Resolution Near-Infrared Study of Seyfert and “Normal” Galaxies. II. Morphology. *ApJ*, 529(1):93–100.
- Kormendy, J. (1979). A morphological survey of bar, lens, and ring components in galaxies: secular evolution in galaxy structure. *ApJ*, 227:714–728.
- Kormendy, J. (1993). Kinematics of extragalactic bulges: evidence that some bulges are really disks. In Dejonghe, H. and Habing, H. J., editors, *Galactic Bulges*, volume 153, page 209.
- Kormendy, J. (2008). Internal secular evolution in disk galaxies: the growth of pseudobulges. In Bureau, M., Athanassoula, E., and Barbuy, B., editors, *Formation and Evolution of Galaxy Bulges*, volume 245, pages 107–112.
- Kormendy, J. (2013). *Secular Evolution in Disk Galaxies*, page 1.
- Kormendy, J., Cornell, M. E., Block, D. L., Knapen, J. H., and Allard, E. L. (2006). Pseudobulges in the Disk Galaxies NGC 7690 and NGC 4593. *ApJ*, 642(2):765–774.
- Kormendy, J., Drory, N., Bender, R., and Cornell, M. E. (2010). Bulgeless Giant Galaxies Challenge Our Picture of Galaxy Formation by Hierarchical Clustering. *ApJ*, 723(1):54–80.
- Kormendy, J. and Kennicutt, Robert C., J. (2004). Secular Evolution and the Formation of Pseudobulges in Disk Galaxies. *ARA&A*, 42(1):603–683.
- Kowalski, M., Rubin, D., Aldering, G., Agostinho, R. J., Amadon, A., Amanullah, R., Balland, C., Barbary, K., Blanc, G., Challis, P. J., Conley, A., Connolly, N. V., Covarrubias, R., Dawson, K. S., Deustua, S. E., Ellis, R., Fabbro, S., Fadeyev, V., Fan, X., Farris, B., Folatelli, G., Frye, B. L., Garavini, G., Gates, E. L., Germany, L., Goldhaber, G., Goldman, B., Goobar, A., Groom, D. E., Haissinski, J., Hardin,

- D., Hook, I., Kent, S., Kim, A. G., Knop, R. A., Lidman, C., Linder, E. V., Mendez, J., Meyers, J., Miller, G. J., Moniez, M., Mourão, A. M., Newberg, H., Nobili, S., Nugent, P. E., Pain, R., Perdereau, O., Perlmutter, S., Phillips, M. M., Prasad, V., Quimby, R., Regnault, N., Rich, J., Rubenstein, E. P., Ruiz-Lapuente, P., Santos, F. D., Schaefer, B. E., Schommer, R. A., Smith, R. C., Soderberg, A. M., Spadafora, A. L., Strolger, L. G., Strovink, M., Suntzeff, N. B., Suzuki, N., Thomas, R. C., Walton, N. A., Wang, L., Wood-Vasey, W. M., and Yun, J. L. (2008). Improved Cosmological Constraints from New, Old, and Combined Supernova Data Sets. *ApJ*, 686(2):749–778.
- Kraljic, K., Bournaud, F., and Martig, M. (2012a). The Two-phase Formation History of Spiral Galaxies Traced by the Cosmic Evolution of the Bar Fraction. *ApJ*, 757(1):60.
- Kraljic, K., Bournaud, F., and Martig, M. (2012b). The Two-phase Formation History of Spiral Galaxies Traced by the Cosmic Evolution of the Bar Fraction. *ApJ*, 757:60.
- Krishnarao, D., Tremonti, C., Fraser-McKelvie, A., Kraljic, K., Boardman, N. F., Masters, K. L., Benjamin, R. A., Haffner, L. M., Jones, A., Pace, Z. J., Zasowski, G., Bershady, M., Bizyaev, D., Brinkmann, J., Brownstein, J. R., Drory, N., Pan, K., and Zhang, K. (2020). The Effect of Bars on the Ionized ISM: Optical Emission Lines from Milky Way Analogs. *ApJ*, 898(2):116.
- Kruk, S. J., Lintott, C. J., Bamford, S. P., Masters, K. L., Simmons, B. D., Häußler, B., Cardamone, C. N., Hart, R. E., Kelvin, L., Schawinski, K., Smethurst, R. J., and Vika, M. (2018). Galaxy Zoo: secular evolution of barred galaxies from structural decomposition of multiband images. *MNRAS*, 473(4):4731–4753.
- Kuchinski, L. E., Madore, B. F., Freedman, W. L., and Trewhella, M. (2001). Quantitative Morphology of Galaxies Observed in the Ultraviolet. *AJ*, 122(2):729–749.
- Lacey, C. and Cole, S. (1993). Merger rates in hierarchical models of galaxy formation. *MNRAS*, 262(3):627–649.

- Laine, S. and Gottesman, S. T. (1998). Neutral hydrogen gas distribution and kinematics in NGC 7479. *MNRAS*, 297(4):1041–1051.
- Laurikainen, E. and Salo, H. (2002). Bar strengths in spiral galaxies estimated from 2MASS images. *MNRAS*, 337(3):1118–1138.
- Laurikainen, E. and Salo, H. (2017). Barlenses and X-shaped features compared: two manifestations of boxy/peanut bulges. *A&A*, 598:A10.
- Laurikainen, E., Salo, H., Athanassoula, E., Bosma, A., Buta, R., and Janz, J. (2013). Statistics of the structure components in S0s: implications for bar-induced secular evolution. *MNRAS*, 430(4):3489–3509.
- Laurikainen, E., Salo, H., Athanassoula, E., Bosma, A., and Herrera-Endoqui, M. (2014a). Milky Way mass galaxies with X-shaped bulges are not rare in the local Universe. *MNRAS*, 444:L80–L84.
- Laurikainen, E., Salo, H., Athanassoula, E., Bosma, A., and Herrera-Endoqui, M. (2014b). Milky Way mass galaxies with X-shaped bulges are not rare in the local Universe. *MNRAS*, 444:L80–L84.
- Laurikainen, E., Salo, H., and Buta, R. (2005). Multicomponent decompositions for a sample of S0 galaxies. *MNRAS*, 362(4):1319–1347.
- Laurikainen, E., Salo, H., Buta, R., and Knapen, J. H. (2007). Properties of bars and bulges in the Hubble sequence. *MNRAS*, 381(1):401–417.
- Laurikainen, E., Salo, H., Buta, R., and Knapen, J. H. (2009). Bars, Ovals, and Lenses in Early-Type Disk Galaxies: Probes of Galaxy Evolution. *ApJL*, 692(1):L34–L39.
- Laurikainen, E., Salo, H., Buta, R., and Knapen, J. H. (2011). Near-infrared atlas of S0-Sa galaxies (NIRS0S). *MNRAS*, 418(3):1452–1490.
- Le Fèvre, O., Abraham, R., Lilly, S. J., Ellis, R. S., Brinchmann, J., Schade, D., Tresse, L., Colless, M., Crampton, D., Glazebrook, K., Hammer, F., and Broadhurst, T. (2000). Hubble Space Telescope imaging of the CFRS and LDSS redshift surveys

- IV. Influence of mergers in the evolution of faint field galaxies from $z \sim 1$. *MNRAS*, 311(3):565–575.
- Lee, G.-H., Woo, J.-H., Lee, M. G., Hwang, H. S., Lee, J. C., Sohn, J., and Lee, J. H. (2012). Do Bars Trigger Activity in Galactic Nuclei? *ApJ*, 750(2):141.
- Leroy, A. K., Walter, F., Brinks, E., Bigiel, F., de Blok, W. J. G., Madore, B., and Thornley, M. D. (2008). The Star Formation Efficiency in Nearby Galaxies: Measuring Where Gas Forms Stars Effectively. *AJ*, 136(6):2782–2845.
- Leroy, A. K., Walter, F., Sandstrom, K., Schruba, A., Munoz-Mateos, J.-C., Bigiel, F., Bolatto, A., Brinks, E., de Blok, W. J. G., Meidt, S., Rix, H.-W., Rosolowsky, E., Schinnerer, E., Schuster, K.-F., and Usero, A. (2013). Molecular Gas and Star Formation in nearby Disk Galaxies. *AJ*, 146(2):19.
- Li, Z., Shen, J., and Kim, W.-T. (2015). Hydrodynamical Simulations of Nuclear Rings in Barred Galaxies. *ApJ*, 806(2):150.
- Li, Z.-Y., Ho, L. C., and Barth, A. J. (2017). The Carnegie-Irvine Galaxy Survey. V. Statistical Study of Bars and Buckled Bars. *ApJ*, 845(1):87.
- Lichtenberg, A. J. and Leiberman, M. A. (1983). *Regular and stochastic motion*.
- Lin, L., Koo, D. C., Willmer, C. N. A., Patton, D. R., Conselice, C. J., Yan, R., Coil, A. L., Cooper, M. C., Davis, M., Faber, S. M., Gerke, B. F., Guhathakurta, P., and Newman, J. A. (2004). The DEEP2 Galaxy Redshift Survey: Evolution of Close Galaxy Pairs and Major-Merger Rates up to $z \sim 1.2$. *ApJ*, 617(1):L9–L12.
- Lin, L., Li, C., Du, C., Wang, E., Xiao, T., Bureau, M., Fraser-McKelvie, A., Masters, K., Lin, L., Wake, D., and Hao, L. (2020). SDSS-IV MaNGA: the indispensable role of bars in enhancing the central star formation of low- z galaxies. *MNRAS*, 499(1):1406–1423.
- Lin, L., Li, C., He, Y., Xiao, T., and Wang, E. (2017). Bar-induced Central Star Formation as Revealed by Integral Field Spectroscopy from CALIFA. *ApJ*, 838(2):105.

- Lin, Y., Cervantes Sodi, B., Li, C., Wang, L., and Wang, E. (2014). The Environment of Barred Galaxies in the Low-redshift Universe. *ApJ*, 796(2):98.
- Łokas, E. L. (2019). Anatomy of a buckling galactic bar. *A&A*, 629:A52.
- López-Sanjuan, C., Balcells, M., García-Dabó, C. E., Prieto, M., Cristóbal-Hornillos, D., Eliche-Moral, M. C., Abreu, D., Erwin, P., and Guzmán, R. (2009). Robust Determination of the Major Merger Fraction at $z = 0.6$ in the Groth Strip. *ApJ*, 694(1):643–653.
- López-Sanjuan, C., Balcells, M., Pérez-González, P. G., Barro, G., Gallego, J., and Zamorano, J. (2010). Spectro-photometric close pairs in GOODS-S: major and minor companions of intermediate-mass galaxies. *A&A*, 518:A20.
- López-Sanjuan, C., Le Fèvre, O., de Ravel, L., Cucciati, O., Ilbert, O., Tresse, L., Bardelli, S., Bolzonella, M., Contini, T., Garilli, B., Guzzo, L., Maccagni, D., McCracken, H. J., Mellier, Y., Pollo, A., Vergani, D., and Zucca, E. (2011). The VVDS-Deep Survey: the growth of bright galaxies by minor mergers since $z = 1$. In Zapatero Osorio, M. R., Gorgas, J., Maíz Apellániz, J., Pardo, J. R., and Gil de Paz, A., editors, *Highlights of Spanish Astrophysics VI*, pages 232–237.
- López-Sanjuan, C., Le Fèvre, O., Ilbert, O., Tasca, L. A. M., Bridge, C., Cucciati, O., Kampczyk, P., Pozzetti, L., Xu, C. K., Carollo, C. M., Contini, T., Kneib, J. P., Lilly, S. J., Mainieri, V., Renzini, A., Sanders, D., Scodreggio, M., Scoville, N. Z., Taniguchi, Y., Zamorani, G., Aussel, H., Bardelli, S., Bolzonella, M., Bongiorno, A., Capak, P., Caputi, K., de la Torre, S., de Ravel, L., Franzetti, P., Garilli, B., Iovino, A., Knobel, C., Kovač, K., Lamareille, F., Le Borgne, J. F., Le Brun, V., Le Floc’h, E., Maier, C., McCracken, H. J., Mignoli, M., Pelló, R., Peng, Y., Pérez-Montero, E., Presotto, V., Ricciardelli, E., Salvato, M., Silverman, J. D., Tanaka, M., Tresse, L., Vergani, D., Zucca, E., Barnes, L., Bordoloi, R., Cappi, A., Cimatti, A., Coppa, G., Koekemoer, A., Liu, C. T., Moresco, M., Nair, P., Oesch, P., Schawinski, K., and Welikala, N. (2012). The dominant role of mergers in the size evolution of massive early-type galaxies since $z \sim 1$. *A&A*, 548:A7.

- Lotz, J. M., Jonsson, P., Cox, T. J., Croton, D., Primack, J. R., Somerville, R. S., and Stewart, K. (2011). The Major and Minor Galaxy Merger Rates at $z \lesssim 1.5$. *ApJ*, 742(2):103.
- Lotz, J. M., Jonsson, P., Cox, T. J., and Primack, J. R. (2010). The effect of mass ratio on the morphology and time-scales of disc galaxy mergers. *MNRAS*, 404(2):575–589.
- Lütticke, R., Dettmar, R. J., and Pohlen, M. (2000). Box- and peanut-shaped bulges. I. Statistics. *A&AS*, 145:405–414.
- Lynden-Bell, D. (1967). Statistical mechanics of violent relaxation in stellar systems. *MNRAS*, 136:101.
- Lynden-Bell, D. (1979). On a mechanism that structures galaxies. *MNRAS*, 187:101–107.
- Lynden-Bell, D. and Kalnajs, A. J. (1972). On the generating mechanism of spiral structure. *MNRAS*, 157:1.
- Maciejewski, W. (2000). Centers of Barred Galaxies: Secondary Bars and Gas Flows. In Combes, F., Mamon, G. A., and Charmandaris, V., editors, *Dynamics of Galaxies: from the Early Universe to the Present*, volume 197 of *Astronomical Society of the Pacific Conference Series*, page 63.
- Majewski, S. R., Schiavon, R. P., Frinchaboy, P. M., Allende Prieto, C., Barkhouser, R., Bizyaev, D., Blank, B., Brunner, S., Burton, A., Carrera, R., Chojnowski, S. D., Cunha, K., Epstein, C., Fitzgerald, G., García Pérez, A. E., Hearty, F. R., Henderson, C., Holtzman, J. A., Johnson, J. A., Lam, C. R., Lawler, J. E., Maseman, P., Mészáros, S., Nelson, M., Nguyen, D. C., Nidever, D. L., Pinsonneault, M., Shetrone, M., Smee, S., Smith, V. V., Stolberg, T., Skrutskie, M. F., Walker, E., Wilson, J. C., Zasowski, G., Anders, F., Basu, S., Beland, S., Blanton, M. R., Bovy, J., Brownstein, J. R., Carlberg, J., Chaplin, W., Chiappini, C., Eisenstein, D. J., Elsworth, Y., Feuillet, D., Fleming, S. W., Galbraith-Frew, J., García, R. A., García-Hernández, D. A., Gillespie, B. A., Girardi, L., Gunn, J. E., Hasselquist, S., Hayden,

- M. R., Hekker, S., Ivans, I., Kinemuchi, K., Klaene, M., Mahadevan, S., Mathur, S., Mosser, B., Muna, D., Munn, J. A., Nichol, R. C., O'Connell, R. W., Parejko, J. K., Robin, A. C., Rocha-Pinto, H., Schultheis, M., Serenelli, A. M., Shane, N., Silva Aguirre, V., Sobek, J. S., Thompson, B., Troup, N. W., Weinberg, D. H., and Zamora, O. (2017). The Apache Point Observatory Galactic Evolution Experiment (APOGEE). *AJ*, 154(3):94.
- Maller, A. H., Dekel, A., and Somerville, R. (2002). Modelling angular-momentum history in dark-matter haloes. *MNRAS*, 329(2):423–430.
- Maller, A. H., Katz, N., Kereš, D., Davé, R., and Weinberg, D. H. (2006). Galaxy Merger Statistics and Inferred Bulge-to-Disk Ratios in Cosmological SPH Simulations. *ApJ*, 647(2):763–772.
- Mandelker, N., Dekel, A., Ceverino, D., DeGraf, C., Guo, Y., and Primack, J. (2017). Giant clumps in simulated high- z Galaxies: properties, evolution and dependence on feedback. *MNRAS*, 464(1):635–665.
- Mandelker, N., Dekel, A., Ceverino, D., Tweed, D., Moody, C. E., and Primack, J. (2014). The population of giant clumps in simulated high- z galaxies: in situ and ex situ migration and survival. *MNRAS*, 443(4):3675–3702.
- Marinova, I. and Jogee, S. (2007). Characterizing Bars at $z \sim 0$ in the Optical and NIR: Implications for the Evolution of Barred Disks with Redshift. *ApJ*, 659(2):1176–1197.
- Márquez, I., Masegosa, J., Durret, F., González Delgado, R. M., Moles, M., Maza, J., Pérez, E., and Roth, M. (2003). The detection of stellar velocity dispersion drops in the central regions of five isolated Seyfert spirals. *A&A*, 409:459–467.
- Martig, M., Bournaud, F., Croton, D. J., Dekel, A., and Teyssier, R. (2012). A Diversity of Progenitors and Histories for Isolated Spiral Galaxies. *ApJ*, 756(1):26.
- Martig, M., Bournaud, F., Teyssier, R., and Dekel, A. (2009). Morphological Quenching of Star Formation: Making Early-Type Galaxies Red. *ApJ*, 707(1):250–267.

- Martig, M., Minchev, I., and Flynn, C. (2014a). Dissecting simulated disc galaxies - I. The structure of mono-age populations. *MNRAS*, 442:2474–2486.
- Martig, M., Minchev, I., and Flynn, C. (2014b). Dissecting simulated disc galaxies - II. The age-velocity relation. *MNRAS*, 443:2452–2462.
- Martin, C. L. (2005). Mapping Large-Scale Gaseous Outflows in Ultraluminous Galaxies with Keck II ESI Spectra: Variations in Outflow Velocity with Galactic Mass. *ApJ*, 621(1):227–245.
- Martin, P. (1995). Quantitative Morphology of Bars in Spiral Galaxies. *AJ*, 109:2428.
- Martin, P. and Friedli, D. (1997). Star formation in bar environments. I. Morphology, star formation rates and general properties. *A&A*, 326:449–464.
- Martinet, L. and Friedli, D. (1997). Bar strength and star formation activity in late-type barred galaxies. *A&A*, 323:363–373.
- Martinez-Valpuesta, I. and Shlosman, I. (2004). Why Buckling Stellar Bars Weaken in Disk Galaxies. *ApJL*, 613(1):L29–L32.
- Martinez-Valpuesta, I., Shlosman, I., and Heller, C. (2006). Evolution of Stellar Bars in Live Axisymmetric Halos: Recurrent Buckling and Secular Growth. *ApJ*, 637(1):214–226.
- Martini, P., Pogge, R. W., Ravindranath, S., and An, J. H. (2001). Hubble Space Telescope Observations of the CfA Seyfert 2 Galaxies: Near-Infrared Surface Photometry and Nuclear Bars. *ApJ*, 562(1):139–151.
- Martini, P., Regan, M. W., Mulchaey, J. S., and Pogge, R. W. (2003). Circumnuclear Dust in Nearby Active and Inactive Galaxies. II. Bars, Nuclear Spirals, and the Fueling of Active Galactic Nuclei. *ApJ*, 589(2):774–782.
- Masters, K. L., Mosleh, M., Romer, A. K., Nichol, R. C., Bamford, S. P., Schawinski, K., Lintott, C. J., Andreescu, D., Campbell, H. C., Crowcroft, B., Doyle, I., Edmondson, E. M., Murray, P., Raddick, M. J., Slosar, A., Szalay, A. S., and Vandenberg, J. (2010). Galaxy Zoo: passive red spirals. *MNRAS*, 405(2):783–799.

- Masters, K. L., Nichol, R. C., Haynes, M. P., Keel, W. C., Lintott, C., Simmons, B., Skibba, R., Bamford, S., Giovanelli, R., and Schawinski, K. (2012). Galaxy Zoo and ALFALFA: atomic gas and the regulation of star formation in barred disc galaxies. *MNRAS*, 424(3):2180–2192.
- Masters, K. L., Nichol, R. C., Hoyle, B., Lintott, C., Bamford, S. P., Edmondson, E. M., Fortson, L., Keel, W. C., Schawinski, K., Smith, A. M., and Thomas, D. (2011). Galaxy Zoo: bars in disc galaxies. *MNRAS*, 411(3):2026–2034.
- McNamara, B. R. and Nulsen, P. E. J. (2007). Heating Hot Atmospheres with Active Galactic Nuclei. *ARA&A*, 45(1):117–175.
- Melvin, T., Masters, K., Lintott, C., Nichol, R. C., Simmons, B., Bamford, S. P., Casteels, K. R. V., Cheung, E., Edmondson, E. M., Fortson, L., Schawinski, K., Skibba, R. A., Smith, A. M., and Willett, K. W. (2014). Galaxy Zoo: an independent look at the evolution of the bar fraction over the last eight billion years from HST-COSMOS. *MNRAS*, 438(4):2882–2897.
- Méndez-Abreu, J., Debattista, V. P., Corsini, E. M., and Aguerri, J. A. L. (2014). Secular- and merger-built bulges in barred galaxies. *A&A*, 572:A25.
- Menéndez-Delmestre, K., Sheth, K., Schinnerer, E., Jarrett, T. H., and Scoville, N. Z. (2007). A Near-Infrared Study of 2MASS Bars in Local Galaxies: An Anchor for High-Redshift Studies. *ApJ*, 657(2):790–804.
- Merritt, D. (1983). Relaxation and tidal stripping in rich clusters of galaxies. I. Evolution of the mass distribution. *ApJ*, 264:24–48.
- Minchev, I. and Famaey, B. (2010). A New Mechanism for Radial Migration in Galactic Disks: Spiral-Bar Resonance Overlap. *ApJ*, 722(1):112–121.
- Miwa, T. and Noguchi, M. (1998). Dynamical Properties of Tidally Induced Galactic Bars. *ApJ*, 499(1):149–166.
- Momose, R., Okumura, S. K., Koda, J., and Sawada, T. (2010). Star Formation Efficiency in the Barred Spiral Galaxy NGC 4303. *ApJ*, 721:383–394.

- Moore, B., Katz, N., Lake, G., Dressler, A., and Oemler, A. (1996). Galaxy harassment and the evolution of clusters of galaxies. *Nature*, 379(6566):613–616.
- Moore, B., Lake, G., Quinn, T., and Stadel, J. (1999). On the survival and destruction of spiral galaxies in clusters. *MNRAS*, 304(3):465–474.
- Morris, M. and Serabyn, E. (1996). The Galactic Center Environment. *ARA&A*, 34:645–702.
- Moster, B. P., Macciò, A. V., Somerville, R. S., Johansson, P. H., and Naab, T. (2010). Can gas prevent the destruction of thin stellar discs by minor mergers? *MNRAS*, 403(2):1009–1019.
- Murray, N., Quataert, E., and Thompson, T. A. (2010). The Disruption of Giant Molecular Clouds by Radiation Pressure & the Efficiency of Star Formation in Galaxies. *ApJ*, 709(1):191–209.
- Nair, P. B. and Abraham, R. G. (2010). On the Fraction of Barred Spiral Galaxies. *ApJl*, 714(2):L260–L264.
- Navarro, J. F., Frenk, C. S., and White, S. D. M. (1997). A Universal Density Profile from Hierarchical Clustering. *ApJ*, 490(2):493–508.
- Newnham, L., Hess, K. M., Masters, K. L., Kruk, S., Penny, S. J., Lingard, T., and Smethurst, R. J. (2020). The H I morphology and stellar properties of strongly barred galaxies: support for bar quenching in massive spirals. *MNRAS*, 492(4):4697–4715.
- Ng, Y. K., Bertelli, G., Chiosi, C., and Bressan, A. (1996). The galactic structure towards the Galactic Centre. III. A study of Baade’s Window: discovery of the bar population? *A&A*, 310:771–796.
- Noeske, K. G., Weiner, B. J., Faber, S. M., Papovich, C., Koo, D. C., Somerville, R. S., Bundy, K., Conselice, C. J., Newman, J. A., Schiminovich, D., Le Floch, E., Coil, A. L., Rieke, G. H., Lotz, J. M., Primack, J. R., Barmby, P., Cooper, M. C., Davis, M., Ellis, R. S., Fazio, G. G., Guhathakurta, P., Huang, J., Kassin, S. A., Martin, D. C., Phillips, A. C., Rich, R. M., Small, T. A., Willmer, C. N. A., and Wilson,

- G. (2007). Star Formation in AEGIS Field Galaxies since $z=1.1$: The Dominance of Gradually Declining Star Formation, and the Main Sequence of Star-forming Galaxies. *ApJ*, 660(1):L43–L46.
- Noguchi, M. (1987). Close encounter between galaxies - II. Tidal deformation of a disc galaxy stabilized by massive halo. *MNRAS*, 228:635–651.
- Ocvirk, P., Pichon, C., and Teyssier, R. (2008). Bimodal gas accretion in the Horizon-MareNostrum galaxy formation simulation. *MNRAS*, 390(4):1326–1338.
- Oh, S., Oh, K., and Yi, S. K. (2012). Bar Effects on Central Star Formation and Active Galactic Nucleus Activity. *ApJS*, 198(1):4.
- Ostriker, J. P. and Peebles, P. J. E. (1973). A Numerical Study of the Stability of Flattened Galaxies: or, can Cold Galaxies Survive? *ApJ*, 186:467–480.
- Overzier, R. A., Heckman, T. M., Kauffmann, G., Seibert, M., Rich, R. M., Basu-Zych, A., Lotz, J., Aloisi, A., Charlot, S., Hoopes, C., Martin, D. C., Schiminovich, D., and Madore, B. (2008). Hubble Space Telescope Morphologies of Local Lyman Break Galaxy Analogs. I. Evidence for Starbursts Triggered by Merging. *ApJ*, 677(1):37–62.
- Pan, Z., Kong, X., and Fan, L. (2013). Green Galaxies in the COSMOS Field. *ApJ*, 776(1):14.
- Park, C., Gott, J., and Choi, Y. (2007). Transformation of Galaxy Morphology and Luminosity Classes. In *American Astronomical Society Meeting Abstracts*, volume 211 of *American Astronomical Society Meeting Abstracts*, page 20.03.
- Patton, D. R., Pritchet, C. J., Carlberg, R. G., Marzke, R. O., Yee, H. K. C., Hall, P. B., Lin, H., Morris, S. L., Sawicki, M., Shepherd, C. W., and Wirth, G. D. (2002). Dynamically Close Galaxy Pairs and Merger Rate Evolution in the CNOC2 Redshift Survey. *ApJ*, 565(1):208–222.
- Patton, D. R., Pritchet, C. J., Yee, H. K. C., Ellingson, E., and Carlberg, R. G. (1997). Close Pairs of Field Galaxies in the CNOC1 Redshift Survey. *ApJ*, 475(1):29–42.

- Peebles, P. J. E. (1982). Anisotropy of the microwave background due to the mass distribution in an open cosmological model. *ApJ*, 259:442–448.
- Peirani, S., Hammer, F., Flores, H., Yang, Y., and Athanassoula, E. (2009). A giant bar induced by a merger event at $z = 0.4$? *A&A*, 496(1):51–56.
- Peletier, R. F., Falcón-Barroso, J., Bacon, R., Cappellari, M., Davies, R. L., de Zeeuw, P. T., Emsellem, E., Ganda, K., Krajnović, D., Kuntschner, H., McDermid, R. M., Sarzi, M., and van de Ven, G. (2007). The SAURON project - XI. Stellar populations from absorption-line strength maps of 24 early-type spirals. *MNRAS*, 379(2):445–468.
- Peng, Y., Maiolino, R., and Cochrane, R. (2015). Strangulation as the primary mechanism for shutting down star formation in galaxies. *Nature*, 521(7551):192–195.
- Peng, Y.-j., Lilly, S. J., Kovač, K., Bolzonella, M., Pozzetti, L., Renzini, A., Zamorani, G., Ilbert, O., Knobel, C., Iovino, A., Maier, C., Cucciati, O., Tasca, L., Carollo, C. M., Silverman, J., Kampczyk, P., de Ravel, L., Sanders, D., Scoville, N., Contini, T., Mainieri, V., Scodreggio, M., Kneib, J.-P., Le Fèvre, O., Bardelli, S., Bongiorno, A., Caputi, K., Coppa, G., de la Torre, S., Franzetti, P., Garilli, B., Lamareille, F., Le Borgne, J.-F., Le Brun, V., Mignoli, M., Perez Montero, E., Pello, R., Ricciardelli, E., Tanaka, M., Tresse, L., Vergani, D., Welikala, N., Zucca, E., Oesch, P., Abbas, U., Barnes, L., Bordoloi, R., Bottini, D., Cappi, A., Cassata, P., Cimatti, A., Fumana, M., Hasinger, G., Koekemoer, A., Leauthaud, A., Maccagni, D., Marinoni, C., McCracken, H., Memeo, P., Meneux, B., Nair, P., Porciani, C., Presotto, V., and Scaramella, R. (2010). Mass and Environment as Drivers of Galaxy Evolution in SDSS and zCOSMOS and the Origin of the Schechter Function. *ApJ*, 721(1):193–221.
- Penny, S. J., Masters, K. L., Smethurst, R., Nichol, R. C., Krawczyk, C. M., Bizyaev, D., Greene, O., Liu, C., Marinelli, M., Rembold, S. B., Riffel, R. A., Ilha, G. d. S., Wylezalek, D., Andrews, B. H., Bundy, K., Drory, N., Oravetz, D., and Pan, K. (2018). SDSS-IV MaNGA: evidence of the importance of AGN feedback in low-mass galaxies. *MNRAS*, 476(1):979–998.

- Percival, W. J., Cole, S., Eisenstein, D. J., Nichol, R. C., Peacock, J. A., Pope, A. C., and Szalay, A. S. (2007). Measuring the Baryon Acoustic Oscillation scale using the Sloan Digital Sky Survey and 2dF Galaxy Redshift Survey. *MNRAS*, 381(3):1053–1066.
- Pérez, I. and Sánchez-Blázquez, P. (2011). Study of stellar populations in the bulges of barred galaxies. *A&A*, 529:A64.
- Pérez, I., Sánchez-Blázquez, P., and Zurita, A. (2009). Study of the stellar line-strength indices and kinematics along bars. I. Bar age and metallicity gradients. *A&A*, 495(3):775–794.
- Perret, V. (2016). DICE: Disk Initial Conditions Environment.
- Perret, V., Renaud, F., Epinat, B., Amram, P., Bournaud, F., Contini, T., Teyssier, R., and Lambert, J. C. (2014). Evolution of the mass, size, and star formation rate in high redshift merging galaxies. MIRAGE - A new sample of simulations with detailed stellar feedback. *A&A*, 562:A1.
- Peschken, N., Athanassoula, E., and Rodionov, S. A. (2017). Forming disc galaxies in major mergers - III. The effect of angular momentum on the radial density profiles of disc galaxies. *MNRAS*, 468(1):994–1004.
- Pfenniger, D. and Friedli, D. (1991). Structure and dynamics of 3D N-body barred galaxies. *A&A*, 252:75–93.
- Portail, M., Gerhard, O., Wegg, C., and Ness, M. (2017). Dynamical modelling of the galactic bulge and bar: the Milky Way’s pattern speed, stellar and dark matter mass distribution. *MNRAS*, 465(2):1621–1644.
- Portail, M., Wegg, C., and Gerhard, O. (2015). Peanuts, brezels and bananas: food for thought on the orbital structure of the Galactic bulge. *MNRAS*, 450:L66–L70.
- Press, W. H. and Schechter, P. (1974). Formation of Galaxies and Clusters of Galaxies by Self-Similar Gravitational Condensation. *ApJ*, 187:425–438.

- Puech, M. (2010). Clumpy galaxies at $z \sim 0.6$: kinematics, stability and comparison with analogues at other redshifts. *MNRAS*, 406(1):535–547.
- Puech, M., Hammer, F., Flores, H., Neichel, B., and Yang, Y. (2009). A forming disk at $z \sim 0.6$: collapse of a gaseous disk or major merger remnant? *A&A*, 493(3):899–906.
- Putman, M. E. (2017). *An Introduction to Gas Accretion onto Galaxies*, volume 430, page 1.
- Quillen, A. C. (2002). Growth of a Peanut-shaped Bulge via Resonant Trapping of Stellar Orbits in the Vertical Inner Lindblad Resonances. *AJ*, 124(2):722–732.
- Quillen, A. C., Frogel, J. A., Kuchinski, L. E., and Terndrup, D. M. (1995). Multiband Images of the Barred Galaxy NGC 1097. *AJ*, 110:156.
- Quillen, A. C., Minchev, I., Sharma, S., Qin, Y.-J., and Di Matteo, P. (2014). A vertical resonance heating model for X- or peanut-shaped galactic bulges. *MNRAS*, 437(2):1284–1307.
- Rahman, N., Bolatto, A. D., Xue, R., Wong, T., Leroy, A. K., Walter, F., Bigiel, F., Rosolowsky, E., Fisher, D. B., Vogel, S. N., Blitz, L., West, A. A., and Ott, J. (2012). CARMA Survey Toward Infrared-bright Nearby Galaxies (STING). II. Molecular Gas Star Formation Law and Depletion Time across the Blue Sequence. *ApJ*, 745(2):183.
- Rautiainen, P. and Salo, H. (2000). N-body simulations of resonance rings in galactic disks. *A&A*, 362:465–586.
- Rautiainen, P., Salo, H., and Laurikainen, E. (2008). Model-based pattern speed estimates for 38 barred galaxies. *MNRAS*, 388(4):1803–1818.
- Rees, M. J. (1984). Black Hole Models for Active Galactic Nuclei. *ARA&A*, 22:471–506.
- Rees, M. J. and Ostriker, J. P. (1977). Cooling, dynamics and fragmentation of massive gas clouds: clues to the masses and radii of galaxies and clusters. *MNRAS*, 179:541–559.

- Reese, A. S., Williams, T. B., Sellwood, J. A., Barnes, E. I., and Powell, B. A. (2007). Photometric Decomposition of Barred Galaxies. *AJ*, 133(6):2846–2858.
- Reynaud, D. and Downes, D. (1998). Kinematics of the gas in a barred galaxy: do strong shocks inhibit star formation? *A&A*, 337:671–680.
- Ribeiro, B., Le Fèvre, O., Cassata, P., Garilli, B., Lemaux, B. C., Maccagni, D., Schaerer, D., Tasca, L. A. M., Zamorani, G., Zucca, E., Amorín, R., Bardelli, S., Hathi, N. P., Koekemoer, A., and Pforr, J. (2017). The VIMOS Ultra-Deep Survey: A major merger origin for the high fraction of galaxies at $2 < z < 6$ with two bright clumps. *A&A*, 608:A16.
- Robertson, B. E. and Bullock, J. S. (2008). High-Redshift Galaxy Kinematics: Constraints on Models of Disk Formation. *ApJL*, 685(1):L27.
- Robichaud, F., Williamson, D., Martel, H., Kawata, D., and Ellison, S. L. (2017). Star formation history in barred spiral galaxies - active galactic nucleus feedback. *MNRAS*, 469(3):3722–3737.
- Rodighiero, G., Daddi, E., Baronchelli, I., Cimatti, A., Renzini, A., Aussel, H., Popesso, P., Lutz, D., Andreani, P., Berta, S., Cava, A., Elbaz, D., Feltre, A., Fontana, A., Förster Schreiber, N. M., Franceschini, A., Genzel, R., Grazian, A., Gruppioni, C., Ilbert, O., Le Floch, E., Magdis, G., Magliocchetti, M., Magnelli, B., Maiolino, R., McCracken, H., Nordon, R., Poglitsch, A., Santini, P., Pozzi, F., Riguccini, L., Tacconi, L. J., Wuyts, S., and Zamorani, G. (2011). The Lesser Role of Starbursts in Star Formation at $z = 2$. *ApJL*, 739(2):L40.
- Rodionov, S. A., Athanassoula, E., and Peschken, N. (2017). Forming disk galaxies in major mergers. II. The central mass concentration problem and a comparison of GADGET3 with GIZMO. *A&A*, 600:A25.
- Romeo, A. B. and Wiegert, J. (2011). The effective stability parameter for two-component galactic discs: is $Q^{-1} \approx Q^{-1}_{stars} + Q^{-1}_{gas}$? *MNRAS*, 416(2):1191–1196.

- Romero-Gómez, M., Athanassoula, E., Masdemont, J. J., and García-Gómez, C. (2007). The formation of spiral arms and rings in barred galaxies. *A&A*, 472(1):63–75.
- Romero-Gómez, M., Masdemont, J. J., Athanassoula, E., and García-Gómez, C. (2006). The origin of rR_1 ring structures in barred galaxies. *A&A*, 453(1):39–45.
- Rosas-Guevara, Y., Bonoli, S., Dotti, M., Zana, T., Nelson, D., Pillepich, A., Ho, L. C., Izquierdo-Villalba, D., Hernquist, L., and Pakmor, R. (2019). The buildup of strongly-barred galaxies in the TNG100 simulation. *arXiv e-prints*, page arXiv:1908.00547.
- Rosen, A. and Bregman, J. N. (1995). Global Models of the Interstellar Medium in Disk Galaxies. *ApJ*, 440:634.
- Rozo, E., Wechsler, R. H., Rykoff, E. S., Annis, J. T., Becker, M. R., Evrard, A. E., Frieman, J. A., Hansen, S. M., Hao, J., Johnston, D. E., Koester, B. P., McKay, T. A., Sheldon, E. S., and Weinberg, D. H. (2010). Cosmological Constraints from the Sloan Digital Sky Survey maxBCG Cluster Catalog. *ApJ*, 708(1):645–660.
- Rubin, K. H. R., Prochaska, J. X., Koo, D. C., Phillips, A. C., Martin, C. L., and Winstrom, L. O. (2014). Evidence for Ubiquitous Collimated Galactic-scale Outflows along the Star-forming Sequence at $z \sim 0.5$. *ApJ*, 794(2):156.
- Saha, K., Martinez-Valpuesta, I., and Gerhard, O. (2012). Spin-up of low-mass classical bulges in barred galaxies. *MNRAS*, 421(1):333–345.
- Saha, K. and Naab, T. (2013). Spinning dark matter haloes promote bar formation. *MNRAS*, 434(2):1287–1299.
- Sakamoto, K., Okumura, S. K., Ishizuki, S., and Scoville, N. Z. (1999). Bar-driven Transport of Molecular Gas to Galactic Centers and Its Consequences. *ApJ*, 525(2):691–701.
- Salo, H. and Laurikainen, E. (2017). Boxy/Peanut/X-Shaped Bulges: Steep Inner Rotation Curve Leads to Barless Face-on Morphology. *ApJ*, 835(2):252.

- Salo, H., Laurikainen, E., Buta, R., and Knapen, J. H. (2010). Bars do Drive Spiral Density Waves. *ApJ*, 715(1):L56–L61.
- Sánchez, A. G., Crocce, M., Cabré, A., Baugh, C. M., and Gaztañaga, E. (2009). Cosmological parameter constraints from SDSS luminous red galaxies: a new treatment of large-scale clustering. *MNRAS*, 400(3):1643–1664.
- Sánchez, S. F., Avila-Reese, V., Rodríguez-Puebla, A., Ibarra-Medel, H., Calette, R., Bershady, M., Hernández-Toledo, H., Pan, K., and Bizyaev, D. (2019). SDSS-IV MaNGA - an archaeological view of the cosmic star formation history. *MNRAS*, 482(2):1557–1586.
- Sánchez, S. F., Kennicutt, R. C., Gil de Paz, A., van de Ven, G., Vílchez, J. M., Wisotzki, L., Walcher, C. J., Mast, D., Aguerri, J. A. L., Albiol-Pérez, S., Alonso-Herrero, A., Alves, J., Bakos, J., Bartáková, T., Bland-Hawthorn, J., Boselli, A., Bomans, D. J., Castillo-Morales, A., Cortijo-Ferrero, C., de Lorenzo-Cáceres, A., Del Olmo, A., Dettmar, R. J., Díaz, A., Ellis, S., Falcón-Barroso, J., Flores, H., Gallazzi, A., García-Lorenzo, B., González Delgado, R., Gruel, N., Haines, T., Hao, C., Husemann, B., Iglésias-Páramo, J., Jahnke, K., Johnson, B., Jungwiert, B., Kalinova, V., Kehrig, C., Kupko, D., López-Sánchez, Á. R., Lyubenova, M., Marino, R. A., Mármol-Queraltó, E., Márquez, I., Masegosa, J., Meidt, S., Mendez-Abreu, J., Monreal-Ibero, A., Montijo, C., Mourão, A. M., Palacios-Navarro, G., Papaderos, P., Pasquali, A., Peletier, R., Pérez, E., Pérez, I., Quirrenbach, A., Relaño, M., Rosales-Ortega, F. F., Roth, M. M., Ruiz-Lara, T., Sánchez-Blázquez, P., Sengupta, C., Singh, R., Stanishev, V., Trager, S. C., Vazdekis, A., Viironen, K., Wild, V., Zibetti, S., and Ziegler, B. (2012). CALIFA, the Calar Alto Legacy Integral Field Area survey. I. Survey presentation. *A&A*, 538:A8.
- Sanders, R. H. and Huntley, J. M. (1976). Gas response to oval distortions in disk galaxies. *ApJ*, 209:53–65.
- Schawinski, K., Lintott, C., Thomas, D., Sarzi, M., Andreescu, D., Bamford, S. P., Kaviraj, S., Khochfar, S., Land, K., Murray, P., Nichol, R. C., Raddick, M. J., Slosar,

- A., Szalay, A., VandenBerg, J., and Yi, S. K. (2009). Galaxy Zoo: a sample of blue early-type galaxies at low redshift*. *MNRAS*, 396(2):818–829.
- Schawinski, K., Thomas, D., Sarzi, M., Maraston, C., Kaviraj, S., Joo, S.-J., Yi, S. K., and Silk, J. (2007). Observational evidence for AGN feedback in early-type galaxies. *MNRAS*, 382(4):1415–1431.
- Schawinski, K., Urry, C. M., Simmons, B. D., Fortson, L., Kaviraj, S., Keel, W. C., Lintott, C. J., Masters, K. L., Nichol, R. C., Sarzi, M., Skibba, R., Treister, E., Willett, K. W., Wong, O. I., and Yi, S. K. (2014). The green valley is a red herring: Galaxy Zoo reveals two evolutionary pathways towards quenching of star formation in early- and late-type galaxies. *MNRAS*, 440(1):889–907.
- Schommer, R. A. and Sullivan, W. T., I. (1976). Do the Ring-Like Structures in the Galaxy NGC 4736 Represent Lindblad Resonances? *Astrophys. Lett.*, 17:191.
- Schwarz, M. P. (1981). The response of gas in a galactic disk to bar forcing. *ApJ*, 247:77–88.
- Seidel, M. K., Falcón-Barroso, J., Martínez-Valpuesta, I., Díaz-García, S., Laurikainen, E., Salo, H., and Knapen, J. H. (2015). The BaLROG project - I. Quantifying the influence of bars on the kinematics of nearby galaxies. *MNRAS*, 451(1):936–973.
- Seigar, M., Carollo, C. M., Stiavelli, M., de Zeeuw, P. T., and Dejonghe, H. (2002). Spiral Galaxies with HST/NICMOS. II. Isophotal Fits and Nuclear Cusp Slopes. *AJ*, 123(1):184–194.
- Sellwood, J. A. (1981). Bar instability and rotation curves. *A&A*, 99(2):362–374.
- Sellwood, J. A. and Gerhard, O. (2020). Three mechanisms for bar thickening. *MNRAS*, 495(3):3175–3191.
- Sellwood, J. A. and Moore, E. M. (1999). On the Formation of Disk Galaxies and Massive Central Objects. *ApJ*, 510(1):125–135.

- Sellwood, J. A. and Wilkinson, A. (1993). Dynamics of barred galaxies. *Reports on Progress in Physics*, 56(2):173–256.
- Semelin, B. and Combes, F. (2002). Formation and evolution of galactic disks with a multiphase numerical model. *A&A*, 388:826–841.
- Sérsic, J. L. (1963). Influence of the atmospheric and instrumental dispersion on the brightness distribution in a galaxy. *Boletín de la Asociación Argentina de Astronomía La Plata Argentina*, 6:41–43.
- Sevenster, M. N. (1999). Speculations on Bar-Driven Evolution of the Galaxy. *Ap&SS*, 265:377–378.
- Shapley, A. E., Steidel, C. C., Pettini, M., and Adelberger, K. L. (2003). Rest-Frame Ultraviolet Spectra of $z \sim 3$ Lyman Break Galaxies. *ApJ*, 588(1):65–89.
- Shaw, M., Axon, D., Probst, R., and Gatley, I. (1995). Nuclear bars and blue nuclei within barred spiral galaxies. *MNRAS*, 274(2):369–387.
- Shen, J. and Sellwood, J. A. (2004). The Destruction of Bars by Central Mass Concentrations. *ApJ*, 604(2):614–631.
- Sheth, K., Elmegreen, D. M., Elmegreen, B. G., Capak, P., Abraham, R. G., Athanassoula, E., Ellis, R. S., Mobasher, B., Salvato, M., Schinnerer, E., Scoville, N. Z., Spalsbury, L., Strubbe, L., Carollo, M., Rich, M., and West, A. A. (2008). Evolution of the Bar Fraction in COSMOS: Quantifying the Assembly of the Hubble Sequence. *ApJ*, 675(2):1141–1155.
- Sheth, K., Melbourne, J., Elmegreen, D. M., Elmegreen, B. G., Athanassoula, E., Abraham, R. G., and Weiner, B. J. (2012). Hot Disks and Delayed Bar Formation. *ApJ*, 758(2):136.
- Sheth, K., Regan, M., Hinz, J. L., Gil de Paz, A., Menéndez-Delmestre, K., Muñoz-Mateos, J.-C., Seibert, M., Kim, T., Laurikainen, E., Salo, H., Gadotti, D. A., Laine, J., Mizusawa, T., Armus, L., Athanassoula, E., Bosma, A., Buta, R. J., Capak, P., Jarrett, T. H., Elmegreen, D. M., Elmegreen, B. G., Knapen, J. H., Koda, J., Helou,

- G., Ho, L. C., Madore, B. F., Masters, K. L., Mobasher, B., Ogle, P., Peng, C. Y., Schinnerer, E., Surace, J. A., Zaritsky, D., Comerón, S., de Swardt, B., Meidt, S. E., Kasliwal, M., and Aravena, M. (2010). The Spitzer Survey of Stellar Structure in Galaxies (S4G). *PASP*, 122(898):1397.
- Sheth, K., Vogel, S. N., Regan, M. W., Thornley, M. D., and Teuben, P. J. (2005). Secular Evolution via Bar-driven Gas Inflow: Results from BIMA SONG. *ApJ*, 632(1):217–226.
- Shibuya, T., Ouchi, M., Kubo, M., and Harikane, Y. (2016). Morphologies of ~190,000 Galaxies at $z = 0-10$ Revealed with HST Legacy Data. II. Evolution of Clumpy Galaxies. *ApJ*, 821(2):72.
- Shin, J., Kim, S. S., Baba, J., Saitoh, T. R., Hwang, J.-S., Chun, K., and Hozumi, S. (2017). Hydrodynamic Simulations of the Central Molecular Zone with a Realistic Galactic Potential. *ApJ*, 841(2):74.
- Shlosman, I., Frank, J., and Begelman, M. C. (1989). Bars within bars: a mechanism for fuelling active galactic nuclei. *Nature*, 338(6210):45–47.
- Sil'chenko, O. K. and Moiseev, A. V. (2006). Nature of Nuclear Rings in Unbarred Galaxies: NGC 7742 and NGC 7217. *AJ*, 131(3):1336–1346.
- Silk, J. (1977). On the fragmentation of cosmic gas clouds. I. The formation of galaxies and the first generation of stars. *ApJ*, 211:638–648.
- Silk, J. (2013). Unleashing Positive Feedback: Linking the Rates of Star Formation, Supermassive Black Hole Accretion, and Outflows in Distant Galaxies. *ApJ*, 772(2):112.
- Silk, J. and Rees, M. J. (1998). Quasars and galaxy formation. *A&A*, 331:L1–L4.
- Simkin, S. M., Su, H. J., and Schwarz, M. P. (1980). Nearby Seyfert galaxies. *ApJ*, 237:404–413.

- Simmons, B. D., Melvin, T., Lintott, C., Masters, K. L., Willett, K. W., Keel, W. C., Smethurst, R. J., Cheung, E., Nichol, R. C., Schawinski, K., Rutkowski, M., Kartaltepe, J. S., Bell, E. F., Casteels, K. R. V., Conselice, C. J., Almaini, O., Ferguson, H. C., Fortson, L., Hartley, W., Kocevski, D., Koekemoer, A. M., McIntosh, D. H., Mortlock, A., Newman, J. A., Ownsworth, J., Bamford, S., Dahlen, T., Faber, S. M., Finkelstein, S. L., Fontana, A., Galametz, A., Grogin, N. A., Grützbauch, R., Guo, Y., Häußler, B., Jek, K. J., Kaviraj, S., Lucas, R. A., Peth, M., Salvato, M., Wiklind, T., and Wuyts, S. (2014). Galaxy Zoo: CANDELS barred discs and bar fractions. *MNRAS*, 445(4):3466–3474.
- Skibba, R. A., Masters, K. L., Nichol, R. C., Zehavi, I., Hoyle, B., Edmondson, E. M., Bamford, S. P., Cardamone, C. N., Keel, W. C., Lintott, C., and Schawinski, K. (2012). Galaxy Zoo: the environmental dependence of bars and bulges in disc galaxies. *MNRAS*, 423(2):1485–1502.
- Skokos, C., Patsis, P. A., and Athanassoula, E. (2002). Orbital dynamics of three-dimensional bars - I. The backbone of three-dimensional bars. A fiducial case. *MNRAS*, 333(4):847–860.
- Smethurst, R. J., Lintott, C. J., Simmons, B. D., Schawinski, K., Marshall, P. J., Bamford, S., Fortson, L., Kaviraj, S., Masters, K. L., Melvin, T., Nichol, R. C., Skibba, R. A., and Willett, K. W. (2015). Galaxy Zoo: evidence for diverse star formation histories through the green valley. *MNRAS*, 450(1):435–453.
- Smirnov, A. A. and Sotnikova, N. Y. (2019). Is the late buckling stage inevitable in the bar life? *MNRAS*, 485(2):1900–1905.
- Solway, M., Sellwood, J. A., and Schönrich, R. (2012). Radial migration in galactic thick discs. *MNRAS*, 422(2):1363–1383.
- Somerville, R. S. and Davé, R. (2015). Physical Models of Galaxy Formation in a Cosmological Framework. *ARA&A*, 53:51–113.
- Sotnikova, N. Y. and Rodionov, S. A. (2003). Mechanisms of the Vertical Secular Heating of a Stellar Disk. *Astronomy Letters*, 29:321–335.

- Soto, E., de Mello, D. F., Rafelski, M., Gardner, J. P., Teplitz, H. I., Koekemoer, A. M., Ravindranath, S., Grogin, N. A., Scarlata, C., Kurczynski, P., and Gawiser, E. (2017). Physical Properties of Sub-galactic Clumps at $0.5 \leq Z \leq 1.5$ in the UVUDF. *ApJ*, 837(1):6.
- Sparre, M. and Springel, V. (2017). The unorthodox evolution of major merger remnants into star-forming spiral galaxies. *MNRAS*, 470(4):3946–3958.
- Spinoso, D., Bonoli, S., Dotti, M., Mayer, L., Madau, P., and Bellovary, J. (2017). Bar-driven evolution and quenching of spiral galaxies in cosmological simulations. *MNRAS*, 465(3):3729–3740.
- Springel, V., Frenk, C. S., and White, S. D. M. (2006). The large-scale structure of the Universe. *Nature*, 440(7088):1137–1144.
- Stewart, K. R., Bullock, J. S., Wechsler, R. H., Maller, A. H., and Zentner, A. R. (2008). Merger Histories of Galaxy Halos and Implications for Disk Survival. *ApJ*, 683(2):597–610.
- Stinson, G. S., Bailin, J., Couchman, H., Wadsley, J., Shen, S., Nickerson, S., Brook, C., and Quinn, T. (2010). Cosmological galaxy formation simulations using smoothed particle hydrodynamics. *MNRAS*, 408(2):812–826.
- Straughn, A. N., Voyer, E. N., Eufrasio, R. T., de Mello, D., Petty, S., Kassin, S., Gardner, J. P., Ravindranath, S., and Soto, E. (2015). A Multiwavelength Study of Tadpole Galaxies in the Hubble Ultra Deep Field. *ApJ*, 814(2):97.
- Sutherland, R. S. and Dopita, M. A. (1993). Cooling Functions for Low-Density Astrophysical Plasmas. *ApJS*, 88:253.
- Taniguchi, Y. and Shioya, Y. (2001). A New Interpretation of Chain Galaxies at High Redshift. *ApJ*, 547(1):146–153.
- Taranu, D. S., Dubinski, J., and Yee, H. K. C. (2013). Mergers in Galaxy Groups. I. Structure and Properties of Elliptical Remnants. *ApJ*, 778(1):61.

- Taylor, P. and Kobayashi, C. (2015). Quantifying AGN-driven metal-enhanced outflows in chemodynamical simulations. *MNRAS*, 452(1):L59–L63.
- Teyssier, R. (2002). Cosmological hydrodynamics with adaptive mesh refinement. A new high resolution code called RAMSES. *A&A*, 385:337–364.
- Thomas, D., Maraston, C., Bender, R., and Mendes de Oliveira, C. (2005). The Epochs of Early-Type Galaxy Formation as a Function of Environment. *ApJ*, 621(2):673–694.
- Thomas, D., Maraston, C., Schawinski, K., Sarzi, M., and Silk, J. (2010). Environment and self-regulation in galaxy formation. *MNRAS*, 404(4):1775–1789.
- Toomre, A. (1964). On the gravitational stability of a disk of stars. *ApJ*, 139:1217–1238.
- Toomre, A. (1977). Mergers and Some Consequences. In Tinsley, B. M. and Larson, Richard B. Gehret, D. C., editors, *Evolution of Galaxies and Stellar Populations*, page 401.
- Toomre, A. (1981). What amplifies the spirals. In Fall, S. M. and Lynden-Bell, D., editors, *Structure and Evolution of Normal Galaxies*, pages 111–136.
- Toomre, A. and Toomre, J. (1972). Galactic Bridges and Tails. *ApJ*, 178:623–666.
- Toth, G. and Ostriker, J. P. (1992). Galactic Disks, Infall, and the Global Value of Omega. *ApJ*, 389:5.
- Tsoutsis, P., Efthymiopoulos, C., and Voglis, N. (2008). The coalescence of invariant manifolds and the spiral structure of barred galaxies. *MNRAS*, 387(3):1264–1280.
- Tubbs, A. D. (1982). The inhibition of star formation in barred spiral galaxies. *ApJ*, 255:458–466.
- Umehata, H., Fumagalli, M., Smail, I., Matsuda, Y., Swinbank, A. M., Cantalupo, S., Sykes, C., Ivison, R. J., Steidel, C. C., Shapley, A. E., Vernet, J., Yamada, T., Tamura, Y., Kubo, M., Nakanishi, K., Kajisawa, M., Hatsukade, B., and Kohno,

- K. (2019). Gas filaments of the cosmic web located around active galaxies in a protocluster. *Science*, 366(6461):97–100.
- Valenzuela, O. and Klypin, A. (2003). Secular bar formation in galaxies with a significant amount of dark matter. *MNRAS*, 345(2):406–422.
- van de Voort, F., Schaye, J., Booth, C. M., and Dalla Vecchia, C. (2011). The drop in the cosmic star formation rate below redshift 2 is caused by a change in the mode of gas accretion and by active galactic nucleus feedback. *MNRAS*, 415(3):2782–2789.
- van der Marel, R. P. and Franx, M. (1993). A New Method for the Identification of Non-Gaussian Line Profiles in Elliptical Galaxies. *ApJ*, 407:525.
- van Starckenburg, L., van der Werf, P. P., Franx, M., Labbé, I., Rudnick, G., and Wuyts, S. (2008). Dynamical properties of a large young disk galaxy at $z = 2.03$. *A&A*, 488(1):99–112.
- Vera, M., Alonso, S., and Coldwell, G. (2016). Effect of bars on the galaxy properties. *A&A*, 595:A63.
- Verley, S., Combes, F., Verdes-Montenegro, L., Bergond, G., and Leon, S. (2007). Star formation in isolated AMIGA galaxies: dynamical influence of bars. *A&A*, 474(1):43–53.
- Vikhlinin, A., Kravtsov, A. V., Burenin, R. A., Ebeling, H., Forman, W. R., Hornstrup, A., Jones, C., Murray, S. S., Nagai, D., Quintana, H., and Voevodkin, A. (2009). Chandra Cluster Cosmology Project III: Cosmological Parameter Constraints. *ApJ*, 692(2):1060–1074.
- Villa-Vargas, J., Shlosman, I., and Heller, C. (2009). Dark Matter Halos and Evolution of Bars in Disk Galaxies: Collisionless Models Revisited. *ApJ*, 707(1):218–232.
- Villa-Vargas, J., Shlosman, I., and Heller, C. (2010). Dark Matter Halos and Evolution of Bars in Disk Galaxies: Varying Gas Fraction and Gas Spatial Resolution. *ApJ*, 719(2):1470–1480.

- Villalobos, Á., Kazantzidis, S., and Helmi, A. (2010). Thick-disk Evolution Induced by the Growth of an Embedded Thin Disk. *ApJ*, 718(1):314–330.
- Vitvitska, M., Klypin, A. A., Kravtsov, A. V., Wechsler, R. H., Primack, J. R., and Bullock, J. S. (2002). The Origin of Angular Momentum in Dark Matter Halos. *ApJ*, 581(2):799–809.
- Voglis, N., Tsoutsis, P., and Efthymiopoulos, C. (2006). Invariant manifolds, phase correlations of chaotic orbits and the spiral structure of galaxies. *MNRAS*, 373(1):280–294.
- Wang, J., Kauffmann, G., Overzier, R., Tacconi, L. J., Kong, X., Saintonge, A., Catinella, B., Schiminovich, D., Moran, S. M., and Johnson, B. (2012). Quantifying the role of bars in the build-up of central mass concentrations in disc galaxies. *MNRAS*, 423(4):3486–3501.
- Weilbacher, P. M., Palsa, R., Streicher, O., Bacon, R., Urrutia, T., Wisotzki, L., Conseil, S., Husemann, B., Jarno, A., Kelz, A., Pécontal-Rousset, A., Richard, J., Roth, M. M., Selman, F., and Vernet, J. (2020). The data processing pipeline for the MUSE instrument. *A&A*, 641:A28.
- Weilbacher, P. M., Streicher, O., Urrutia, T., Jarno, A., Pécontal-Rousset, A., Bacon, R., and Böhm, P. (2012). Design and capabilities of the MUSE data reduction software and pipeline. In Radziwill, N. M. and Chiozzi, G., editors, *Software and Cyberinfrastructure for Astronomy II*, volume 8451 of *Society of Photo-Optical Instrumentation Engineers (SPIE) Conference Series*, page 84510B.
- Weiner, B. J., Coil, A. L., Prochaska, J. X., Newman, J. A., Cooper, M. C., Bundy, K., Conselice, C. J., Dutton, A. A., Faber, S. M., Koo, D. C., Lotz, J. M., Rieke, G. H., and Rubin, K. H. R. (2009). Ubiquitous Outflows in DEEP2 Spectra of Star-Forming Galaxies at $z = 1.4$. *ApJ*, 692(1):187–211.
- Weinmann, S. M., van den Bosch, F. C., Yang, X., and Mo, H. J. (2006). The Dependence of Galaxy Type on Host Halo Mass. *arXiv e-prints*, pages astro-ph/0607585.

- Weinzirl, T., Jogee, S., Khochfar, S., Burkert, A., and Kormendy, J. (2009). Bulge n and B/T in High-Mass Galaxies: Constraints on the Origin of Bulges in Hierarchical Models. *ApJ*, 696(1):411–447.
- White, S. D. M. (1984). Angular momentum growth in protogalaxies. *ApJ*, 286:38–41.
- White, S. D. M. and Frenk, C. S. (1991). Galaxy Formation through Hierarchical Clustering. *ApJ*, 379:52.
- White, S. D. M. and Rees, M. J. (1978). Core condensation in heavy halos: a two-stage theory for galaxy formation and clustering. *MNRAS*, 183:341–358.
- Whyte, L. F., Abraham, R. G., Merrifield, M. R., Eskridge, P. B., Frogel, J. A., and Pogge, R. W. (2002). Morphological classification of the OSU Bright Spiral Galaxy Survey. *MNRAS*, 336(4):1281–1286.
- Wozniak, H. (2007). The distribution of stellar population age in galactic bars. *A&A*, 465(1):L1–L4.
- Wozniak, H. and Champavert, N. (2006). Lifetime of nuclear velocity dispersion drops in barred galaxies. *MNRAS*, 369(2):853–859.
- Wozniak, H. and Michel-Dansac, L. (2009). Formation of young boxy/peanut bulges in ringed barred galaxies. *A&A*, 494(1):11–20.
- Wuyts, E., Rigby, J. R., Gladders, M. D., and Sharon, K. (2014). A Magnified View of the Kinematics and Morphology of RCSGA 032727-132609: Zooming in on a Merger at $z = 1.7$. *ApJ*, 781(2):61.
- Yoshida, N. (2008). Protostar formation in the early universe. In Hunt, L. K., Madden, S. C., and Schneider, R., editors, *Low-Metallicity Star Formation: From the First Stars to Dwarf Galaxies*, volume 255, pages 18–23.
- Yoshino, A. and Yamauchi, C. (2015). Box/peanut and bar structures in edge-on and face-on nearby galaxies in the Sloan Digital Sky Survey - I. Catalogue. *MNRAS*, 446(4):3749–3767.

Zanella, A., Le Floch, E., Harrison, C. M., Daddi, E., Bernhard, E., Gobat, R., Strazzullo, V., Valentino, F., Cibinel, A., Sánchez Almeida, J., Kohandel, M., Fensch, J., Behrendt, M., Burkert, A., Onodera, M., Bournaud, F., and Scholtz, J. (2019). A contribution of star-forming clumps and accreting satellites to the mass assembly of $z \sim 2$ galaxies. *MNRAS*, 489(2):2792–2818.